

# **Titanium nitride thin films for sensor applications**

Master of Science thesis by  
Mathias Hausladen

Supervisors: Jakob Kjelstrup-Hansen and Kasper  
Thilsing-Hansen in collaboration with Serguei Chiriaev  
and Nis Dam Madsen

Hand-in date: 02.06.2014

Examination date: 18.06.2014

In corporation with Mads Clausen Institute (SDU  
Sønderborg), NanoSYD and Danfoss A/S



## Preface

This thesis has been submitted to partially fulfill the requirements of obtaining the Masters of Science degree in Engineering at the University of Southern Denmark (SDU). The experiments were conducted at NanoSYD and the Mads Clausen Institute (MCI) of the SDU.

The master's project formed an integrated part of a larger research project that is carried out in collaboration between the SDU and Danfoss A/S concerning the development of new strain gauge sensors. The goal of this project is to reduce the resistivity drift of a potential sensor material and measure the gauge factor. The project involves the fabrication of thin films, tuning deposition parameters, and analyzing the thin films with various characterization methods to extract information about the atomic composition, electrical characteristics, and morphology.

At this point, I would like to thank Jakob Kjelstrup-Hansen (Associate Professor at MCI, SDU) and Serguei Chiriaev (Development specialist, Danfoss A/S) for giving me the opportunity of working on an industry related project with a steep learning curve. Furthermore, I would like to thank Jakob for his guidance during the overall project. Also, I would like to thank Kasper Thilising-Hansen (Technical Manager of Cleanroom at MCI, SDU) and Nis Dam Madsen (Industrial Postdoc at MCI (SDU) / Danfoss A/S) for their extensive technical assistance concerning the production and characterization processes and theory related support during this project. I am thankful for the opportunity to work and learn alongside these motivated and highly dedicated scientists.



---

Mathias Hausladen

## Abstract

Recently, a growing demand for inexpensive pressure sensors, which can provide accurate and reliable measurements of the pressures that occur when fuels are incinerated at high temperatures, can be observed. Thin film ceramic materials such as titanium nitride ( $\text{TiN}_x$ ) pose a promising solution to realize low cost high temperature sensors, which fulfill the needed requirements.

Danfoss A/S has established requirements for the sensors material, which include (a) resistivity drift of the potential sensor material being below  $\pm 2\%$  at an operating temperature of up to  $250^\circ\text{C}$  during 150 hours, a gauge factor (GF) of 3 to 5 or higher, and a temperature coefficient of resistance (TCR) below  $100 \text{ ppm}/^\circ\text{C}$ .

The overall research approach was to study the impact of the deposition pressure, nitrogen flow, and the target power on the resistivity stability, thin film stoichiometry, and structure. This has been done by a commercial material analyzer (DMA Q800) has been modified in order to measure the gauge factors and TCR.

During the research it was found that a low deposition pressure results in thin films with a higher density and lower resistivity drift over time. In the case of the MCI NanoSYD deposition system, the main chamber deposition pressure was adjusted to be around  $2,2\text{E-}3 \text{ mbar}$ .

Three sputter target modes were related to the resistivity stability performance of the thin films. Both the metallic target mode with a low nitrogen reactive gas flow and the poisoned target mode with a high reactive nitrogen flow showed stable resistivities. The remaining mode, the area between the metallic and poisoned target modes, was resulting in thin films with a high resistivity drift over time at room temperature; thus this area should be avoided.

Two samples from the metallic and poisoned target mode, which both had a resistivity drift of below  $\pm 2\%$  at an operating temperature of  $200^\circ\text{C}$  during 360 hours, were analyzed with regard to their gauge factor. The poisoned target mode sample measured a gauge factor of around 5,08 and a TCR of around  $99,4 \text{ ppm}/^\circ\text{C}$  and the metallic target mode sample resulted in a gauge factor of around 1,54 and a TCR of around  $-10,8 \text{ ppm}/^\circ\text{C}$ .

The results for the poisoned target mode should be further analyzed because they are close to the desired requirement stated by Danfoss A/S.

## Contents

|   |    |
|---|----|
| Preface.....  | i  |
| Abstract .....  | ii |
| 1. Introduction.....  | 1  |
| 1.1. Project background .....                                 | 1  |
| 1.2. Project goals .....                                      | 2  |
| 1.3. Outline.....   | 3  |
| 2. Theory.....  | 4  |
| 2.1. Strain gauge sensors.....                                | 4  |
| 2.1.1. Strain gauge working principle .....                   | 6  |
| 2.1.2. Temperature coefficient of resistance (TCR).....       | 8  |
| 2.2. Sputtering techniques .....                              | 9  |
| 2.2.1. Working principle DC, RF and reactive sputtering ..... | 9  |
| 2.2.1.1. Plasma .....   | 11 |
| 2.2.1.2. Ion-surface interaction .....                        | 12 |
| 2.2.1.3. Reactive sputtering.....                             | 13 |
| 2.2.1.5. Target integrity .....                               | 14 |
| 2.2.1.6. Arcing.....  | 14 |
| 2.2.2. Thin film structure .....                              | 15 |
| 2.2.2.1. Processing parameters .....                          | 15 |
| 2.2.2.2. Structure-zone diagrams (SZD).....                   | 15 |
| 2.3. Energy-dispersive X-ray spectroscopy (EDX) .....         | 16 |
| 2.3.1. Generation of x-rays.....                              | 18 |
| 2.3.2. Continuum x-rays (Bremsstrahlung).....                 | 20 |
| 2.4. Resistivity - Four-point probe .....                     | 21 |
| 2.5. Thin film stress .....                                   | 24 |
| 2.6. X-Ray Diffraction (XRD).....                             | 25 |
| 3. Fabrication and characterization equipment.....            | 28 |
| 3.1. Cryofox - thin film deposition system .....              | 28 |
| 3.2. Deposition log book.....                                 | 28 |
| 3.3. Wafer substrate information.....                         | 28 |
| 3.4. Four point probe – electrical resistivity.....           | 28 |
| 3.5. AFM – thin film thickness .....                          | 29 |
| 3.6. EDX – atomic composition.....                            | 29 |

|          |  |    |
|----------|--|----|
| 3.7.     | SEM – top and cross-section images .....   | 30 |
| 3.8.     | Dektak - stress measurements .....   | 30 |
| 3.9.     | XRD – crystal structure .....  | 30 |
| 3.10.    | Oven - accelerated life test.....  | 30 |
| 3.11.    | Tube furnace post-annealing.....   | 30 |
| 4.       | Experimental introduction TiN <sub>x</sub> and TiO <sub>x</sub> N <sub>y</sub> project recap ..... | 31 |
| 5.       | Post-annealing investigations.....   | 33 |
| 6.       | TiN resistivity stability - research strategy .....  | 37 |
| 7.       | TiN resistivity stability – experiments, results and discussions.....                              | 38 |
| 7.1.     | Pressure series.....   | 38 |
| 7.1.1.   | Resistivity.....   | 39 |
| 7.1.2.   | Atomic composition .....   | 42 |
| 7.1.3.   | Thin film structure .....  | 42 |
| 7.1.4.   | Crystal structure .....  | 43 |
| 7.1.5.   | Density.....   | 44 |
| 7.1.6.   | Conclusion .....   | 44 |
| 7.2.     | Nitrogen flow series at 300W.....  | 45 |
| 7.2.1.   | Deposition system characteristics and hysteresis.....  | 45 |
| 7.2.2.   | Depositions.....   | 47 |
| 7.2.3.   | Resistivity.....   | 49 |
| 7.2.4.   | Atomic composition .....   | 52 |
| 7.2.5.   | Crystal structure .....  | 52 |
| 7.2.6.   | Conclusion .....   | 53 |
| 7.3.     | Power series .....   | 54 |
| 7.3.1.   | Deposition system characteristics.....   | 54 |
| 7.3.2.   | Depositions.....   | 55 |
| 7.3.3.   | Resistivity.....   | 57 |
| 7.3.4.   | Atomic composition .....   | 61 |
| 7.3.5.   | Crystal structure .....  | 63 |
| 7.3.6.   | Residual stress .....  | 63 |
| 7.3.7.   | Conclusion .....   | 64 |
| 7.4.     | Nitrogen flow series at 600W.....  | 65 |
| 7.4.1.   | Depositions.....   | 66 |
| 7.4.1.1. | Deposition parameters during production.....   | 66 |

|        |  |     |
|--------|--|-----|
| 7.4.2. | Resistivity.....   | 68  |
| 7.4.3. | Atomic composition .....                                   | 70  |
| 7.4.4. | Thin film stress .....                                     | 71  |
| 7.4.5. | Conclusion .....   | 72  |
| 7.5.   | Overall stability research conclusion and outlook .....    | 73  |
| 8.     | Initial gauge factor experiments.....                      | 75  |
| 8.1.   | DMA Q800 3-point bending .....                             | 75  |
| 8.2.   | DMA electro-mechanical holder design.....                  | 78  |
| 8.2.1. | Analytical strain evaluations.....                         | 80  |
| 8.3.   | Strain sensitive pattern .....                             | 81  |
| 8.4.   | Depositions.....   | 83  |
| 8.5.   | Gauge factor results .....                                 | 83  |
| 8.6.   | Conclusion and outlook.....                                | 87  |
| 9.     | Overall project conclusion.....                            | 88  |
|        | Bibliography.....  | 90  |
| 10.    | Appendix.....  | 94  |
| 10.1.  | Project time table .....                                   | 94  |
| 10.2.  | Initial project description .....                          | 95  |
| a.     | Fabrication and characterization equipment appendix .....  | 97  |
| A1.    | Correction factor calculation example .....                | 97  |
| A2.    | Resistivity calculation .....                              | 100 |
| A3.    | Cryofox DC procedure .....                                 | 101 |
| A4.    | Cryofox error analysis and optimization .....              | 103 |
| A5.    | Cryofox sample placement.....                              | 108 |
| A6.    | Deposition log book .....                                  | 109 |
| A7.    | Wafer substrate information .....                          | 117 |
| A8.    | Four point probe procedure.....                            | 118 |
| A9.    | Four point probe measurement repeatability experiment..... | 121 |
| A10.   | AFM lift-off structure .....                               | 123 |
| A11.   | EDX procedure .....  | 124 |
| A12.   | EDX measurement standard .....                             | 128 |
| A13.   | EDX relative concentration and error calculations .....    | 129 |
| A14.   | SEM top-view and Cross-section images .....                | 133 |
| A15.   | Stress wafer measurements and calculations.....            | 134 |

|   |     |
|---|-----|
| A16. XRD quick start guide .....                            | 137 |
| A17. Tube furnace annealing procedure .....                 | 139 |
| b. Post-annealing experiments.....                          | 140 |
| c. Pressure series appendix.....                            | 152 |
| C1. Substrates and placement – pressure series.....         | 152 |
| C2. Accelerated lifetime testing experiment.....            | 153 |
| C3. Pre and post EDX for accelerated life test samples..... | 154 |
| C4. AFM and SEM thickness measurements .....                | 155 |
| C5. SEM top-view and cross-section view images.....         | 156 |
| C6. Density measurement experiment.....                     | 158 |
| d. Nitrogen flow series at 300 W appendix .....             | 160 |
| D1. Substrates and placement .....                          | 160 |
| D2. Sample thickness.....                                   | 161 |
| D3. Sample deposition data observations.....                | 162 |
| D4. Pressure evolution during deposition .....              | 163 |
| D5. Target arcing investigations .....                      | 163 |
| D6. SEM cross-section images.....                           | 168 |
| e. Power series appendix .....                              | 170 |
| E1. Substrates and placement – power series .....           | 170 |
| E2. Sample deposition data observations .....               | 171 |
| f. Nitrogen flow series 600W appendix.....                  | 172 |
| F1. XRD – nitrogen series 600W .....                        | 172 |
| g. Gauge factor experiments.....                            | 173 |
| G1. Ansys and Comsol beam deflection models .....           | 173 |
| G2. Initial gauge factor measurement.....                   | 175 |
| G3. DMA software measurement steps.....                     | 180 |
| G4. Load displacement performance experiment .....          | 181 |
| G5. Strain sensitive resistor substrate design .....        | 182 |
| G6. Gauge factor measurement test.....                      | 185 |
| G7. Substrate and substrate placement.....                  | 189 |
| G8. Step by step production instructions.....               | 191 |

## 1. Introduction

### 1.1. Project background

Machinery working at high pressure, such as power generators or engines in air crafts and container ships must become more efficient in order to reduce energy consumption and pollution of the environment. To achieve this, it is essential to have stable sensors that can provide accurate and reliable measurements of the pressures that occur when fuels are incinerated at high temperatures.

The major challenge is that nowadays there are no pressure sensors at an affordable price, which are accurate and stable enough in these high temperature environments. Yet on the other side there is a growing demand for inexpensive pressure sensors, which are capable of operating at high temperatures (above 150 °C and up to 400 °C) and harsh environments (e.g. chemically aggressive media). The existing sensors on the market use expensive materials and have high fabrication costs, which makes them economically infeasible in numerous industrial applications.

Thin film ceramic materials such as titanium nitride ( $\text{TiN}_x$ ) and titanium oxynitride ( $\text{TiO}_x\text{N}_y$ ) pose a promising solution to realize low cost, high temperature sensors, which fulfill the needed requirements.

This master's project forms an integrated part of a larger research project that is carried out in collaboration between the University of Southern Denmark (SDU) and Danfoss A/S.

The project team consists of five people:

- Nis Dam Madsen (Industrial Postdoc at MCI (SDU) / Danfoss A/S)
- Mathias Hausladen (Master Student, MCI, SDU)
- Kasper Thilsing-Hansen (Technical Manager of Cleanroom at MCI, SDU)
- Jakob Kjelstrup-Hansen (Associate Professor at MCI, SDU)
- Serguei Chiriaev (Development specialist, Danfoss A/S)

The master's project is managed through weekly meetings together with Nis, Kasper and Jakob to coordinate the work, discuss experimental problems, and evaluate the project progress.

Furthermore detailed project logs and time plans make sure, that the project milestones are on track. (See appendix "Project time table" page94)

## 1.2. Project goals

The initial project formulation of this masters' project suggested a focus on titanium oxynitride ( $\text{TiO}_x\text{N}_y$ ), but the actual focus of this project report is on the titanium nitride system (see appendix "Initial project description" page 95). The incentive for this was, to first optimize the  $\text{TiN}_x$  system, before adding further complexity to the parameter space, by using the oxygen pulsing to create  $\text{TiO}_x\text{N}_y$  thin films. Furthermore, research of  $\text{TiO}_x\text{N}_y$  performed prior to this project indicated, that the  $\text{TiN}_x$  thin film system had the lowest resistance drift at room temperature.

The stable operation at elevated temperatures is a challenge for piezoresistive pressure sensors. High temperatures cause the resistivity of the thin film material to drift. One important mechanism causing the resistivity drift could be oxidation.

In order to establish a foundation for the future  $\text{TiO}_x\text{N}_y$  research, one first has to know how the oxygen pulsing modifies the actual  $\text{TiN}_x$  system. This requires comprehensive knowledge about how the processing parameters of the NanoSYD deposition system are affecting the  $\text{TiN}_x$  thin film structure and properties. Furthermore understanding and minimizing the resistivity drift, which in essence is related with an optimization of the existing  $\text{TiN}_x$  thin film structure, is a key milestone for tailoring the material, so it can be employed as a strain gauge material.

Danfoss A/S has the following requirements for the sensors material: [1]

- 1) The resistivity drift of the potential sensor material should be below  $\pm 2\%$  at an operating temperature of up to  $250^\circ\text{C}$  during 150 hours. This requirement had the highest priority in the masters' projects and therefore the main focus of this masters' project was on the deposition process parameter space and the characterization of the thin films with regard to their electrical resistivity drift, thin film composition and structure.
- 2) A gauge factor (GF) of 3 to 5 or higher. A small part of the masters' project was allocated to contribute to the modifications of a commercial material analyzer (DMA Q800), to be able to measure an electromechanical gauge factor (electrical resistance as a function of strain).
- 3) An absolute value of the temperature coefficient of resistance (TCR) below  $100 \text{ ppm}/^\circ\text{C}$ . It was mentioned that the TCR can be compensated by a Wheatstone configuration by Danfoss A/S, which makes this requirement a low priority for this masters' project.

### 1.3. Outline

This thesis is divided into several chapters.

Chapter 1 presents the project background, the motivation, and the team behind the project and the project goals for this master's project.

Chapter 2 contains the theory related to this project. It starts by introducing the basic strain gauge theory, which includes an overview of strain gauge sensor types and an explanation of the strain gauge working principle. Afterwards, the sputtering technique for the thin film depositions is introduced and related parameters are discussed, followed by an introduction to thin film structures. Also, the underlying theory for different characterization methods is presented in this chapter, which includes atomic composition analysis, electrical characteristics, thin film stress, and crystal structures.

Chapter 3 is listing the different fabrication, experimental, and characterization techniques, that were developed and used throughout this project.

Chapter 4 summarizes the main results of previous research conducted related to titanium nitride and titanium oxynitride at MCI Sønderborg, on which this masters project is based.

Chapter 5 shows a brief investigation of post-annealing and the effects on the resistivity drift.

Chapter 6 explains the research strategy for the titanium nitride resistivity stability

Chapter 7 shows the results, discussions, and conclusions of the titanium nitride stability research. The experiments include investigations of the effect of key deposition parameters; the main chamber pressure, the nitrogen flow, and the target power on the thin film resistivity and its stability at temperatures up to 200 °C; furthermore, thin film composition, morphology, crystal orientation, and residual stress were investigated.

Chapter 8 gives an overview of the ongoing gauge factor setup development. Initial experimental results are presented.

The report is concluded by summarizing the main results and making suggestions for future improvements and work.

## 2. Theory

### 2.1. Strain gauge sensors

A strain gauge is a sensing device, which converts mechanical displacement into an electric signal. Strain gauge sensors are used for pressure sensors, structural analyses, experimental stress analysis, vibration and torque measurements, deformation monitoring of components, crack or strain monitoring in buildings [2] and bridges, medical and education applications, research and development applications within automotive, oil/gas and aerospace applications. [3]

A large application sector for strain gauges is the pressure monitoring in high pressure applications such as engines, fuel systems, or power generators.

Also in particular, the stress analysis is a vital part of the structural design and optimization process of parts, which need to be lighter and thinner to increase the efficiency of the overall product, while still maintaining their strength to assure safety and economic feasibility (e.g. within automotive or aerospace industry for fuel consumption optimization to decrease CO<sub>2</sub> output). Generally, stress is defined as an internal resisting force and strain is the displacement and deformation, which occurs due to the stress. [4] Stress and strain may occur when an external force, pressure, moments, or heat is applied on a stationary object. Currently there is no technology that can measure and evaluate stress directly, but the strain on the surface of an object can be measured by strain gauges in order to get an estimate of an object's internal stresses. [5]

The strain gauge market is divided into three sensor types, which are bonded-metal foil gauges, diffused semiconductor strain gauges, and thin film strain gauges. [6]

The dominating strain gauge type is the foil type, which is available in a wide variety of shapes and sizes with gauge factor values from 2-5. The design uses a patterned resistive foil, which is mounted on a backing material and applied with adhesive bonding agent to an object, for which the strain is monitored. When the foil is subjected to stress the electrical resistance of the foil will change linearly with strain. For this type of strain gauge the proper mounting is important, because the adhesive bonding agent needs to transmit the strain properly from the object to the foil diaphragm. Furthermore the adhesive bonding agent is working as an electrical insulator between the foil grid and the surface. [4] [7] Drawbacks are the low resistivity of the metals and a low gauge factor. In order to increase the gauge a large meander structure can be employed, but this minimizes the potential of using this type of gauge for small dimensional applications. [6]

The second sensor type is the semiconductor strain gauge, which is based on the piezoresistive effect of silicon or germanium. It tends to have gauge factors of -125 to +200 for single crystal silicon and +/-30 for polysilicon. The design uses resistor elements, which are diffused into a silicon wafer substrate by e.g. doping. This makes the overall structure much smaller and less costly compared to metal foil strain gauge sensors. Also higher resistances, sensitivity, accuracy and repeatability can be achieved. Furthermore a wider pressure range and a stronger output signal can be measured. The disadvantage of these types of strain gauges is that they are more sensitive to temperature variations (restricted to below 120 °C [8]) and drift compared to metallic foil sensors. [4] [7]

The third types of sensor, is based on thin film materials. For the thin film strain gauges, which have a thickness of typically below 10 micrometer, a ceramic electrical insulation is deposited on the stressed surface. On top of the insulator, small resistor elements are deposited by physical vapor deposition (e.g. sputtering). Then wires are attached to the bonding pads and an encapsulation will protect the final device thin film. The strain gauge factors are around 2 but can be tuned depending on the chemical composition of the thin film (e.g. increasing gauge factors by using nitrides or oxides). The advantages are that no adhesive bonding is necessary, because the resistor elements are molecular bonded on the substrate, which makes the bonding also very stable. [9] Furthermore, this results in less resistivity drift, because the sensor becomes part of the whole device. Also the strain gauge can be applied to all kind of base materials. It is very small, has a robust performance, good long-term stability and superior accuracy. [7] [9] Thin film sensors also don't require special machining of the substrates on which they will be mounted. Also thin film strain gauges have a lower impact on the physical characteristics of the system in which they are placed (e.g. turbine blades at a high rotational speed will behave differently if a heavy strain gauge is mounted on the blades). [10] The drawbacks are that specialized equipment is needed for the deposition and the whole process is only economical at large volume. In addition there might be design constraints due to the deposition equipment. [11]

Basically when choosing a strain gauge, the primary considerations are about the operating temperature, the nature of the strain which needs to be measured, and the stability requirements. [7]

### 2.1.1. Strain gauge working principle

Strain is determined by the elasticity of the material, the magnitudes and directions of the applied forces, and the geometry of the material under loading.

If a tension force is applied along the x-axis of a 3-dimensional cube made of a isotropic linearly elastic material, it will elongate by  $\Delta L$  in the x-direction and contract in the y and z-direction by  $\Delta L'$ . (See figure 1)

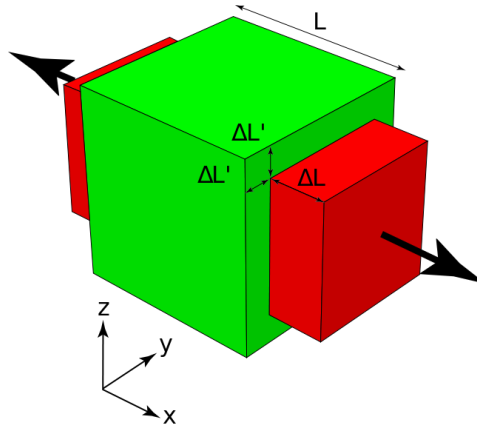


Figure 1 – A cube made of isotropic linearly elastic material with sides of length “L”. Tension along x-axis is applied. Green cube is unstrained. Poisson ratio = 0.5 (constant volume). Red cube is expanded in x-direction by  $\Delta L$  and contracted in y and z direction by  $\Delta L'$ . Source: [http://en.wikipedia.org/wiki/Poisson's\\_ratio](http://en.wikipedia.org/wiki/Poisson's_ratio) (22.05.2014)

The longitudinal x-axial strain is then expressed by (eq.1) and the transverse y-axial strain by (eq.2):

$$\epsilon_{x\_axial} = \frac{\Delta L_x}{L_x} \quad (\text{eq.1})$$

$$\epsilon_{y\_transverse} = \frac{\Delta L_y}{L_y} \quad (\text{eq.2})$$

Where  $\Delta L_x$  and  $\Delta L_y$  is the change in length in the respective axis and  $L_x$  and  $L_y$  is the initial length in the respective axis

The ratio between transverse and longitudinal strain is called the poisson's ratio and is defined as: [5]

$$\nu = - \frac{\epsilon_{transverse}}{\epsilon_{axial}} \quad (\text{eq.3})$$

Figure 2 shows a strain sensitive pattern with electrical terminals, which is mounted on top of a beam without any applied force. In figure 2 (b) a force is applied causing a positive strain (tensile) to the beam. The strain sensitive pattern is stretched and becomes narrower, which increases the resistance at the measurement terminals. Figure 2 (c) shows the opposite scenario where a negative strain (compression) is occurring, causing the area of the strain sensitive pattern to become thicker, which results in a resistance decrease.

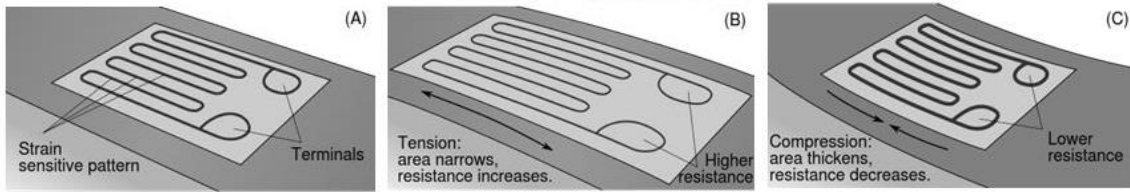


Figure 2 - Strain sensitive pattern [12]

This behavior is defined by the piezoresistive effect, which describes the change of electrical resistivity for a semiconductor or metal when a mechanical strain is applied.

The resistance [ $\Omega$ ] of an unstrained metal gauge resistor with length ( $l$ ) and cross-sectional area ( $A$ ) is expressed by:

$$R = \rho \frac{l}{A} \quad (\text{eq. 4})$$

where  $\rho$  is the bulk resistivity [ $\Omega \cdot \text{m}$ ] of the material.

When a strain is applied to the resistor, the resistance value changes based on dimensional changes of its length and cross-sectional area. For a piezoresistor under uniaxial loading the macroscopic behavior of the change in resistance is linearly related to the applied strain and can be expressed by

$$\frac{\Delta R}{R} = G \cdot \frac{\Delta l}{l} \quad (\text{eq. 5})$$

The proportional constant  $G$  is called “gauge factor” and if isolated an expression for the gauge factor can be established:

$$G = \frac{\frac{\Delta R}{R}}{\frac{\Delta l}{l}} = \frac{\Delta R}{R \cdot \varepsilon} \quad (\text{eq. 6})$$

From eq.6 it can be seen that the gauge factor is a ratio between the relative change of electrical resistance and the applied mechanical strain at constant temperature. [13]

Basically, the gauge factor is a material property, which relates the sensitivity of the gauge to strain and determines a material suitability as a strain gauge material. [10] The higher the Gauge factor, the larger is the change in resistance for a given strain, which in other words increases the sensitivity of the sensor.

Normally, the resistance of a resistor is measured along its longitudinal axis. In case an external force is applied on a component, additional strain components are introduced, so longitudinal and transverse strains are present at the same time, yet one of them is normally clearly dominant. [13]

The Gauge factor can also be expressed in terms of the poisson ratio and resistivity:

$$G = \frac{\frac{\Delta R}{R}}{\varepsilon} = 1 + 2\nu + \frac{\frac{\Delta \rho}{\rho}}{\varepsilon_x} \quad (\text{eq. 7})$$

In the case where the resistivity change upon strain is zero or negligible, the gauge factor is: [14]

$$G = 1 + 2\nu \quad (\text{eq.8})$$

It should be noted that a true piezoresistor will change its resistivity upon induced strain. Metal resistors predominantly change their resistance upon strain because of dimensional changes such as deformation of shape, which is the reason of the lower gauge factor compared to e.g. silicon based sensors (see eq.8). Silicon is a true piezoresistor because its resistivity is changing as a function of strain, which results in a larger gauge factor (see eq.7). [13]

### 2.1.2. Temperature coefficient of resistance (TCR)

The temperature coefficient of resistance (TCR) is used to characterize a resistor and is defined as the change in resistance as a function of temperature:

$$TCR = \frac{(R_2 - R_1)}{R_1 \cdot (T_2 - T_1)} \cdot 10^{-6} \quad (\text{eq. 9})$$

Where

TCR is in ppm/°C (ppm: parts per million)

R<sub>1</sub>: resistance [Ω] at room temperature

R<sub>2</sub>: resistance [Ω] at operating temperature

T<sub>1</sub>: room temperature [°C]

T<sub>2</sub>: operating temperature [°C]

Collisional effects in a material (e.g. wire) normally are increasing with increasing temperature. A larger temperature coefficient means that the electrical resistance will increase more when the operating temperature is increased. [15]

For a strain gauge sensor the TCR has to be considered because when the ambient temperature changes, the output readings of the strain gauge sensor will be not reliable any more due to changes in the sensor materials resistance, resulting in a wrong strain measurement. The TCR value can be compensated by a wheat stone configuration, where the resistors are on the same chip and are made of the same material. [1]

## 2.2. Sputtering techniques

Sputtering is a physical vapor deposition technique, which is used within an array of industries such as semiconductors (integrated circuits), tool bit coatings, windows (double-pane windows), optics (anti-reflective coatings), data storage devices, e.g. hard disc, CD and DVD production, and the technique also has an important role in making efficient solar cells. The sputter techniques are used to deposit material on an atomic level, which establishes strong bonds between the substrate and atoms creating uniform, low cost and extremely thin films. [16] [17]

In this project, titanium nitride thin films on glass and silicon wafer substrates were produced by direct current (DC) sputtering of a titanium target in an inert argon atmosphere with additional flow of nitrogen.

### 2.2.1. Working principle DC, RF and reactive sputtering

Figure 3 shows the basic principle of DC-sputtering. DC sputtering is using a top electrode (cathode), where a negative DC voltage is applied. At the cathode, the conductive source material (target, e.g. titanium) is placed from which the thin film should also be made of.

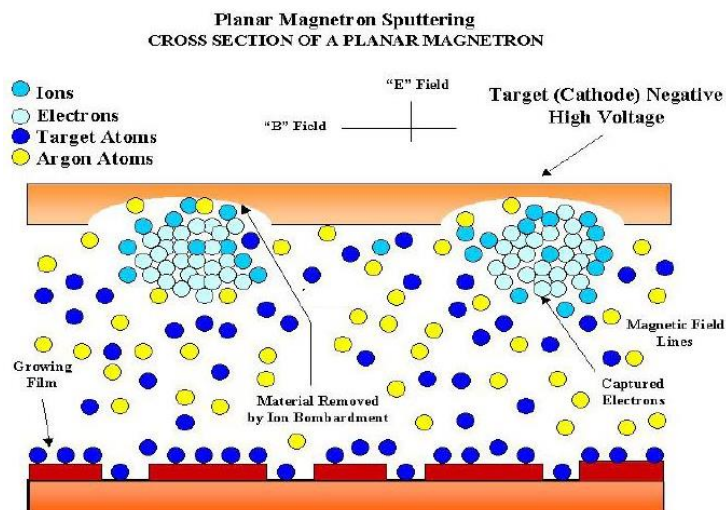


Figure 3 - DC sputtering working principle [18]

The bottom electrode (anode) consists of a grounded metal plate. This is where the wafer is placed, on which the thin film will be deposited. In the beginning, an inert gas (typically argon) is introduced at a low pressure into the chamber. Argon has a low ionization potential and its inertness inhibits it to form compounds at the target surface. [18]

A constant negative DC voltage of a few hundred volts is established between the magnetron across the gas, causing an ionization of the argon gas atoms, which creates plasma. The magnetron is mounted behind the target and provides a magnetic field, which increases the ionization rate of the argon gas. The positive argon ions in the plasma are then accelerated by the electric field to the

cathode where they strike and sputter atoms from the target. These atoms are then traveling through the plasma as vapor and condense on the surface of the wafer forming a thin film. The crucial point with DC sputtering is that the target acts as an electrode in the DC mode. To avoid a charge build the target material must be conductive. If the target would be insulating, positive argon ions coming from the plasma would strike the negatively charged insulating target, causing an accumulation of a positive charge at the target surface, which would decrease the negative surface voltage, necessary to sustain the glow discharge; resulting in a shutdown of the plasma. [16] [19] [20] [17]

For insulating target materials, e.g. oxides or nitrides, radio frequency (RF)-sputtering can be used. The underlying working principle of sputtering is similar for all sputtering technologies. The differences between the different sputter technologies are in the process of how the ion bombardment of the target is realized. Figure 4 left shows the basic principles of RF-sputtering. To solve this problem of a charge buildup for insulating targets, RF-sputtering is using a high-frequency (13.56 MHz) alternating voltage.

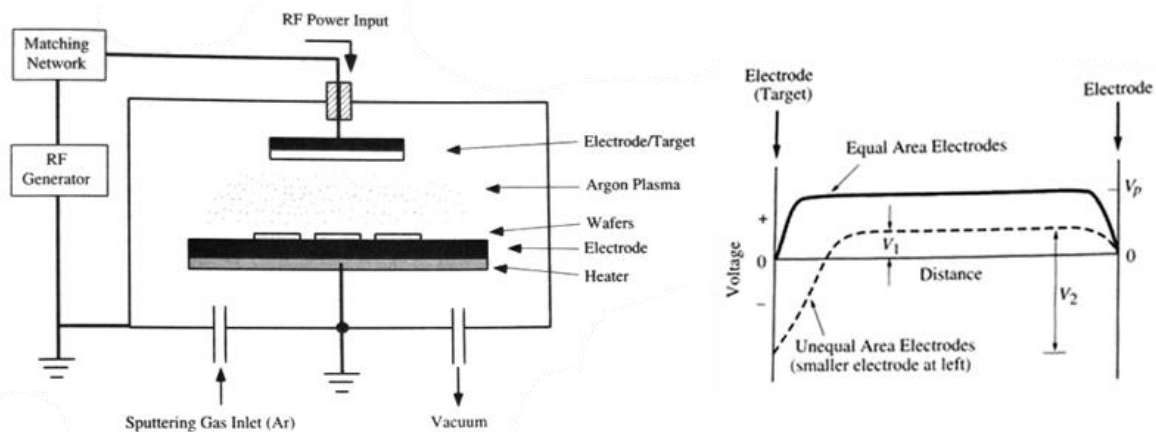


Figure 4 - Silicon VLSI Technology (Fundamentals, Practice and Modelling) by James D. Plummer – p. 549 (left) and Steady state voltage distribution in RF-powered sputtering system. (Wafer is placed on right electrode) ([1] p. 548) (right)

The positive charge build-up at the target is neutralized by electron bombardment over each cycle, resulting in a steady state voltage distribution between target and wafer, which keeps the glow discharge and plasma running (see figure 4 right). [20] For frequencies less than about 50 kHz the electron and ions in the plasma are mobile and both will follow the switching of the anode and cathode, which will result in sputtering of both the target and the wafer and for frequencies above 50 kHz the heavy ions can't follow the switching, but the fast electrons can neutralize any positive charge build-up at the target. [21] The electrodes need to have different areas for RF-sputtering. The electrode with the smaller area has a higher negative potential with respect to the plasma than the other electrode, so it is bombarded with higher energy ions. [22] [23]

### 2.2.1.1. Plasma

Plasma describes an ionized gas containing electrons, ions, and neutral atomic and molecular species. The plasma is initiated by a discharge, when a sufficiently high DC voltage is applied between two metal electrodes, which are positioned in a gaseous environment at low pressure. The discharge in a gas is triggered when an electron, which is close to the cathode, is accelerated towards the anode by the applied electric field. While moving the electron gains energy and may collide with a neutral gas atom, knocking out an electron which ionizes that gas atom. The two free electrons are then accelerated and collide with additional two neutral gas atoms ionizing them, and so on. Simultaneously, the electric field is pushing the positively charged ions towards the cathode, where they collide with the target material, ejecting particles and secondary electrons. The secondary electrons also are accelerated by the electric field towards the anode, which will increase the already started charge multiplication within the argon gas. This effect continues until the current is high enough to cause a gas breakdown. [24] The breakdown voltage necessary to start a discharge or electric arc between two electrodes in gas as a function of pressure and gap length between the electrodes is given by Paschen's law:

$$V_B = \frac{APd}{\ln(Pd)+B} \quad (\text{eq. 10})$$

where A and B are constants, which depend upon the gas composition, and "Pd" is the product of the pressure (P) and the distance (d) between the electrodes. The gas composition determines the minimum break down voltage and at which distance it will occur. [24] Figure 5 shows the Paschen curves plotted for V<sub>B</sub> vs. Pd:

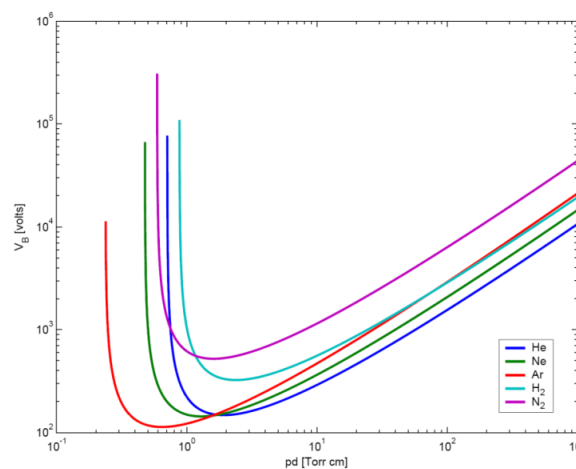


Figure 5 - Paschen curves for a number of gases ([http://en.wikipedia.org/wiki/File:Paschen\\_Curves.PNG](http://en.wikipedia.org/wiki/File:Paschen_Curves.PNG) 04.05.2014)

At a high Pd value, an electron will collide with a lot of gas molecules while traveling from cathode to anode. Due to the more frequent collisions the electrons energy is reduced, which makes it more

difficult to ionize gas molecules. A higher voltage for the electrons is needed in order to gain sufficient energy to ionize enough gas molecules to produce an avalanche breakdown in the gas.

At a small Pd value, the electrons mean free path is longer and electrons will accumulate a lot of energy, but less ionizing collisions occur due to the smaller pressure. In this case a higher voltage is needed to ionize enough gas molecules in order to start an avalanche breakdown. It is important that the distance between the electrodes is large enough, so the electrons can gain enough kinetic energy to continue the ionization.

### 2.2.1.2. Ion-surface interaction

The ion interactions with the cathode or substrate are important parts of the plasma processing and the understanding is important for the production and tuning of thin films. An incoming ion can be subject to one or more of the interactions in figure 6:

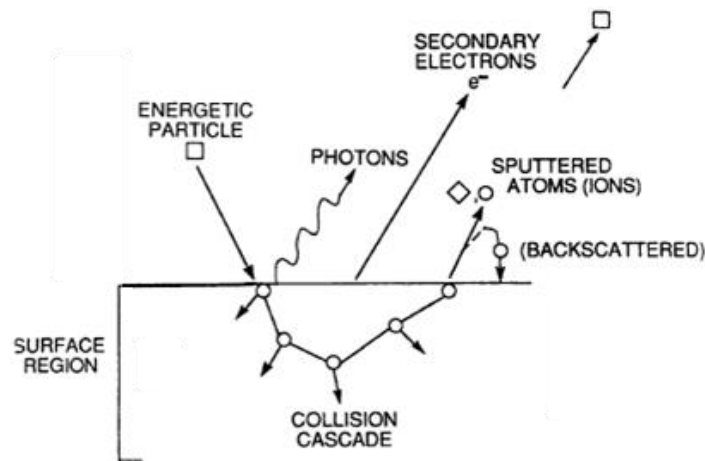


Figure 6 – Energetic-particle bombardment effects on surfaces and growing films [24]

Generally, incoming ions cause sputtering of surface atoms when impacting with the target surface.

The efficiency of the sputtering process can be expressed as the sputter yield which is defined as:

$$S = \frac{\text{number of sputtered atoms}}{\text{Incident particles}} \quad (\text{eq. 11})$$

The sputter yield depends on the density, binding energy and mass of the target material atoms. Furthermore, the sputtering gas is controlling the sputter yield. Gasses with heavier atoms and gas ions with higher incident energy will increase the sputtering yield.

Side effects of the ion bombardment of the target surface can be chemical reactions, altering of the surface morphology, surface heating and the emission of secondary electrons. One important factor

controlling the probability of which surface-ion interaction occurs is the kinetic energy of the ions, which can be influenced by the applied sputter power. [24]

### 2.2.1.3. Reactive sputtering

In this project DC-sputtering is combined with reactive sputtering to achieve the deposition of titanium nitride. Reactive gas, in this case Nitrogen ( $N_2$ ), is introduced into the sputtering chamber in addition to the Argon plasma. Titanium is then sputtered in the presence of nitrogen. During the reactive process,  $N_2$  will dissociate into atomic nitrogen, which reacts with the sputtered titanium atoms. The reaction between the atomic nitrogen and the sputtered titanium will occur on the surface of e.g. the wafer or on the titanium target itself. [20]

### 2.2.1.4. Hysteresis

Figure 7 shows the hysteresis effect observed in reactive sputtering. Two stable states are shown going from metal to compound target (poisoned) mode and reverse. From state A to state B a compound formation on the metal target is occurring.

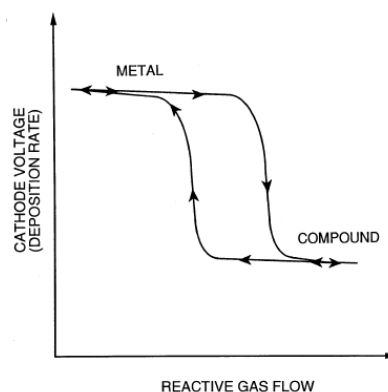


Figure 7 - "Hysteresis curve for both cathode voltage and deposition rate vs. reactive gas flow rate at constant discharge current" [24]

It is known that the sputter rate for metals drops when compounds forms on the target, which can be observed in a decrease in deposition rate because of the lower sputter yields of compounds compared to metals. [25] The sputter yield for a metal is significantly higher than the sputter yield for a compound. The drop in cathode voltage for higher reactive gas flows is caused by the higher secondary electron emission from the compound formed on the target, which lowers the plasma impedance. [24] To correct for the hysteresis a high-pumping speed system can be used for which the hysteresis will be less pronounced and at some point the hysteresis disappears, which is feasible in small lab setups, but not in large sized industrial systems. Also for small target area sizes the hysteresis is less pronounced. [26] Before each deposition, the target can be cleaned by pure argon sputtering, so the pure-metal surface and deposition rates are restored. [24]

### 2.2.1.5. Target integrity

When using planar magnetron sputtering, the target erodes most in the area where the plasma is most intense, which is called the racetrack (see figure 8)

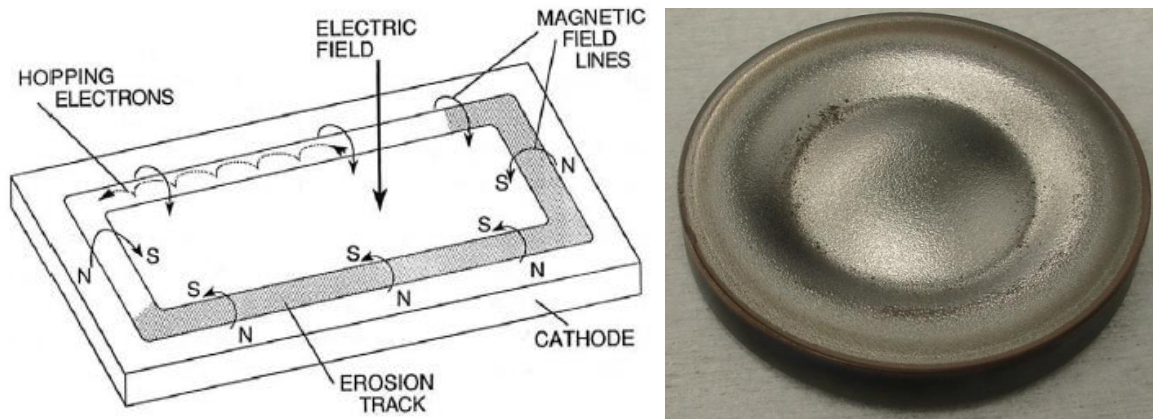


Figure 8 – “Applied fields and electron motion in the planar magnetron “ [24] (left) and Ti target with racetrack (right)

The reason for the racetrack is that the electric and magnetic field lines on the cathode are forcing the electrons to drift around in a cyclical hopping motion, causing the plasma to be most intense in this region.

The racetrack formation results in low process efficiency because only 10-30% of the target's surfaces area is used. The uniformity of the deposited thin film is also influenced by the racetrack formation, and the non-uniform plasma erosion shortens the target lifetime because of mechanical tensile stress, that can cause fractures in the target. Also the target can lose contact to the water-cooled backing plate, which will cause problems due to thermal stresses caused by ion bombardment and heating of the target. Furthermore, while the racetrack is getting deeper, the surrounding target area becomes more insulating due to the formation of compound insulator films such as nitrides or oxides, while the racetrack itself stays metallic. This inhomogeneous metal loss during the reactive sputtering process increases the probability of arcing. [24]

### 2.2.1.6. Arcing

For metal targets that are used in reactive sputtering it is not uncommon to become poisoned (forming a different surface composition compared to the bulk material) e.g. the formation of dielectric oxides or nitrides. When ions sputter away material from a dielectric, a positive surface charge builds up and at a certain point the ion bombardment stops. But given a large charge buildup, a breakdown of the insulating films can be caused on local positions on the target, which causes arcing over the target. This results in the formation of craters, which erode the target. Furthermore, it can cause sputtering of liquid droplets that incorporates defects in the produced thin films. [24]

## 2.2.2. Thin film structure

The thin film structure is controlling properties, such as morphology and crystallinity. In order to produce thin films with e.g. a desired target resistivity drift, the parameters causing the thin film structure need to be studied.

### 2.2.2.1. Processing parameters

The electrical, mechanical, optical, and morphological properties of thin films vary significantly with the deposition conditions. The reactive gas flow and partial pressure, total pressure, deposition temperature, and sputtering power are important parameters.

The chamber pressure is important because it directly influences the kinetic energy of the source atoms that are impinging on the growing thin film. The atoms' kinetic energy can be controlled by changing the background gas pressure. [24] An increase in pressure reduces the total energy at the substrate because energy is lost from increased collisions and interactions of the particles during the travel to the substrate. [26] The substrate temperature and sputtering power are influencing the crystallinity of the thin film. At higher temperatures, the grain size is getting larger. [24]

The reactive gas flow and partial pressure are influencing the stoichiometry of the thin film. In sputtering, also argon ions may hit the surface of the growing film. The ratio between ionized atoms and source atoms that hit the growing thin film, has an important role on the morphology and crystallites of the thin film. [27] Generally in thin film deposition, the higher the deposition temperature is, the better the film properties are, because of improved film density, which also results in a lower resistivity for conducting materials. [20]

### 2.2.2.2. Structure-zone diagrams (SZD)

A structure zone diagram qualitatively illustrates the effect of important deposition parameters for relatively thick (>100 nm) films. [28] [24]

Figure 9 shows a structure zone diagram for which the substrate temperature  $T^*$  is a generalized temperature, which includes the homologous temperature ( $T_H = T_{\text{roomtemp}} / T_{\text{meltingpoint}}$ ), plus a temperature shift caused by the potential energy from arriving particles on the substrate. The potential energy includes the cohesive energy, which is released when two atoms form a crystal (e.g. nitrogen and titanium during reactive sputtering).  $E^*$ -axis is showing the normalized energy flux on a logarithmic scale, which describes heating effects and displacement by the kinetic energy of bombarding particles. This axis is also related to the pressure and power induced to the system because the higher the pressure or power is, the higher the kinetic energy of the incoming particles will be. Furthermore, the z-axis which is called  $t^*$ , shows the net film thickness. [28]

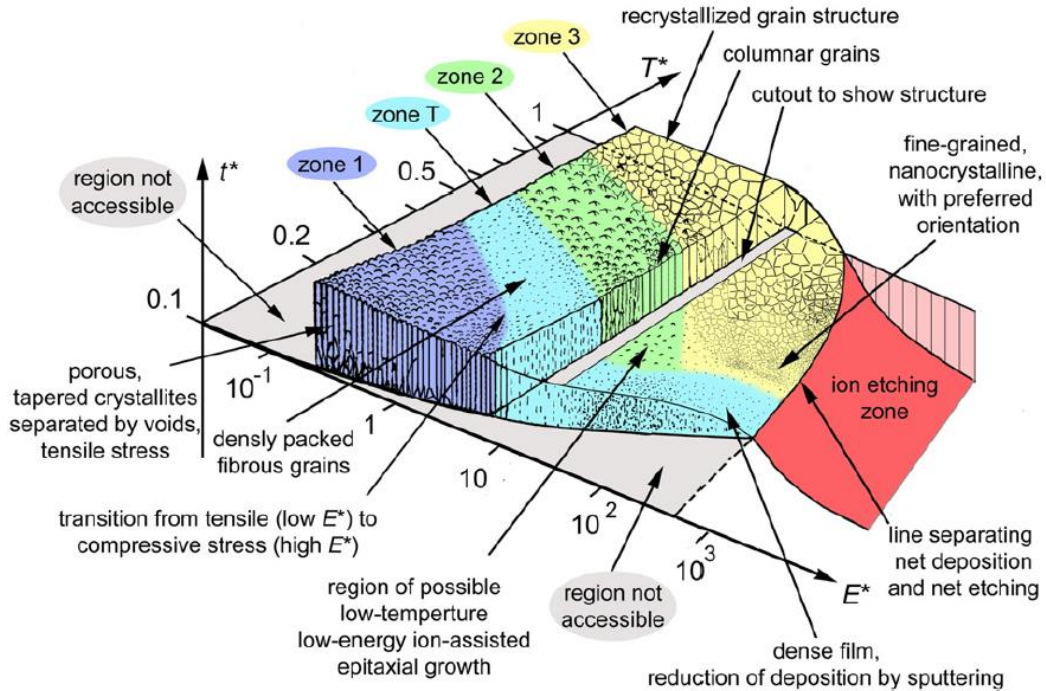


Figure 9 - Structure zone diagram of films deposited by energetic deposition. “The boundaries between zones are gradual and for illustration only. The numbers on the axes are for orientation only — the actual values depend on the material and many other conditions and therefore the reader should avoid reading specific values or predictions.” Andre Anders, *Thin Solid Films* 518 (2010) 4087–4090.

Zone 1 is characterized by continued nucleation of grains due to low adatom mobility. The grain structure is fine of texture and fibrous, pointing in the direction of the arriving vapor flux. At the boundaries, there is a high density of pores and lattice imperfections, which are visible as voids and a tensile stress distribution. Zone T is a transition zone between zone 1 and 2. The surface diffusion is high, but the grain structure is inhomogeneous, which is caused by a strongly limited grain boundary diffusion that leads to inhomogeneous v-shaped grains through the film thickness. Zone 2 is at higher temperatures and the surface diffusion is still high, but the grain size increases with increasing temperature, which leads to more uniform columnar grains throughout the entire thin film thickness. Zone 3 is at even higher temperatures, where diffusion and recrystallization result in dense film with large grains. [28] For this project the deposition is done at room temperature, which means that the actual tuning parameter change will mostly be along the  $E^*$  axis within zone 1 and zone T.

### 2.3. Energy-dispersive X-ray spectroscopy (EDX)

Energy dispersive X-Ray spectroscopy (EDX) is a method for the chemical microanalysis of material and is performed with a scanning electron microscope (SEM), which is equipped with an X-ray spectrometer. Figure 10 shows the main components of an EDX system, which consists of an x-ray detector, a pulse processor that measures the voltage pulses corresponding to x-ray energies, and a PC for data collection.

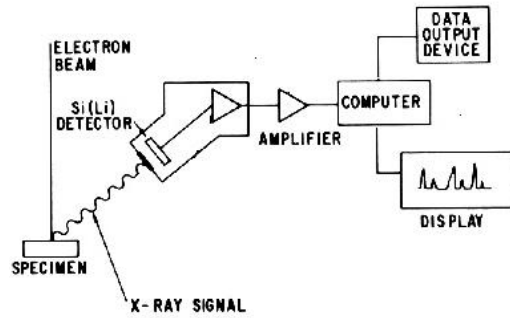


Figure 10 - Energy dispersive spectroscopy setup source: [http://ion.asu.edu/descript\\_ed.shtm](http://ion.asu.edu/descript_ed.shtm) (21.05.2014)

A sample is bombarded with a focused electron beam, which generates x-rays within the sample. The EDX solid state detector picks up the x-rays and generates a small current. Common Si-based detectors are e.g. “lithium-drifted silicon” Si(Li) or SDD, which are cooled down to cryogenic temperatures (e.g. -30 to -180 °C) with liquid nitrogen. The signal is collected by the detector. An amplifier converts the signal into a voltage corresponding to the x-ray energies and amplifies the voltage. The magnitude of the voltage pulse is proportional to the x-ray energy, and the energy of the x-rays is characteristic for each specific element which has emitted them. The voltage signal is then sent to a computer that measures the voltage pulses over a period of time. The data are then analyzed and a spectrum of the number of emitted x-rays vs. their energy is created. The atomic composition of the analyzed sample can then be determined based on the spectrum (see figure 11). Each element has a unique atomic structure which allows a unique set of peaks on each element's x-ray spectrum. [29] [30] [17]

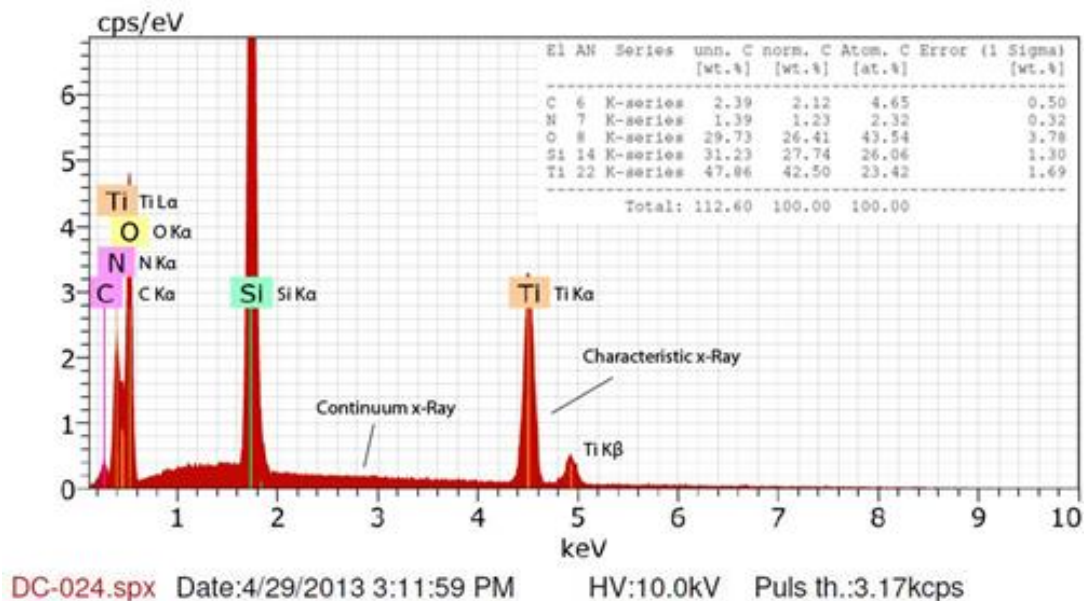


Figure 11 – EDX example spectrum

### 2.3.1. Generation of x-rays

EDS determines the elemental composition of a material by analyzing the characteristic x-ray energies. Characteristic and continuum x-rays are produced during the inelastic interaction of the SEM beam electrons with the sample. Characteristic x-rays are produced, when inner shell electrons from the sample atoms are ejected. These x-rays can be seen as peaks on the EDX spectrum. [30]

Figure 12 (left) shows the physical process of the x-ray generation. An incident high energy beam electron ( $E_0$ ) collides with the sample atom. If the incoming SEM beam electron has enough kinetic energy to overcome the binding energy of the particular inner K shell electron, it will eject the inner shell electron from the atoms K shell, which ionizes the atom.

The binding energy is characteristic for each electron in the atom and the energy required to ionize an atom is called critical ionization energy. In order to successfully excite x-rays with an electron beam, the beam energy should be 1.5 to 3 times higher than the critical ionization energy.

The now vacant position in the atom's K shell is filled by an electron from an outer shell (L3). The excess energy is emitted as a characteristic X-ray quantum, which in this case is the energy difference between the K and L3 shell:  $E_x = E_k - E_{L3}$ . The energy of the emitted x-ray is characteristic for the material's atomic number from which it was emitted. [30]

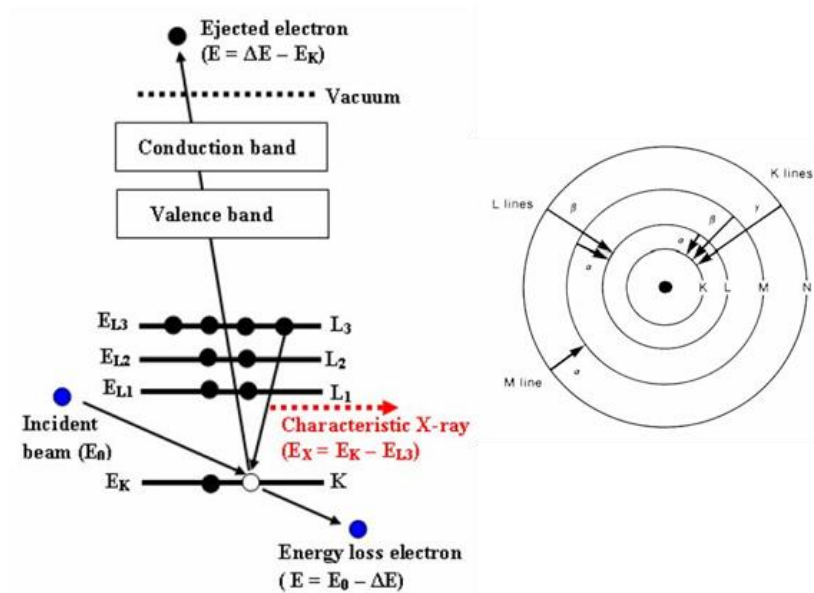


Figure 12 - Creation of characteristic x-rays [27](left) and atom model showing x-ray emission [2] (right)

The names for the characteristic x-rays from figure 11 are based on the shell in which the initial electron vacancy appears and the shell from which an electron travels in order to fill the vacancy.

If, for example, an electron from the K-shell is knocked out by one of the SEM beam electrons and an electron from the L-shell fills the empty spot, then  $K\alpha$  x-rays are emitted. In the case where the electron falls two shells from the M-shell to the K-shell, the emitted x-ray is called  $K\beta$  x-ray. If the initial electron vacancy occurs in the L-shell and an electron from the M-shell falls to the L-shell, then the emitted x-ray is named  $L\alpha$  x-ray (see figure 12 right). [30]

For the case, when the initial vacancy occurs in the K shell, the most probable transition will be an L to K transition, which is the reason why the  $K\alpha$  x-rays (L to K transition) are more intense on the spectrum than  $K\beta$  x-rays. On the other hand the  $K\beta$  x-rays (M to K transition) have a higher energy compared to the  $K\alpha$  x-rays (L to K transition), because the energy difference between the M and K-shell is higher than the difference from the L to K-shells. Also  $M\alpha$  x-rays (N to M transition) will have a smaller energy than  $L\alpha$  x-ray (M to L transition), which again will have smaller energy than the  $K\alpha$  x-rays (L to K transition). This means that the energy that is released from the electron transitions between adjacent shells in the outer shells is less compared to the inner shell transitions. [30]

The energy of the EDX spectra lines from figure 11 is defined by the element and which type of electron transition occurs within an atom. Hereby the intensity of the line depends on the probability of producing an electron vacancy, the probability of an electron transition to fill the vacancy, the probability of an actual x-ray emission, and the concentration of the element within in sample. [31]

The empirical Moseley's law states that, in the case where the K, L or M line energy is known, the atomic number of the element that is producing the line can be determined and thus the element can be identified. From figure 13 it can be seen, that with an increasing atomic number the energy of the x-rays also increases. [17]

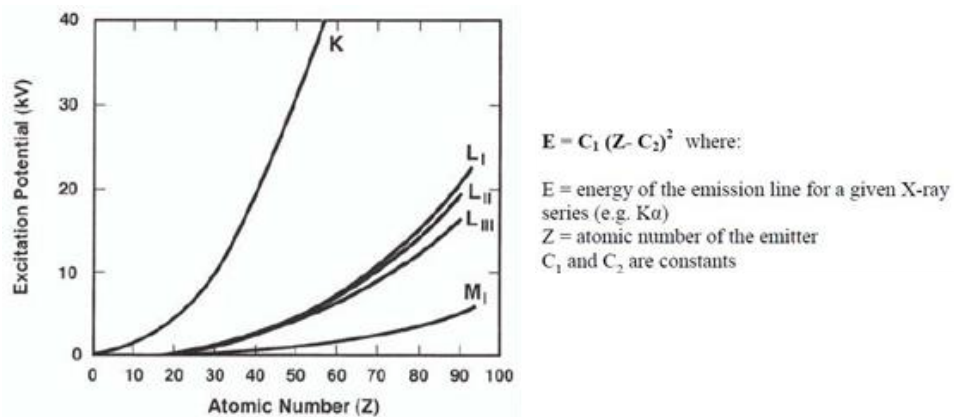


Figure 13 - excitation potential (kV) vs. atomic number (z) [30]

Generally, the higher the atomic number Z is, the higher the peak energy. [31] Low atomic number elements will mostly emit x-rays from the K series, intermediate elements will emit x-ray of L-series,

and heavy elements (high atomic number) will emit x-rays from M series or a mixture of L and M. EDX makes it possible to record a broad spectrum and simultaneously get information about a wide range of elements in the specimen. [17]

The surface sensitivity of EDX is controlled by the penetration range of the x-rays, which is a function of the density of the sample material. Generally, the penetration depths of the x-rays range from 0.5 to 5 micrometer, which makes the EDX method less surface sensitive than e.g. Auger electron spectroscopy (about 5-10nm). [30] [17] (See figure 14)

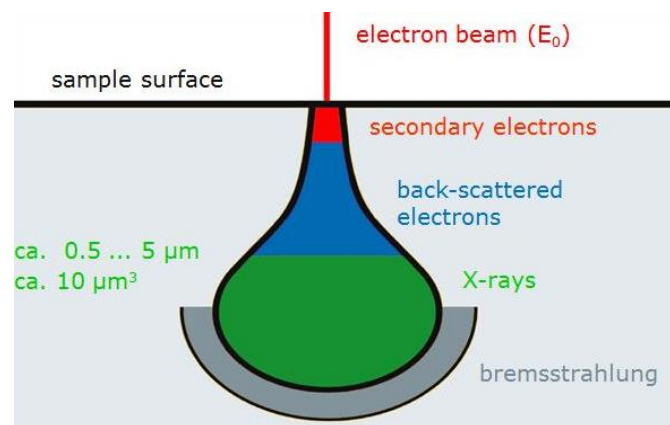


Figure 14 - X-ray range - Principles of Electron Beam Microanalysis – source: Bruker EDX user school (PowerPoint)

The penetration depth can be increased by increasing the primary electron energy, which increases the x-ray signal. Yet this decreases the x-ray spatial resolution, which makes it harder to resolve the different element energies. [31] Further limitations are the peak overlapping of many elements. The accuracy of the spectrum is also influenced by the roughness of the sample. [32]

### 2.3.2. Continuum x-rays (Bremsstrahlung)

The continuum x-rays (Bremsstrahlung) occur when beam electrons are interacting with the electrical field of the sample atoms nucleus. During this interaction, the beam electrons are losing kinetic energy, which will be detected as continuum x-rays. The energies of the emitted x-ray photons are directly linked to how close a beam electron is interacting with the coulomb field of the nucleus. If the interaction is close, then the beam electron will lose more energy and the emitted x-ray photon will be more energetic.

The continuum x-ray and can be seen as a continuous background on the EDX spectrum and they are not characteristic (see figure 15). The intensity of the continuum x-ray increases with atomic number, probe current, and acceleration voltage. [30] [33]

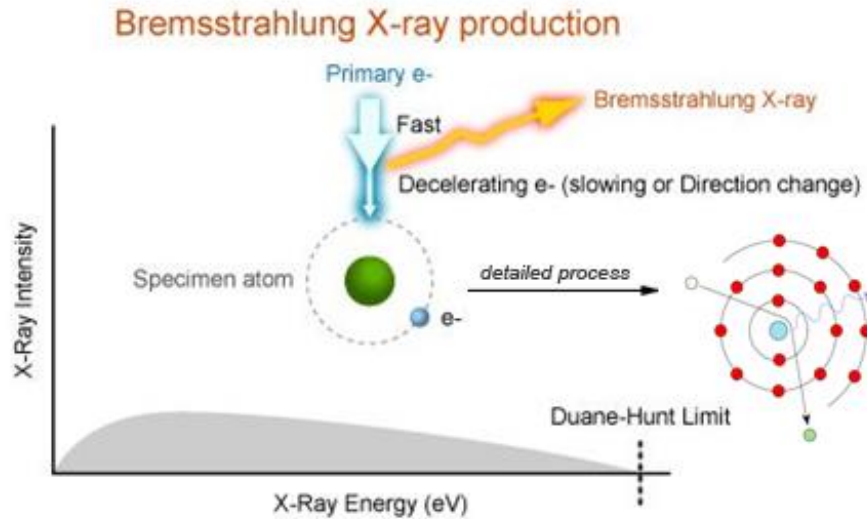


Figure 15 - Bremsstrahlung x-rays (energies between zero and Duane-Hunt limit) [33] [31]

The wavelength and energy of an x-ray can be expressed by the following equation, where  $h$ =plank's constant and  $c$ =speed of light.

$$\lambda \text{ (nm)} = \frac{h \cdot c}{E \text{ (keV)}} = \frac{1.2398}{E \text{ (keV)}} \quad (\text{eq. 12})$$

The continuum x-rays with the highest energy will have the smallest wavelength, which is called the Duane-Hunt limit. At this limit the energy of the continuum x-ray background goes to zero (see figure 15). [30] [33] [17]

## 2.4. Resistivity - Four-point probe

The 4-point probe method is an electrical impedance measurement technique, which is used to measure the electrical sheet resistance of a conductive material. The sheet resistance is defined as the resistance value of one single layer of conductive or semi-conductive material and it is denoted  $\Omega$ -per-square. Based on the sheet resistance, the electrical resistivity [ohm-cm] can be calculated if the thin film thickness is known. Resistivity is an inherent property that quantifies a material's opposition to current flow. [34]

Figure 16 depicts the working principle of a four point probe. A DC current is forced through the two outer probes that are called "force probes". The two inner probes are measuring the voltage and are called "sense probes".

The four point probe can measure low resistances, because the current and voltage electrodes are separated. In the case of a two-point-probe, the current running through the probes is causing a

voltage drop across the sample, probe contacts, and the force wires, which makes the actual resistance measurement inaccurate.

To achieve a more accurate resistance measurement, the four-point-method uses two voltage “sense probes” placed between the current probes (see figure 16 left). By using this setup, almost no current flows through the voltage sensing probes (see figure 16 right). According to ohms law ( $U=R \cdot I$ ), the voltage drop is then very small, which makes it possible to measure the resistance of the sample without the added resistances of the wires and contact probes [35] [17]

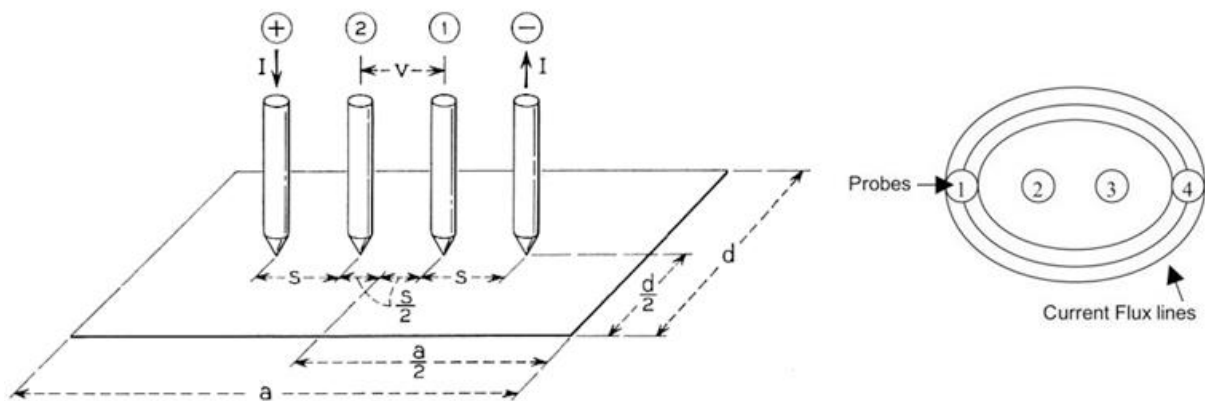


Figure 16 - 4 point probe schematics with probe spacing “s” and sample dimensions; length “a” and width “d” [36] (left) and current flux of 4 point probe (right) [35]

In order to achieve consistently good measurements, there are 5 assumptions which should be fulfilled:

1. The measurement should be conducted at room temperature (23 °C)
2. The spacing between the probe points is constant
3. The distance between the sample edge and the nearest probe tip should at least be 10 times the spacing between the probe points.
4. The four probe tips have a uniform contact pressure with the thin film
5. The conducting film thickness should be less than 40% of the spacing between the probe tips

Based on these assumptions, the 4-point probe measures the sheet-resistance in ohms per square: [17]

$$R_s = \frac{V}{I} \cdot C \quad (\text{eq: 13})$$

$R_s$  = Ohms per square  
 $V$  = voltage measured between probes 2 and 3 (voltage)  
 $I$  = magnitude of source current (amps)  
 $C$  = correction factor

The “Lucas Labs” four point probe station manual suggests using a correction factor of 4.5324 if the above mentioned requirements are fulfilled. [37] Yet, it should be noted that the correction factor of 4.5324 is mathematically derived based on the assumption that the samples size is infinite and that the current flux lines seen in figure 16 right are not influenced by geometrical constraints for which the following relation holds:

$$R_s = \frac{V}{I} \cdot \frac{\pi}{\ln 2} = \frac{V}{I} \cdot 4.5324 \quad (\text{eq: 14})$$

In the case of a finite sample, the correction factor is adjusted based on the probe spacing ( $s$ ), sample length ( $a$ ) and sample width ( $d$ ) (see figure 16 left).

Equation 15 expresses the total voltage between the inner voltage sensing probes. The expression for “ $1/C$ ”, where “ $C$ ” is the correction factor, was used to calculate the adjusted correction factors throughout this project. A calculation example can be found in appendix “A1. Correction factor calculation example” page 97 and a detailed derivation of the mathematics in the referenced article [36].

$$V = I\rho_s \frac{1}{\pi} \left[ \frac{\pi}{d} + \ln \left( 1 - e^{-\frac{4\pi}{d}} \right) - \ln \left( 1 - e^{-\frac{2\pi}{d}} \right) + \sum_{m=1}^{\infty} a_m \right] \quad (\text{eq: 15})$$

↓  
Expression for 1/C

$V$  = voltage measured between probes 2 and 3 (voltage)

$I$  = magnitude of source current (amps)

$\rho$  = the sheet resistivity

$d$ : normalization of distance “ $d$ ” divided by probe spacing “ $s$ ”

$a_m$ : summation term (see “A1. Correction factor calculation example” page 97)

$C$  = correction factor

Furthermore, based on the sheet-resistance, it is possible to calculate the resistivity (ohm-cm) of the thin film: [34]

$$\rho = R_s \cdot t \quad (\text{eq: 16})$$

$\rho$  = the volume resistivity ( $\Omega$  cm)

$R_s$  = sheet resistance ( $\Omega$  per square)

$t$  = sample thickness (cm)

Also one could calculate the thin film thickness if the resistivity is known. [38] [37]

The validity of the sheet resistance and the calculated resistivity depends on the correction factor, which is influenced by the sample dimensions and the probe spacing. A wrong correction factor, e.g.

caused by a change in probe heads with different probe spacing, will influence the material characterization results and can lead to false interpretations. For this it is important to use the right correction factor if e.g. samples with different geometries are compared with each other.

An example of obtaining the resistivity for a titanium nitride sample can be found in appendix “A2. Resistivity calculation” page 100.

## 2.5. Thin film stress

During the deposition process residual stresses may develop, which can cause a strain in the deposited thin film, observed as tensile or compressive stress.

A negative stress value means compressive stress and a positive stress value means tensile stress. In the case where the thin film is facing upwards, internal tensile stresses will bend the substrate concave upward and compressive stresses convex outward (see figure 17). Tensile stresses can cause a film fracture whereas compressive stresses can cause wrinkling and adhesion loss of the thin film. [24]

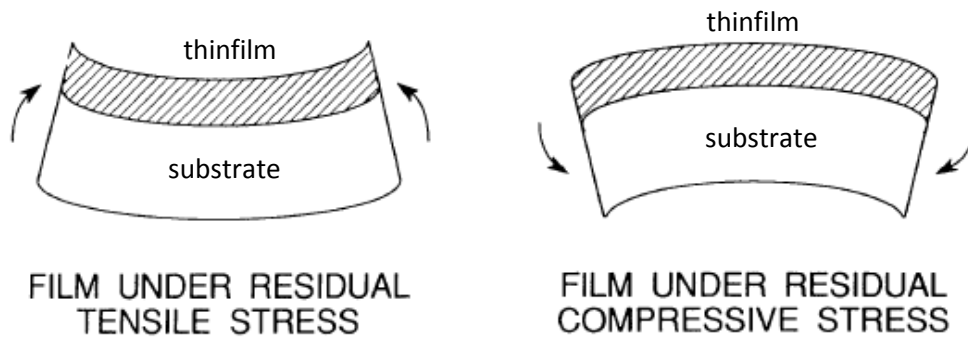


Figure 17 - Tensile film stress (left), compressive film stress (right) [24]

The internal thin film stress can be measured by the curvature method using the “Stoney” equation. This formula relates the curvature of the substrate to the stress in the thin film [39]:

$$\sigma_f = \frac{E_s}{6(1-\nu_s)} \cdot \frac{t_s^2}{t_f} \cdot \left( \frac{1}{R_{post}} - \frac{1}{R_{pre}} \right) \quad (\text{eq: 17})$$

$\sigma_f$  = plane stress component in the film

$t_f$  = thickness of the thin film

$E_s$  = Young's modulus of the substrate

$\nu_s$  = Poisson ratio for the substrate

$h$  = thickness of the substrate

$R_{pre}$  and  $R_{post}$  = radius of curvature of substrate before and after deposition

The substrate thickness should be much larger compared to the thin film thickness. In the case of this project, the substrate thickness is 200 micro meters and the thin film thickness is around 400 nm. As long as the deflections are small compared to the substrate thickness, these simple theories will provide accurate results. [24]

There are variations of the “Stoney” formula depending on the substrates’ material characteristics. For an elastically anisotropic substrate, such as single crystal silicon wafers, the “Stoney” equation for Si(100) wafers is [39]:

$$\sigma_f = \frac{h^2}{6(s_{11}^{Si} + s_{12}^{Si}) \cdot t_f} \cdot \left( \frac{1}{R_{post}} - \frac{1}{R_{pre}} \right) \quad (\text{eq: 18})$$

Where  $s_{11}^{Si}$  and  $s_{12}^{Si}$  are elements of the compliance tensors (young’s modulus as a function of direction) of silicon.

The factor  $\frac{1}{s_{11}^{Si} + s_{12}^{Si}}$  is called biaxial modulus (M) of Si(100) for which the numerical value is:

$$M_{(001)}^{Si} = \frac{1}{s_{11}^{Si} + s_{12}^{Si}} = 180 \text{ GPa} \quad (\text{eq: 19}) [39] [40]$$

which yields to:

$$\sigma_{Si(100)} = \frac{180 \text{ GPa} \cdot h^2}{6 \cdot t_f} \cdot \left( \frac{1}{R_{post}} - \frac{1}{R_{pre}} \right) \quad (\text{eq: 20}) [39]$$

The stress determination accuracy depends on the validity of the elastic theory, which includes the film & substrate, their geometries, deflections, and composite properties. [24] A calculation example of the stress can be found in the appendix “A15. Stress wafer measurements and calculations” page 134

## 2.6. X-Ray Diffraction (XRD)

X-ray diffraction is a nondestructive technique used to characterize crystalline materials and determine the atomic structure of crystals. [41] The x-rays wavelength is about 0.1-10 Ångström. This makes it possible to extract information about interatomic distances, bond angles, phase identification, texture & preferential orientation, and the crystallite sizes. [42] [43]

Crystals have a periodic structure which consists of unit cells placed into a lattice. A unit cell may contain one or several atoms in a fixed arrangement (see figure 18). [41]

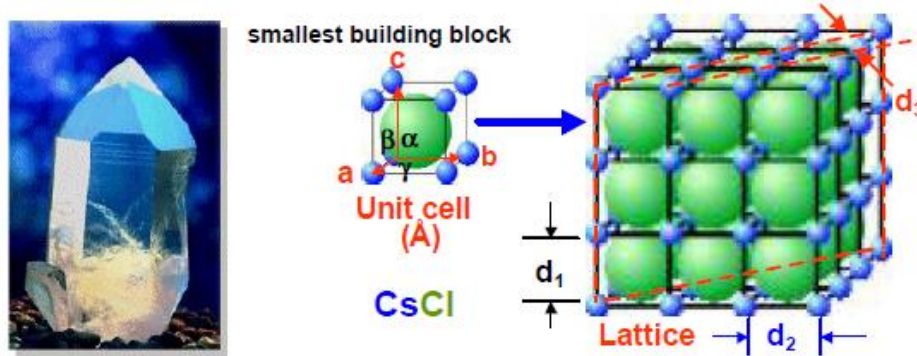


Figure 18 - Crystal lattice with unit cell [41]

A crystal consists of planes of atoms that are placed at a distance “d” from each other. The length is describes by “a,b,c” and the angle between lengths “a,b,c” are described by “alpha, beta, gamma”. These lattice parameters can be determined by XRD. [41]

XRD uses electromagnetic radiation (x-rays) which is directed on a sample and is elastically scattered (diffracted) by electrons from the regular array of crystal atoms in the sample. This creates a regular array of spherical waves, that will interfere constructively and destructively with each other, resulting in maxima and minima. The interference maxima’s are in a few specific directions, which can be determined by “Bragg’s” law: [43]

$$n\lambda = 2d\sin\theta \quad (\text{eq. 21})$$

$n = \text{integer}$

$\lambda = x - \text{ray wavelength}$

$d = \text{distance between crystal lattice planes}$

$\theta = \text{diffraction angle}$

Figure 19 shows the diffraction of x-rays within a crystalline material, showing the x-ray source and detector. “Bragg’s” law is predicting a maximum for each lattice spacing “d” at a characteristic angle “ $\theta$ ” and is fulfilled when the path length difference of the x-rays is equal to  $n\lambda$  (green lines). [43]

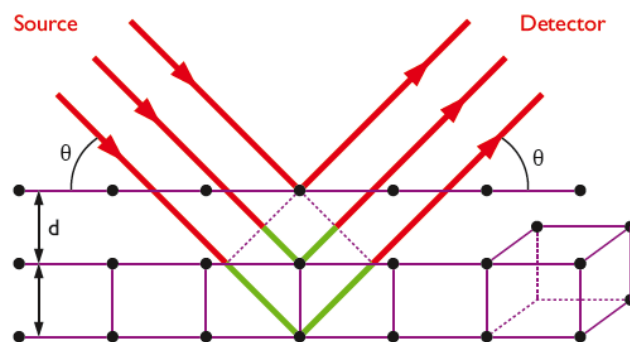


Figure 19- “Diffraction of X-rays in a crystalline material” [43]

The incidence and refracted angles are measured during the XRD experiment. By plotting the detected x-ray intensities as a function of angle “ $\theta$ ” a characteristic x-ray diffraction pattern is generated. [43] Figure 20 shows the XRD pattern for titanium nitride samples produced by reactive sputtering at different target modes. The peak intensities at various diffracted angles are used to find the crystallographic orientations of the tested sample. The intensity is the total area under a peak. [42]

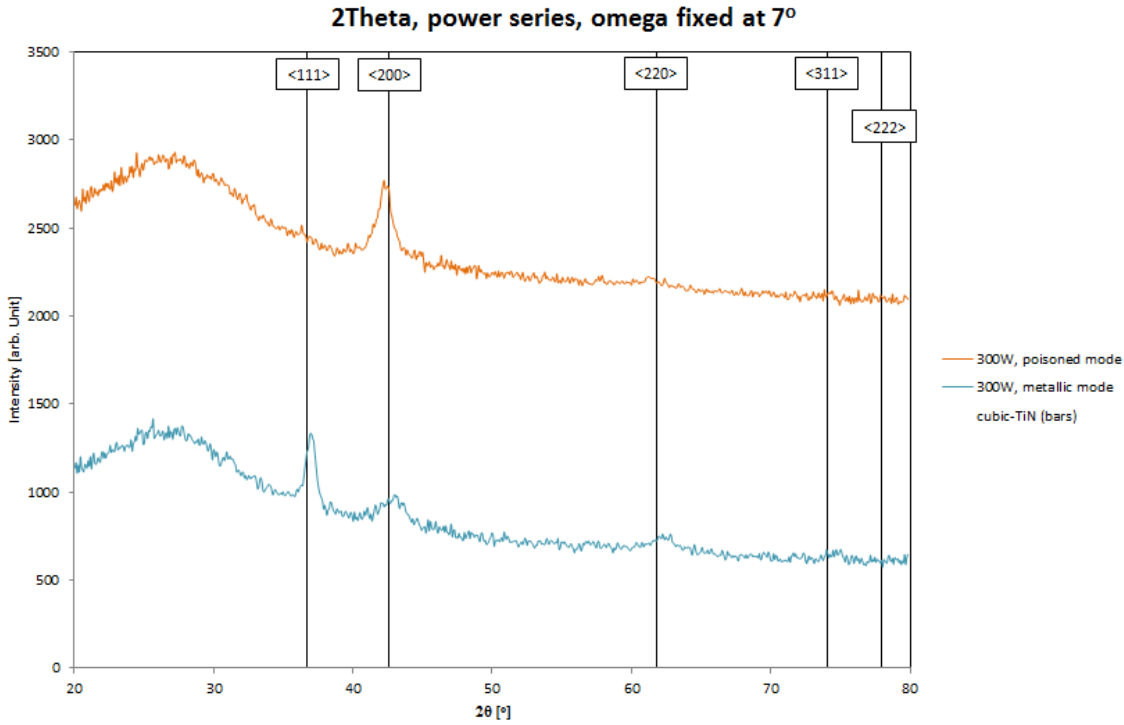


Figure 20- XRD pattern of TiN and reference patterns. Grazing incident X-ray diffraction patterns ( $\omega=7^\circ$ ) The reflection angles from cubic TiN are shown as bars. The large “bumps” in the spectra stem from the amorphous BK-7 glass substrates.

### **3. Fabrication and characterization equipment**

This chapter briefly mentions the fabrication and characterization techniques used in this project. Furthermore, it refers to relevant step-by-step manuals and calibrations experiments.

#### **3.1. Cryofox - thin film deposition system**

The thin films in this project were produced with the “Polytechnik Cryofox Explorer 600” using DC magnetron sputtering combined with reactive sputtering. An example deposition step by step procedure can be found in appendix “A3. Cryofox DC procedure” page 101.

A major challenge throughout this project was a deposition failure rate of over 50% due to several reactive sputtering related problems. Metal flakes from the surrounding chamber plates and the target shutter were causing the plasma to permanently shut down during the deposition process. A procedure has been developed to address these problems and increase the production yield (see appendix “A4. Cryofox error analysis and optimization” page 103). Furthermore an experiment regarding the thin film thickness and its position on the deposition holder was conducted, which can be seen in appendix: “A5. Cryofox sample placement” page 108. It was found that the thin film thickness drops by about 20% from the middle to the edge position of a 100mm Si(100) wafer. The conclusion was to always place the samples for the various characterization methods centered and in the same position to increase the reproducibility.

#### **3.2. Deposition log book**

A deposition logbook for all produced samples can be found in appendix “A6. Deposition log book” page “109”

#### **3.3. Wafer substrate information**

Information about the wafer substrates used in this project can be found in appendix: “A7. Wafer substrate information” page 117. The wafers were diced with a dicing saw (disco DAD-2H5) to achieve the desired sample geometries.

#### **3.4. Four point probe – electrical resistivity**

The electrical characteristics of the produced thin films have been measured by a four point probe system from “Lucas labs” using a four point probe head with a probe spacing of 1 mm. The station was combined with a “Keithley 2450” source meter for measuring the sheet resistance of the produced samples. The substrate used for the measurements was a 25x25 BK7 double-sided polished, 500 micrometer thick, silicon glass wafer. It is good practice to make at least 4 measurements and it is important to take out the sample between each measurement to obtain the correct statistics for comparing different samples. The four point probe measurement procedure can be found in appendix “A8. Four point probe procedure” page 118.

Furthermore, a position repeatability experiment was conducted in order to determine the relative error associated with the placement position of the four point probe on the sample. It was found, that the relative error for the placing of the probe in the middle of the sample over a course of 10 tries is around 1,4% for the 25x25mm sample with regard to the resistance measurement. The resistance standard deviation was 0,442  $\Omega$  and the resistivity standard deviation was 4,87068E-05  $\Omega$ . This relative difference should be considered when evaluating the resistivity drift over time. The experimental details can be seen in appendix “A9. Four point probe measurement repeatability experiment” page 121.

### 3.5. AFM – thin film thickness

The thicknesses of the thin films, that have been produced on 10x10mm Si(100) wafer substrates, were measured with an Atomic force microscope (AFM) (Veeco Dimension 3100) using “tapping mode”. In order to measure the thin film thickness accurately, a photolithographic and lift-off procedure was used to create a small pattern on the substrate, which makes it possible to measure the thin film thickness with a tolerance of about +/- 1-2nm (see figure 21).

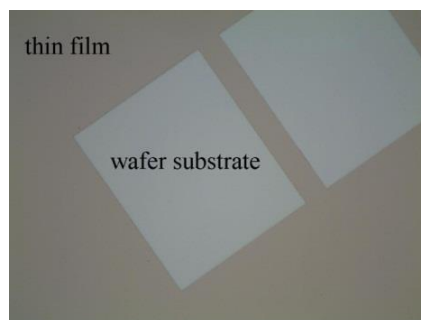


Figure 21 - Picture taken with Digital inspection microscope (Nikon LV100D) 5x-0.15A1 - Ti\_N=0%

The production recipe can be found in appendix “A10. AFM lift-off structure” page 123.

### 3.6. EDX – atomic composition

The atomic concentration of the thin films have been measured on 10x10mm Si(100) wafer samples and were carried out with an SEM and a Quantax EDX System from Bruker. The procedure can be found in appendix at “A11. EDX procedure” page 124 and “A12. EDX measurement standard” page 128. Calculations and explanations related to the EDX error and relative atomic concentration, which were used for plotting the EDX data, can be found in appendix “A13. EDX relative concentration and error calculations” page 129.

### **3.7. SEM – top and cross-section images**

For the top-view and cut section images, a scanning electron microscope (SEM) (Hitachi S-4800 system) with a cold field-emission electron source was used. A measurement description can be found in appendix “A14. SEM top-view and Cross-section images” page 133.

### **3.8. Dektak - stress measurements**

The wafer radius for the stress measurements were performed with a contact profilometer (Veeco Dektak 150) using a diamond stylus which is laterally moved in contact mode across the sample. The substrates were 25x3 mm P7 silicon wafers with a thickness of 200 micro meters. A description about the procedure can be found in appendix “A15. Stress wafer measurements and calculations” page 134.

A detailed description and pictures about the mentioned equipment can be found at <http://www.nanosyd.dk/cleanroom/en/page/equipment>.

### **3.9. XRD – crystal structure**

The XRD measurements have been performed with an „X’Pert PRO MPD” X-ray Diffraction System from “PANanalytical” in Odense by Kasper Thilasing Hansen and Nis Dam Madsen. More information can be found in appendix “A16. XRD quick start guide” page 137.

### **3.10. Oven - accelerated life test**

In order to accelerate the resistivity drift over time, the thin film samples were placed in an oven made by “Electrolux”. For a more detailed setup description see appendix “C2. Accelerated lifetime testing experiment” page 153

### **3.11. Tube furnace post-annealing**

The quartz tube furnace from “Barnstead-Thermolyne” was used for high temperature annealing of up to 900 °C. An operation procedure can be found in appendix “A17. Tube furnace annealing procedure” page 139.

#### 4. Experimental introduction TiN<sub>x</sub> and TiO<sub>x</sub>N<sub>y</sub> project recap

As mentioned in the preface, the reactive sputtering of titanium nitride was initially started as a small project in the end of 2012 during my 7<sup>th</sup> semester of my master's at the "Mads Clausen Institute". The goal was to investigate if it was possible to create titanium nitride thin films by conventional RF sputtering with an additional flow of nitrogen. It was the intention to investigate if the "Cryofox Explorer 600 LT" system from the NanoSYD clean room facility is actually able to deposit titanium nitride thin films. During that project, titanium nitride thin films were produced at the NanoSYD clean room and optical constants such as refractive index (n), extinction coefficient (k), and transmission spectra were extracted and evaluated. It was found by comparison with other group's results that the properties of the produced thin films have similar qualitative tendencies for n, k, and the transmission spectra for 400-800 nm spectral range, which indicated that it was possible to produce titanium nitride thin films. [23]

In the beginning of 2013 during my 8<sup>th</sup> semester on the master's at the Mads Clausen Institute, the project was continued. Due to an interest from Danfoss A/S regarding new pressure sensor materials the purpose of that study was, to investigate the possibilities of creating titanium oxynitride (TiO<sub>x</sub>N<sub>y</sub>) thin films, using DC reactive magnetron sputtering with a constant nitrogen flow and a periodically pulsed O<sub>2</sub> flow rate.

A chemical analysis of the thin film atomic composition was carried out by using the at that point new energy dispersive X-Ray spectroscope (EDX) and an electrical characterization of the thin films by a four point probe system was conducted.

During the first 10 weeks of that project, flow meters were installed in the Cryofox, enabling the adjustment of the gas flows in "standard cubic centimeters per minute" (sccm). Titanium nitride thin films were produced at varying nitrogen flow rates and analyzed by EDX in order to determine the flow rate that would result in a saturation of nitrogen content. The saturation parameters for titanium nitride (TiN<sub>x</sub>) were then used as the basis for the titanium oxynitride (TiO<sub>x</sub>N<sub>y</sub>) research.

From the results in figure 22 the "atomic composition [%] vs. oxygen duty cycle [%] (% of T)" where the duty cycle is defined as the pulse time " $T_{\text{on\_oxygen}}$ " divided by the total pulse period " $T$ " is shown. The total pulsing period was  $T=18\text{s}$ . From the results it can be seen that with an increasing oxygen duty cycle the atomic thin film composition of oxygen is increased, which indicates that the pulsed oxygen flow method is working. For titanium nitride at a duty cycle of 0% an atomic composition of oxygen of about 23,4% +/- 4,11% was measured, despite of no oxygen flow during the deposition.

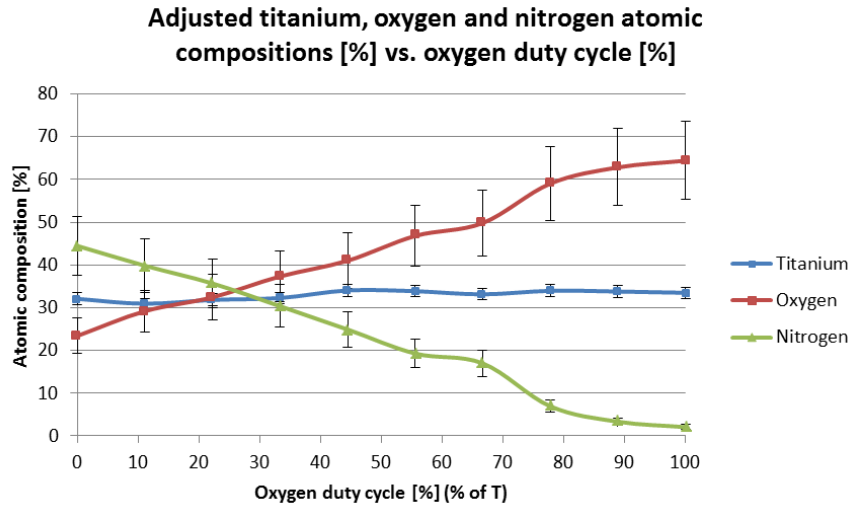


Figure 22- Adjusted titanium, oxygen and nitrogen atomic compositions [%] vs. oxygen duty cycle [%]

Based on qualitative and quantitative comparisons of the obtained results, it was concluded that it is possible to adjust the film composition by reactive magnetron sputtering with pulsed oxygen flow at the NanoSYD facilities. Similar results were obtained by two other research groups. [17]

Figure 23 shows the normalized sheet resistance for the produced samples over a time frame of 10 day (note that the graphs are shifted up by 1 with respect to each other for a quick qualitative overview of the resistance stability over time).

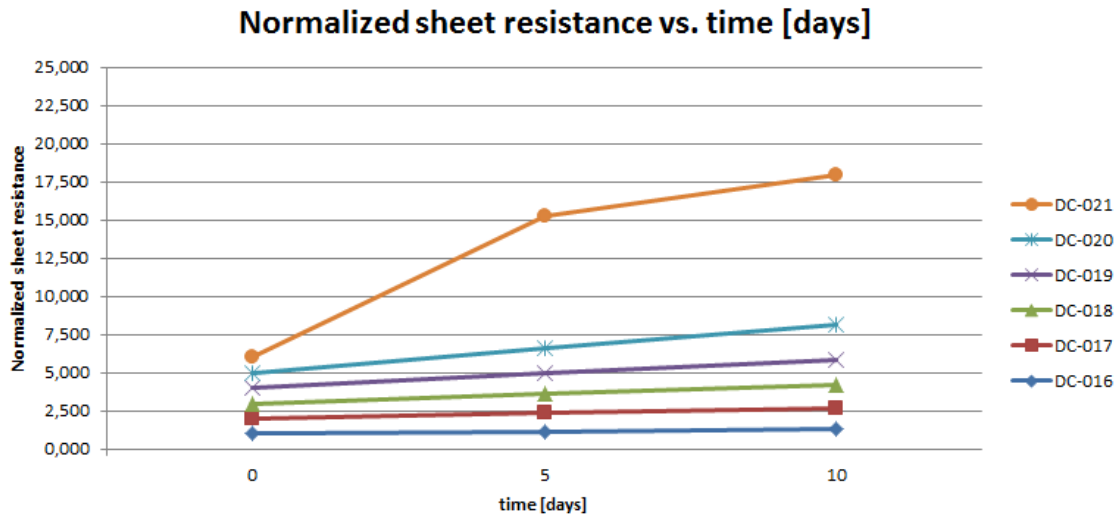


Figure 23 – Normalized sheet resistance vs. time [days]

It can be seen that the sheet resistance at room temperature is changing over time. It was also found that the oxygen content over time is increasing, which is consistent with an oxidation of the thin films, explaining the change in resistance over time. It was observed that with increasing oxygen duty cycle during the deposition, the thin films became increasingly unstable with regards to their resistance drift. Sample DC-016 shows the lowest sheet resistance with about 29% over 2 weeks.

An investigation by a cross-sectional scanning He-ion microscopy (SHIM) image of thin film DC-016 revealed a columnar porous thin film structure (see figure 24).

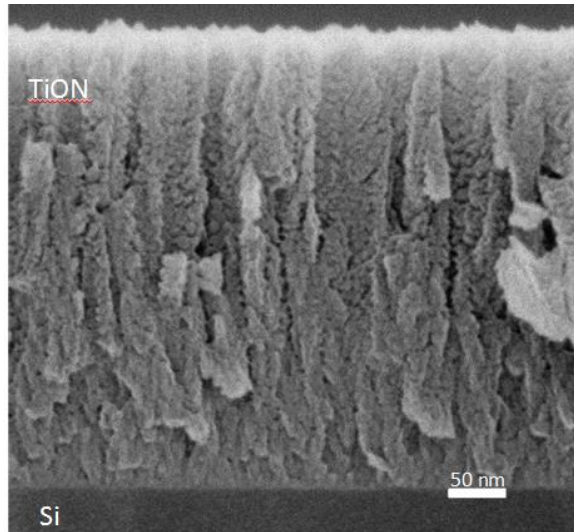


Figure 24 – Cross-sectional scanning He-ion microscopy (SHIM) image of DC-016

The porosity is believed to lower the stability of the films by increasing the chance of through film oxidation. This is believed to be the origin of the large resistance drift observed in figure 23. [24]

## 5. Post-annealing investigations

A high temperature experiment at 500 °C and 900 °C using a tube furnace was set up and performed during an initial resistivity stability investigation in corporation with Nis Dam Madsen. The overall idea was proposed by visiting professor Paulo Fichtner (UFRGS, Porto Alegre). The purpose was to study the effect of introducing a periodic pulse of O<sub>2</sub> gas into the deposition of titanium nitride thin films with the goal of interrupting the columnar structure in the TiN thin films. Four thin films were produced by using RF sputtering with the Cryofox 600 Explorer deposition system (see figure 25).

| Deposition Parameters:            | Film A (RF-029) | Film B (RF-028) |
|-----------------------------------|-----------------|-----------------|
| Target                            | 2-inch Ti       | 2-inch Ti       |
| RF Power                          | 360 W           | 360 W           |
| N <sub>2</sub> flow               | 5 sccm          | 5 sccm          |
| O <sub>2</sub> flow (pulse)       | 0               | 2 sccm          |
| Ar flow                           | 20 sccm         | 20 sccm         |
| Base Pressure                     | 5,00E-5 mbar    | 5,00E-5 mbar    |
| Substrate temperature             | 20 °C           | 20 °C           |
| Thickness                         | 400 nm          | 400 nm          |
| Tooling factor                    | 31              | 31              |
| Expected rate                     | 0,8 Å/s         | 0,8 Å/s         |
| T <sub>on</sub> /T <sub>off</sub> | 0 / 99.9s       | 5 s / 250 s     |
| Layer thickness                   | 400 nm          | 20 nm           |
| No. of layers                     | 1               | 20              |

Figure 25 - Deposition parameters for the layered annealing series.

The pulsing period was chosen so that the titanium nitride layer thickness would be 20 nm per layer. It was assumed that 5 seconds of oxygen flow at 2 sccm should be enough to produce a few monolayers of oxide on top of the titanium nitride layers to interrupt the columnar growth.

The annealing parameters are listed in figure 26:

| <b>Annealing Parameters:</b>  | <b>Annealing 1</b>                             | <b>Annealing 2</b>                            |
|-------------------------------|--|---|
| T <sub>max</sub>              | 500 °C   | 900 °C  |
| Outgassing                    | Min. 15 minutes @ 1 scfh, Ar 4.0 (99.99%) flow | Min. 15 minutes @ 1 scfh Ar 4.0 (99.99%) flow |
| Hold time at T <sub>max</sub> | 1 h  | 1 h   |
| Heating time                  | 6-7 min  | 12-13 min                                     |
| Cooling time                  | 1,5h (samples are exposed to air at 100 °C)    | 2h (samples are exposed to air at 100 °C)     |
| Ar flow rate                  | 0.5 L/min                                      | 0.5 L/min                                     |
| Pressure                      | Flow through vacuum oil cooled to 0 °C         | Flow through vacuum oil cooled to 0 °C        |

Figure 26 - Annealing parameters for Film A and Film B.

Argon gas was bubbled through vacuum oil cooled with ice to ensure an oil partial pressure below 10E-08 mbar. The oil should prevent back diffusion of oxygen into the furnace. However, the atmosphere is not expected to be oxygen free, since the argon gas purity as well as the tubing to the furnace isn't perfect.

The samples were placed in the furnace at room temperature. The tube was outgassed with Ar for 15 minutes before the heating was started to insure a clean atmosphere during the annealing. The outgassing time was calculated from the tube volume and the flow rate.

After the annealing was done, the samples were taken out below 100 °C to reduce oxygen reaction post-annealing. The sheet resistance was measured right before and right after the annealing procedure.

There was an issue with oxygen leakage due a crack in the tube for the annealing at 900 °C for thin film "A (RF-029)" (not layered). The error analysis and picture, together with the entire study results, are shown in appendix "Post-annealing experiments" page 140 with detailed explanations, setup images, and graphs.

From EDX measurements it was observed that with increasing temperature the nitrogen content is decreasing and the oxygen content is increasing for both thin films. At 900 °C, no nitrogen content was measured, which indicates that the measured thin film composition is that of titanium dioxide (TiO<sub>2</sub>) for both non-layered and layered thin film. The non-layered thin film shows an oxygen to titanium ratio of 1,81 and the layered thin film 1,92 (see figure 27).

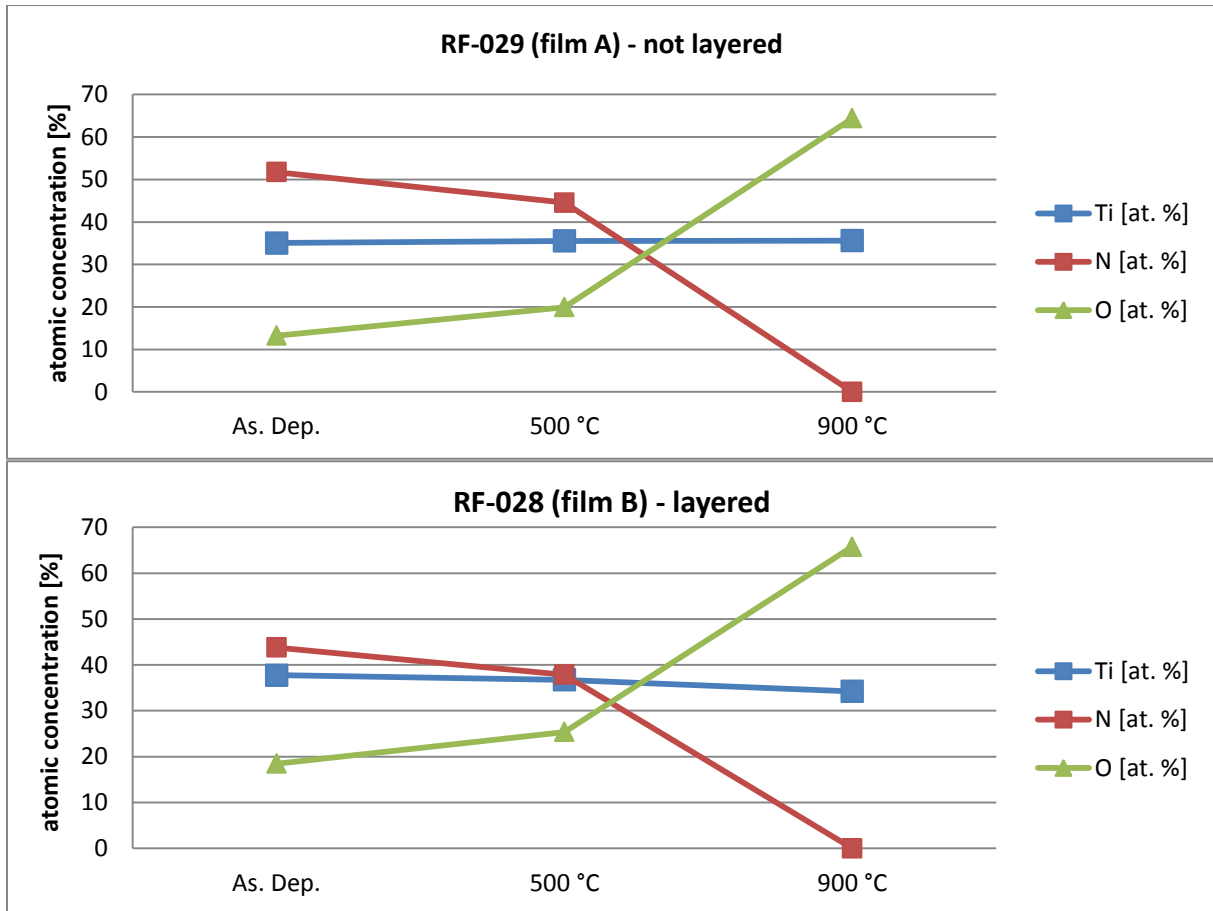


Figure 27 – EDX measurements for RF-029 (film-A non-layered) (top image) and RF-028 (film-B layered) (bottom image)

Additional SEM and XRD measurements showed that the highest annealing temperature of 900 °C resulted in the formation of large TiO<sub>2</sub> crystallites, which are insulating and therefore not suitable for a strain gauge material (figure 28). The annealing at 900 °C should be avoided.

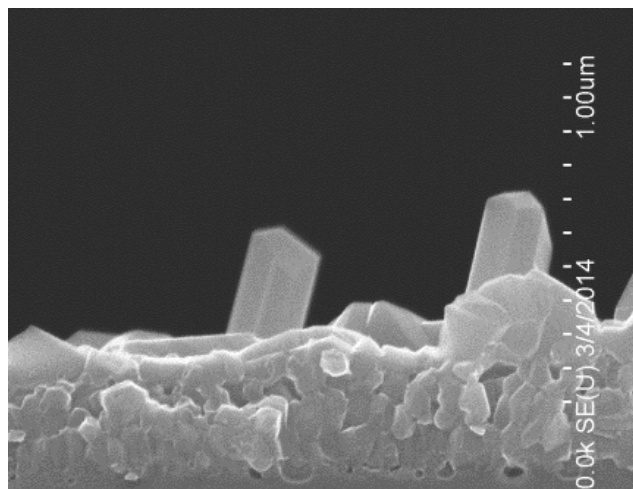


Figure 28 - SEM image, RF-028 (film B) – layered, showing TiO<sub>2</sub> crystals. Picture taken at 10kV, working distance=9,5mm x50,0k magnification

Film A (non-layered) was measured to have an as-deposited resistivity of 1,58 mΩ·cm, while film B (layered) had an as-deposited resistivity of 4,35 mΩ·cm. From the resistivity measurements, it also was found that the annealing of 3 hours at 500 °C caused a resistivity increase of 5x for the layered and 70x for the non-layered thin film respectively. The large increase for the non-layered sample was due to a crack in the quartz tube; thus the focus here will be on the layered thin film results.

After 3 hours of annealing at 500 °C, the resistivity normalized by the post-annealing resistivity was tracked for 29 days (see figure 29). Note that the annealed film has been normalized by the post-annealing resistivity. Overall, the resistivity of the annealed sample appears to be more stable with an increase of 3,6% over 29 days compared to the as-deposited sample with 8% increase over 29 days.

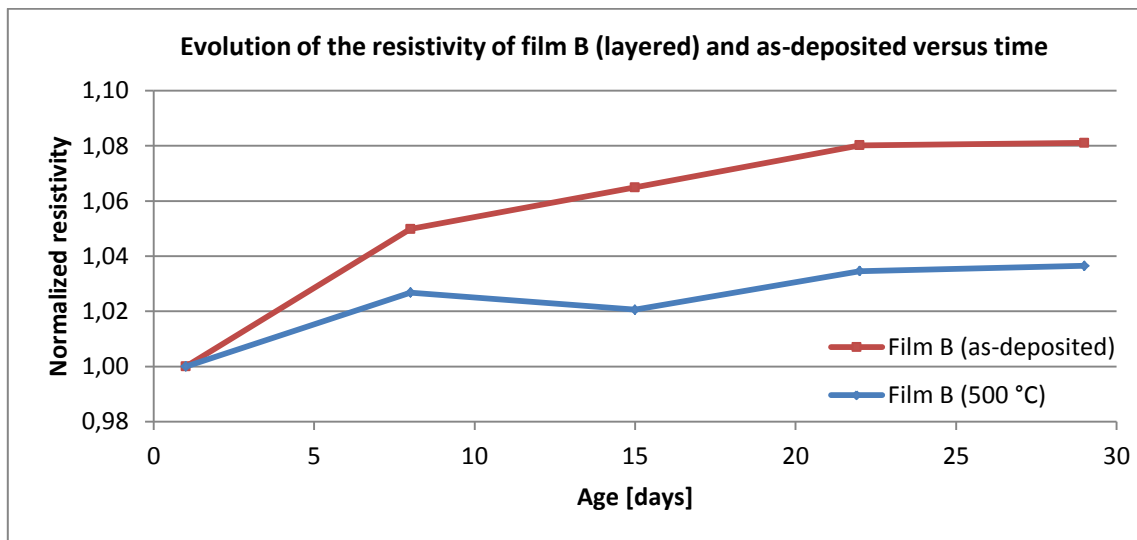


Figure 29 –Normalized resistivity vs. age [days] (note: annealed film normalized by the post-annealing resistivity)

Also, it was found that the resistivity of the as-deposited non-layered sample is slightly more stable than the layered sample during aging at room temperature.

### Conclusion

It was found that the layered film annealed at 500 °C is more stable than the non-annealed sample during aging at room temperature. Regarding the performance of the layered vs. non-layered annealed samples, it is not possible to draw any conclusions because of the crack that occurred in the quartz tube during the annealing experiment of the non-layered sample. Based on the SEM pictures, it seems that oxygen pulsing can be used to break up the columnar structure of TiN films (SEM), yet this should be evaluated closer by taking images of the cross-section layered thin film with a tunneling electron microscope offered by Paulo Fichtner (UFRGS, Porto Alegre). Overall temperatures of 500-600 °C should not be exceeded due to limitations of the production facilities at Danfoss. [1]

## 6. TiN resistivity stability - research strategy

At that point of time in the project, the annealing oven was broken due to a fracture in the quartz tube and the RF-sputtering of Cryofox system had a failure yield of over 60%. Therefore the decision was made, to propose further annealing post-annealing experiments, and use DC-sputtering while tuning the deposition parameters of the system in order to achieve thin films with a lower resistivity drift.

Thin film DC-016 from figure 24, which was deposited at Ar: 40 sccm, N<sub>2</sub>: 10 sccm, a power of 300 W at a main chamber pressure of  $5,90 \cdot 10^{-3}$  mbar, shows a porous structure, which seems to be in the beginning of zone 1 in the structure zone diagram (see figure 9 page 16). Based on the results of the previous research, the main goal of this masters project is to achieve thin films with a resistivity drift of below  $\pm 2\%$  at an operating temperature of up to 250°C during 150 hours in order to create the basis for further strain gauge research. The turning parameters are generally set by the limitations of the deposition system. The system used throughout this project has three main parameters, which can be adjusted to achieve higher quality titanium nitride thin films. First, the chamber pressure can be controlled by the amount of argon flow [sccm] during the deposition; secondly the nitrogen flow [sccm] can be controlled and finally the target power can be controlled.

Looking again at the structure zone diagram (see figure 9 page 16), it can be seen that the mentioned parameters could mainly lead to a shift along the E\*-axis. The deposition is performed at room temperature which seems to make the movement along the T\*-axis more rigid.

The overall approach was to study the impact of the main chamber pressure, nitrogen flow, and the target power on the resistivity stability, thin film stoichiometry, and structure. The experiments were carried out in collaboration with Nis Dam Madsen and Kasper Thilising Hansen.

## 7. TiN resistivity stability – experiments, results and discussions

### 7.1. Pressure series

The objective of this experiment was to investigate if more dense films can be achieved at lower deposition pressures and if the oxygen content of the titanium nitride films is reduced, which should help to avoid excessive oxidation and resistivity drift over time. Generally, it is known that a lower deposition pressure is increasing the film density. [28] To investigate the film stability, the sheet resistivity was measured as a function of time and accelerated life tests have been conducted. Furthermore, the composition and structure was investigated with EDX and XRD, respectively.

The thin films have been deposited at constant target power at room temperature by DC-sputtering using the Cryofox Explorer 600. The deposition parameters for the various samples are given in figure 30. Based on previous experiments, the expected deposition rate was around 1,3 Å/s. The thin film thickness was chosen based on previous experimental experience, which resulted in proper EDX measurements.

| Parameters     | Value(s)           |
|----------------|--------------------|
| DC Power       | 300 W              |
| N2 flow        | 5 sccm             |
| Ar flow        | 10, 15, 20, 30, 40 |
| Base Pressure  | 5,00E-5 mbar       |
| Temperature    | Room temperature   |
| Thickness      | 400 nm             |
| Tooling factor | 27                 |
| Expected rate  | 1,3 Å/s            |

Figure 30 - Parameters for the pressure series variation

A variation of substrates was used for the different characterization techniques. A list and placement instructions can be found in appendix “C1. Substrates and placement – pressure series” page 152.

Figure 31 shows the deposition system characteristics for the main chamber pressure [mbar] and deposition rate [Å/s] versus the total flow (Argon [sccm] + Nitrogen [sccm]) for the parameters in figure 30. Note that the nitrogen flow is kept constant and only the argon flow is changed.

It can be seen that the pressure/total flow relationship is close to linear with the slope being the pumping speed of the system. There is also an increase in the deposition rate as the argon flow is increased, which may indicate that the target becomes more metallic. Whereas when the argon flow is reduced at constant nitrogen flow, it seems probable that the target becomes more poisoned, resulting in a reduction of sputter yield and thus lower deposition rate. This behavior is also observed by other groups. [44]

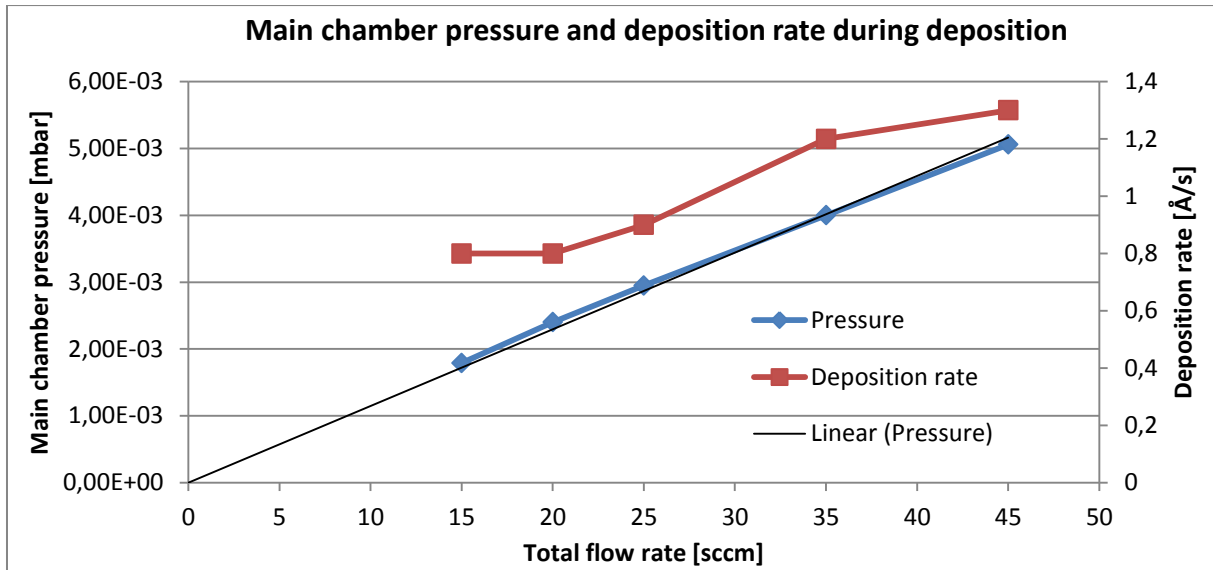


Figure 31 – Main chamber pressure [mbar] and deposition rate [Å/s] during deposition vs. total flow [sccm]

### 7.1.1. Resistivity

Figure 32 shows the resistivity of the samples produced with various argon flows at constant nitrogen flow and measured as-deposited by the four point probe. The as-deposited measurements in this project were performed on the same day on which the sample was produced.

It can be seen that the samples produced at lower pressure (lower Argon flow) have a lower resistivity. Furthermore, it can be seen that the resistivity is increasing with increasing chamber pressure (higher argon flow).

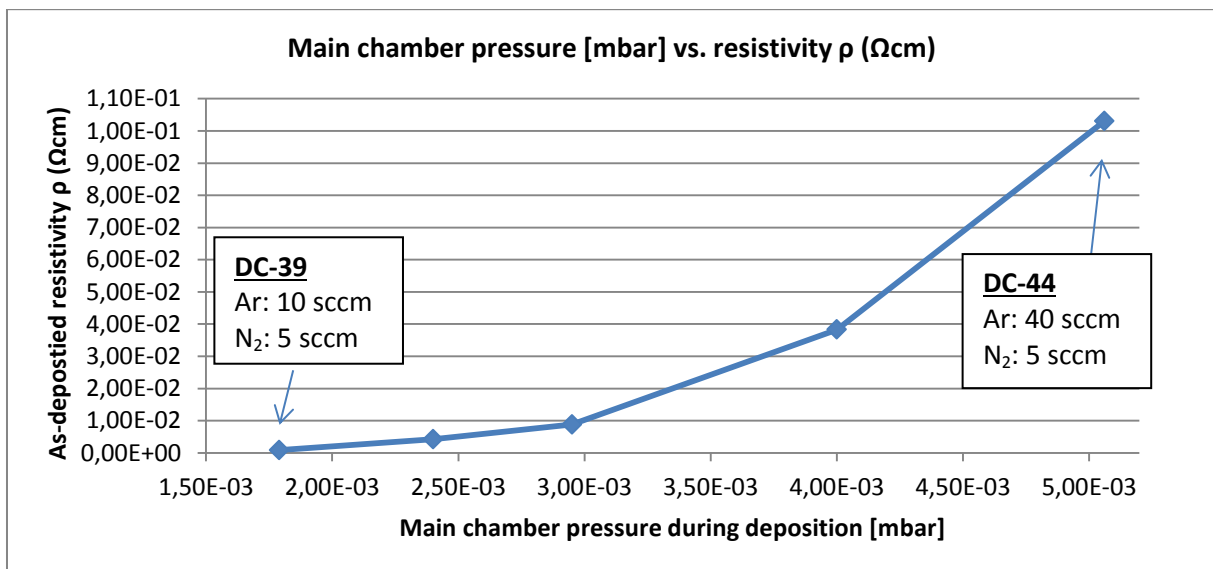


Figure 32 – Main chamber pressure during deposition [mbar] vs. As-deposited resistivity  $\rho$  ( $\Omega\text{cm}$ ) in ambient environment

### 7.1.1.1. Accelerated life test

The accelerated life test was carried out by placing the samples in an oven at 100 °C for 1 hour in ambient atmosphere followed by a four point measurement. This process was repeated four times. Before each measurement each sample was given a cool down time of 10-15 minutes. See appendix “C2. Accelerated lifetime testing experiment” page 153.

Figure 33 shows the results for the accelerated life test plotted as normalized resistivity versus time [hours]. Sample DC-044 (Ar: 40 sccm) was excluded because of invalid measurement results. The pre-accelerated measurements, that were taken on the same day, are plotted at t=0 hours. It should be mentioned that the resistivity normalization will always be done with regard to the as-deposited sheet resistance. The plotted samples have different production dates (maximum 5 days) resulting in different shelf-lifetimes at ambient environment, that causes the offset at t=0 hours.

The resistivity of sample DC-39 changed by 1,1%, DC-40 changed by 23%, DC-41 by 85% and DC-43 by 275% during the 4 hours accelerated life time experiment at 100 °C. It can be seen, that sample DC-039, which was produced at the lowest pressure (1,79E-03 mbar), has the lowest resistivity drift over time compared to the other samples, which have been produced at a gradually higher pressure.

Generally, it can be observed that at lower deposition pressure the thin film resistivity over time is more stable, whereas at higher pressure the resistivity drift is gradually larger.

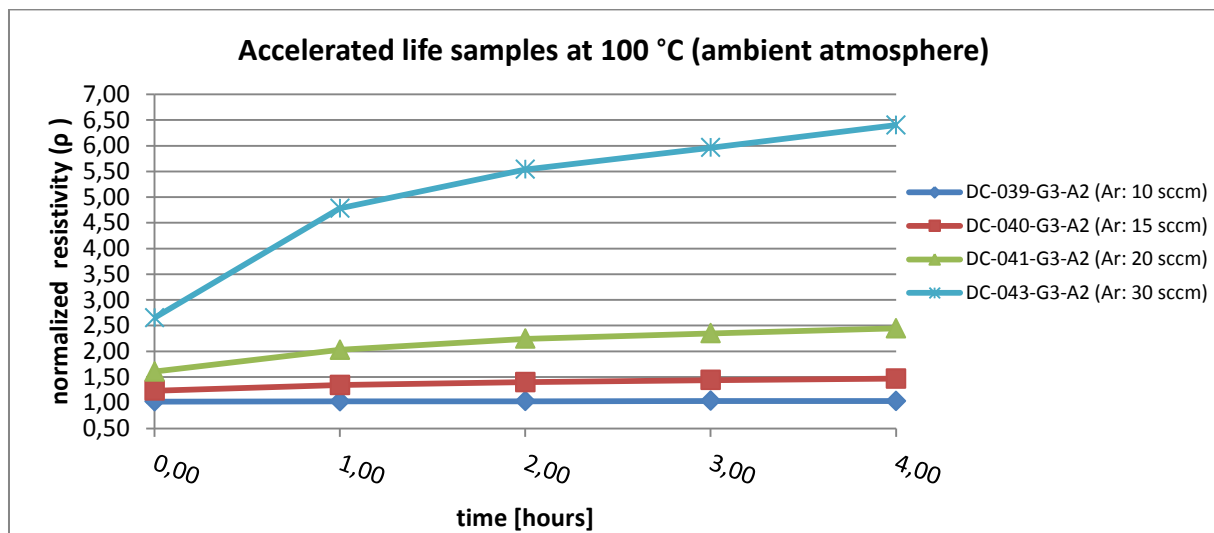


Figure 33 - Accelerated life samples normalized resistivity ( $\rho$ ) versus time [hours]

It should be noted that the atomic concentration in percentage between the pre- and post-accelerated life time measurements is lower than the corresponding measurement error. Based on these observations, it seems that the accelerated life time tests at 100 °C have no measurable effect on the thin film stoichiometry. (See appendix “C3. Pre and post EDX for accelerated life test samples” page 154) Also thickness measurements have been performed with both AFM and SEM cross-section,

showing no significant difference between the two techniques' results (See appendix "C4. AFM and SEM thickness measurements" page 155).

**7.1.1.2. Stability at room temperature**

Figure 34 shows the thin film resistivity measurements at room temperature in ambient conditions conducted over the time frame of 35 days. The resistivity of the films was measured every week in order to follow the stability of the films. The resistivity is normalized with regard to the as-deposit measurements. Again it is observed that the sample produced at the lowest pressure (DC-39) has a superior resistivity stability with 3,6% increase after 34 days. DC-40 changes 31% after 34 days, DC-41 changes 78% after 34 days, DC-43 changes 227% after 33 days and DC-044 changes 604% after 33 days. Based on the resistivity data, it is clear that the deposition pressure has a significant impact on the resistivity drift.

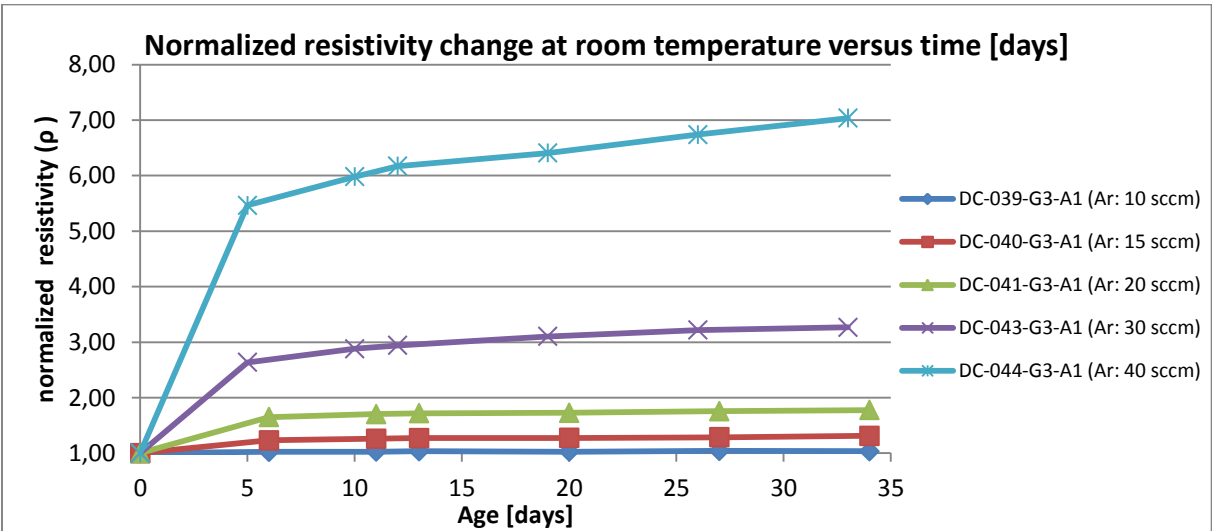


Figure 34 - Normalized resistivity change at room temperature versus time [days]

Figure 35 highlights the resistivity change of sample DC-39 with 3,6% over the time frame of 34 days at room temperature.

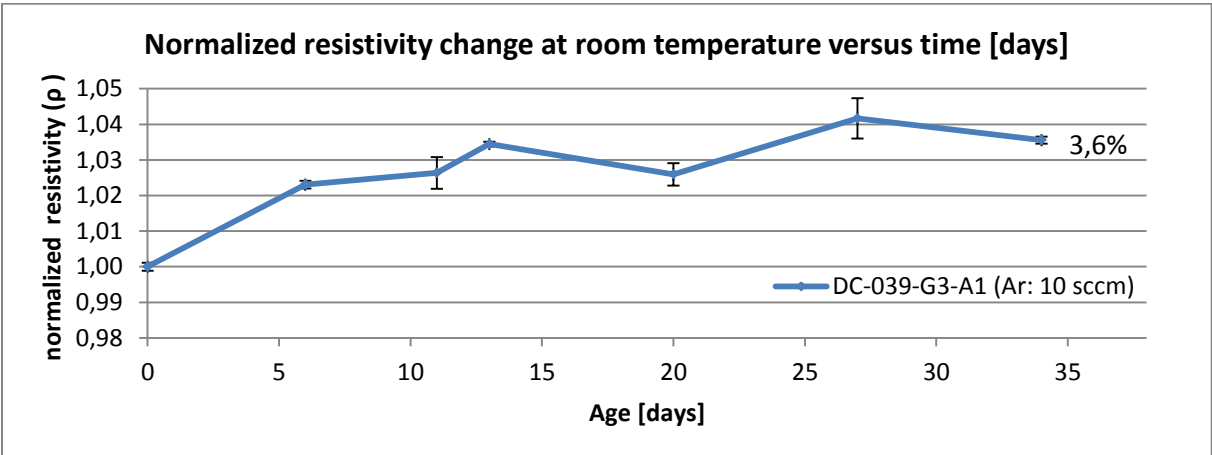


Figure 35 - Normalized resistivity change at room temperature versus time [days] for DC-39

### 7.1.2. Atomic composition

Figure 36 shows the as-deposited atomic concentrations measurement by EDX. It can be observed that the atomic concentration of oxygen is increasing with an increase in argon flow (increase in main chamber pressure).

DC-039 (lowest resistivity, Ar: 10 sccm, N<sub>2</sub>: 5 sccm), produced at the lowest pressure (1,79E-03 mbar), shows an atomic oxygen concentration offset of about 9%. On the other hand DC-044 (highest resistivity drift, Ar: 40 sccm, N<sub>2</sub>: 5 sccm), which was produced at the highest pressure (5,06E-03 mbar), shows an atomic oxygen concentration offset of about 36%.

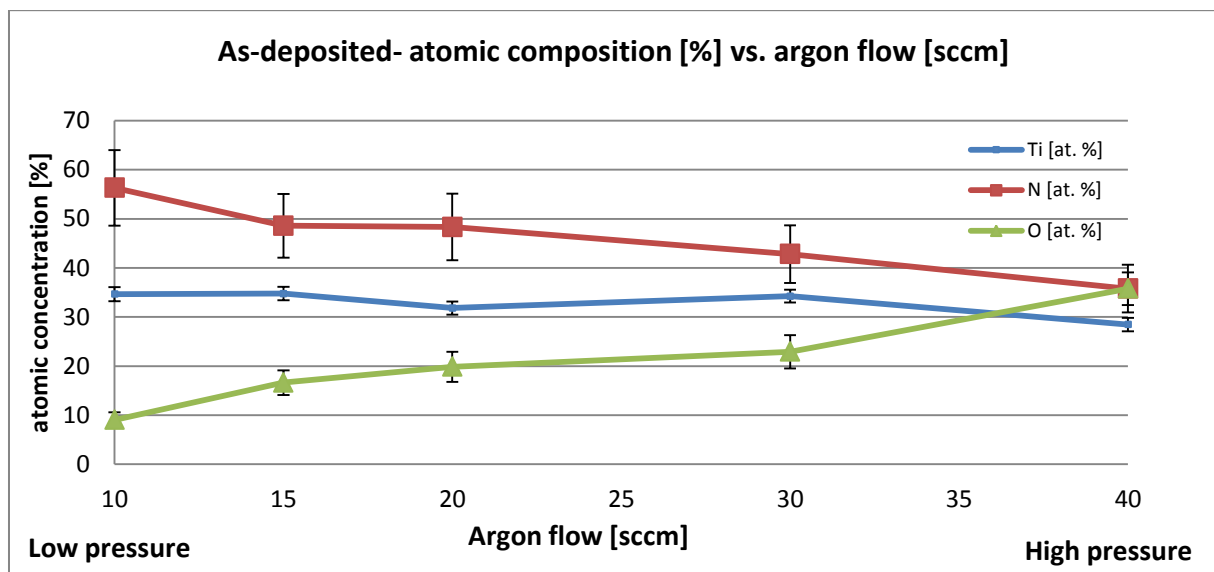


Figure 36 – As-deposited - atomic composition [%] vs. argon flow [sccm]

Furthermore, it can be observed, that the atomic concentration of nitrogen [%] decreases with an increasing argon flow (increasing main chamber pressure). The titanium atomic concentration stays fairly stable for the various argon flow rates. Generally, it can be observed, that at the lowest pressure the oxygen content is smallest and comparing the results from figure 34 with figure 36 it can be seen, that an increase of atomic oxygen results in a larger resistivity drift over time.

### 7.1.3. Thin film structure

SEM top-view and cross-section images have been made in order to investigate the thin film thickness and morphology (see appendix “C5. SEM top-view and cross-section view images” page 156). The top-view images show no clear differences.

Figure 37 shows the SEM cross-section and top-view images for the low and high pressure sample (note that the pictures have not been modified). It seems that DC-044 shows a more porous structure, indicating that the films are denser at the lower pressures; yet this is a more subjective

result, because for a clear conclusion a helium-ion microscope would be needed to achieve Nano-scale resolution.

The resistivity change for DC-044 over the time frame of 33 days was about 167x higher compared to DC-039, which is a quite remarkable impact on the resistivity drift.

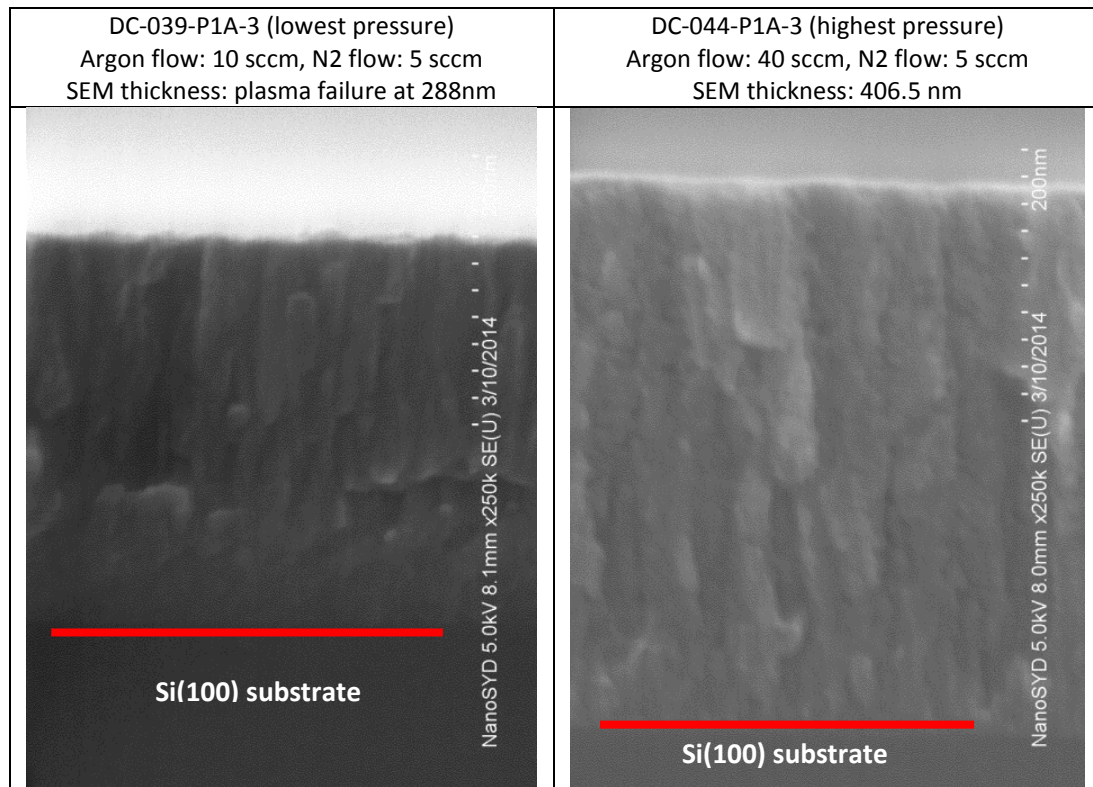


Figure 37– SEM cross-section images taken at 250k magnification, working distance around 8mm.

#### 7.1.4. Crystal structure

XRD measurements were performed by Nis Dam Madsen and Kasper Thilising-Hansen with the goal of analyzing the phase content of the thin films. Figure 38 shows the x-ray diffraction patterns for the produced samples. The grazing incident X-ray diffraction patterns were taken at  $\omega=7^\circ$  and the reflection angles from cubic titanium nitride ( $\text{TiN}_x$ ) are shown as bars. It should be noted that the large “bumps” in the spectra are caused by the amorphous BK-7 glass substrates.

It can be observed that the film crystallinity is increasing with decreasing pressure. There is a clear increase in the peak intensities as the pressure is lowered. Furthermore, the diffraction peaks fit very well with the cubic- $\text{TiN}_x$  structure<sup>1</sup> for the sample produced at the lowest pressure. A small shift of the peak positions are observed with increasing deposition pressure.

<sup>1</sup> PDF card no: 01-087-0629

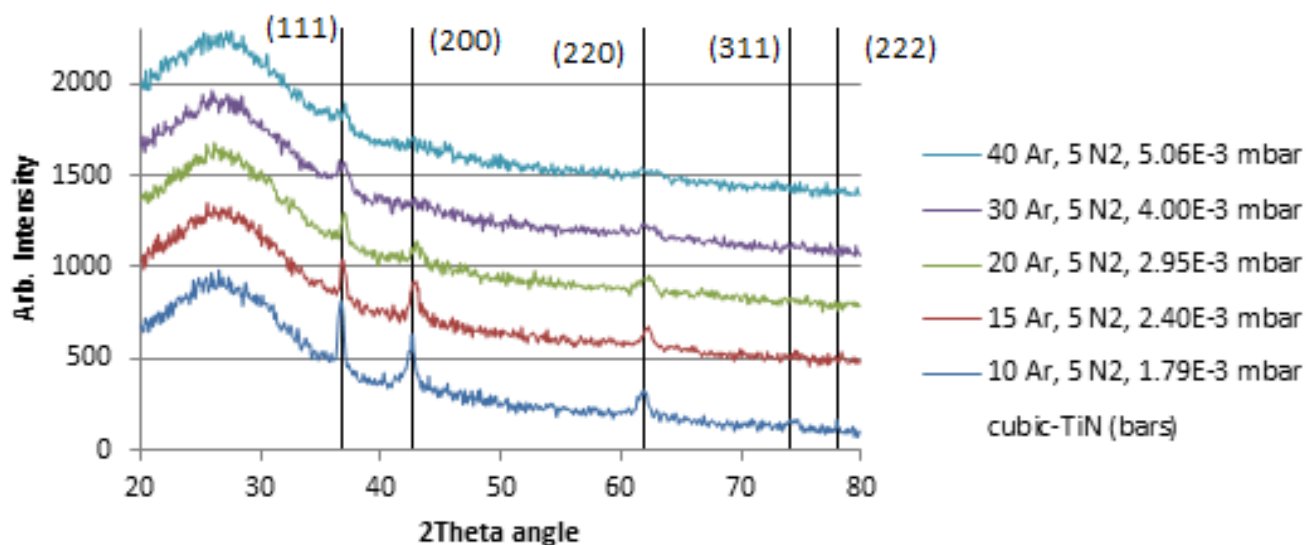


Figure 38 - X-ray diffraction patterns – pressure series

### 7.1.5. Density

Density measurements were taken by Nis Dam Madsen and Kasper Thilising-Hansen. The density is determined for the highest and lowest pressure by making an additional deposition with substrates that have been weighted with a high precision weight (+/-0.01 mg) at the “University of Southern Denmark” in Odense. See appendix “C6. Density measurement experiment” page 158 for a detailed experimental description.

It was found that the density for the low pressure sample was 4,0 g/cm<sup>3</sup> and for the high pressure sample 2,7 g/cm<sup>3</sup>. For comparison, the tabulated value for the density of TiN<sub>x</sub> is 5.22 g/cm<sup>3</sup>, while pure Ti has a density of 4.51 g/cm<sup>3</sup>.<sup>2,3</sup> From the obtained measurements it can be seen in a quantitative way that the low pressure samples are denser than the high pressure samples.

### 7.1.6. Conclusion

Overall it was shown through this study that at a lower pressure, a lower atomic concentration of oxygen [%] is measured. The low pressure thin films show a higher crystallinity and a higher density. These improved characteristics reduce the resistivity drift, which results in a more stable resistivity over time at both room temperature (3,6% over 34 days) and at 100 °C (1,1% over 4 hours).

Still an oxygen offset of 9% was detected for the low pressure sample DC-39, which should be reduced more, in order to see if the resistivity drift becomes even lower.

<sup>2</sup> Source: <http://en.wikipedia.org/wiki/Titanium> (24.05.2014)

<sup>3</sup> Source: [http://en.wikipedia.org/wiki/Titanium\\_nitride](http://en.wikipedia.org/wiki/Titanium_nitride) (24.05.2014)

## 7.2. Nitrogen flow series at 300W

The next investigation concerns the nitrogen flow and its impact on the electrical characteristics of the thin film. The focus of this study was to investigate the influence of the sputter gas composition on the stability of the thin film resistivity. Furthermore, a correlation between structural and compositional characterization results is intended.

The incentive is to decrease the oxygen content of the thin films, so pure titanium nitride is produced, with the hypothesis, that this might decrease the resistivity drift even more compared to the results of the pressure series. From the pressure series it was found, that a low pressure yields desired results, so for the nitrogen flow series the main chamber pressure will be kept constant at a low level during the depositions.

### 7.2.1. Deposition system characteristics and hysteresis

The first step was to extract hysteresis curves for the Argon/Nitrogen flow ratios [sccm] at (Ar=20; N<sub>2</sub>=0), (Ar=18; N<sub>2</sub>=2), (Ar=16; N<sub>2</sub>=4), (Ar=14; N<sub>2</sub>=6), (Ar=12; N<sub>2</sub>=8), (Ar=10; N<sub>2</sub>=10) in order to observe the stability of the main chamber pressure [mbar]. Note that the total flow (Ar + N<sub>2</sub>) is kept constant. The chamber pressure should stay stable for the various argon and nitrogen flow combinations because it's important to only change the nitrogen flow in order to be able to evaluate its impact on the thin film characteristics. Figure 39 shows the results from the first hysteresis run based on the above mentioned argon/nitrogen flow combinations.

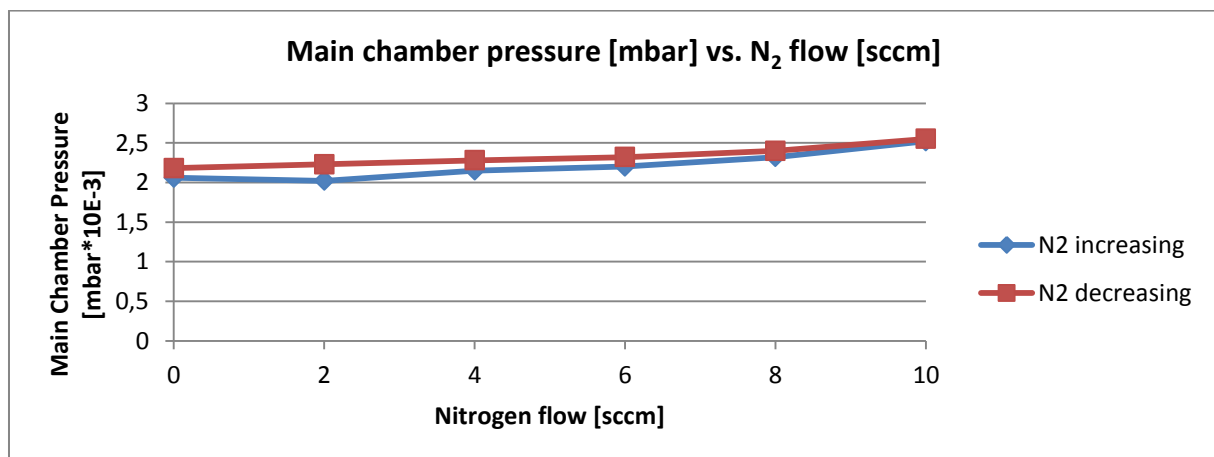


Figure 39 - Main chamber pressure [mbar] vs. nitrogen flow [sccm]

It can be observed, that the increase in nitrogen flow from N<sub>2</sub>=0 sccm to N<sub>2</sub>=10 sccm will result in a pressure increase of about 18%. For a more conclusive investigation, the pressure should be kept more constant at a low level.

In the next step the different argon and nitrogen flow rate combinations that result in a stable and low main chamber pressure were experimentally extracted. This was done via the cryofox interface

by manually changing the flow rates and recording the rate, DC bias voltage over the target, and main chamber pressure. Figure 40 shows deposition parameters, which result in a stable main chamber pressure at a constant target power of 300 W.

| Ar flow [sccm] | N <sub>2</sub> flow [sccm] | Rate [Å/s] | DC bias voltage [V] | Main Chamber Pressure [mbar*10E-3] | Total flow |
|----------------|----------------------------|------------|---------------------|------------------------------------|------------|
| 18             | 0                          | 1,8        | 384                 | 2,03                               | 18         |
| 18             | 1                          | 1,9        | 383                 | 2,03                               | 19         |
| 16             | 3                          | 1,6        | 427                 | 2,06                               | 19         |
| 12             | 5                          | 0,8        | 434                 | 1,99                               | 17         |
| 9              | 7                          | 0,6        | 457                 | 2,03                               | 16         |

Figure 40 – Deposition parameters yielding stable main chamber pressure [mbar\*10E-3] (first run)

Figure 41 shows the nitrogen flow [sccm] vs. main chamber pressure [10E-3 mbar] for (argon/nitrogen) ratios (18:0), (18:1), (16:3), (12:5), (9:7) from figure 40 for increasing and decreasing runs. It can be seen that the main chamber pressure stays fairly constant and the percentage difference between highest and lowest pressure during the first run is about 3.4% and for the consecutive run 5.5% which is acceptable for the nitrogen flow investigations.

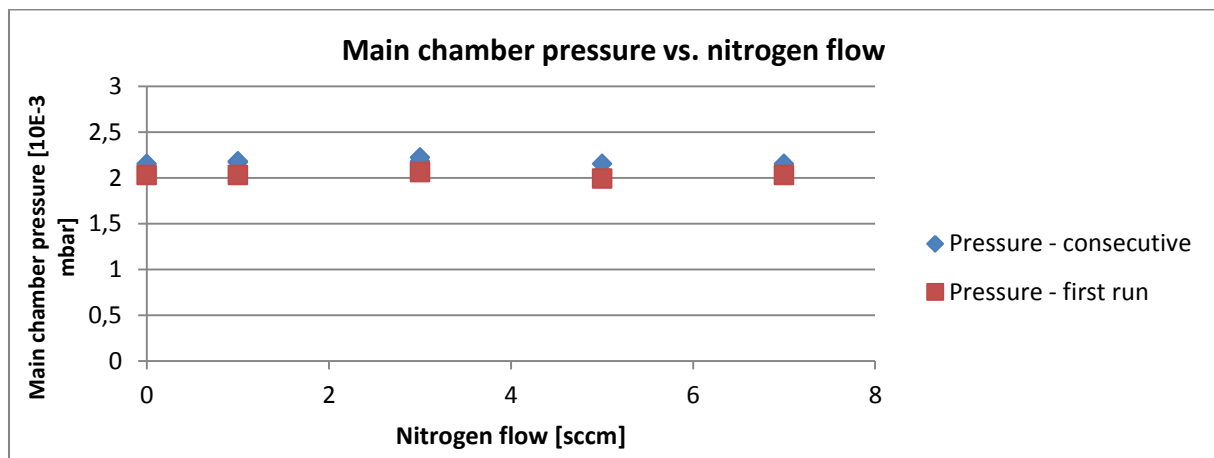


Figure 41 – Main chamber pressure [10E-3 mbar] vs. nitrogen flow [sccm]

Figure 42 shows the hysteresis for the nitrogen flow vs. deposition rate [Å/s] and total flow [sccm]. It can be seen, that the deposition rate decreases with an increase in nitrogen flow, which seems to be caused by target poisoning.

Note also that, in order to keep a stable main chamber pressure, the total flow is adjusted by the argon flow, which causes the total flow to be fluctuating. Yet the goal is to keep the main chamber pressure stable because that parameter has a very high impact on the thin film characteristics.

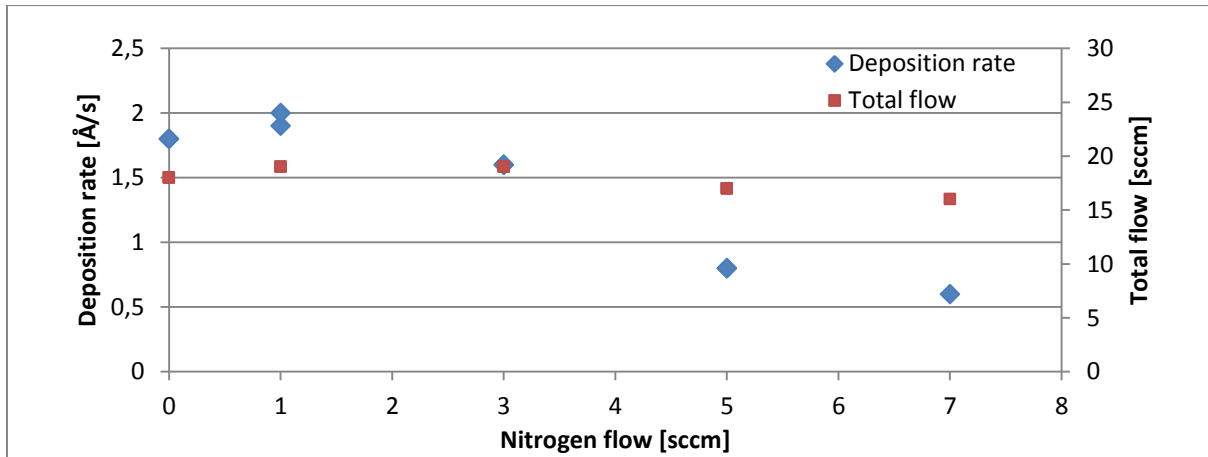


Figure 42 – Deposition rate [Å/S] and total flow [sccm] vs. nitrogen flow [sccm]

### 7.2.2. Depositions

Figure 43 shows the adjusted parameters used during the deposition in order to achieve a stable low main chamber pressure of around 2,20-2,26E-03 mbar at a power of 300 W. The maximum pressure difference between the samples is about 2,7%, which is acceptable.

| Sample | Ar flow [sccm] | N <sub>2</sub> flow [sccm] | Total flow [sccm] | N <sub>2</sub> /total flow ratio | Rate [Å/s] | DC Voltage [V] | Main Chamber Pressure [mbar*10E-3] | Thickness [nm] by AFM |
|--------|----------------|----------------------------|-------------------|----------------------------------|------------|----------------|------------------------------------|-----------------------|
| DC-054 | 19             | 0                          | 19                | 0                                | 2,0        | 519            | 2,20E-03                           | 290                   |
| DC-055 | 19             | 1                          | 20                | 0,05                             | 2,0        | 510            | 2,20E-03                           | 283                   |
| DC-053 | 18             | 2                          | 20                | 0,10                             | 1,9        | 543            | 2,23E-03                           | 324                   |
| DC-051 | 16             | 3                          | 19                | 0,16                             | 1,1        | 437            | 2,23E-03                           | 320                   |
| DC-050 | 12             | 5                          | 17                | 0,29                             | 0,6        | 468            | 2,23E-03                           | 313                   |
| DC-049 | 9              | 7                          | 16                | 0,44                             | 0,6        | 462            | 2,26E-03                           | 339                   |

Figure 43 – Adjusted deposition parameters recorded during deposition

Additional deposition parameters are shown in figure 44:

| Parameters     | Value(s)              |
|----------------|-----------------------|
| DC Power       | 300W                  |
| N2 flow        | 0, 1, 2, 3, 5, 7      |
| Ar flow        | 19, 19, 18, 16, 12, 9 |
| Base Pressure  | 5,00E-5 mbar          |
| Temperature    | RT                    |
| Thickness      | 400 nm                |
| Tooling factor | 27                    |

Figure 44 - Additional parameters for the nitrogen flow variation series

Detailed information about the substrates used and their placement can be found in appendix “D1. Substrates and placement” page 160.

#### 7.2.2.1. Deposition parameters during deposition

During the deposition of the samples the main chamber pressure [mbar], deposition rate [Å/s], and cathode voltage [V] were observed. Details about the raw data can be found in appendix “D3. Sample deposition data observations” page 162 and “D4. Pressure evolution during deposition” page 163.

From figure 45 it can be seen that the deposition rate for the investigated samples is decreasing with an increasing nitrogen/total flow ratio. Sample DC-54, 55, 53 have a low nitrogen/total flow ratio (0 – 0,10) for which the sputter deposition happens in the metallic target mode. Samples DC-51, 50, 49 have a higher nitrogen/total flow ratio (0,16-0,44) for which the deposition rate is lower, which is due to a poisoned target mode, where N<sub>2</sub> is reacting with the titanium target, forming a compound. Samples DC-51 and DC-53 seem to be on the border of their respective target modes. The samples produced in this transitional mode seem to have a higher deposition rate drift over time. For an industrial production purposes, the metallic mode would be favorable because of the higher deposition rates resulting in a higher production output.

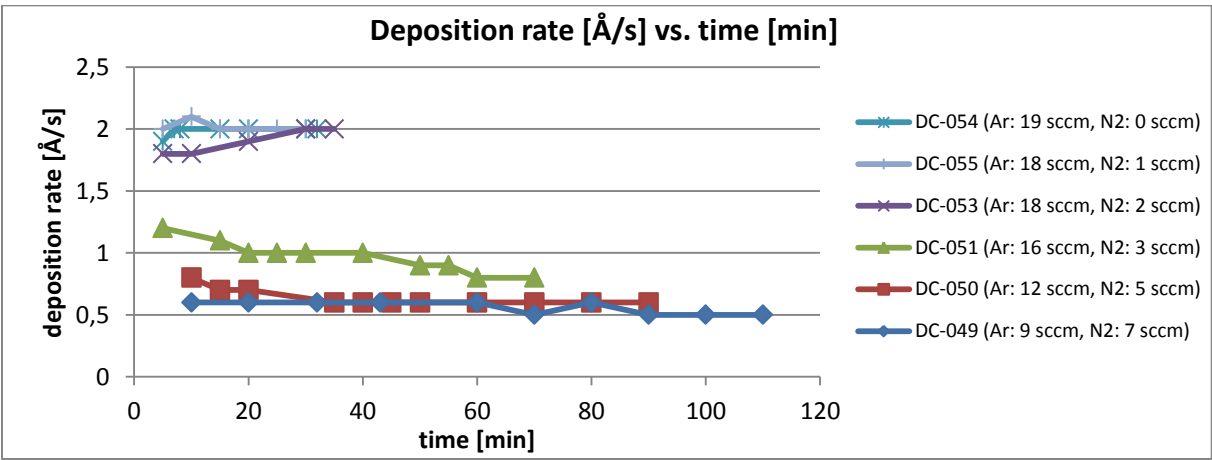


Figure 45 – deposition rate [Å/s] vs. time [min]

Figure 46 shows the average deposition rate [Å/s] versus nitrogen/total flow ratio. It can be observed that the average deposition rate is significantly reduced when operating the sputtering process with a nitrogen/total flow ratio over 0,1.

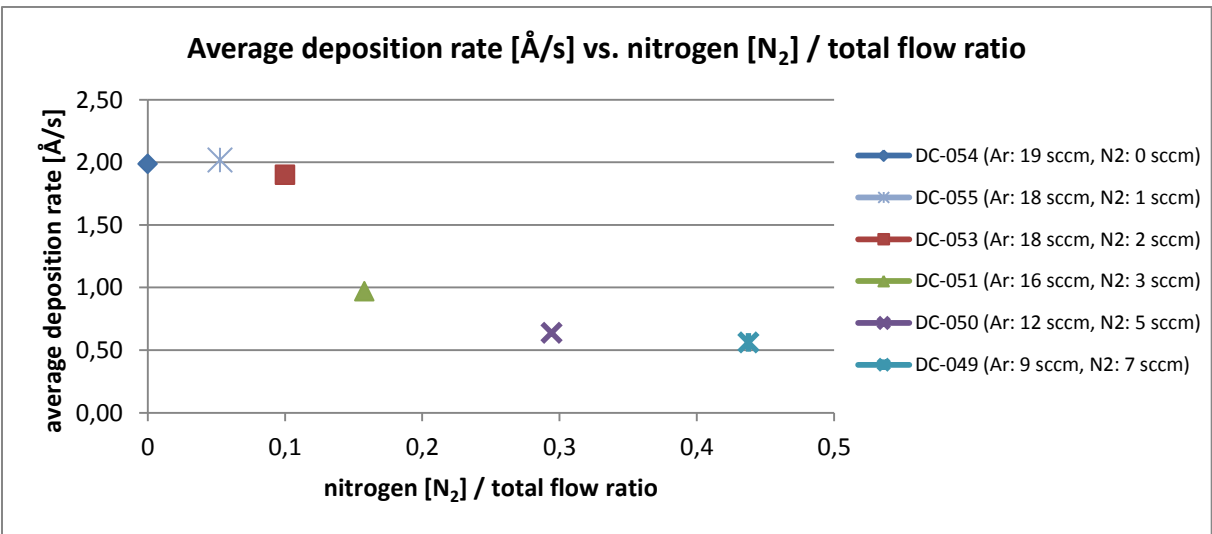


Figure 46 – average deposition rate [Å/s] vs. nitrogen [N<sub>2</sub>] / total flow ratio

Figure 47 shows the cathode voltage [V] versus time [min]. A difference for the cathode voltage evolution of the poison and metallic target mode can be observed. The cathode voltage for poisoned mode samples is increasing while for metallic mode it's decreasing over time. A possible explanation for the cathode evolution for DC-49,50,51 could be the increased target poisoning with N<sub>2</sub> causing it to be more insulating over time, which increases the needed voltage in order to keep the plasma operational. In the metallic mode, the target becomes more conductive and the cathode voltage drops.

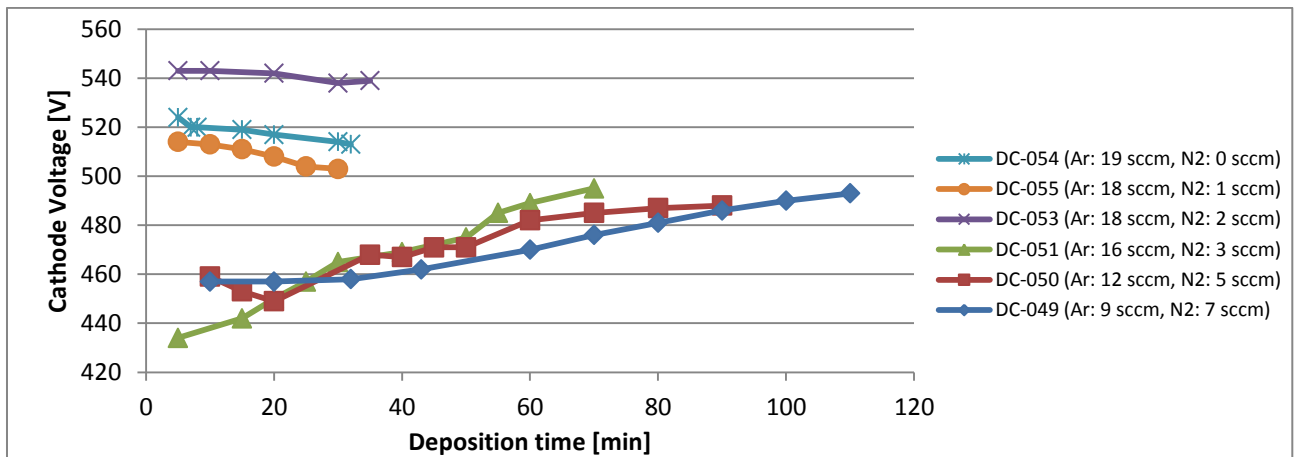


Figure 47 - cathode voltage [V] vs. time [min]

It should be mentioned that, during the nitrogen investigation series, arcing around the target was observed. The consequences for the future could be to polish the target in case the racetrack is becoming too deep and also to increase the sputtering time of the target in pure argon at the beginning of the deposition process (SOAK2) from 6 to 15 minutes in order to get rid of target compound formation from earlier reactive sputtering processes. Details about this investigation can be found in appendix “D5. Target arcing investigations” page 163.

### 7.2.3. Resistivity

Figure 48 shows the as-deposit resistivity [ $\Omega\text{cm}$ ] versus the N<sub>2</sub>/total flow ratio. It can be observed, that with an increase in N<sub>2</sub>/total flow ratio the resistivity is increasing. Comparing the results to the bulk resistivities at room temperature for titanium ( $420\text{ n}\Omega\cdot\text{m}$ )<sup>4</sup> and titanium nitride (ceramic) ( $1,3\text{M}\Omega\cdot\text{m}$ )<sup>5</sup>, it can be seen that an increase in resistivity with larger nitrogen/total flow ratio can be expected. Also other research groups are reporting an increase in thin film resistivity from titanium to titanium nitride. [45]

<sup>4</sup> <http://en.wikipedia.org/wiki/Titanium> (26.05.2014)

<sup>5</sup> <https://www.memscet.org/material/titaniumnitridetinbulk/> (26.06.2014)

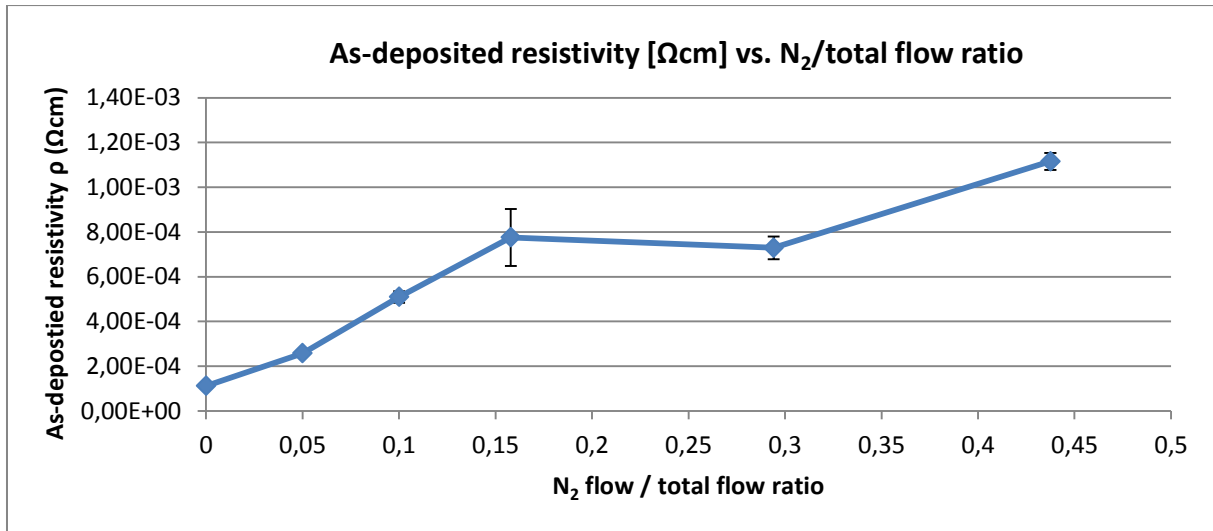


Figure 48 – As-deposited resistivity [Ωcm] vs. N<sub>2</sub>/total flow ratio

Figure 49 shows the results of an accelerated life time test performed similar to the pressure series. The experiment was conducted for 18 hours at 100 °C in ambient atmosphere. It can be seen that both samples DC-51 and DC-53 are unstable compared to the rest of the samples. DC-51 has a resistivity increase of 18% and DC-53 of 19% over the time frame of 18 hours at 100 °C. Note the off-set at t=0 [hours] is caused by different production times as explained in the pressure series. Interestingly, DC-51 and DC-53 are both the samples which are in the “transitional” sputtering mode, which might indicate that this area should be avoided in order to stabilize the resistivity of the thin films.

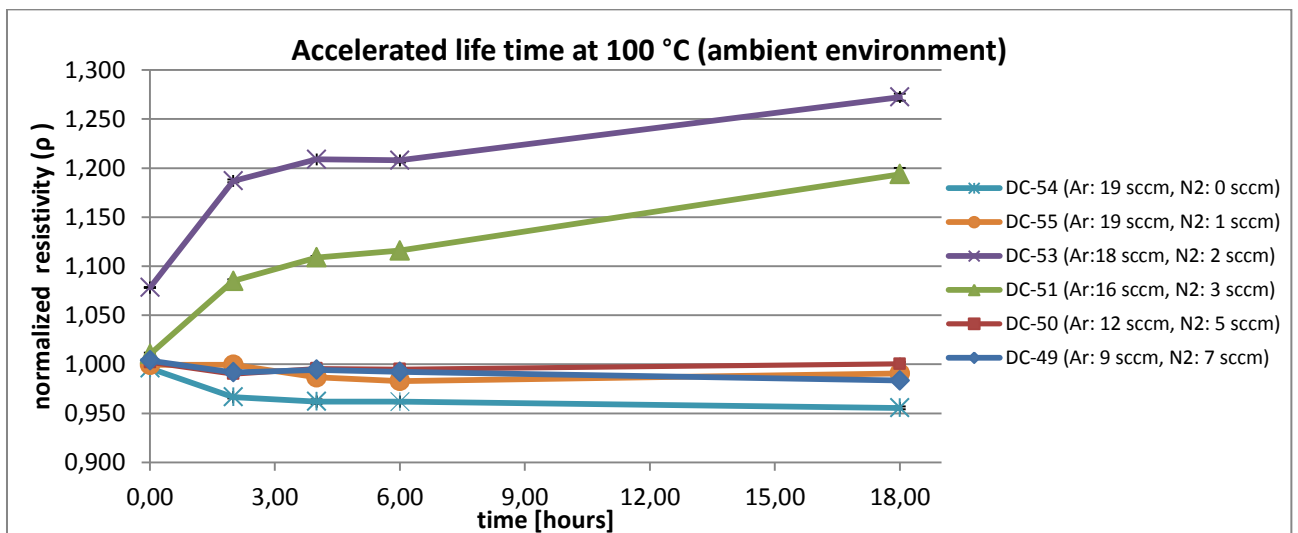


Figure 49 - accelerated life time experiments for nitrogen series at 100 °C (substrates BK7-A2)

Figure 50 shows a zoom-in on the best performing accelerated life time samples from the nitrogen series shown in figure 49. Based on the results, it can be seen, that the samples with the highest N<sub>2</sub>/total flow ratio, which are DC-49 and DC-50, have a resistivity drift of -2,1% and 0,2% respectively

for t=0h to t=18h. Samples DC-54 and DC-055 (low N<sub>2</sub>/total flow ratio) show a resistivity drift of -4,04% and -0,88% for t=0h to t=18h. The “pure” titanium sample DC-054 is not stable enough with more than 4% resistivity drift. Note that the samples have a slight offset at t=0h due to different shelf-lifetimes as discussed before.

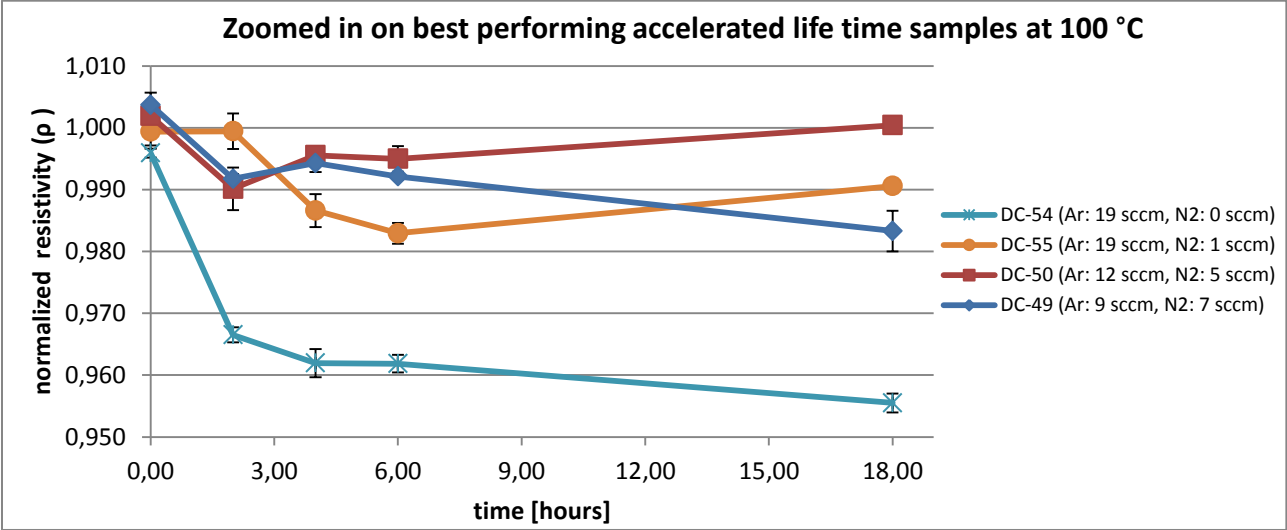


Figure 50 - zoomed in on best performing accelerated life time samples from nitrogen series at 100 °C

Figure 51 shows the resistivity stability for the samples at room temperature in ambient environment. Similar to the accelerated life test, it can also be observed that both “transitional” samples DC-051 and DC-053 are unstable with 7% and 13% resistivity drift respectively within 35 days. DC-49 and DC-50 perform well with 0,4% and 1,0% resistivity drift within 35 days and DC-55 with 0,8% within 29 days. The pure titanium sample DC-54 also performs well with 1,43% with regard to its resistivity drift at room temperature within 29 days. The data also indicate that “pure” titanium seems to have a higher resistivity drift at elevated temperatures.

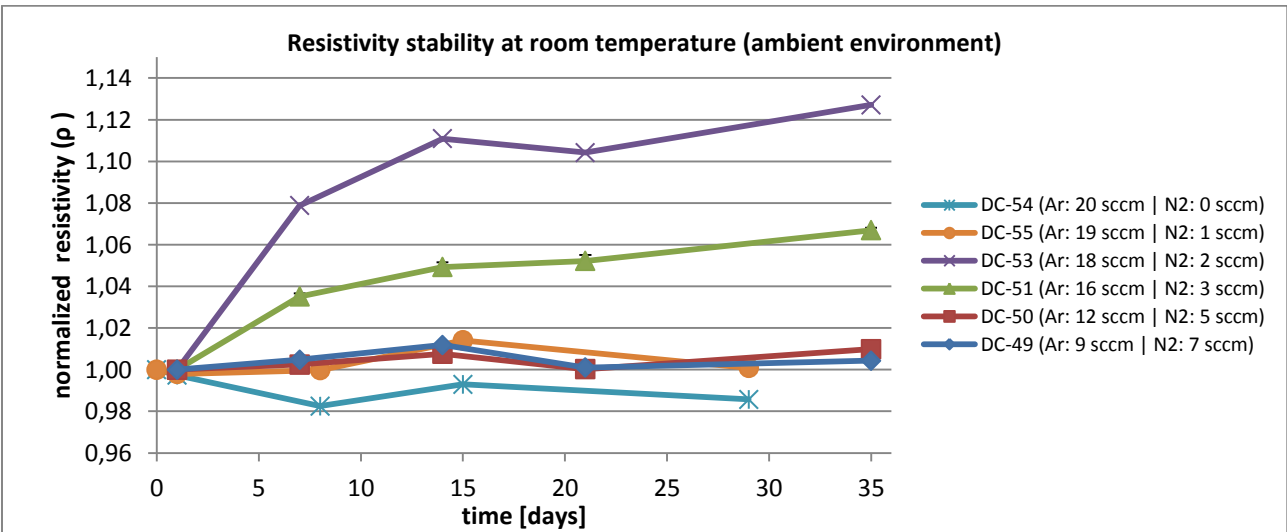


Figure 51 - resistivity [Ωcm] vs. time [days] at room temperature for the reference substrates BK7-A1

#### 7.2.4. Atomic composition

Figure 52 shows the results of the EDX analysis. DC-54 should be pure titanium, yet there is a small offset in nitrogen atomic concentration of about 10%. DC-55 shows a nitrogen-to-titanium ratio of about 1,25 with no traces of oxygen. Note that this is another key achievement, since now “pure” titanium nitride can be produced. It is interesting that the nitrogen-to-titanium ratio is above 1 for the films deposited with a  $N_2$ /total flow above 0,10. For the increasing  $N_2$ /total flow ratio, it seems that the atomic concentration for nitrogen, oxygen and titanium is stabilizing for the samples with a  $N_2$ /total flow ratio from around 0,30. The nitrogen-to-titanium ratio is stabilizing around 1,43. A nitrogen-to-titanium ratio of 1,63 has been observed by “Lemperière 1984” for films deposited in the poisoned target mode and it was suggested that the nitrogen is located in the grain boundaries, which causes the nitrogen-to-titanium ratio to exceed unity. [46] Furthermore, there seems to be a slightly higher oxygen atomic concentration level of above 10% for the unstable thin films DC-53 and DC-51.

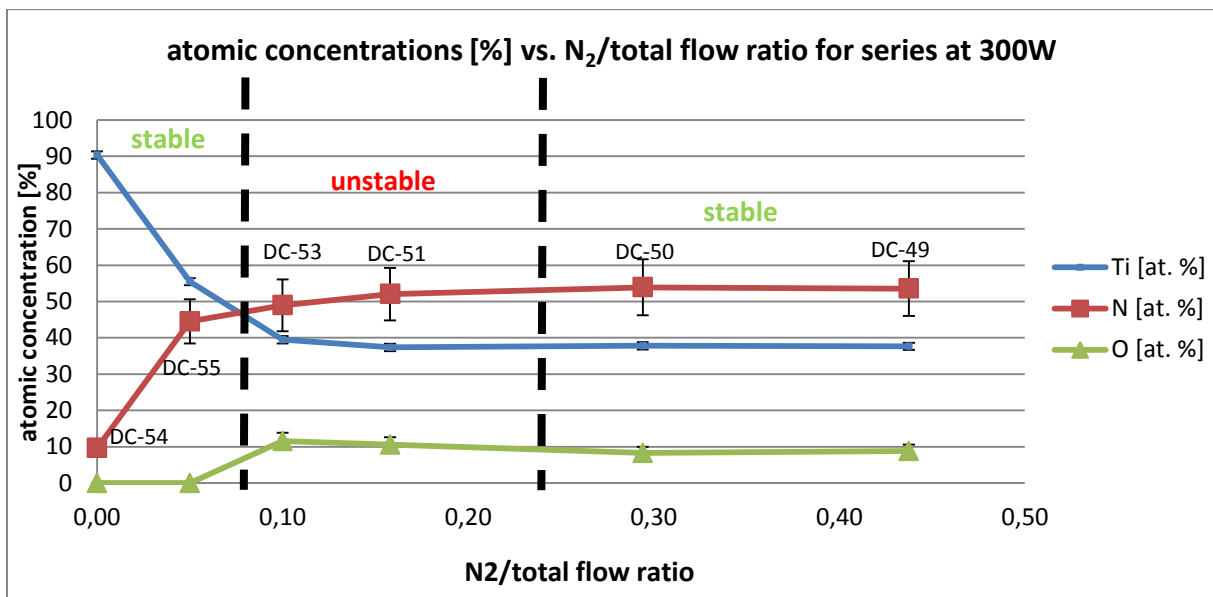


Figure 52 – EDX analysis - atomic concentrations [%] vs.  $N_2$ /total flow ratio

#### 7.2.5. Crystal structure

XRD measurements were performed by Kasper Thilising-Hansen with the goal of analyzing the phase content of the thin films. Figure 53 shows the x-ray diffraction patterns for the produced samples. The grazing incident X-ray diffraction patterns were taken at  $\omega=7^\circ$  and the reflection angles from cubic titanium nitride ( $TiN_x$ ) are shown as bars. A correlation between a strong (111) cubic-TiN texture and the unstable films seems to exist. It seems that the unstable thin films have a stronger (111) texture. Note also the shift from a (111) to (200) texture as the nitrogen flow increases.

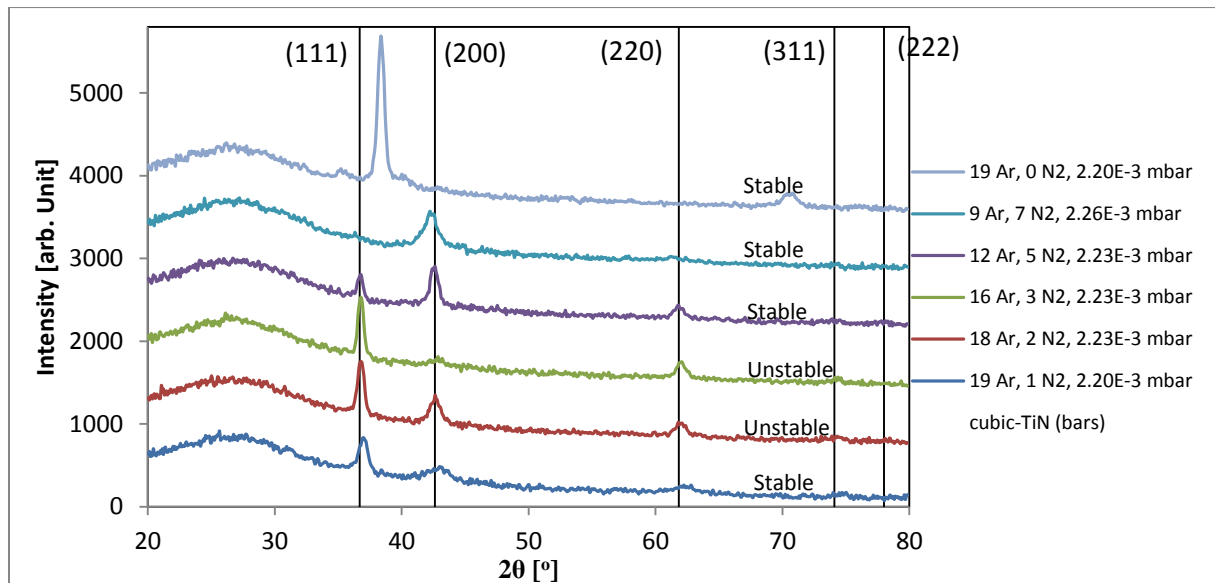


Figure 53 – XRD spectra - grazing incident X-ray diffraction patterns ( $\omega=7^\circ$ ). The reflection angles from cubic TiN are shown as bars. The large “bumps” in the spectra stem from the amorphous BK-7 glass substrates.

The thin film cross-section also has been evaluated with an SEM, but the results are not conclusive because of a too low resolution (see appendix “D6. SEM cross-section images” page 168). The samples should be evaluated when the new helium-ion microscope is operational.

### 7.2.6. Conclusion

Generally, there have been some interesting results during the nitrogen flow study. It was found, that, at the metallic mode and poisoned mode of reactive sputtering, the thin film resistivity drift is lower compared to the resistivity drift for samples that were produced at intermediate flows between metallic and poisoned target mode. The intermediate target mode samples were unstable.

From the EDX results, slightly higher oxygen contents were observed for the unstable thin films and from the XRD measurements a stronger (111) texture for the unstable thin films was observed.

The results indicate that stable thin films can be achieved by producing them in either metallic or in poisoned target mode, at a main chamber pressure of around  $2,2E-03$  mbar.

### 7.3. Power series

The following experiments have been conducted with the intention of finding out how the target power is affecting the titanium nitride thin film resistivity drift over time. In this research, the focus will be on evaluating samples from the metallic and poisoned target mode at different target powers. To investigate the film stability, the sheet resistivity was measured as function of time and an accelerated life test was conducted. Additional EDX measurements were taken and a characterization of the thin film residual stress was performed.

#### 7.3.1. Deposition system characteristics

Before the depositions were started, characterization curves at 150W, 300W, 450W, 600W and 750W were extracted. Figure 54 shows the characteristic curves. The total flow (Ar+N<sub>2</sub>) was kept constant at 19 sccm. The various argon/nitrogen combinations were (Ar=19 sccm : N<sub>2</sub>=0 sccm), (18:1), (17:2), (16:3), [...], (5:14), (4:15).

The goal was to determine where the metallic and poisoned target modes are located with respect to the nitrogen flow. Furthermore, in this way the range of attainable powers were surveyed before the experiment was started. Based on these characteristic curves, the nitrogen flow was chosen for the different target powers, so that the depositions will be at roughly similar points on the characteristic curves with respect to the metallic and poisoned target modes.

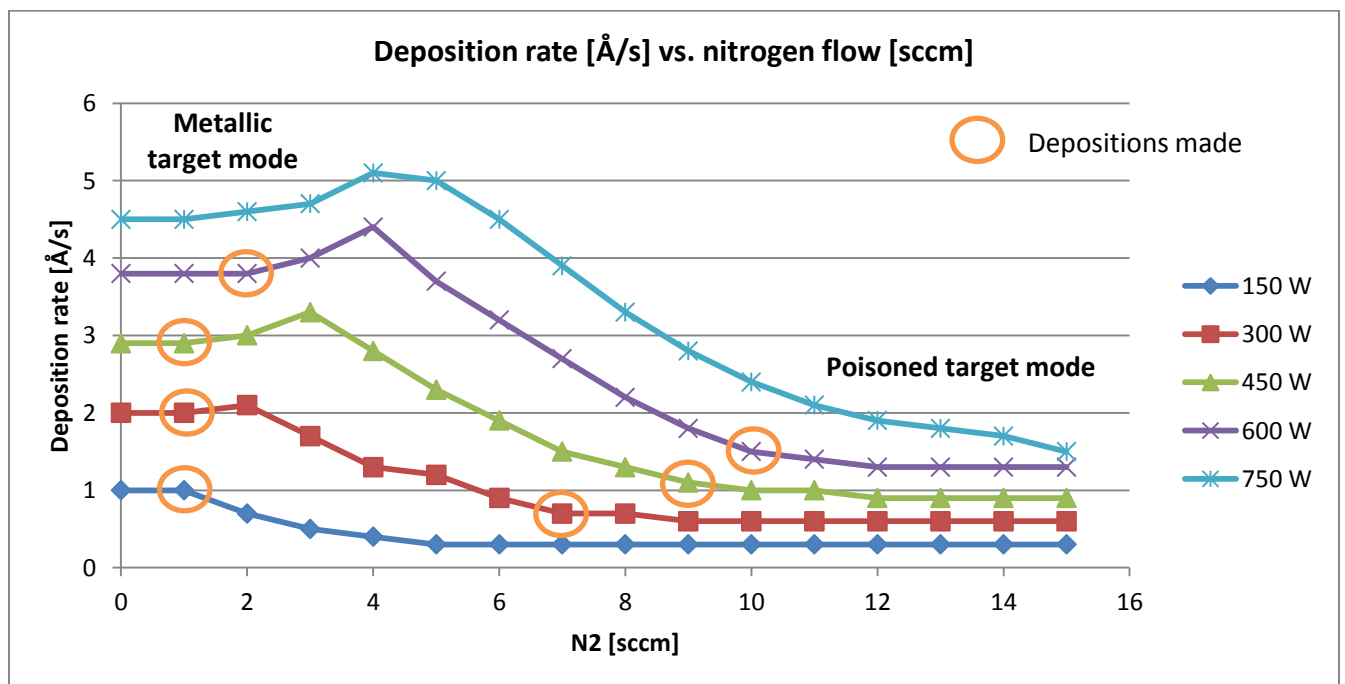


Figure 54 – Characteristic curves for N<sub>2</sub> [sccm] vs. deposition rate [Å/s]

Figure 55 shows the main chamber pressure vs. “N<sub>2</sub>/total flow ratio”. It can be observed that the main chamber pressure is increasing with an increasing “N<sub>2</sub>/total flow ratio”. This effect has to be

counteracted during the deposition by adjusting the argon flow so the main chamber pressure will be set to the desired level.

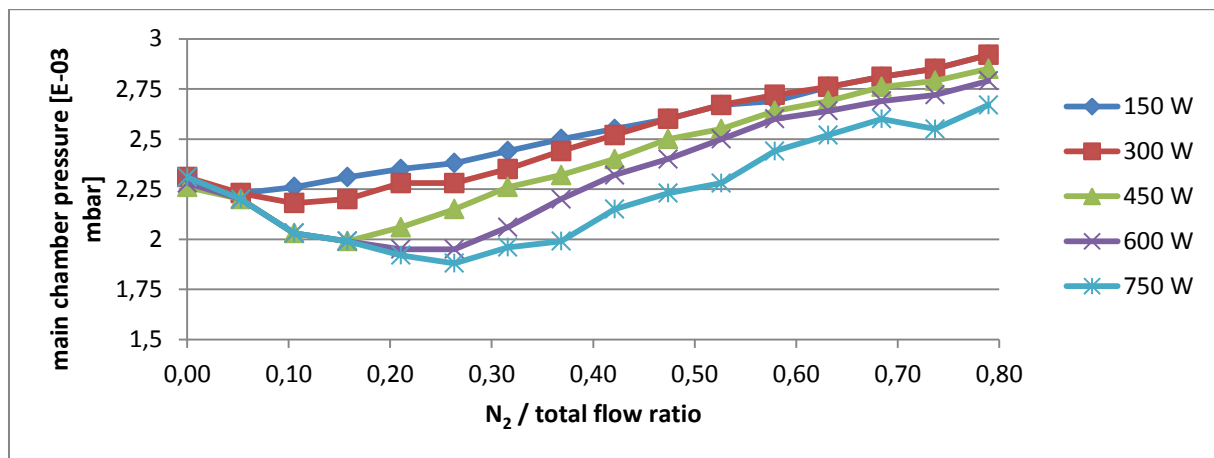


Figure 55 – Main chamber pressure [E-03 mbar] vs. N<sub>2</sub>/total flow ratio

### 7.3.2. Depositions

Figure 56 and figure 57 show the adjusted deposition parameters for the produced samples. Overall, it was important to keep the pressure at a low level (around 2,2E-03 mbar). For this the argon flow was adjusted manually during the deposition. Samples at 750 W were not produced due to technical problems in that region, which were causing a shut-down of the deposition system. The poisoned mode sample for 150W also created challenges and due to an extremely low deposition rate it was decided to cancel it. It should be mentioned that samples DC-49 and DC-55 are coming from the “nitrogen series 300W” experiments (see page 47).

| Sample | Date     | Power [W] | Argon [sccm] | Nitrogen [sccm] | Main chamber pressure [mbar] | Thickness AFM (400 nm desired) | Target state  |
|--------|----------|-----------|--------------|-----------------|------------------------------|--------------------------------|---------------|
| DC-59  | 04.04.14 | 150       | 18           | 1               | 2,20-2,26E-03                | 378 nm                         | Metallic mode |
| DC-55  | 26.03.14 | 300       | 19           | 1               | 2,18-2,20E-03                | 299 nm                         | Metallic mode |
| DC-49  | 20.03.14 | 300       | 9            | 7               | 2,18-2,26E-03                | 339 nm                         | Poisoned mode |
| DC-57  | 02.04.14 | 450       | 19           | 1               | 2,20-2,23E-03                | 308 nm                         | Metallic mode |
| DC-63  | 07.04.14 | 450       | 8            | 9               | 2,20-2,31E-03                | 282 nm                         | Poisoned mode |
| DC-61  | 04.04.14 | 600       | 18           | 2               | 2,23-2,26E-03                | 310 nm                         | Metallic mode |
| DC-62  | 02.04.14 | 600       | 6            | 10              | 2,20-2,32E-03                | 323 nm                         | Poisoned mode |

Figure 56 – Produced samples with deposition parameters

| Fixed parameters | Value(s)     |
|------------------|--------------|
| Desired pressure | 2.2E-3 mbar  |
| Base Pressure    | 5,00E-5 mbar |
| Temperature      | RT           |
| Thickness        | 400 nm       |
| Tooling factor   | 27           |

Figure 57 - Parameters for the pressure series variation

Detailed information about the substrates used and their placement can be found in appendix “E1. Substrates and placement – power series” page 170.

### 7.3.2.1. Deposition parameters during production

During the deposition of the samples, the main chamber pressure [mbar], deposition rate [ $\text{\AA}/\text{s}$ ], and cathode voltage [V] were observed. Figure 58 shows the main chamber pressure vs. time for the produced thin films. It was observed, that the samples deposited in the poisoned target mode have a higher pressure increase over time compared to the samples deposited in the metallic target mode. Also, above  $N=10$  sccm it was not possible to adjust the main chamber pressure for the poisoned target mode, because the argon flow was becoming too low to sustain the plasma.

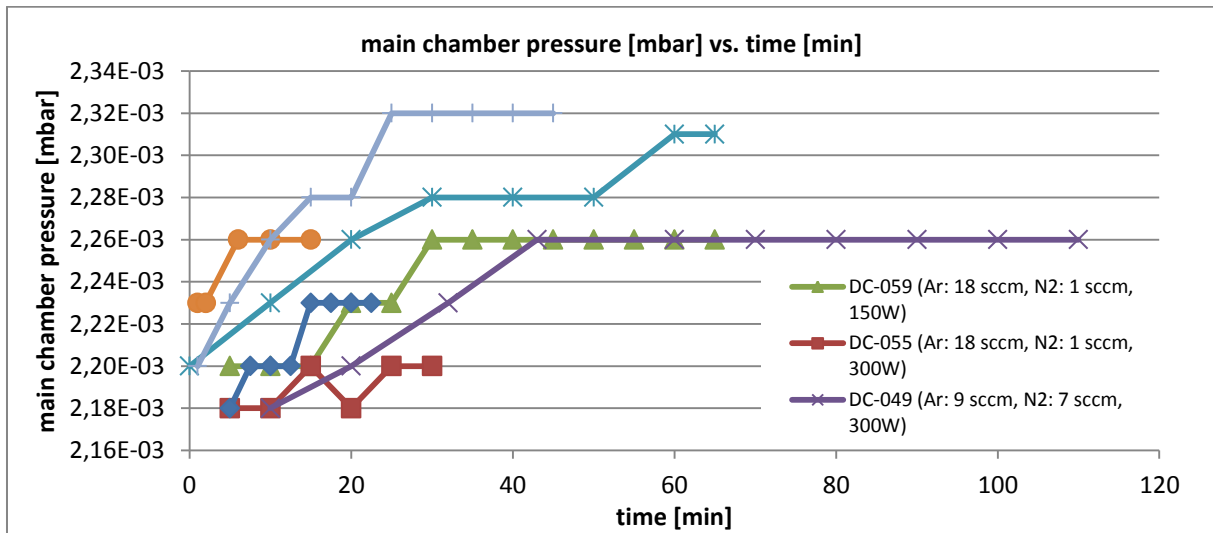


Figure 58- main chamber pressure [mbar] vs. time [min] for metallic target mode from 150W to 600W

Figure 59 shows the deposition rate [ $\text{\AA}/\text{s}$ ] vs. time [min] for the evaluated samples. Generally, it can be seen, that an increase in power will increase the deposition rate for both metallic and poisoned mode sputtered samples, which will decrease the overall deposition time.

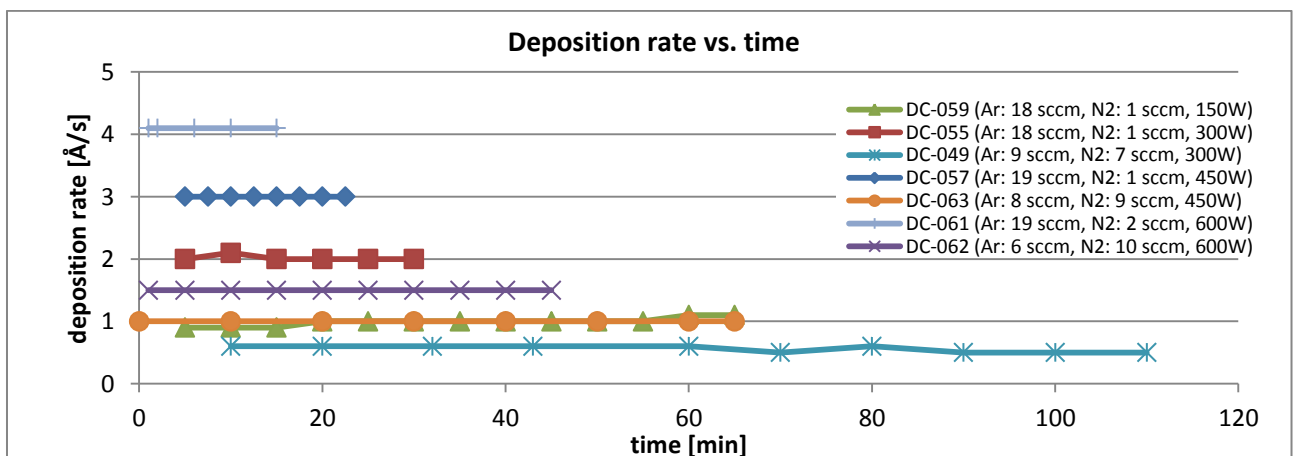


Figure 59 – Deposition [ $\text{\AA}/\text{s}$ ] rate vs. time [min]

Figure 60 shows the cathode voltage [V] versus time [min] for the produced samples. It can be observed that the cathode voltage is increasing with increasing power. Also an increase in  $N_2/\text{total}$

flow ratio seems to increase the cathode voltage, which might be connected to target poisoning as seen in the nitrogen series (300W) figure 47 page 49. Overall, the cathode voltage is stable throughout the depositions. Note that sample DC-049 had been produced during the “nitrogen series (300W)” experiments. More drift over time is observed for samples from that experimental series with regard to their cathode voltage compared to the samples produced during the power series experiments. The target used during the power series experiments is just half as thick and mounted on a copper back plate, which might explain the more stable cathode voltage.

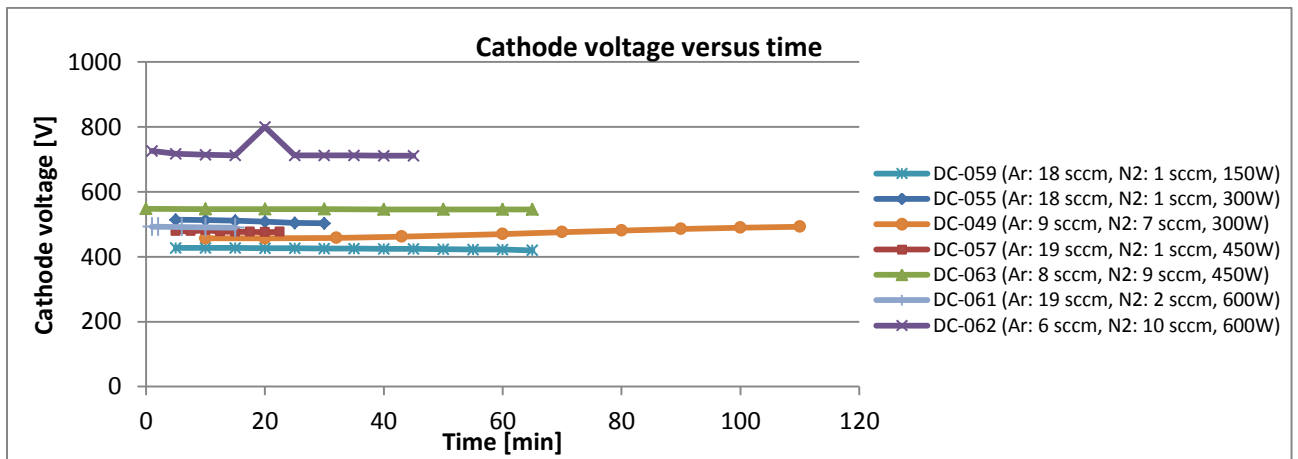


Figure 60 - cathode voltage [V] vs. time [min]

Further details about the data for the main chamber pressure, deposition rate and cathode voltage can be found in appendix “E2. Sample deposition data observations” page 171.

### 7.3.3. Resistivity

From figure 61 it can be observed, that an increase in target power results in a decrease of the as-deposited resistivity for both metallic and poisoned target mode. The lower resistivity could indicate that the thin films become denser with fewer defects at higher target power.

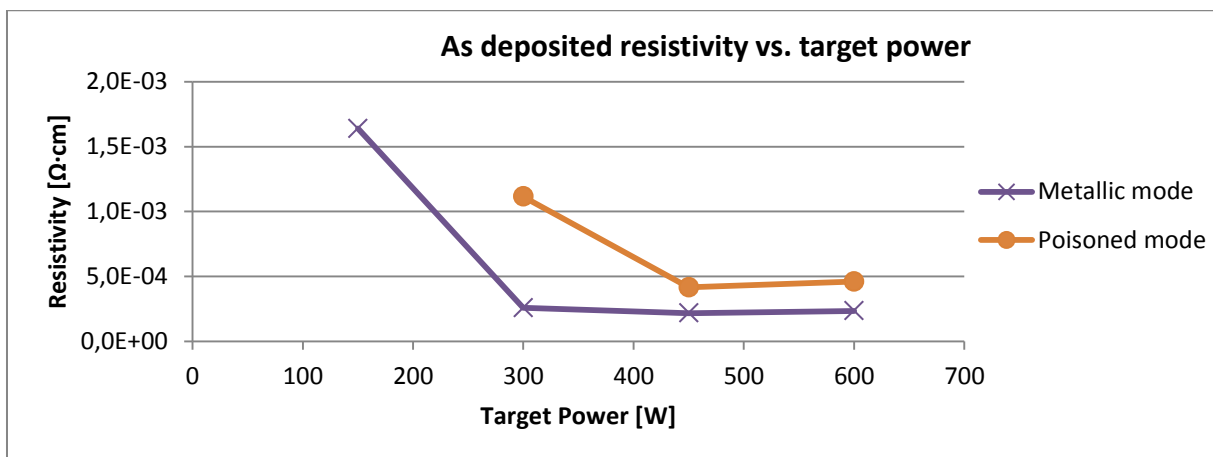


Figure 61 – As-deposited resistivity [Ω·cm] vs. target power [W]

Figure 62 shows the accelerated life time experimental results at 100 °C performed in ambient atmosphere. It can be observed, that sample DC-59, which was produced at 150 W in metallic target mode, is unstable with a resistivity drift of 517% over the time frame of 18 hours at 100 °C.

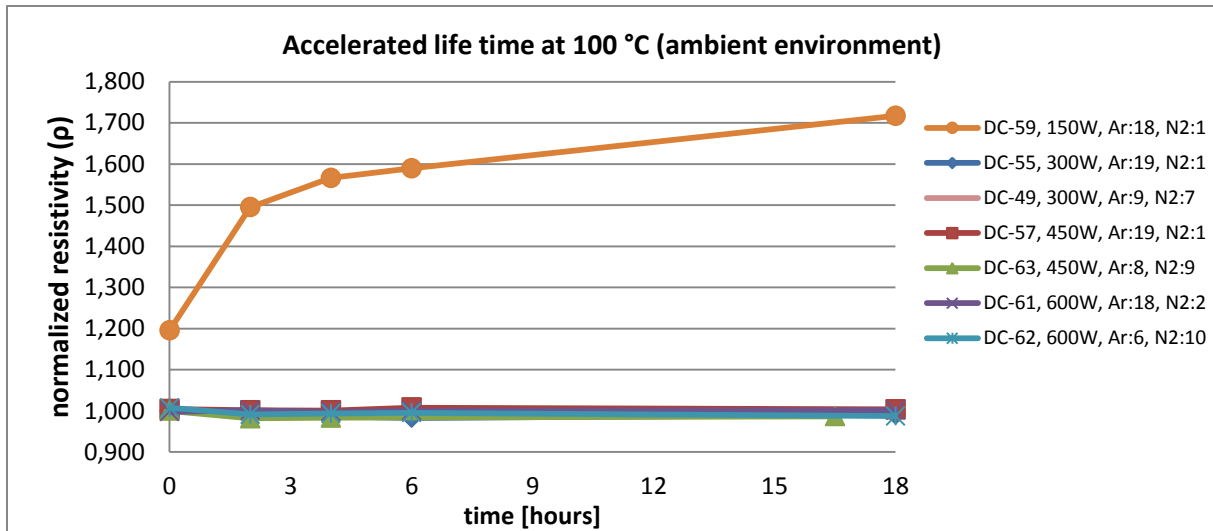


Figure 62 - Accelerated life time at 100 °C (ambient environment)

Figure 63 shows a zoomed in version on the stable samples of the accelerated life time experiments from figure 62. It seems that both poisoned mode and metallic mode samples perform well within a 2% resistivity drift window at 100°C for 18 hours in ambient atmosphere. The resistivity values from t=0h to the respective times seen in figure 63 are DC-55 (metallic): -0,88% ; DC-49 (poisoned): -1,8% ; DC-57 (metallic): 0,08% ; DC-63 (poisoned): -1,3 ; DC-61 (metallic): 0,3% and DC-62 (poisoned): -2%.

Based on the data the poisoned target mode samples have a larger resistivity change compared to the metallic target mode samples.

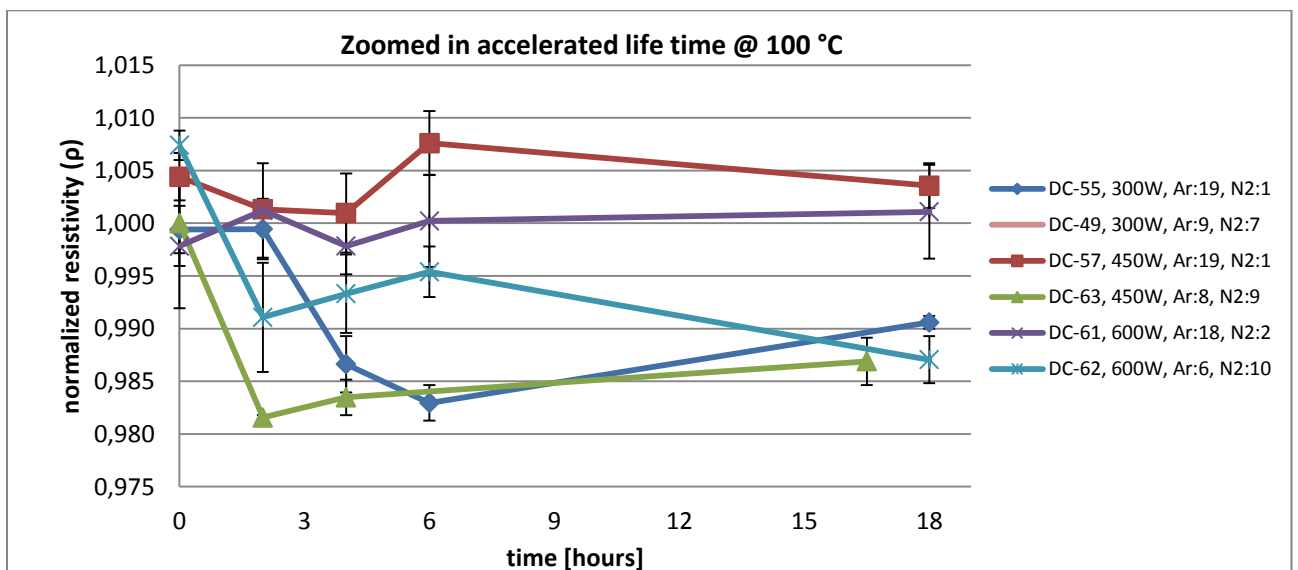


Figure 63 - Zoomed in accelerated life time @ 100 °C

Figure 64 shows the resistivity stability at room temperature in ambient atmosphere for up to 30-45 days. Also, here it can be observed that sample DC-59 (150W, metallic mode) is unstable with a resistivity drift of 34% over the time frame of 30 days. Due to a production error only one substrate of DC-63 existed, which was used for the accelerated tests.

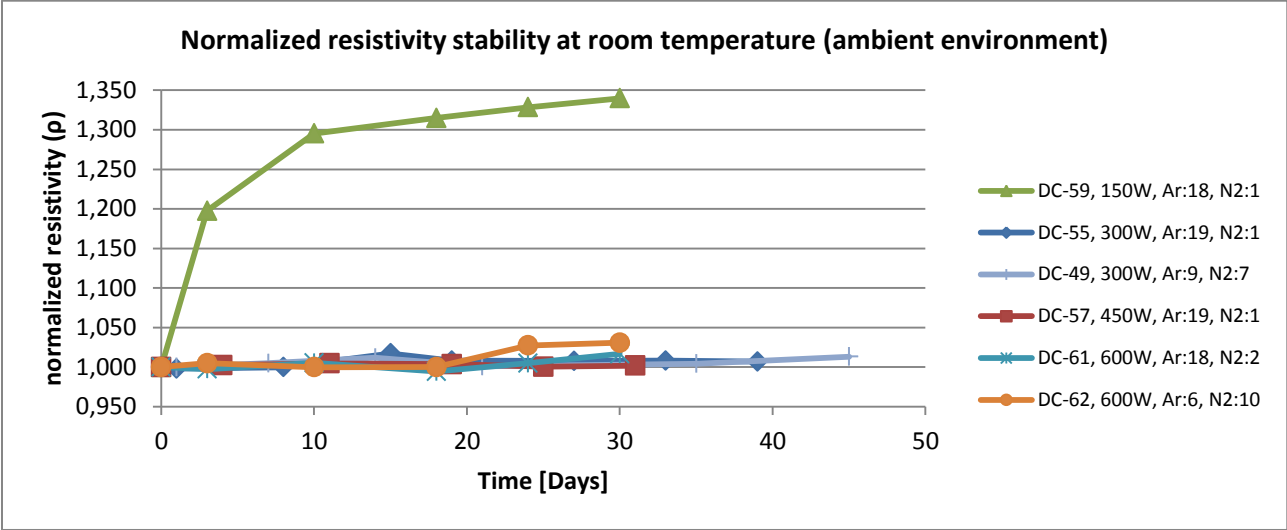


Figure 64 – Normalized resistivity stability at room temperature (ambient environment)

Figure 65 shows a zoom-in on the stable samples from figure 64. It can be observed that all samples except DC-62 (600W, poisoned mode) are stable within a 2% resistivity drift window. For DC-62, a generally larger measurement error has been observed, which could indicate a higher sensitivity with regard to the four point probe placement for this particular sample. The resistivity drift value from t=0days to the respective times are DC-55=0,7% @30 days ; DC-49=1,3% @45 days ; DC-57=0,19% @ 31 days; DC-61=1,7% @30 days ; DC-62=3,1% @30 days. Also at room temperature the poisoned target mode samples seem to be more unstable compared to the metallic target mode samples.

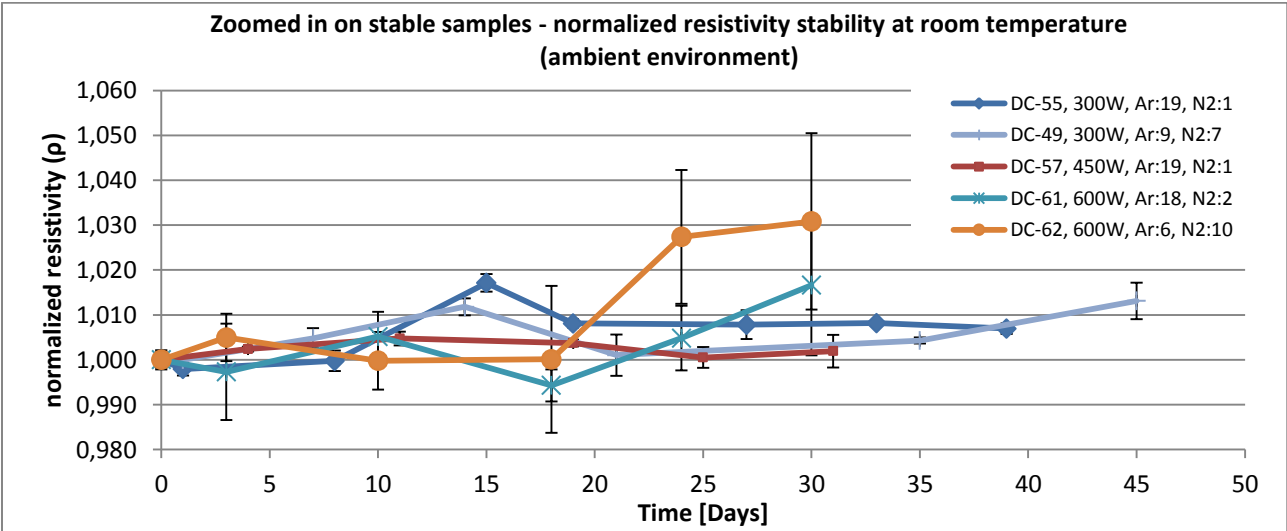


Figure 65 – Normalized resistivity stability at room temperature (ambient environment) (zoomed in on stable samples)

The next step was to increase the accelerated life test temperature from 100 °C to 200 °C for the tested samples in figure 65. Note that at this point the maximum achievable testing conditions were at 200 °C. Sample DC-59 (150W, metallic mode) was excluded of this research because it already proofed unstable at 100 °C.

Figure 66 shows the resistivity stability results at 200 °C performed at ambient atmosphere. It can be observed that all samples have an initial large resistivity drift, but after about 56 hours of annealing the resistivity drift stabilizes. There seems to be a trend that the poisoned mode samples resistivity is initially decreasing and the metallic mode samples resistivity is initially increasing.

Both poison and metallic mode samples perform well within the 2% resistivity drift window for the time frame from t=56h to t=358h of 358 hours (about 12,5 days) at 200 °C.

It can be seen that samples DC-62 (600W, poisoned mode), DC-63 (450W, poisoned mode) and DC-55 (300W, metallic mode) have the lowest resistivity drift with -0,12%, 0,31% and 0,31% respectively. This indicates that the target power is not necessarily the controlling factor with regard to the resistivity stability.

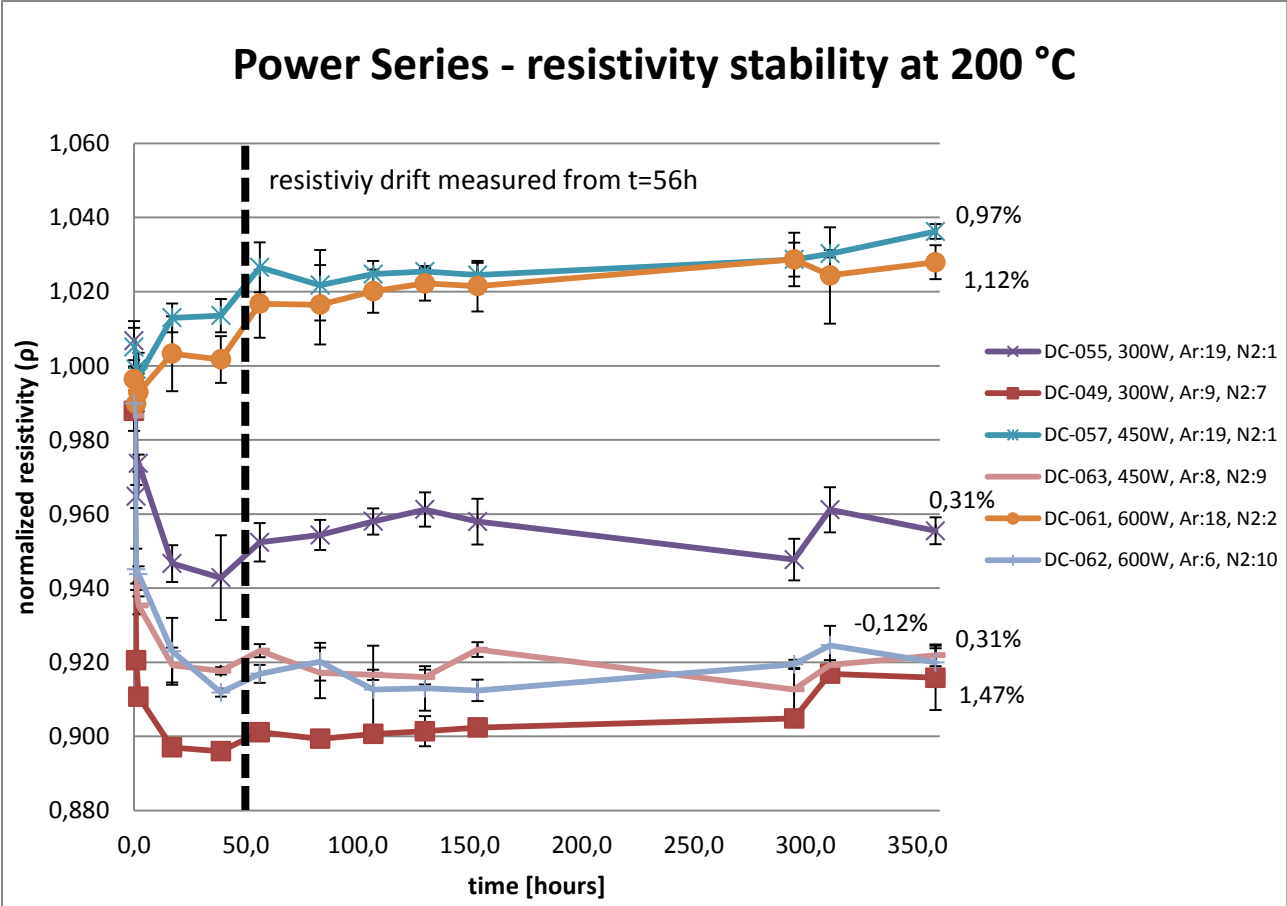


Figure 66 - power Series - resistivity stability at 200 °C. Values on right side depict resistivity drift from t=56h to t=360h.

### 7.3.4. Atomic composition

Figure 67 shows the atomic concentration of the samples produced in metallic target mode from 150W to 600W. It can be observed that the unstable sample DC-59 (150W, metallic) is the only sample containing oxygen. It was previously observed from the pressure and nitrogen series experiments that the thin films containing more than 10% atomic concentration oxygen tend to have an unstable resistivity drift over time. Possible reasons for the elevated oxygen content for sample DC-59 could be the low deposition rates, that could result in relatively higher oxygen incorporation during the thin film growth from the background oxygen gas compared to the samples made at higher deposition rates.

Also, a smaller energy flux from the target to the substrate during the deposition at lower powers could indicate that the thin films are more unstable because of oxygen entering the thin film post deposition.

Note that sample DC-59 (150W, metallic mode) is on the intermediate target mode regime in figure 54 page 54, for which it was observed earlier during the nitrogen series (300W), that these samples are unstable with regard to their resistivity drift. It can be seen that for sample DC-55 (Ar:19sccm N<sub>2</sub>:1sccm, 300W), DC-57 (Ar:19sccm, N<sub>2</sub>:1sccm, 450W) and DC-61 (Ar:18sccm, N<sub>2</sub>:2sccm, 600W) no oxygen was detected. The nitrogen-to-titanium ratio is below 1 for the samples produced at 300W to 600W, which can be expected for the metallic target mode samples.

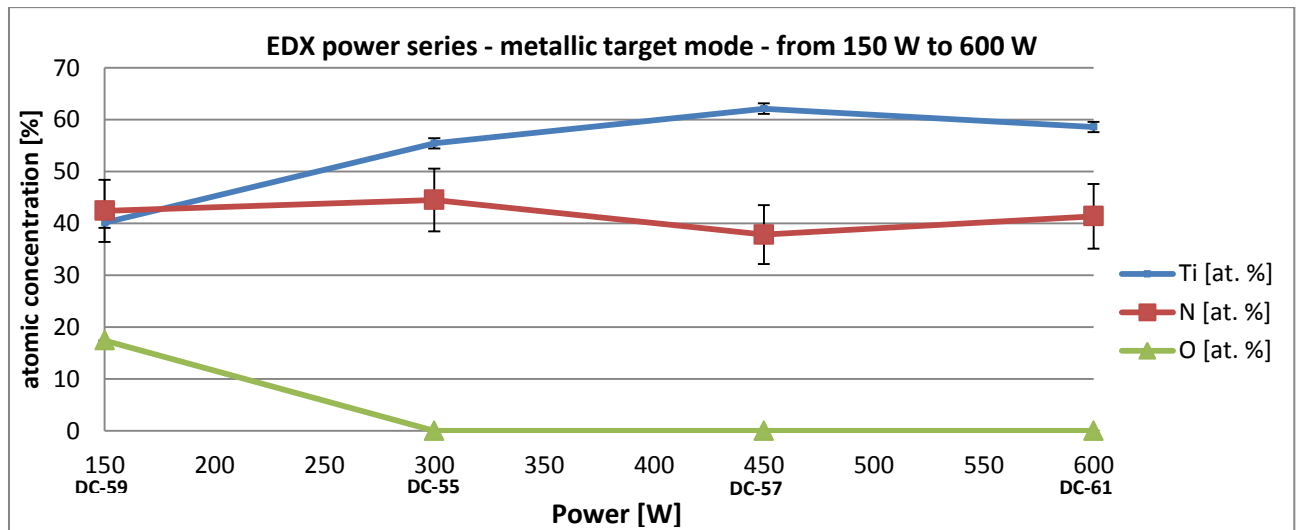


Figure 67– EDX power series - metallic target mode - power 150 W to 600 W

Figure 68 shows the EDX results for the stoichiometry evolution from metallic to poisoned mode for the samples produced at 300W, 450W and 600W. Generally, it can be observed that the nitrogen content is increasing from metallic to poisoned target mode, which is expected due to the higher nitrogen content of the reactive gas. Also, an increase in oxygen is observed for metallic to poisoned

mode samples, which might come from the increased amount of nitrogen gas reacting with the background oxygen gas. The titanium content decreases in each scenario from metallic to poisoned mode and the nitrogen-to-titanium ratio for the poisoned samples is always above 1, whereas the nitrogen-to-titanium ratio for metallic mode samples is always below 1. [46]

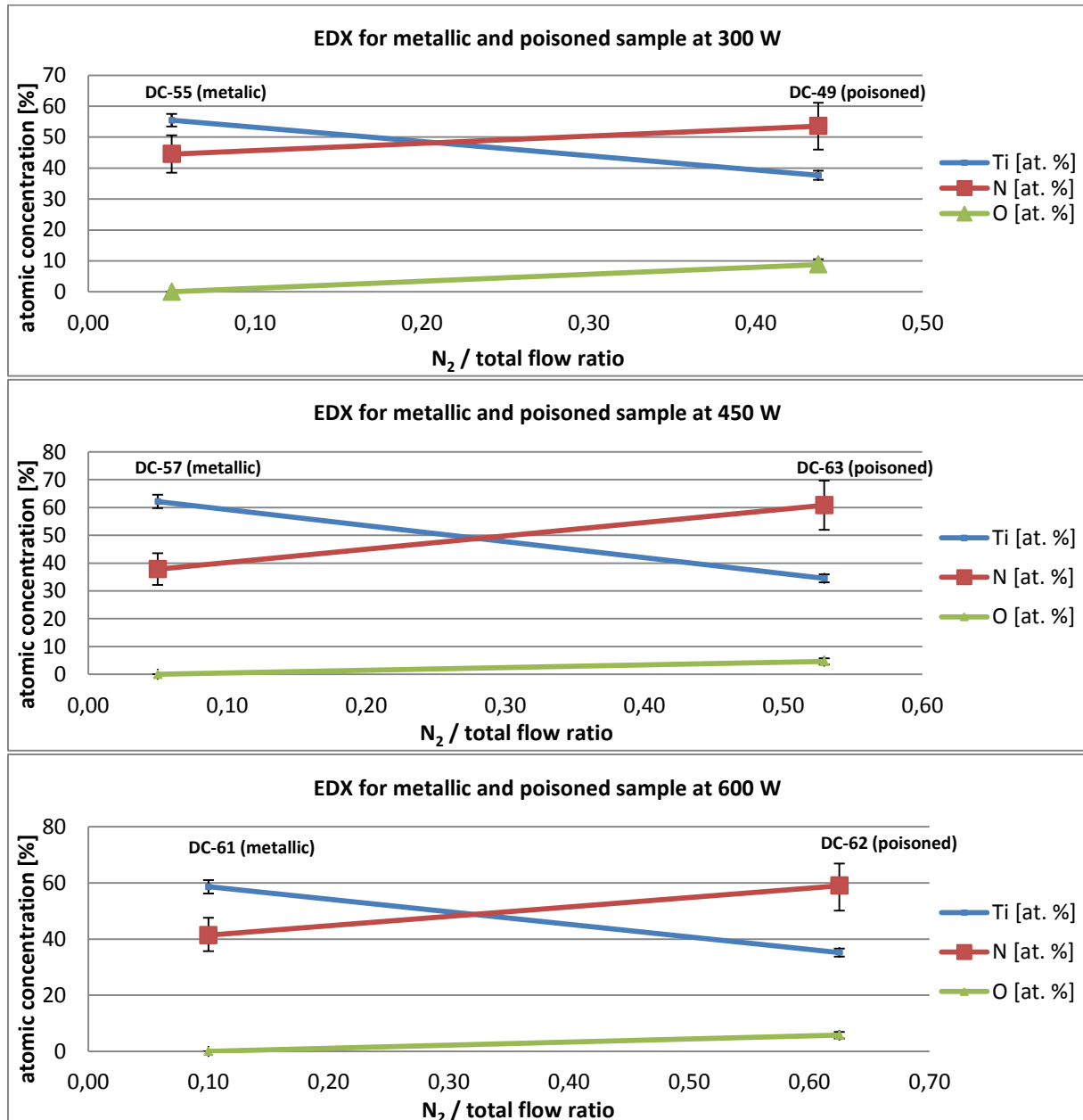


Figure 68– EDX for metallic and poisoned sample at 300W, 450W and 600W

Generally the thin film composition and resistivity performance seems to depend more on the working point situated on the characteristic curves from figure 54 page 54 (reactive gas composition) than the power supplied to the target.

### 7.3.5. Crystal structure

Figure 69 shows the XRD measurements performed by Kasper Thilasing-Hansen with the goal of analyzing the phase content of the thin films. A shift in texture from (111) to (200) crystal orientation is observed for metallic to poisoned target mode thin films. No correlation between the resistivity stability and crystal structure could be found because both samples with (111) and (200) crystal orientations show a stable resistivity, except DC-59, 150W, which shows a mixture of (111) and (200) crystal orientations.

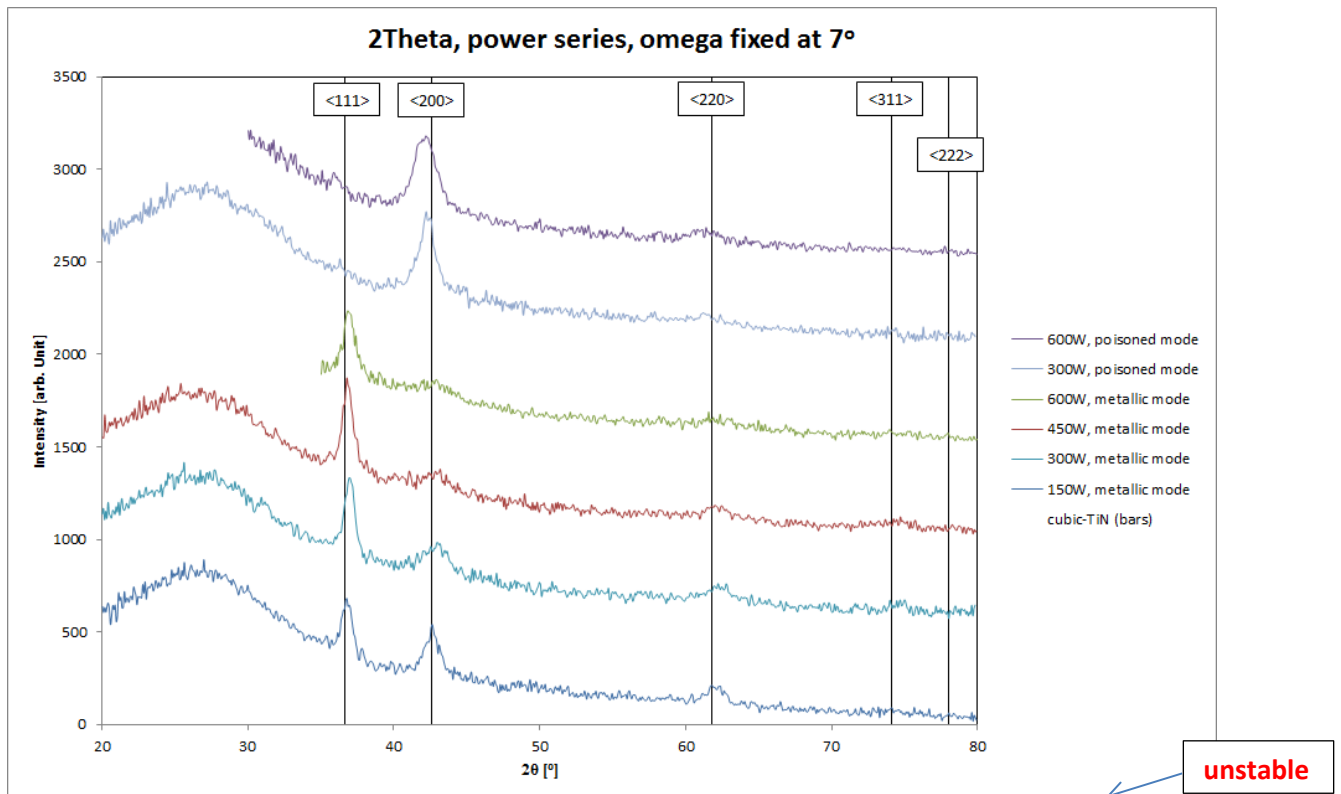


Figure 69 – XRD spectra - Grazing incident X-ray diffraction patterns ( $\omega=7^\circ$ ). The reflection angles from cubic TiN are shown as bars. The large “bumps” in the spectra stem from the amorphous BK-7 glass substrates.

### 7.3.6. Residual stress

The substrate curvature is measured before and after the deposition in order to determine thin film stresses. Figure 70 shows the thin film stress [GPa] versus sputter target power [W] for the produced samples. Due to technical and logistic problems, the poisoned mode sample for 300 W and 150 W are missing and still need to be produced.

The metallic mode samples show a tensile residual stress and have a (111) texture, while the poisoned mode show compressive residual stress and have a (200) texture. Furthermore, it can be seen that both tensile and compressive stresses are increasing with increasing target power. For the poisoned and metallic mode samples, the stress is highest at 600 W with -1,88 GPa and 0,85 GPa

respectively. The increase of residual stress with increasing power is believed to be connected with the increased kinetic energy bombardment of the incoming particles. Also, an increase in cathode voltage from metallic to poisoned mode could be related to the thin film stress (see figure 60 page 57).

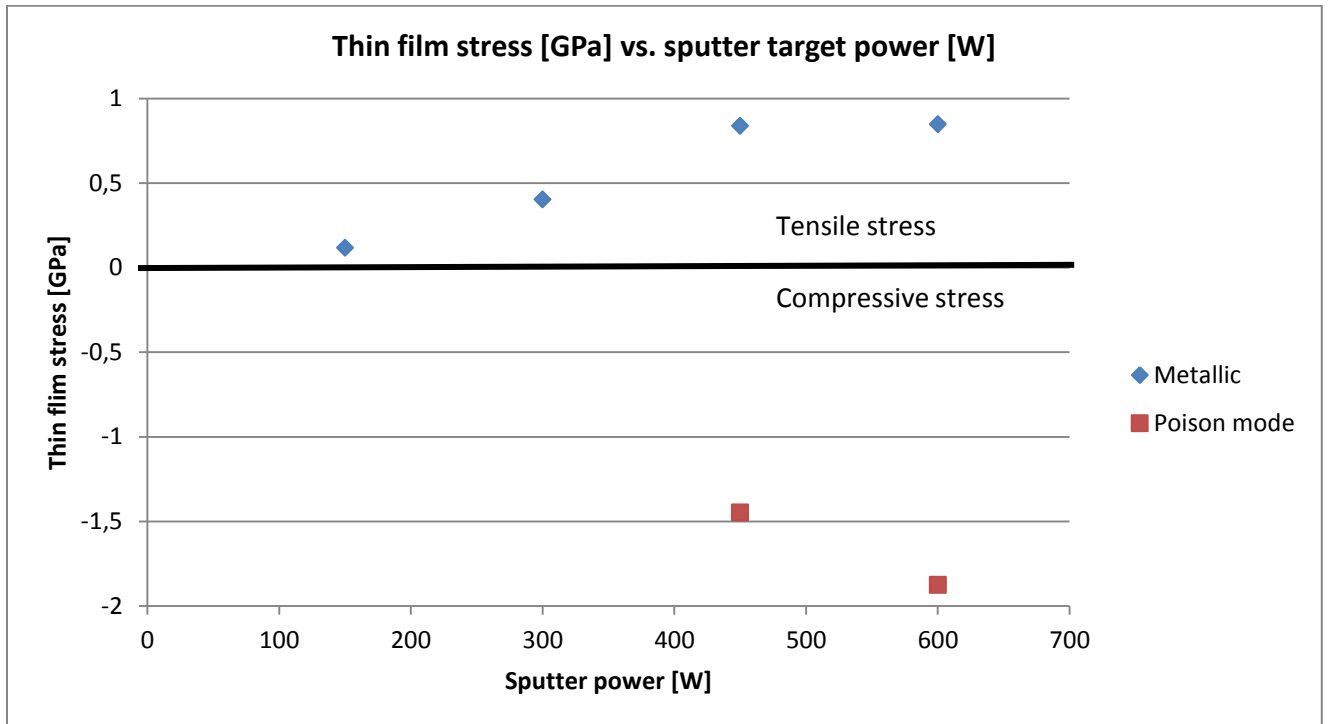


Figure 70 - Thin film stress [GPa] vs. sputter power [W]

### 7.3.7. Conclusion

Based on the results, it seems that the target power shows no controlling influence on the thin film resistivity stability. A stability test at 200 °C for 15 days in ambient atmosphere showed that the most stable samples were produced at 300W-metallic, 450W-poisoned and 600W-poisoned. The working point along the characteristic curves (figure 54 page 54) seems to be a more influencing factor with regards to the resistivity stability.

It was furthermore found that the residual stress is increasing with target power. The highest compressive and tensile stresses were found for the samples produced at 600 W.

For a final product the tolerance to the magnitude of the residual stress at higher powers has to be evaluated. From a mass production point-of-view the higher sputter target power is beneficial because it increases the overall production yield due to lower production times.

## 7.4. Nitrogen flow series at 600W

During the power series, it was found that both metallic and poisoned target modes yield stable thin films with regard to their resistivity drift over time at 200 °C at 300W, 450W and 600W.

In the first nitrogen series at 300W, on page 49 it was observed that the films in the transition between metallic and poison mode were unstable, which to be had researched more closely in order to get confirmation on these results. Also, during the power series, it was found that the stress is tensile for the films made in the metallic mode, while the films made in the poison mode had a compressive residual stress. The transitional area needed further study since stress measurements were not carried out in the first nitrogen series.

The following experiment investigates the intermediate target modes at a target power of 600W and a nitrogen flow at  $N_2=4, 6 \text{ \& } 8 \text{ sccm}$  as shown in figure 71. An extra sample at  $N_2=1 \text{ sccm}$  (metallic mode) was also produced. For nitrogen flows above  $N_2=10 \text{ sccm}$  the adjusted argon flow is getting too low in order to sustain the plasma at the desired pressure level of around  $2,2E-03 \text{ mbar}$ .

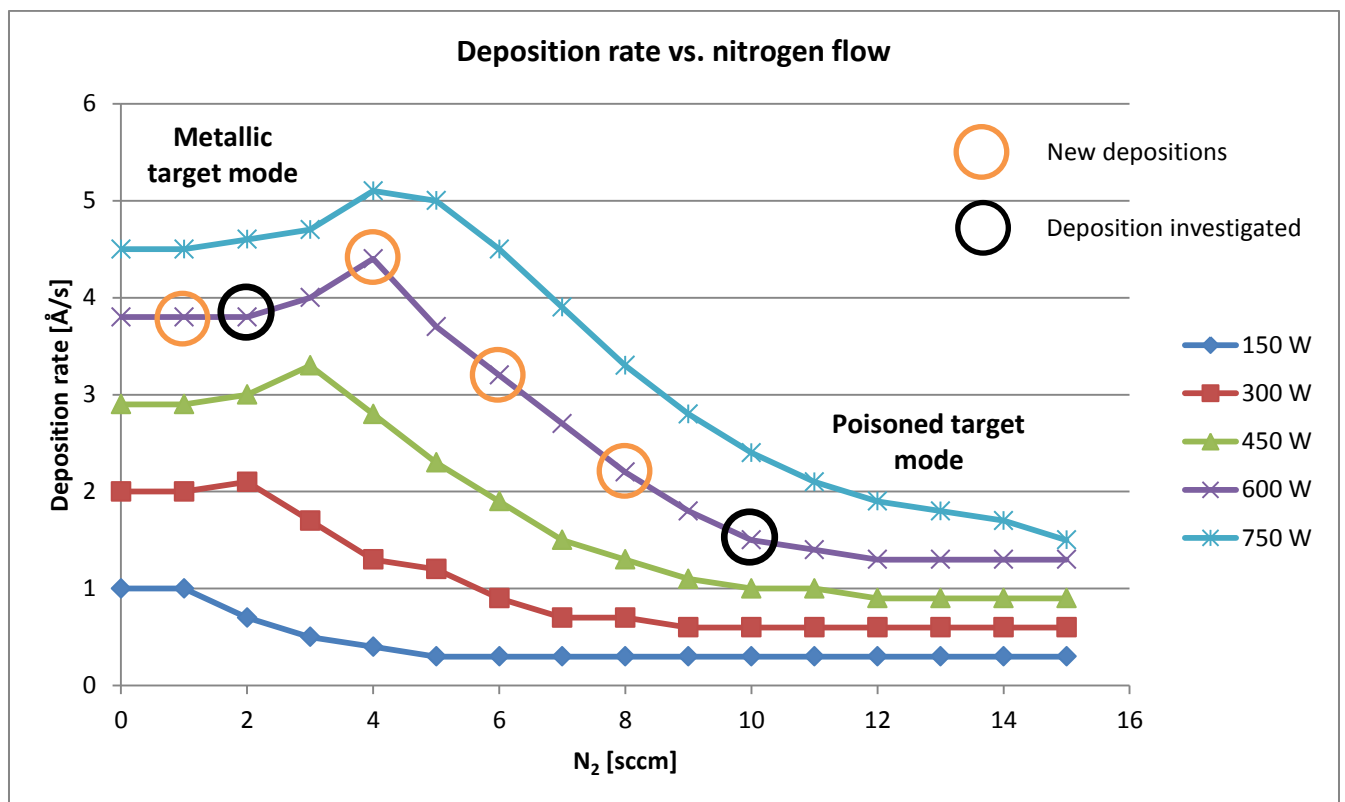


Figure 71 – Characteristic curves for  $N_2$  [sccm] vs. deposition rate [Å/s]

The setup and experimental procedures used during this experiment are similar to the one used during the power series experiments (see appendix “E1. Substrates and placement – power series” page 170).

### 7.4.1. Depositions

The deposition parameters for the experiment are given in figure 72 and figure 73.

| Sample | Production date | Argon [sccm] | Nitrogen [sccm] | Main chamber pressure [mbar] | Thickness AFM (400 nm desired) | Target state  | Comment                  |
|--------|-----------------|--------------|-----------------|------------------------------|--------------------------------|---------------|--------------------------|
| DC-060 | 04.04.14        | 19           | 1               | 2,20-2,23E-03                | 301 nm                         | Metallic mode | N <sub>2</sub> series II |
| DC-061 | 04.04.14        | 18           | 2               | 2,23-2,26E-03                | 310 nm                         | Metallic mode | Power series             |
| DC-062 | 02.04.14        | 6            | 10              | 2,20-2,32E-03                | 323 nm                         | Poison mode   | Power series             |
| DC-066 | 22.04.14        | 17           | 4               | 2,20E-03                     | 350 nm                         | Intermediate  | N <sub>2</sub> series II |
| DC-067 | 22.04.14        | 13           | 6               | 2,20E-03                     | 348 nm                         | Intermediate  | N <sub>2</sub> series II |
| DC-068 | 22.04.14        | 10           | 8               | 2,26E-03                     | 306 nm                         | Poison mode   | N <sub>2</sub> series II |

Figure 72 – Produced samples with deposition parameters

| Fixed parameters | Value(s)     |
|------------------|--------------|
| Target power     | 600 W        |
| Desired pressure | 2.2E-3 mbar  |
| Base Pressure    | 5,00E-5 mbar |
| Temperature      | RT           |
| Thickness        | 400 nm       |
| Tooling factor   | 27           |

Figure 73 - Parameters for the pressure series variation

#### 7.4.1.1. Deposition parameters during production

During the deposition of the samples, the main chamber pressure [mbar], deposition rate [ $\text{\AA}/\text{s}$ ], and cathode voltage [V] were observed. Figure 74 shows the main chamber pressure vs. time from metallic to poisoned target mode at 600W. It can be seen that the samples deposited in the poisoned target mode have a higher pressure increase over time compared to the samples deposited in the metallic target mode. For DC-67 and DC-68, the main chamber pressure was adjusted during the deposition by tuning the argon flow, causing the sharp decline seen on the graphs.

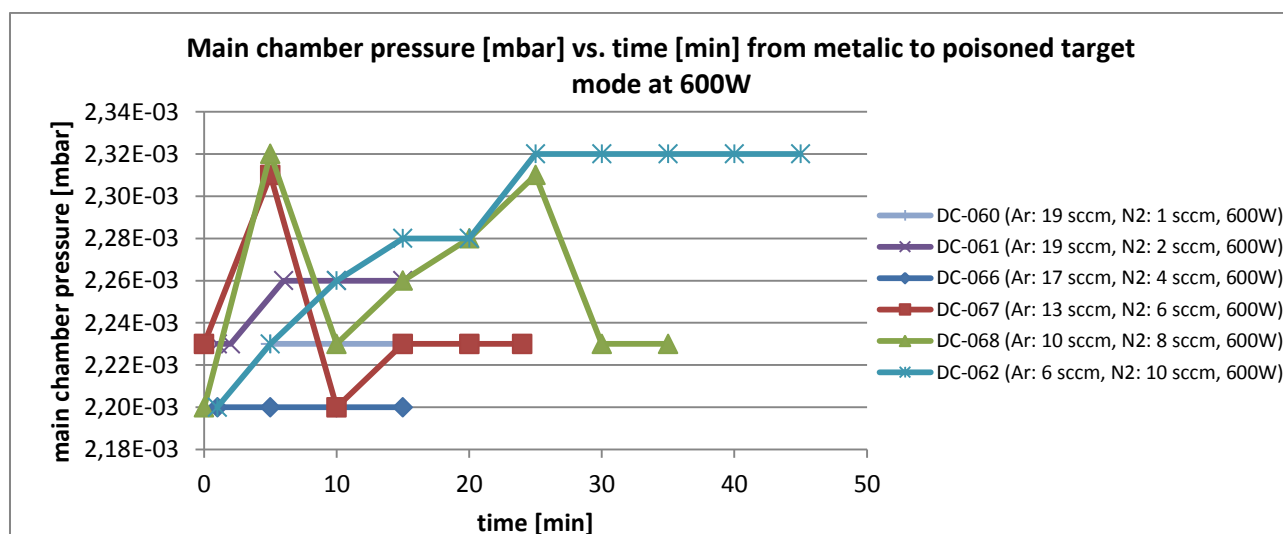


Figure 74 - Main chamber pressure [mbar] vs. time [min] at 600W

Figure 75 shows the deposition rate versus time for a deposition series including metallic, intermediate, and poisoned target modes at 600 W. Generally, the deposition rates of the samples produced in the poisoned target mode are lower compared to the metallic target mode. The impact of the target mode is clearly visible with regards to the deposition rate and thus the overall deposition time. The higher the N<sub>2</sub>/total flow ratio, the lower the deposition rate will be.

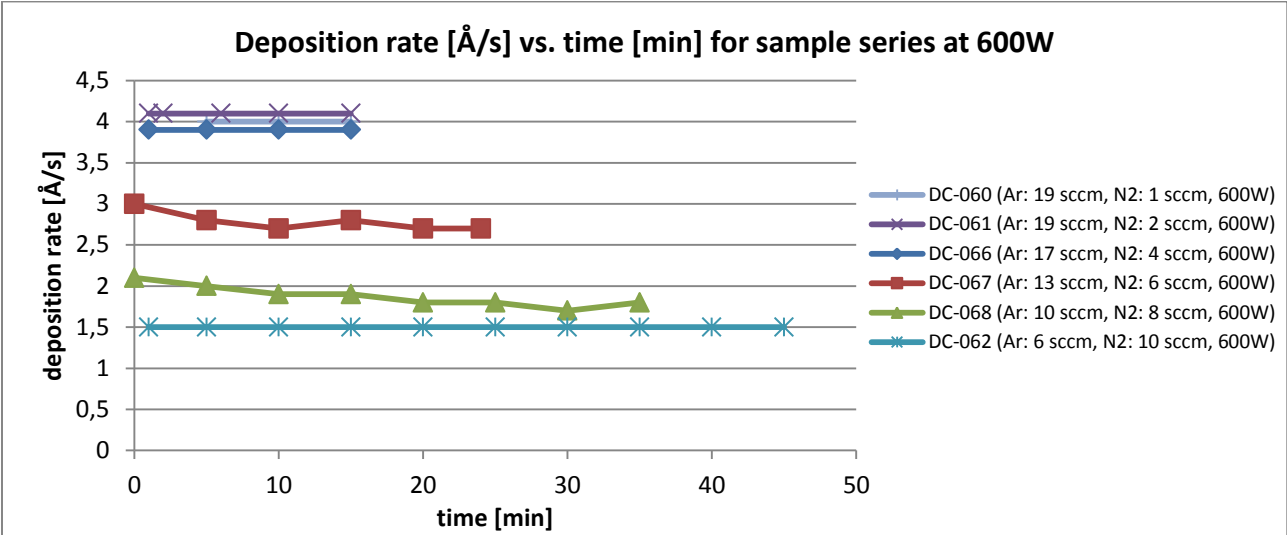


Figure 75 - Deposition rate vs. time series at 600W

Figure 76 show the cathode voltage versus time for the produced samples. It can be observed that the cathode voltage is increasing from metallic to poisoned target mode, yet overall it is rather stable throughout the deposition. It can be seen that for DC-62, which has the highest N<sub>2</sub>/total flow ratio, the cathode voltage is starting to be at the maximum of 800V, which also sets limitations concerning a nitrogen flow above 10 sccm at a main chamber pressure of around 2,2E-03 mbar.

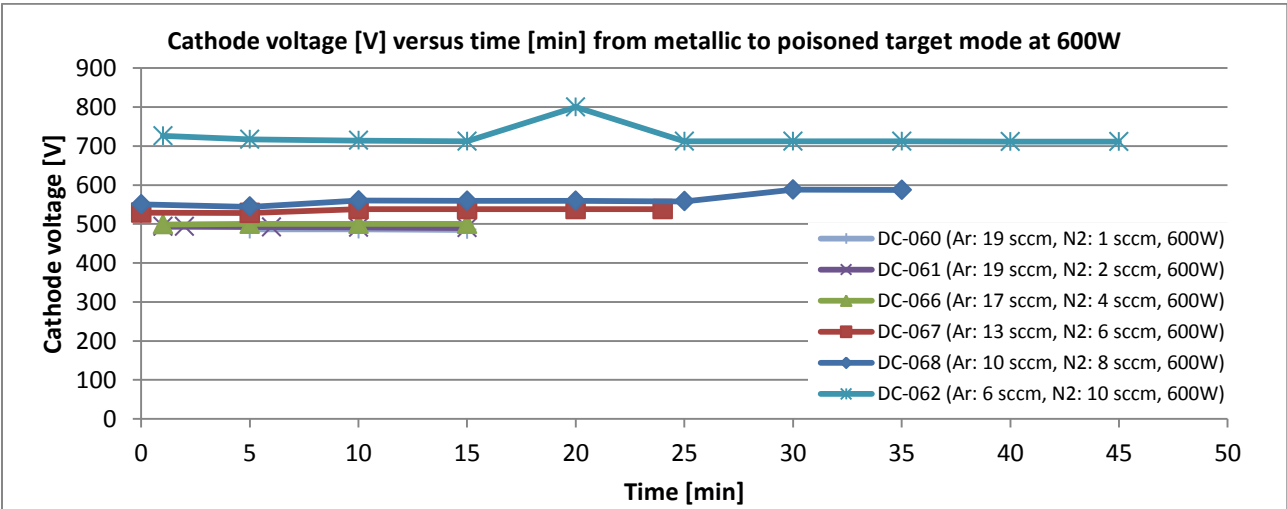


Figure 76 – Cathode voltage [V] vs. time [min]

### 7.4.2. Resistivity

The earlier nitrogen series showed that films made in-between the metallic and poisoned target mode are unstable. Figure 77 shows the resistivity drift over time at 200 °C in ambient atmosphere for up to 328-358 hours (13,5-15 days). It can be observed, that the two intermediate mode samples DC-66 ( $N_2=4$  sccm) and DC-67 ( $N_2=6$  sccm) are unstable with a resistivity increase of 52% and 62% respectively.

Sample DC-68 ( $N_2=8$  sccm) seems to be stable, which could indicate that the poisoned target mode starts around  $N_2=8$  sccm, when operating at a main chamber pressure of around  $2,2E-3$  mbar.

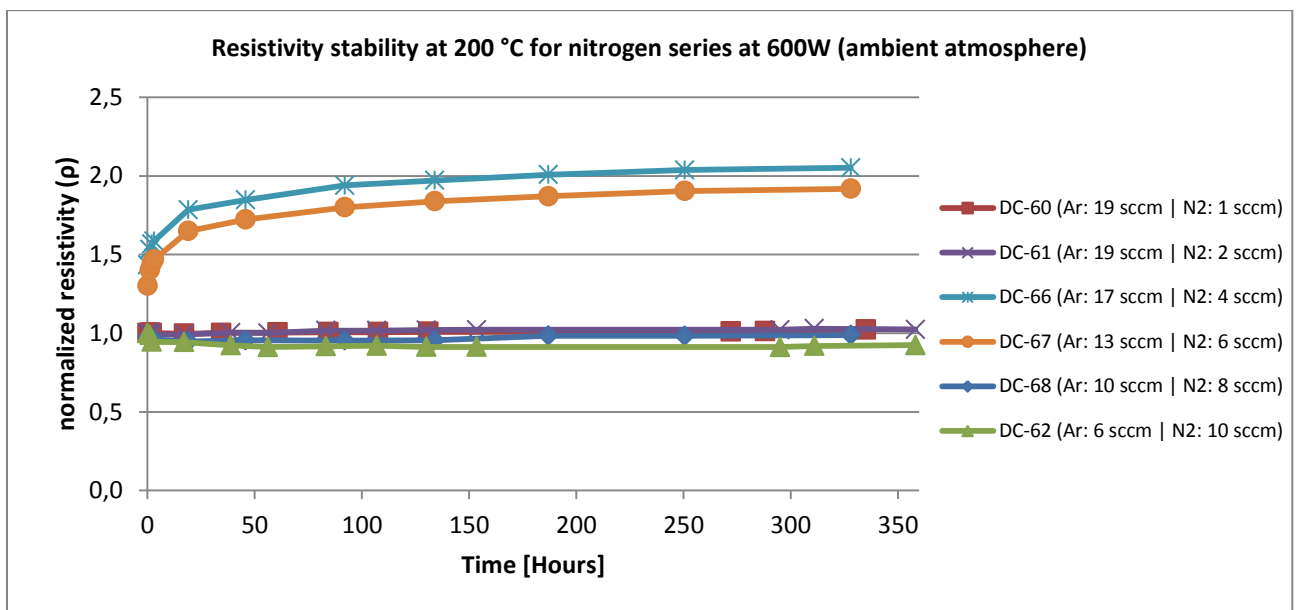


Figure 77 – Resistivity stability at 200 °C (ambient Atmosphere)

Figure 78 is a zoomed-in version of the stable thin films from figure 77.

It can be observed that there is an initial large drift for the poisoned mode samples and a smaller initial drift for the metallic mode samples, which both seem to slow down after about 56 hours of annealing at 200 °C similar to the power series experiments.

The thin films with the lowest resistivity drift are DC-60 (0,86%) and DC-61 (1,12%) in metallic target mode), and DC-62 (0,31%) in poisoned target mode. DC-68 has is semi-stable with a resistivity drift of 3,34% from  $t=56h$  to  $t=328h$ . Measured from  $t=0h$  to  $t=328h$  the drift is about 1,2%, yet the resistivity drift of DC-68 is a bit more unpredictable at this point and needs further testing.

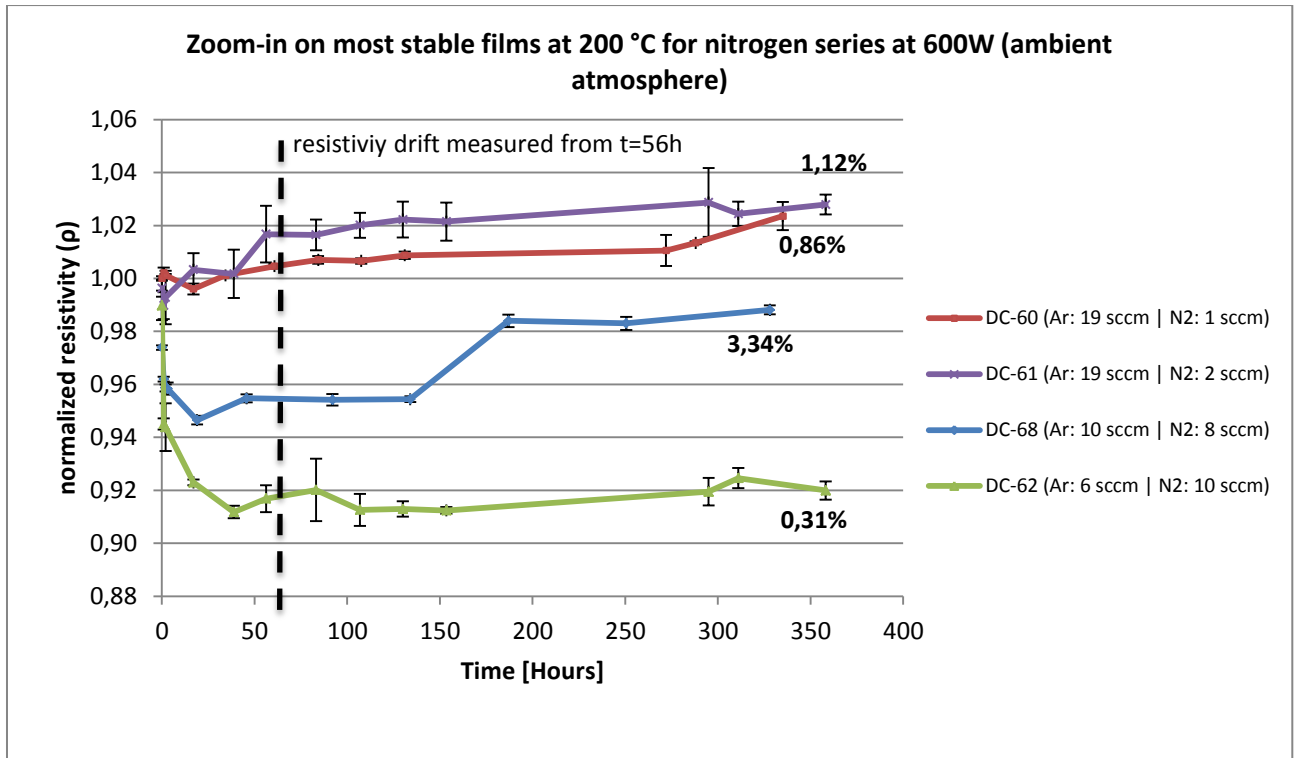


Figure 78 – Zoom-in on most stable films at 200 °C for nitrogen series at 600W (ambient atmosphere). Values on right side depict resistivity drift from t=56h to t=360h

Figure 79 shows the resistivity stability at room temperature for up to 16-30 days. Also, here it can be seen that the resistivity drift for the samples produced at the intermediate target mode is largest. DC-66 and DC-67 are both unstable with an resistivity increase of 11,8% and 7% respectively during 16 days. Sample DC-62 appears to be unstable, but note the large measurement errors of 1,5-2,0% for the last three data points. Overall, these results are similar to the results at 200 °C from figure 77.

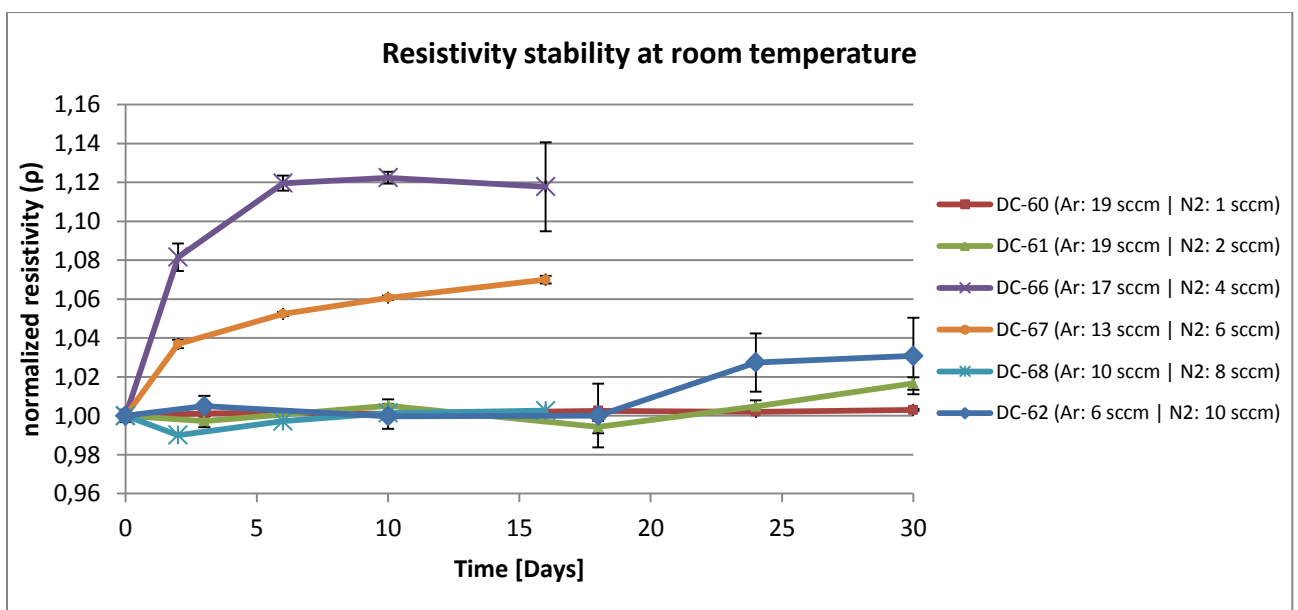


Figure 79 - Resistivity stability at room temperature

Figure 80 shows the as-deposited resistivity vs. nitrogen flow results for the nitrogen series at 300W and 600W. The thin films produced within the nitrogen region between the metallic and poisoned target mode showed unstable resistivity drifts. Based on these information, the nitrogen flow areas of  $N_2=4-6$  sccm for 600W and  $N_2=2-3$  for 300W should be avoided when running the depositions at a main chamber pressure of around  $2,2E-03$  mbar.

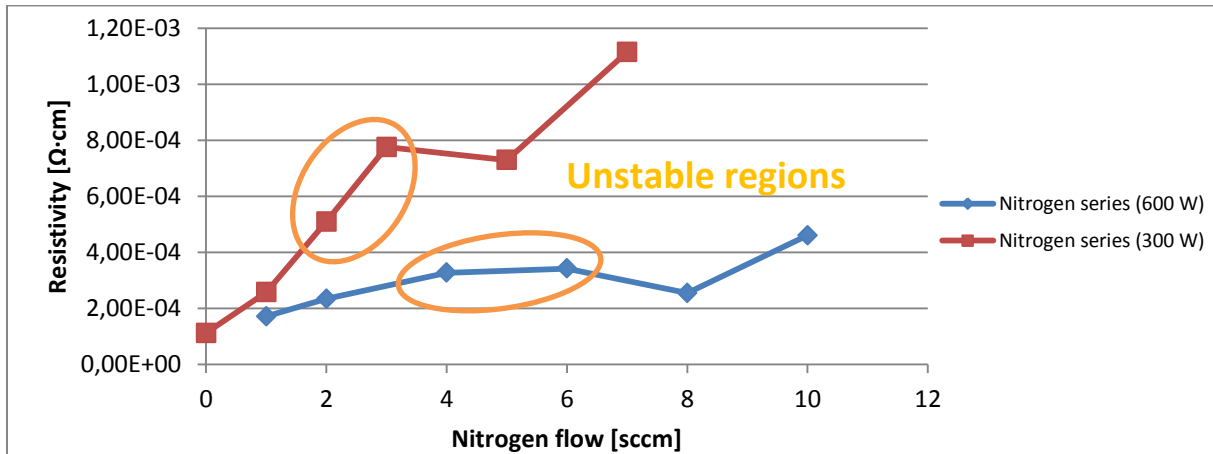


Figure 80 - Resistivity [Ω-cm] vs. nitrogen flow [sccm] and unstable regions

### 7.4.3. Atomic composition

Figure 81 shows the EDX results for the investigated samples. It can be observed that slightly higher oxygen contents were detected in the unstable thin films. This is similar to the results of the nitrogen series done at 300 W. DC-60 and DC-61 have a predominantly titanium stoichiometry with no measurable oxygen atomic concentration and low nitrogen-to-titanium ratios of 0,23 and 0,71, which is expected for the metallic mode sputtering. Similar to the nitrogen series at 300W, the nitrogen-to-titanium ratio is above 1 for the films deposited with a  $N_2$ /total flow ratio above 0,20. The nitrogen-to-titanium ratio stabilizes around 1,75. [46]

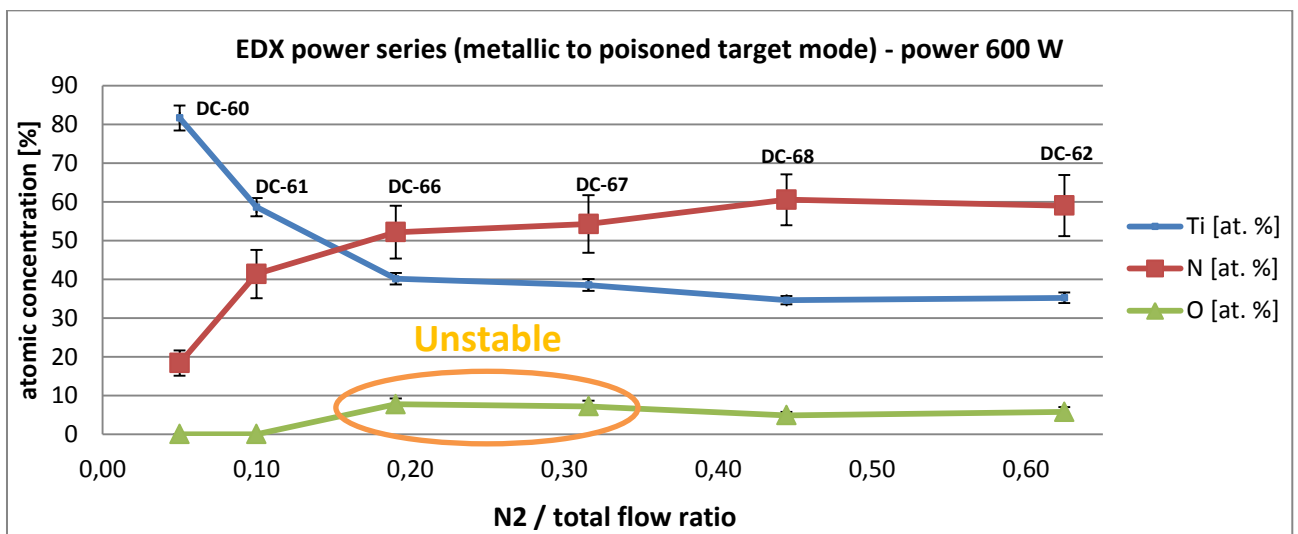


Figure 81 - EDX power series (metallic to poisoned target mode) - power 600 W

The XRD measurements yielded no clear indication of how far the texture is influencing the resistivity stability for the 600 W nitrogen series (see “F1. XRD – nitrogen series 600W” page 172).

#### 7.4.4. Thin film stress

The substrate curvature is measured before and after the deposition in order to determine thin film stresses. Figure 82 shows the thin film stress [GPa] versus sputter power [W] for the investigated samples.

It can be observed that the residual stress is lower for the samples produced at the intermediate target mode compared to the residual stress for samples produced in the metallic and poisoned target mode.

Overall, it can be seen that the nitrogen content during the deposition has a significant impact on the intrinsic thin film stress. From the results, it can be seen that the thin films with a low nitrogen/total flow ratios (metallic mode) have tensile stress, whereas for high nitrogen/total flow ratios the stress is compressive as seen before in the power series experiments. A maximum for the tensile stress can be observed for DC-61 at around 0,10 “N<sub>2</sub> flow/total flow”.

The very compressive stress levels for DC-62, which was produced in poisoned target mode, could be related to an increase in cathode voltage (see figure 76, page 67). Yet, the higher resistivity drift for intermediate flows cannot be connected to a high residual thin film stress. An educated guess could be that the lower residual stress of the intermediate samples is caused by a porous thin film structure, which prohibits the build-up of internal stress due to voids. This has to be investigated closer with the helium ion-microscope.

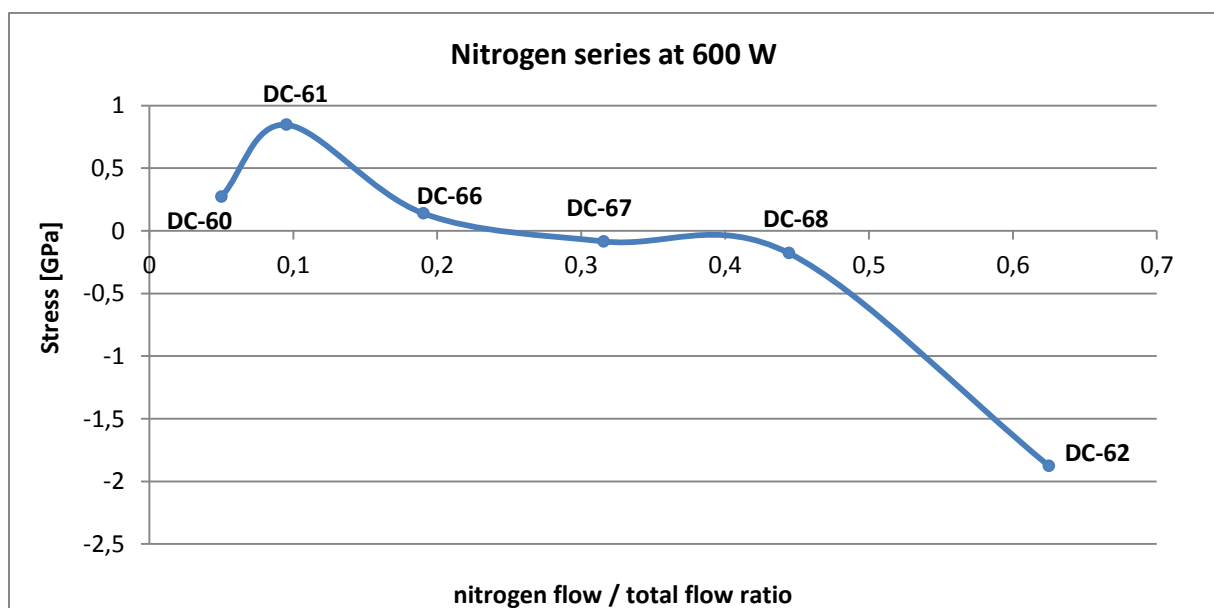


Figure 82 - Stress [GPa] vs. nitrogen flow / total flow ratio

#### 7.4.5. Conclusion

Overall, it was found that the behavior that was observed during the nitrogen series at 300W is similar to the one for 600 W.

It was found that DC-62 (maximum poisoned mode), which consists of about 59% atomic nitrogen, 35% atomic titanium, and 6% atomic oxygen, has the lowest resistivity drift from  $t=56\text{h}$  to  $t=358\text{h}$  with about 0,31%. This thin film also has the lowest deposition rate ( $1,5 \text{ \AA/s}$ ) of all the samples in the nitrogen series experiment at 600W.

Alternatively, DC-60 and DC-61, which were produced in the metallic target mode regime, show resistivity stabilities of 0,86% for  $t=56\text{h}$  to  $t=335\text{h}$  and 1,12% for  $t=56\text{h}$  to  $t=358\text{h}$  respectively. The depositions rates of these two samples are much higher with around  $4 \text{ \AA/s}$ , which would reduce the production time by about 67% from 45 minutes to 15 minutes per deposition.

It is suggested to increase the time frame for DC-068 (poisoned mode), to evaluate how the resistivity stability will develop after 360 hours at  $200^\circ\text{C}$  or higher.

Furthermore, it was found that the transitional samples are unstable. It still has to be analyzed why the transitional samples are unstable. For this, helium-ion microscope pictures of the thin film cross-section for evaluating the porosity might deliver the necessary answers, since the stress and XRD measurements were inconclusive.

## 7.5. Overall stability research conclusion and outlook

The goal was to produce a sensor material with a resistivity drift of below  $\pm 2\%$  at an operating temperature of up to  $250^\circ\text{C}$  during 150 hours.

The outcome of the experimental investigation was an analysis of the deposition equipment process parameter space, which yielded in the extraction of the optimal deposition parameters for stable titanium nitride thin films. The stable thin films have a resistivity drift of below  $\pm 2\%$ , at an operating temperature of  $200^\circ\text{C}$  during 360 hours, which is close to the target temperature of  $250^\circ\text{C}$ .

Figure 83 shows a resistivity stability map, which depicts the deposition rate [ $\text{\AA}/\text{s}$ ] vs. reactive nitrogen gas flow [sccm] for target powers of 150W to 750W. Note that the performed depositions are marked by a color code, which is rating the resistivity stability.

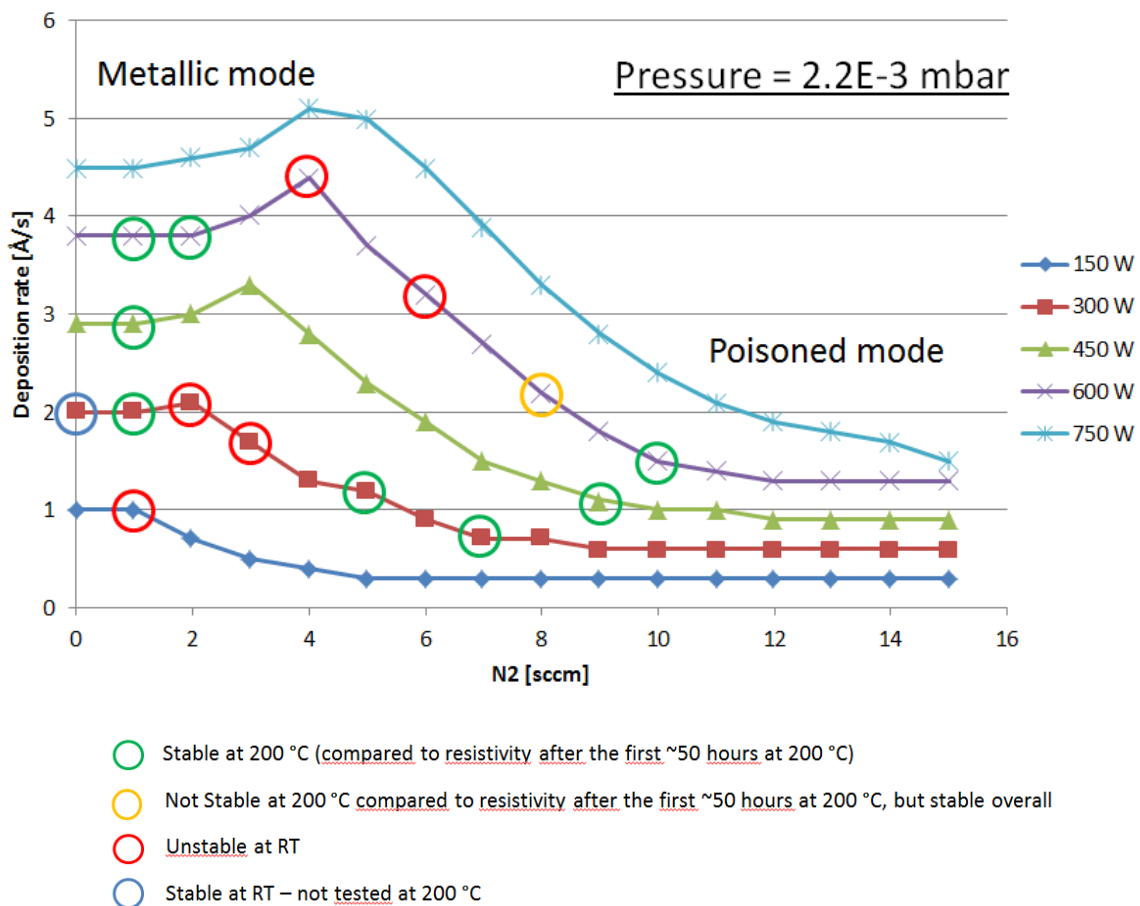


Figure 83 – Resistivity stability map based on the obtained experimental results from the pressure-, nitrogen (300W)-, power- and nitrogen (600W) series investigations

During the research it was found that a low deposition pressure results in thin films with a higher density and lower resistivity drift over time. In the case of the MCI NanoSYD deposition system, the main chamber deposition pressure was adjusted to be around  $2,2\text{E-}3$  mbar.

Three target modes were related to the resistivity stability performance of the thin films. The metallic target mode with a low nitrogen reactive gas flow and higher deposition rates resulted in thin films with good resistivity stability over time. The poisoned target mode with a high nitrogen reactive gas flow and lower deposition rates also resulted in thin films with good resistivity stability over time. Furthermore it was found that an initial annealing of the thin films helps to stabilize the resistivity drift after 56 hours.

The area between the metallic and poisoned target modes was resulting in thin films with a high resistivity drift over time at room temperature, thus this area should be avoided.

### **7.5.1. Outlook**

Overall the results are promising and research from other groups indicate that as a resistor the titanium nitride system can be operated at 350 °C for 10 years using a 800 nm thick oxide passivation layer. [45] In the case of this project, bottom contact electrodes can be developed on which the TiN thin film is deposited, followed by a thick oxide passivation layer deposited by RF-sputtering using the Cryofox system.

The missing depositions for 300W, 450W and 600W should be made in order to complete the resistivity stability map. Furthermore cross-section images with the soon to be installed helium-ion microscope should be conducted, to figure out why the transitional area is unstable.

Regarding the resistivity stability research, automated high temperature in-situ measurements should be designed and performed. The goal could be to measure several sample resistivity's' continuously at 300 °C or 400 °C for a time frame of 30 days or more. The automatization would decrease possible measurement errors and increase the repeatability of the measurements. Also the monitoring of a more exact resistivity drift development over time will be possible in that way.

The stability research procedures and experiments which were developed throughout this project can be applied to a new sensor material study. This will also significantly speed up the material research because most of the key equipment and procedures are operational.

## 8. Initial gauge factor experiments

The following chapter will provide an overview of the initial gauge factor experiments. The work is still on-going and there are unanswered questions with regard on how to optimally determine the strain and thickness of the samples.

### 8.1. DMA Q800 3-point bending

Figure 84 shows the commercial dynamical mechanical material analyzed (DMA Q800) and a standard 3-point bending clamp holder. The maximum force that can be applied is 18N with a force accuracy of  $10^{-4}$  N and a displacement resolution of 1 nm. Furthermore, the temperature can be adjusted between -150 °C to 600 °C with an isothermal stability of 0,1 °C. [47]



Figure 84 – DMA Q800 (DMA=dynamic mechanical analysis) (left), 3-point bending clamp (right) [47]

With the 3-point bending clamp, the DMA can measure the beam deflection and strain. For this a sample is center placed on stationary support under a moveable clamp. A pulling force is applied to the sample by the moveable clamp, causing the sample to bend downwards and resulting in a deflection and strain (see figure 85).

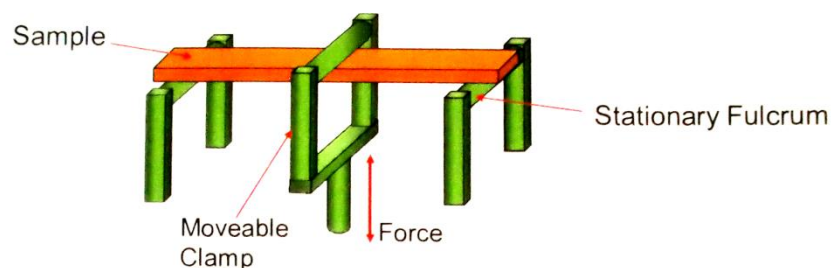


Figure 85 – 3-point bending setup [48]

The deflection and strain can also be calculated analytically by using the “Euler-Bernoulli” beam theory. The maximum deflection ( $w$ ) for a beam that is subject to a central point load can be expressed as [49]:

$$W \frac{L}{2} = \frac{PL^3}{48EI} \quad (\text{eq. 22})$$

Where,

W: deflection [m]

L: length of the beam [m]

P: point load [N]

E: young's modulus [GPa]

I: area moment of inertia [m<sup>4</sup>]

The area moment of inertia for a rectangular beam is defined as:

$$I_x = \frac{1}{12} bh^3 \quad (\text{eq. 23})$$

Where,

b: beam width [m]

h: beam height [m]

Figure 86 shows a comparison between measured, simulated, and calculated displacement curves for a 3-point bending setup with a center load. The beam dimensions were 50mm x 12mm x 525um and the young's modulus was assumed at 169 GPa. [40]

The ANSYS and COMSOL simulations are based on both 3D CAD models of the setup and a finite element analysis (FEA) to obtain the beam displacement for various loads. The DMA Q800 data were obtained by an actual measurement with the original DMA 3-point-clamp. For the Euler beam theory the maximum displacement was calculated for beams with thicknesses of 500um, 525um, and 550um. It can be observed that the displacement-load relationship is linear for all four methods.

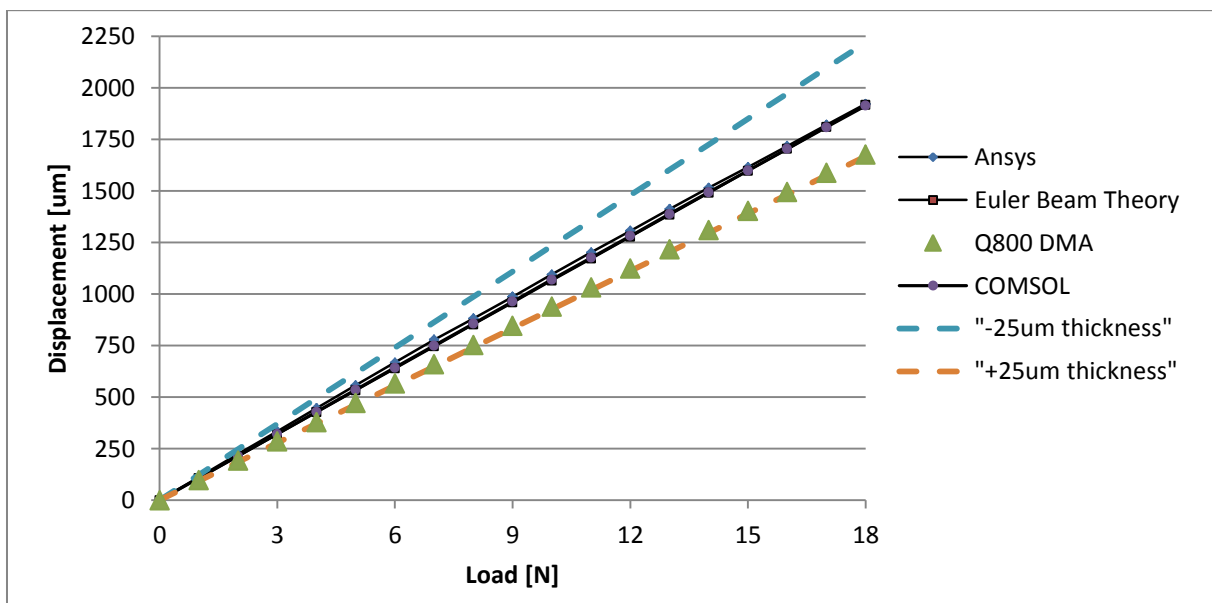


Figure 86 – Comparison between measured DMA displacement curve and analytically beam displacement curves extracted from finite element analysis ANSYS and COMSOL models

Figure 87 shows the error in displacement between the actual DMA Q800 measurement and analytical beam displacement by ANSYS, COMSOL and Euler beam theory from figure 86.

| DMA Q800 – ANSYS error |        | DMA Q800 – COMSOL error |        | DMA Q800 – Euler beam theory error |        |
|------------------------|--------|-------------------------|--------|------------------------------------|--------|
| Min.                   | Max.   | Min.                    | Max.   | Min.                               | Max.   |
| 12,79%                 | 15,35% | 8,74%                   | 12,58% | 9,29%                              | 12,42% |

Figure 87 –Error between actual DMA Q800 measurement and analytical ANSYS, COMSOL, Euler beam theory

Generally, it was observed that the error between actual and analytical displacement is lowest for small loads and increasing while going to larger loads. Overall, the FEA and Euler beam theory yield similar displacement results. It can be said that it is possible to determine the beam displacement analytically with an maximum error of around 12,4% compared to the actual measurement using the Euler beam theory. Yet, from figure 86 it can be seen that the Euler beam theory for a beam with 550 um results in a similar displacement to the actual beam measurement, performed with a beam with thickness 525um. This also raises the question of how accurate the DMA Q800 calibration needs to be and how accurate the wafer thickness information from the manufacturer is in order to extract accurate DMA measurements. (See appendix “G1. Ansys and Comsol beam deflection models” page “173”)

The average strain along the x-axis for the area where a resistor element is placed on the beam is expressed by:

$$\langle \epsilon_x \rangle = - \frac{z_0 \cdot P}{2EI} \cdot \left[ \frac{l}{2} - \frac{l_0}{2} \right] \quad (\text{eq. 24})$$

Where,

$z_0$ : half of the wafer thickness [m]

P: pointload [N]

E: youngs modulus [GPa]

I: area moment of inertia [m<sup>4</sup>]

l: beam length [m]

$l_0$ : resistor length [m]

Equation 24 was derived by Nis Dam Madsen based on the Bernoulli beam strain expression (eq. 25) in combination with the Bernoulli deflection equation (eq. 22) yielding the strain as a function of position.

$$\langle \epsilon_x \rangle = -Z \cdot \frac{d^2w}{dx^2} \quad (\text{eq. 25})^6$$

Eq. 24 was used during the initial test strain measurements.

<sup>6</sup>[http://en.wikipedia.org/wiki/Euler%E2%80%93Bernoulli\\_beam\\_theory#Strain\\_in\\_an\\_Euler.E2.80.93Bernoulli\\_beam](http://en.wikipedia.org/wiki/Euler%E2%80%93Bernoulli_beam_theory#Strain_in_an_Euler.E2.80.93Bernoulli_beam) (01.06.2014)

## 8.2. DMA electro-mechanical holder design

The DMA Q800 was not build for electrical measurements. One of the tasks for the overall research project was to design a solution that makes it possible to measure the electrical resistance of a thin film while applying a mechanical load with the DMA. Initial gauge factor experiments were performed by Nis Dam Madsen and Mathias Hausladen with a holder extension designed and manufactured by Kasper Thilsing-Hansen (See appendix: “G2. Initial gauge factor measurement “175”). Based on the experience gained from these initial tests, Nis Dam Madsen designed a new prototype holder, which was manufactured from a prototyping polymer material with a CNC milling machine by Reiner Hübel (MCI, Engineer) (see figure 88).

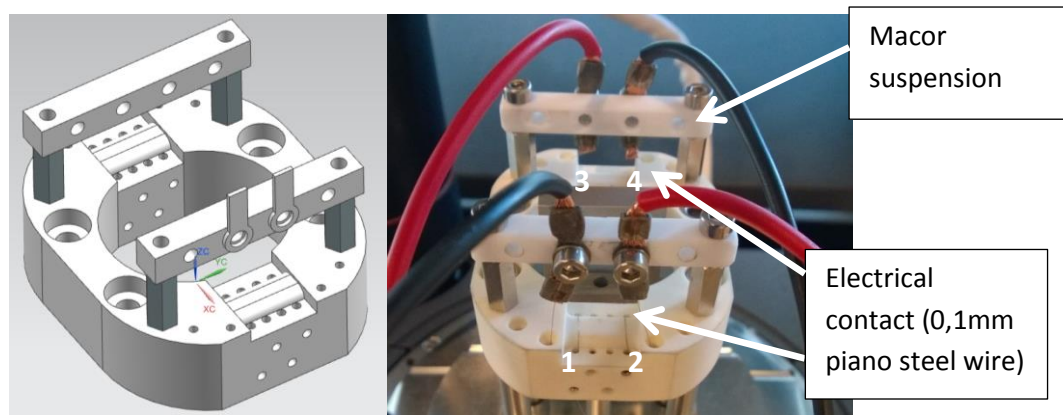


Figure 88 – Siemens PLM CAD by Nis Dam Madsen (left) and prototype holder v1 with contact wires to Keithley 2400 mounted on DMA by Rainer Hübel, Nis Dam Madsen and Mathias Hausladen (right)

The sample features of the holder include a suspension length of 40 mm and a total length of 56,8 mm for a sample width of maximum 13 mm. The electrical contacts consist of four piano wire contacts in each corner. The piano steel wires have a thickness of 0,1mm and are electrically connected via circular crimp connectors to the “macor” suspension bars fittings, which in the current version are connected together with a shielded high temperature (538 °C) 4-lead cable (see figure 89).

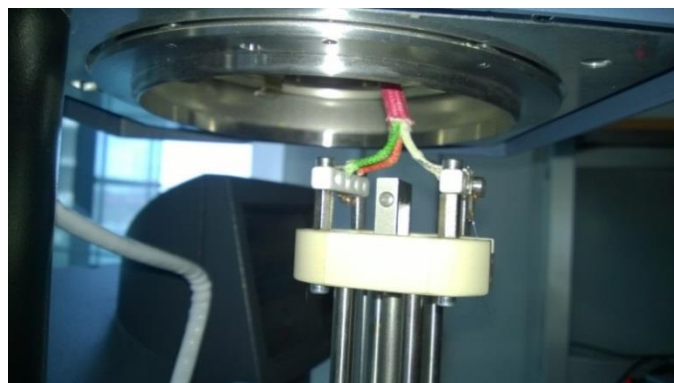


Figure 89 – showing DMA holder with high temperature 4-lead cable connected to the macor suspension bars with circular copper crimp connectors combined with 0,1mm steel piano wire to establish contact to the sample

The ongoing goal is to manufacture a holder from “macor”, which is a machinable glass ceramic for industrial applications. The material is rated for continuous use up to 800 °C, which makes it possible to utilize the achievable high temperature range of the DMA Q800. Furthermore, the material is electrical insulating, which insures that interferences from the electrical contacts on the mechanical loading are avoided.

The current setup consisting of the DMA Q800, which is controlled via a stationary PC, can be seen in figure 90. In combination a source meter (Keithley 2450) is connected to the piano steel wires via a high temperature cable collecting the resistance measurements when receiving a trigger signal via a self-made script, which was written by Nis Dam Madsen. The script is uploaded to the Keithley via USB and runs independently; writing measurements to a text file when receiving a trigger signal from the DMA Q800. In the end, one text file from the DMA Q800 and from the Keithley 2450 is created. For the data analysis a Matlab program was written by Nis Dam Madsen to analyze the two separate text documents, which enables the user to generate plots of e.g the gauge factor vs. temperature, TCR, and load displacement performance graphs.



Figure 90 – DMA connected to source meter (Keithley 2400) via high temperature cable. The DMA is controlled via the PC.

After loading the sample onto the holder, closing the furnace, and starting the measurement process, the DMA program will set the temperature at 40 °C followed by a loading and unloading procedure which will ensure that the sample has proper electrical contact to the piano steel wires. Afterwards, a load from 2N to 7N and back to 3N with a step size of 1N is applied. For each step the resistance, deflection, and temperature is logged. The entire cycle is repeated for temperatures from 40 °C to 60

°C with a temperature step size of 10 °C (see appendix “G3. DMA software measurement steps” page “180”).

### 8.2.1. Analytical strain evaluations

For a center loaded 3-point bending setup it is expected that the displacement of the beam is linear proportional to the load. During the strain gauge experiments with the in-house manufactured holder, it was found that the load [N] vs. displacement [ $\mu\text{m}$ ] relationship tends to be non-linear for lower loads. For higher loads the relationship becomes linear (see figure 91) (see appendix “G4. Load displacement performance experiment” page “181”).

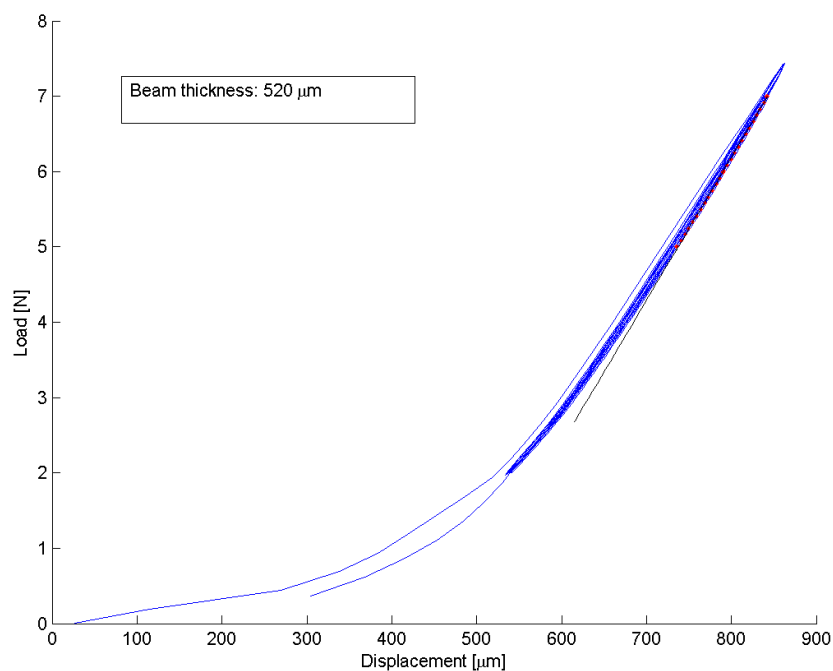


**Figure 91 – load displacement performance. Note the non-linear behavior in the beginning. At a certain load the relationship becomes linear. From the linear part (red line) the experimental data concerning the resistance change are extracted.**

It is expected that there should be a non-linear behavior during the initial part of the loading on the wires. It is design after that the wires will have a spring effect, which ensure the electrical contact. Other contributions to the non-linear load displacement behavior can be due to the material properties of the prototype holder.

The strain can be measured by the DMA Q800 with the original clamp holder, but in the case of this project, where a modified clamp is used, the strain measurements can't be trusted. Also at the current point it is unknown how the DMA Q800, calculates the strain. In the case when the strain should be measured by the DMA Q800 the sample holder must be “near perfect” like the holder that

got supplied with the DMA machine, and the calibration must be correct. Also, the sample thickness must be measured very accurately.

In the case where the beam dimensions (thickness) it not known, the calculated strain cannot be trusted. To measure the beam thickness, the slope of the load-displacement curve at the highest loads was used to determine the thickness from the Euler-Bernoulli equation by assuming that the modulus and the other dimensions are correct. When looking at eq. 22 it can be seen that the deflection is proportional with the load. The slope of the load displacement curve should be:

$$\frac{L^3}{48EI} \quad (\text{eq. 26})$$

When substituting "I" (area moment of inertial) we get:

$$\frac{L^3}{48E \frac{1}{12} bh^3} \quad (\text{eq. 27})$$

Where,

L: length of the beam [m]

E: young's modulus [GPa]

b: beam width [m]

h: beam height [m]

Equation 27 is then set equal to the slope of the measured load-displacement graph and the thickness of the beam is then isolated. To avoid the influence of the wires the slope is taken at the highest loads (see figure 91). Now the dimensions of the Si beam are assumed to be known "precisely" and the strain can be calculated from the Euler-Bernoulli equation by knowing the load and support points. That means that we can calculate the strain from the load alone. The load-displacement graph is only used to determine the thickness. [50]

### 8.3. Strain sensitive pattern

Strain sensitive patterns were designed with „L-edit“ and a high resolution flexible lithography film mask was manufactured by the company “Microlitho”<sup>7</sup>. Figure 92 shows a longitudinal bottom contact strain sensitive pattern. The gold bottom contacts were deposited by e-beam evaporation using a 5 nm layer of titanium (adhesion layer) and a 100nm gold layer for electrical contact. In a separate process using a shadow mask, a 20mm x 5mm x 400nm TiN resistor is deposited on top of the bottom contacts. A similar design exists for transverse gauge factor measurements using a 12mm

---

<sup>7</sup> <http://www.microlitho.co.uk>

x 5 mm x 400nm transverse resistor. Due to at the moment untraceable adhesion problems related to the gold layer, the current use for this type of strain pattern is not possible.

Yet, initial test strain gauge measurements with the new holder, using transverse and longitudinal Ti/Au bottom contact electrodes with a resistors thin film (DC-45, Ar:15 sccm, N<sub>2</sub>: 5 sccm) produced with a target power of 300W at a pressure of 2,38E-3 mbar, were conducted before the adhesion problems occurred. It was found that the gauge factor for the longitudinal bottom contact resistor was around 5,38 and for the transverse resistor around 3,67. A five digit precision on the resistivity measurement was obtained with a little drift on the last digit. See appendix "G6. Gauge factor measurement test" page "185" for a detailed experimental description and calculation data.



Figure 92 – Longitudinal bottom contact - example sample for gauge factor measurements

Another strain sensitive pattern which was developed was a meander structure pattern. The overall meander structure dimensions are 5150 x 5150µm. The resistor lines are 50µm thick and have a spacing of 100 µm (see figure 93).

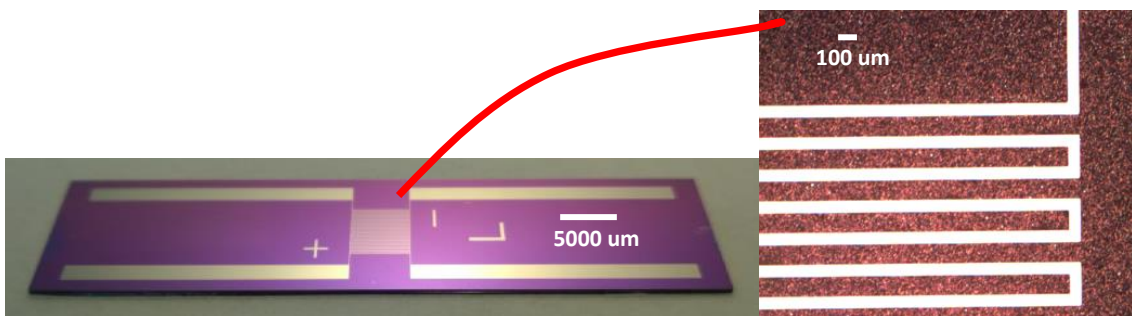


Figure 93 - Longitudinal meander structure - example sample for gauge factor measurements (left), zoom in on part of meander structure pattern

Additional test measurements concerning the meander structure were performed and confirmed that the meander structure is useful for extracting a gauge factor. Details about the masks and production procedure can be found in appendix "G5. Strain sensitive resistor substrate design" page 182 and "G8. Step by step production instructions" page 191

## 8.4. Depositions

During the end of this project, after the stability research was conducted and the strain gauge setup was starting to become operational, a strain gauge and TCR investigation for the most promising samples made during the stability research was started, which at this point is still ongoing.

Due to technical problems related to a new target, which was double the thickness of the previous target, it was not possible to deposit the best performing resistivity drift thin film DC-62 (Ar:6 sccm, N2: 10 sccm, 600W, poisoned) because the DC-bias voltage maxed out at 800V, causing the power and deposition rate to drop. Instead, sample DC-68 (Ar:10 sccm, N2: 8 sccm, 600W, poisoned) and DC-61 (Ar:19 sccm, N2: 2sccm, 600W, metallic) were reproduced. DC-68 had a resistivity drift of 3,34% from t=56h to t=360h at 200 °C in ambient atmosphere, but its overall drift from t=0h to t=360h was 1,19% and becoming stable at t=190h (see figure 66 page 60).

Figure 94 and figure 95 show the parameters of the produced gauge factor samples on longitudinal meander structure gauge factor samples.

| Sample | Production date | Argon [sccm] | Nitrogen [sccm] | Pressure [mbar] | Target state | Gauge factor sample                         |
|--------|-----------------|--------------|-----------------|-----------------|--------------|---|
| DC-68  | 22.04.14        | 10           | 8               | 2,26E-03        | poisoned     | Lift-off meander structure samples (LT-007) |
| DC-72  | 07.05.14        | 19           | 2               | 2,26E-03        | metallic     | Lift-off meander structure samples (LT-009) |

Figure 94 – produced samples with deposition parameters

| Fixed parameters | Value(s)     |
|------------------|--------------|
| Target power     | 600 W        |
| Desired pressure | 2.2E-3 mbar  |
| Base Pressure    | 5,00E-5 mbar |
| Temperature      | RT           |
| Thickness        | 400 nm       |
| Tooling factor   | 27           |

Figure 95 - Parameters for the pressure series variation

Information about the substrates used and their placement and the lithography parameters used to produce the meander structure can be found in appendix “G7. Substrate and substrate placement” page “189” and appendix “G8. Step by step production instructions” page “191”

## 8.5. Gauge factor results

Figure 96 shows the load [N] vs. displacement [ $\mu\text{m}$ ] curves for the produced longitudinal meander strain patterns DC-68 and DC-72. For a load of 5N to 7N the load displacement relationship is linear. For that part of the curve the beam thickness is extracted.

The beam thickness given by the manufacturer is 500um, which results in a percentage difference of 4% and 16% for DC-68 and DC-72 respectively. It has to be further investigated in how far the manufacturer’s specification about thickness is accurate. Bending tests with the original holder and clamp should be performed, for which the thickness is extracted and compared to the self-made holder thickness results.

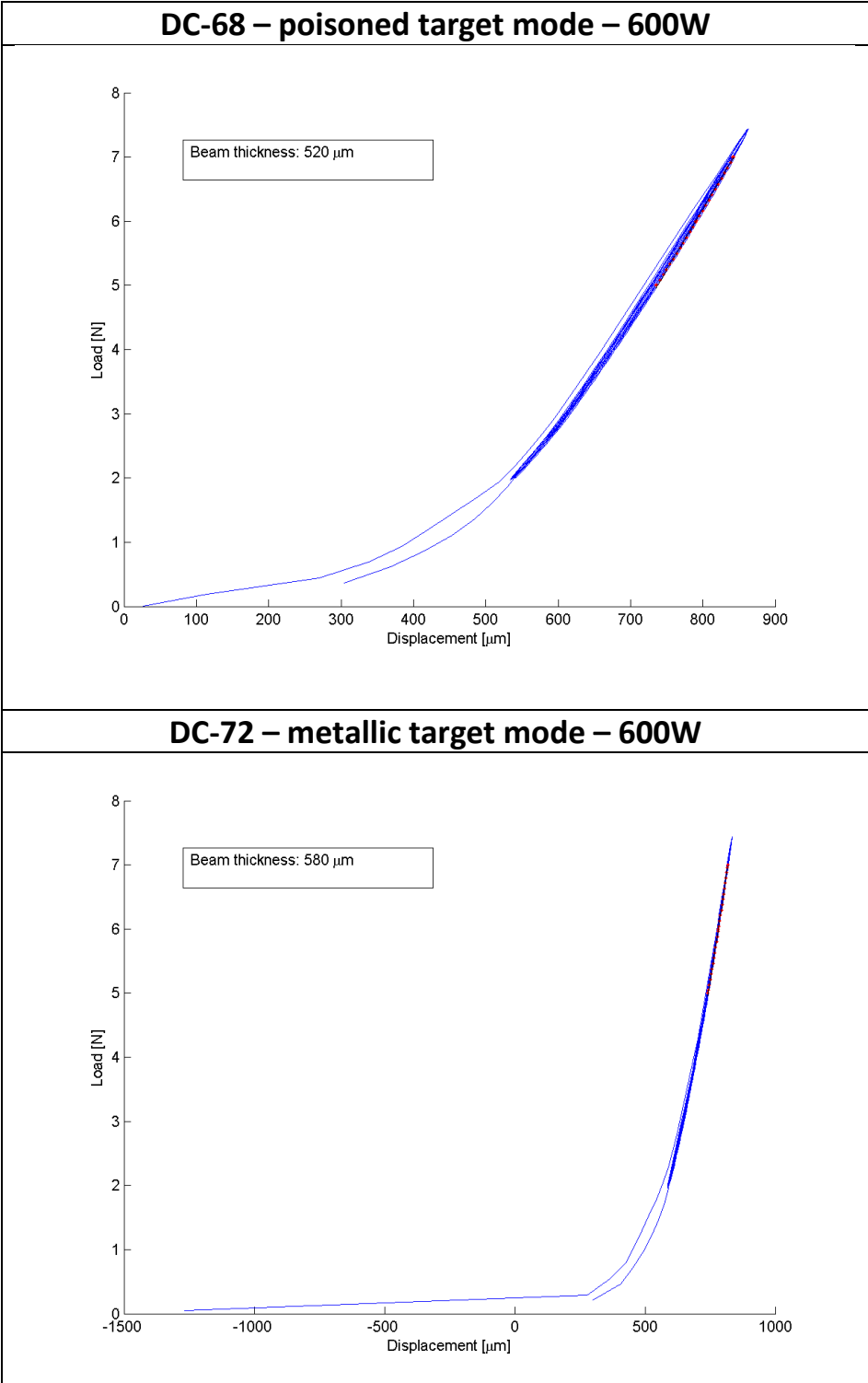


Figure 96 – load [N] vs. displacement [µm] curves for meander strain patterns DC-68 and DC-72

Figure 97 shows the gauge factor measurements for the produced meander strain patterns DC-68 and DC-72. The poisoned target mode sample (DC-68) shows a gauge factor of 5,08, whereas the metallic target mode sample (DC-72) has a considerable lower gauge factor with 1,54. Note that the program used to analyze the gauge factor uses the maximum strain instead of the strain presented in eq.24, which underrates the gauge factor a bit.

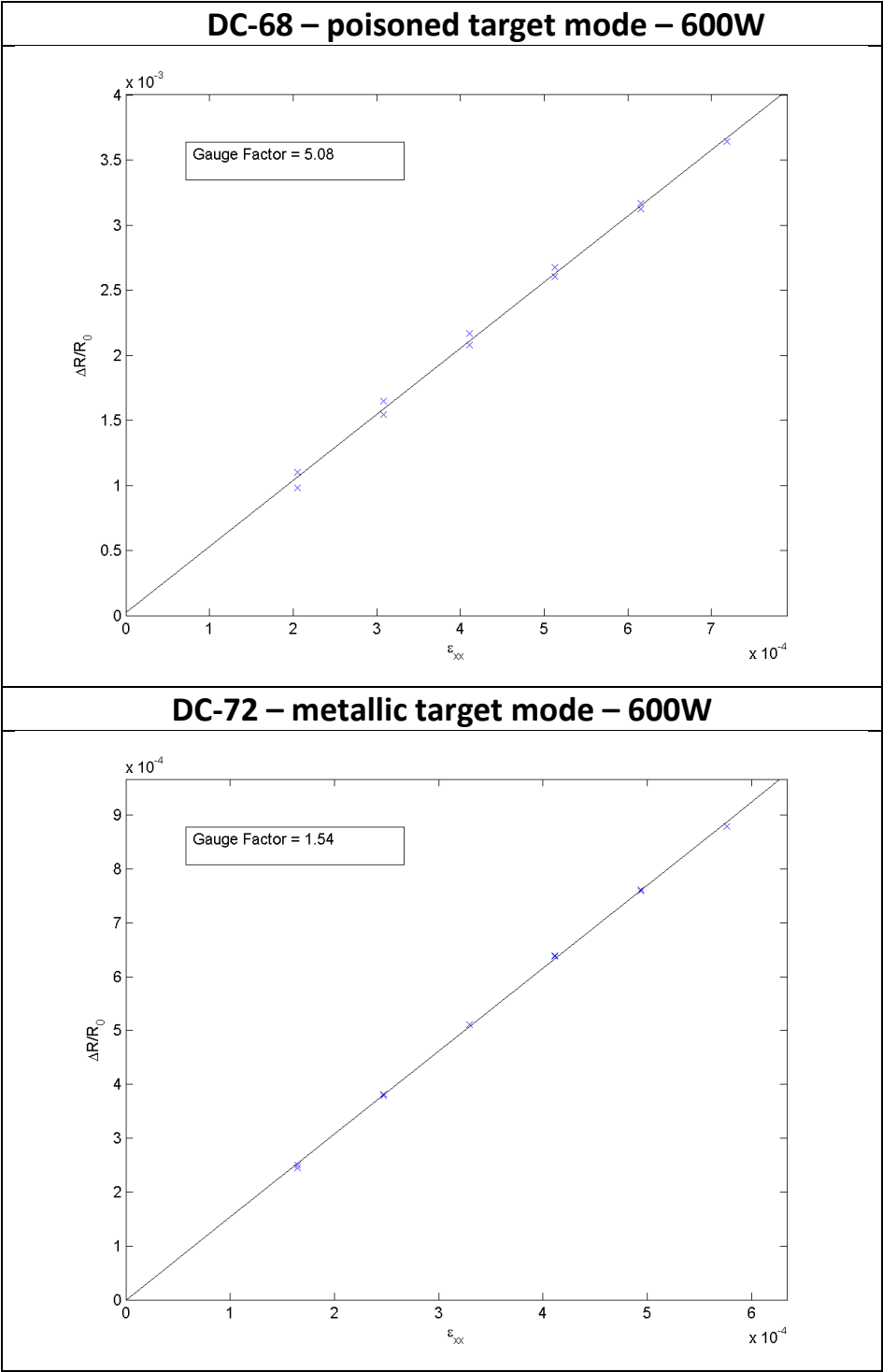


Figure 97 – Gauge factor measurements DC-68-poisoned (left) and DC-72-metallic (right)

Figure 98 shows the resistance change vs. temperature for the produced meander strain patterns DC-68 and DC-72. The TCR is extracted from the slope of the resistance vs. temperature measurements. For DC-68 a TCR value of 99,4 ppm/°C is measured and for DC-72 a TCR value of -10,8 ppm/°C. The TCR value of DC-68 is fulfilling the requirement. For DC-72 a negative TCR value is observed, which means that the material resistance is getting lower with increasing temperature.

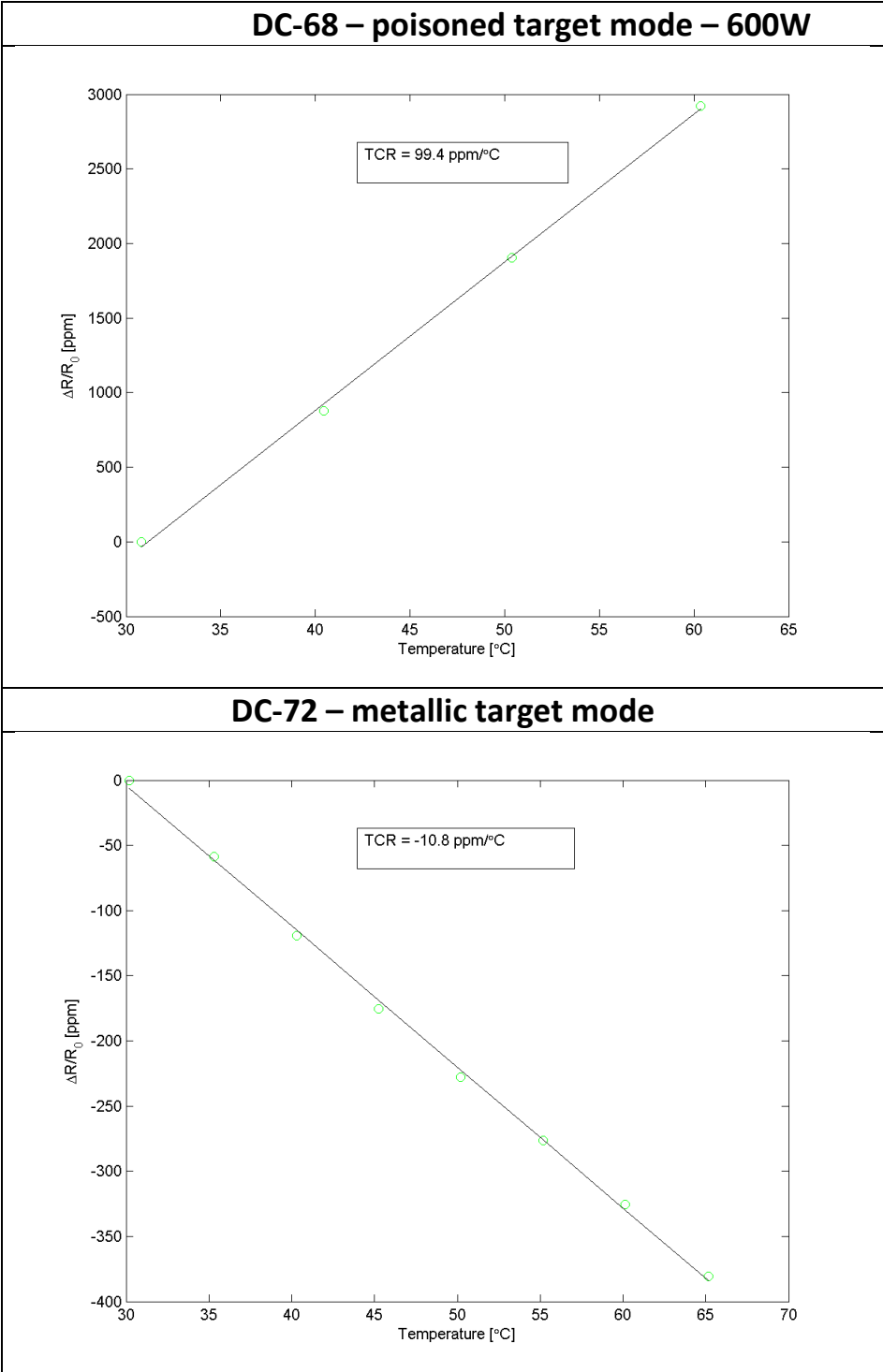


Figure 98 – Temperature coefficient of resistance for DC-68-poisoned (left) and DC-72-metallic (right)

## 8.6. Conclusion and outlook

Gauge factor requirement of 3 to 5 or higher and an absolute value of the temperature coefficient of resistance (TCR) below 100 ppm/ °C were required by Danfoss A/S.

The results of the short initial gauge factor screening investigations shows that the poisoned target mode sample DC-68 has a gauge factor of around 5,08 and a TCR of around 99,4 ppm/°C. The metallic target mode sample DC-72 shows a gauge factor of around 1,54 and a TCR of around -10,8 ppm/ °C.

The results for DC-68 are promising results, which show that the success criteria can be met with the titanium nitride (TiN) system running in poisoned target mode. Yet, as stated before, the strain gauge measurements are still ongoing and the presented samples can be viewed as indicators for which research direction is most promising.

### 8.6.1. Outlook

The next step will be to optimize the models used to determine the beam thickness and strain based of the load-displacement curves. For this the proper high temperature macor sample-holder has to be manufactured by Reiner Hübel. After this, bending experiments, which compare the macor and original DMA holder measurement results (load-displacement curves, beam thickness, strain) should be conducted.

At that point, a gauge factor series at 600W for various nitrogen flows should be conducted based on the information from the resistivity stability experiments.

This will also check for the reproducibility of the presented samples DC-68 and DC-72 in this report. The overall goal should be to characterize the gauge factor and TCR at temperatures above 250 °C using the DMA.

Furthermore, long-term mechanical testing at elevated temperature should be introduced with the aim of testing the fatigue and fracture limits of the titanium nitride system.

## 9. Overall project conclusion

Recently, a growing demand for inexpensive pressure sensors, which can provide accurate and reliable measurements of the pressures that occur when fuels are incinerated at high temperatures, can be observed. Thin film ceramic materials such as titanium nitride ( $\text{TiN}_x$ ) pose a promising solution to realize low cost high temperature sensors, which fulfill the needed requirements.

Danfoss A/S has established requirements for the sensors material, which include (a) resistivity drift of the potential sensor material being below  $\pm 2\%$  at an operating temperature of up to  $250^\circ\text{C}$  during 150 hours, a gauge factor (GF) of 3 to 5 or higher, and a temperature coefficient of resistance (TCR) below 100 ppm/  $^\circ\text{C}$ .

During this project a significant amount of time was invested to set up experimental procedure and creating new setup.

The experimental post-annealing investigation of RF-sputtered thin films using  $\text{O}_2$ -pulsing to incorporate different layers into the thin film in order to break up the columnar growth and with the goal to prevent through film oxidation, found that the layered film annealed at  $500^\circ\text{C}$  is more stable than the non-annealed sample during aging at room temperature. Based on the SEM pictures, it seems that oxygen pulsing can be used to break up the columnar structure of TiN films (SEM), but this should be investigated further with a helium-ion microscope or tunnel electron microscope. Furthermore, it was found that annealing at  $900^\circ\text{C}$  will result in changes of the TiN thin film to pure  $\text{TiO}_2$  with large crystals.

The resistivity stability research was studying the impact of the deposition pressure, nitrogen flow, and the target power on the resistivity stability, thin film stoichiometry, and structure.

During the research it was found that a low deposition pressure results in thin films with a higher density and lower resistivity drift over time. In the case of the MCI deposition system, the main chamber deposition pressure was adjusted to be around  $2,2\text{E}-3$  mbar.

Three sputter target modes were related to the resistivity stability performance of the thin films. Both the metallic target mode with a low nitrogen reactive gas flow and the poisoned target mode with a high reactive nitrogen flow showed stable resistivities. The remaining mode, the area between the metallic and poisoned target modes, was resulting in thin films with a high resistivity drift over time at room temperature; thus this area should be avoided.

A commercial material analyzer (DMA Q800) has been modified in order to measure the gauge factors and TCR. Two samples from the metallic and poisoned target mode, which both had a resistivity drift of below  $\pm 2\%$  at an operating temperature of 200 °C during 360 hours, were analyzed with regard to their gauge factor. The poisoned target mode sample measured a gauge factor of around 5,08 and a TCR of around 99,4 ppm/°C and the metallic target mode sample resulted in a gauge factor of around 1,54 and a TCR of around -10,8 ppm/ °C.

The results for the poisoned target mode should be further analyzed because they are close the desired requirement stated by Danfoss A/S.

## Bibliography

- [1] D. A. Serguei Chiriaev (Development specialist, Interviewee, *Sensor material requirements*. [Interview]. 2014.
- [2] T. Nagayama, M. Ruiz-s, B. Spencer, K. Mechitov und a. G. Agha, „Wireless strain sensor development for civil infrastructure,“ *1st Int. Workshop on Networked Sensing Systems*, pp. 97-100, 2004.
- [3] PCM Ltd., „What is a Strain Gauge?,“ [Online]. Available: <http://www.pcm-uk.com/straingauge-whatisastraingauge.html>. [Zugriff am 30 april 2014].
- [4] Omega, „Introduction to Strain Gages,“ [Online]. Available: <http://www.omega.com/prodinfo/StrainGages.html>. [Zugriff am 30 april 2014].
- [5] Kyowa electronic instruments LTD, „What´s a Strange Gauge?,“ [Online]. Available: <http://www.kyowa-ei.com>. [Zugriff am 30 april 2014].
- [6] Y. Hou, „Aluminum Nitride and Chromium Nitride Thin Films for Strain Gauge Application,“ Delft Institute of Microsystems and Nanoelectronics, Delft University of Technology, July 25th, 2010.
- [7] automationwiki.com, „Types of Strain Gauges,“ [Online]. Available: [http://automationwiki.com/index.php?title=Types\\_of\\_Strain\\_Gauges](http://automationwiki.com/index.php?title=Types_of_Strain_Gauges). [Zugriff am 30 april 2014].
- [8] S. Kim und K.D.Wise, „Temperature sensitivity in silicon piezoresistive pressure transducers,“ Bd. IEEE Transactions on Electron Devices, pp. 802-810, 1983.
- [9] R. Repas, „Sensor Sense: Thin-Film Sputtering Deposition Strain Sensors,“ Machine Design, [Online]. Available: <http://machinedesign.com/technologies/sensor-sense-thin-film-sputtering-deposition-strain-sensors>. [Zugriff am 11 mai 2014].
- [10] J. D. Wrbanek, G. C. Fralick und a. G. W. Hunter, „Thin Film Ceramic Strain Sensor Development for Harsh Environments,“ NASA, 2006.
- [11] DJ Instruments - a dynisco company, „Why Bonded Foil?,“ [Online]. Available: [http://www.djstruments.net/stuff/contentmgr/files/0/d75ccc7f8c8442c181152bdcc9f93cb4/pdf/why\\_bonded\\_foil.pdf](http://www.djstruments.net/stuff/contentmgr/files/0/d75ccc7f8c8442c181152bdcc9f93cb4/pdf/why_bonded_foil.pdf). [Zugriff am 30 april 2014].
- [12] Izantux, „Strain Gauge Visualization,“ WikiCommons, [Online]. Available: <http://en.wikipedia.org/wiki/File:StrainGaugeVisualization.svg#filelinks>. [Zugriff am 30 april 2014].
- [13] C. Liu, *Foundations of MEMS*, Prentice Hall; 2 edition, 2011.

- [14] Faculty of Engineering and Technology University of Jordan, „STRAIN GAUGES,“ [Online]. Available:  
<http://fetweb.ju.edu.jo/staff/me/jyamin/Measurement%20Course/STRAIN%20GAUGES.pdf>.  
 [Zugriff am 01 mai 2014].
- [15] resistorguide, „Temperature Coefficient of Resistance,“ [Online]. Available:  
<http://www.resistorguide.com/temperature-coefficient-of-resistance/>. [Zugriff am 23 may 2014].
- [16] wiseGeek, „What Is DC Magnetron Sputtering?,“ wiseGeek, [Online]. Available:  
<http://www.wisegeek.com/what-is-dc-magnetron-sputtering.htm>. [Zugriff am 29 april 2013].
- [17] M. Hausladen, „Reactive sputtering of Titanium oxynitride thinfilm,“ Supervisors: Jakob Kjelstrup Hansen and Kasper Thilsing Hansen, Sønderborg Denmark, 2013.
- [18] *MAK - Owners Operation and maintenance manual of the MAK sputtering sources*, MeiVac Inc.
- [19] U. o. Colorado, „Physics of Thin Films - PES 449 / PHYS 549,“ University of Colorado, [Online]. Available: <http://www.uccs.edu/~tchriste/courses/PHYS549/549lectures/sputtertech.html>.  
 [Zugriff am 20 april 2013].
- [20] J. D. Plummer, *Silicon VLSI Technology (Fundamentals, Practice and Modelling)*, Prentice Hall; 1 edition (July 24, 2000) ISBN-10: 0130850373.
- [21] T. M. Christensen, „<http://www.uccs.edu>,“ University of Colorado - Colorado Springs, 3 March 2000. [Online]. Available:  
<http://www.uccs.edu/~tchriste/courses/PHYS549/549lectures/sputtertech.html>. [Zugriff am 28 Oktober 2012].
- [22] „Universidad de Sevilla,“ [Online]. Available:  
[http://asignatura.us.es/aplasma/PDF/TPM2012\\_6B.pdf](http://asignatura.us.es/aplasma/PDF/TPM2012_6B.pdf). [Zugriff am 2 December 2012].
- [23] M. Hausladen, „Reactive sputtering of titanium nitride,“ Supervisors: Jakob Kjelstrup-Hansen and Kasper Thilsing-Hansen, Sønderborg Denmark, 2012.
- [24] M. Ohring, *Materials Science of Thin Films. Deposition and Structure*, Academic Press; Second Edition, 2001.
- [25] J.E.Sundgren, B.O.Johansson und S.E.Karlsson, „Mechanisms of reactive sputtering of titanium nitride and titanium carbide,“ *Thin Solid Films*, Bd. 105, pp. 353-366, 1983.
- [26] D. Depla und S. Mahieu, *Reactive Sputter Deposition*, Berlin: Springer-Verlag, 2008.
- [27] H. Windischman, „Intrinsic stress in sputter deposited thin film,“ *Solid State and Materials Sciences*, Bd. 17, Nr. 6, pp. 547-596, 1992.

- [28] A. Anders, „A structure zone diagram including plasma-based deposition and ion etching,“ *Bd. Thin Solid Films* 518 (2010) 4087–4090.
- [29] H. F. Ounsi, „Quantitative and Qualitative Elemental Analysis of Different Nickel–Titanium Rotary Instruments by Using Scanning Electron Microscopy and Energy Dispersive Spectroscopy,“ *Volume 34, Issue 1, January 2008, Pages 53–55*.
- [30] B. Hafner, „Energy Dispersive Spectroscopy on the SEM,“ [Online]. Available: [http://www.charfac.umn.edu/instruments/eds\\_on\\_sem\\_primer.pdf](http://www.charfac.umn.edu/instruments/eds_on_sem_primer.pdf). [Zugriff am 6 April 2013].
- [31] Bruker Nano, *EDS User School Powerpoint slides*, [www.bruker-nano.com](http://www.bruker-nano.com), 2013.
- [32] U. o. C. Riverside, „Central Facility for Advanced Microscopy and Microanalysis,“ [Online]. Available: <http://micron.ucr.edu/public/manuals/EDS-intro.pdf>. [Zugriff am 20 April 2013].
- [33] Australian microscopy & microanalysis research facility, „Bremsstrahlung X-ray generation,“ [Online]. Available: <http://www.ammrf.org.au/myscope/analysis/eds/xraygeneration/bremsstrahlung/>. [Zugriff am 19 04 2013].
- [34] Keithley Instruments, Inc., „Resistivity Measurements Using the Model 2450 SourceMeter® SMU Instrument and a Four-Point Collinear,“ 2013.
- [35] Mircoworld, „Four Point Probe Resistivity,“ [Online]. Available: <http://de.scribd.com/doc/132957898/4PP-resistivity>. [Zugriff am 28 April 2013].
- [36] F.M.Smits, „Measurement of Sheet Resistivities with the Four-Point Probe,“ *The bell system technical journal*, 1958.
- [37] Lucas Signatone Corp., *302 Resistivity Stand - installation and operation manual*, 392-J Tomkins Ct Gilroy, CA 95020 USA: Lucas Labs.
- [38] BRIDGE Technology, „Sheet Resistance and the Calculation of Resistivity or Thickness,“ [www.bridgetec.com](http://www.bridgetec.com), [Online]. Available: <http://www.four-point-probes.com/short.html>. [Zugriff am 29 4 2013].
- [39] G. Janssen, M. Abdalla, F. Keulen, B.R.Pujada und B. Venrooy, „Celebrating the 100th anniversary of the Stoney equation for film stress,“ *Thin solid films*, Bd. 517, pp. 1858-1867, 2009.
- [40] M. A. Hopcroft, W. D.Nix und T. W.Kenny, „What is the Young’s Modulus of Silicon,“ *Journal of microelectromechanical systems*, Bd. 19, Nr. 2, 2010.
- [41] Portland State University, „X-ray diffraction (XRD),“ [Online]. Available: <http://web.pdx.edu/~pmoeck/phy381/Topic5a-XRD.pdf>. [Zugriff am 08 05 2014].

- [42] H. z. Loye, „X-Ray Diffraction - HOW IT WORKS - WHAT IT CAN AND WHAT IT CANNOT TELL US,“ University of south Carolina - Chemistry and Biochemistry, [Online]. Available: [http://www.chem.sc.edu/faculty/zurloye/XRDTutorial\\_2013.pdf](http://www.chem.sc.edu/faculty/zurloye/XRDTutorial_2013.pdf). [Zugriff am 08 marts 2014].
- [43] Philips Innovation Services, „X-Ray Diffraction (XRD),“ [Online]. Available: <http://www.innovationservices.philips.com/sites/default/files/materials-analysis-xrd.pdf>. [Zugriff am 08 05 2014].
- [44] K. Khojier<sup>1</sup>, H. Savaloni, E. Shokrai, Z. Dehghani und N. Z. Dehnavi, „Influence of argon gas flow on mechanical and electrical properties of sputtered titanium nitride thin films,“ *Journal of Theoretical and Applied Physics* 2013, 7:37, <http://www.jtaphys.com/content/7/1/37>.
- [45] Y. L. Cheng, J. Wei, F. H. Shih und Y. L. Wanga, „Stability and Reliability of Ti/TiN as a Thin Film Resistor,“ *ECS Journal of Solid State Science and Technology*, 2 (1) Q12-Q15, 2013.
- [46] G. Lemperière und J. M. Poitevin, „Influence of the nitrogen partial pressure on the properties of D.C. sputtered titanium and titanium nitride films,“ *Thin Solid Films*, Bd. 3, pp. 339-349, 1984.
- [47] TA-Instruments, „tainstruments.com,“ [Online]. Available: <http://www.tainstruments.com/product.aspx?siteid=11&id=25&n=3>. [Zugriff am 28 may 2014].
- [48] TA-Instruments, *DMA Training Course material*, Sønderborg, 2013.
- [49] eFunda (engineering Fundamentals), „Beam Diagram and Calculations,“ [Online]. Available: [https://www.efunda.com/formulae/solid\\_mechanics/beams/casestudy\\_display.cfm?case=simple\\_centerload](https://www.efunda.com/formulae/solid_mechanics/beams/casestudy_display.cfm?case=simple_centerload). [Zugriff am 28 may 2014].
- [50] N. D. Madsen, Interviewee, *Calculation of beam thickness based on load-displacement curves*. [Interview]. 1 june 2014.

## 10. Appendix

### 10.1. Project time table

| A  | B   | C        | D        | E        | F        | G        | H        | I        | J        | K        | L         | M         | N         | O         | P         | Q         | R         | S         |
|--|---|----------|----------|----------|----------|----------|----------|----------|----------|----------|-----------|-----------|-----------|-----------|-----------|-----------|-----------|-----------|
| <b>General timetable for Master project part 2 [30 ECTS]</b> |   |          |          |          |          |          |          |          |          |          |           |           |           |           |           |           |           |           |
| <b>Main project parts</b>                                    | <b>Milestones</b>   | <b>1</b> | <b>2</b> | <b>3</b> | <b>4</b> | <b>5</b> | <b>6</b> | <b>7</b> | <b>8</b> | <b>9</b> | <b>10</b> | <b>11</b> | <b>12</b> | <b>13</b> | <b>14</b> | <b>15</b> | <b>16</b> | <b>17</b> |
| TiO <sub>x</sub> N <sub>y</sub> stability research           | Investigate the influence of post annealing of the stability of the TiO <sub>x</sub> N <sub>y</sub> films, using pipe oven, four point probe and EDX. Also compare RF with DC sputtering and vary the partial pressure during the deposition (investigate TiO <sub>x</sub> N <sub>y</sub> tuning options) | x        | x        | x        | x        | x        | x        | x        | x        | x        | x         | x         | x         |           |           |           |           |           |
| DMA setup  | Calibrating DMA setup, making an experimental procedure, finding error sources, calibration sample  |          |          |          |          |          | x        | x        | x        |          | x         |           |           |           |           |           |           |           |
| Gauge factor   | Characterize the electrical and electromechanical properties of various TiO <sub>x</sub> N <sub>y</sub> films using DMA setup and EDX (at room temperature and elevated temperatures)   |          |          |          |          |          |          |          | x        |          |           |           |           |           | x         |           | x         |           |
| Report writing   | Writing the report including appendix   |          |          |          |          |          |          |          |          |          |           | x         | x         | x         | x         | x         | x         | x         |

## 10.2. Initial project description

### Titanium oxynitride thin films for sensor applications

Supervisors: Jakob Kjelstrup-Hansen ([jkh@mci.sdu.dk](mailto:jkh@mci.sdu.dk)) and Kasper Thilsing-Hansen ([kth@mci.sdu.dk](mailto:kth@mci.sdu.dk))

Project made in collaboration with Danfoss Industrial Automation (Serguei Chiriaev

[shiryaev@danfoss.com](mailto:shiryaev@danfoss.com))

**Introduction:** One of the major trends in the present market for pressure sensors is the rapidly growing demand for devices capable of operating at high temperature (above 150°C and up to 400°C) and in harsh environments such as in chemically aggressive media. The existing sensors at the market are based on expensive materials and fabrication costs, which make them too expensive for numerous applications at the industrial market.

A possible solution to this problem is sensors based on thin films of titanium oxynitride, which is a promising material for sensors to be used in harsh environments, and which can be produced at low production costs. The implementation of titanium oxynitride in sensors, however, requires a detailed investigation of how the processing parameters affect the material properties such as electrical resistivity, temperature coefficient of resistance, electromechanical gauge factor and the long-term stability of these properties.

**Goals and milestones:** This master project will focus on deposition of titanium oxynitride ( $\text{TiO}_x\text{N}_y$ ) via reactive sputtering and characterization of the resulting thin films in terms of electrical and electromechanical properties. The initial part of the project will concentrate on setting up facilities for characterizing the electromechanical gauge factor of  $\text{TiO}_x\text{N}_y$  thin films under conditions up to 300°C. A commercial material analyzer (DMA Q800) will be used, but needs to be modified to be able to measure electrical resistance as a function of strain of the  $\text{TiO}_x\text{N}_y$  thin film. This also includes the design of the test structures incl. substrate and resistor dimensions. Once the set-up is operational and the test substrates have been designed and realized, the project will focus on the investigation of how the sputter deposition conditions affect the material properties, i.e. electrical resistivity, temperature coefficient of resistance, electromechanical gauge factor and the long-term stability of these properties

**The milestones are:**

- **Part 1**

- Determine the optimum geometry for a silicon test substrate that can be used in the 3-point bending clamp system for the material analyzer using COMSOL simulations.
- Design and realize a high-temperature stable electrical connector, which can be mounted on the material analyzer clamp system.
- Design a resistor layout (e.g. using a Wheatstone bridge) based on the COMSOL simulations that makes it possible to measure small resistance variations incl. the design of the necessary lithography masks.
- Realize a test sample and characterize the gauge factor both at room temperature and at an elevated temperature.

- **Part 2**

- Deposit  $\text{TiO}_x\text{N}_y$  thin films via reactive sputtering under different deposition conditions thereby changing the stoichiometry of the resulting thin film.
- Determine the chemical composition of the deposited films using Energy-Dispersive X-ray microscopy (EDX).
- Characterize the electrical and electromechanical properties of the  $\text{TiO}_x\text{N}_y$  films.
- Investigate the influence of post-annealing on the stability of the  $\text{TiO}_x\text{N}_y$  films.

## a. Fabrication and characterization equipment appendix

### A1. Correction factor calculation example

Four point probe measurement experiment with a sample dimension of  $a_{dim}=15mm$ ,  $d_{dim}=15mm$  and probe spacing  $s=1mm$

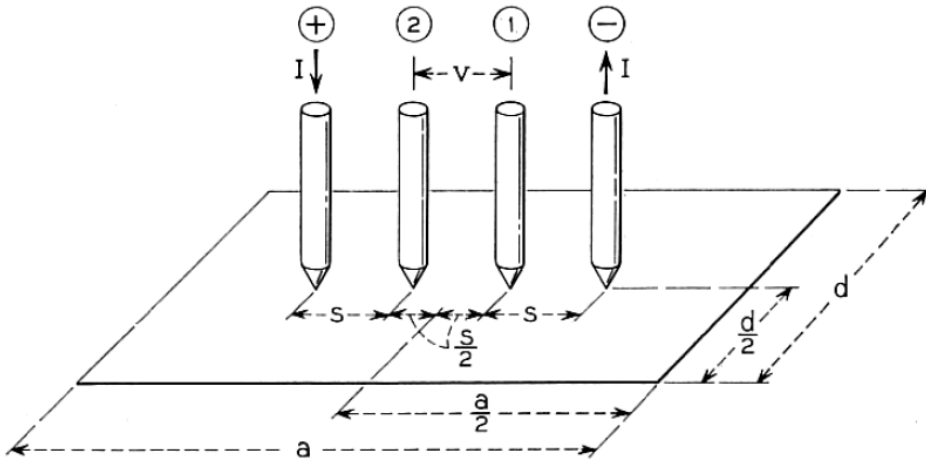


Figure 99- 4 point probe schematics with probe spacing “s” and sample dimensions; length “a” and width “d” [36]

First the dimensions are normalized with regard to the probe spacing in order to keep the calculations more generalized:

$$d \text{ is used for } \frac{d_{dim}}{s} \quad \rightarrow \quad d = \frac{d_{dim}}{s} = \frac{15mm}{1mm} = 15 \quad (\text{eq: 1})$$

$$a \text{ is used for } \frac{a_{dim}}{s} \quad \rightarrow \quad d = \frac{a_{dim}}{s} = \frac{15mm}{1mm} = 15 \quad (\text{eq: 2})$$

From [36] the following formulas have been derived:

$$V = I\rho_s \frac{1}{\pi} \left[ \frac{\pi}{d} + \ln(1 - e^{-4\pi/d}) - \ln(1 - e^{-2\pi/d}) + \sum_{m=1}^{\infty} a_m \right]$$

*sheet resistivity*  
(defined same way as “sheet resistance” in article)
*Expression for 1/C*

“sheet resistivity” is defined in the same way as “sheet resistance” so in this case ( $\rho_s = R_s$ ) [ohm-square]

$$\rho_s = \frac{V}{I} \cdot C \rightarrow V = I \cdot \rho_s \cdot \frac{1}{C} \quad (\text{eq: 3})$$

and where the correction factor is expressed as "1/C":

$$\frac{1}{C} = \frac{1}{\pi} \left[ \frac{\pi}{d} + \ln \left( 1 - e^{-\frac{4\pi}{d}} \right) - \ln \left( 1 - e^{-\frac{2\pi}{d}} \right) + \sum_{m=1}^{\infty} a_m \right] \quad (\text{eq.4})$$

for which the summation term for "a<sub>m</sub>" is expressed as:

$$a_m = \frac{1}{m} e^{-2\pi(a-2)m/d} \frac{(1 - e^{-6\pi m/d})(1 - e^{-2\pi m/d})}{(1 + e^{-2\pi a m/d})} \quad (\text{eq.5})$$

which for m=1 is:

$$a_m = e^{\frac{-2\pi(a-2)}{d}} \cdot \frac{(1 - e^{-\frac{6\pi}{d}}) \cdot (1 - e^{-\frac{2\pi}{d}})}{(1 + e^{-\frac{2\pi a}{d}})} \quad (\text{eq.6})$$

Based on the normalized dimensions "a<sub>m</sub>" is calculated:

$$a_m = e^{\frac{-2\pi(a-2)}{d}} \cdot \frac{(1 - e^{-\frac{6\pi}{d}}) \cdot (1 - e^{-\frac{2\pi}{d}})}{(1 + e^{-\frac{2\pi a}{d}})} \quad (\text{eq.7})$$

Based on the normalized dimensions "a<sub>m</sub>" is calculated:

$$a_m = e^{\frac{-2\pi(15-2)}{15}} \cdot \frac{(1 - e^{-\frac{6\pi}{15}}) \cdot (1 - e^{-\frac{2\pi}{15}})}{(1 + e^{-\frac{2\pi \cdot 15}{15}})} = 0.001054665 \quad (\text{eq.8})$$

Where from eq.9:

$$\frac{1}{C} = \frac{1}{\pi} \left[ \frac{\pi}{15} + \ln \left( 1 - e^{-\frac{4\pi}{15}} \right) - \ln \left( 1 - e^{-\frac{2\pi}{15}} \right) + 0.001054665 \right] = 0.2279 \quad (\text{eq.10})$$

Which can be calculated to the correction factor by:

$$C = \frac{1}{\frac{1}{C}} = \frac{1}{0.227902177} = 4.387847502 \sim 4.3878 \quad (\text{eq.11})$$

Figure 100 lists correction factors for various geometries. It can be seen that as the sample size increase, the correction factor goes against 4.5434, which is the correction factor for an infinite large sample.

| $d/s$    | circle diam $d/s$ | $a/d = 1$ | $a/d = 2$ | $a/d = 3$ | $a/d \geq 4$ |
|----------|-------------------|-----------|-----------|-----------|--------------|
| 1.0      |                   |           |           | 0.9988    | 0.9994       |
| 1.25     |                   |           |           | 1.2467    | 1.2248       |
| 1.5      |                   |           | 1.4788    | 1.4893    | 1.4893       |
| 1.75     |                   |           | 1.7196    | 1.7238    | 1.7238       |
| 2.0      |                   |           | 1.9454    | 1.9475    | 1.9475       |
| 2.5      |                   |           | 2.3532    | 2.3541    | 2.3541       |
| 3.0      | 2.2662            | 2.4575    | 2.7000    | 2.7005    | 2.7005       |
| 4.0      | 2.9289            | 3.1137    | 3.2246    | 3.2248    | 3.2248       |
| 5.0      | 3.3625            | 3.5098    | 3.5749    | 3.5750    | 3.5750       |
| 7.5      | 3.9273            | 4.0095    | 4.0361    | 4.0362    | 4.0362       |
| 10.0     | 4.1716            | 4.2209    | 4.2357    | 4.2357    | 4.2357       |
| 15.0     | 4.3646            | 4.3882    | 4.3947    | 4.3947    | 4.3947       |
| 20.0     | 4.4364            | 4.4516    | 4.4553    | 4.4553    | 4.4553       |
| 40.0     | 4.5076            | 4.5120    | 4.5129    | 4.5129    | 4.5129       |
| $\infty$ | 4.5324            | 4.5324    | 4.5324    | 4.5325    | 4.5324       |

Figure 100 - correction factor C for the measurement of sheet resistivity's with the fur point probe

## A2. Resistivity calculation

Example for sample DC-66-BK7-A2 (25x25 mm, thin film thickness: 350 nm)

Four measurements are taken. Between each measurement the sample is removed and placed again under the four point probe. This is done in order to account for possible placement errors.

Resistance measurement results with average resistance:

|                 |       |
|-----------------|-------|
| M1 ( $\Omega$ ) | 2,019 |
| M2 ( $\Omega$ ) | 2,019 |
| M3 ( $\Omega$ ) | 2,011 |
| M4 ( $\Omega$ ) | 2,016 |
| Avg. $\Omega$   | 2,017 |

The standard deviation of the 4 measurements is calculated by excel using the "STDEV" function.

$$\sigma\text{-resistance } (\Omega) = \text{STDEV}(2,019; 2,019; 2,011; 2,016) = 0,004 \Omega$$

Then the sheet resistance is calculated by multiplying the average resistance with the correction factor C:

$$R_s = R_{avg} \cdot C = 2,017 \cdot 4,4791 = 9,03 \Omega/sq$$

The error on the sheet resistance is calculated by:

$$\sigma\text{-sheet resistance } (\Omega) = \sigma\text{-resistance } (\Omega) \cdot \text{correction factor [cm]} = 0,004 \Omega \cdot 4,4791 = 0,01792 \Omega/sq$$

Then the resistivity is calculated by:

$$\rho = R_s \cdot t = 9,03 \frac{\Omega}{sq} \cdot 350E-07cm = 3,16E-04 \Omega cm$$

The error on the resistivity is calculated by:

$$\begin{aligned} \sigma\text{-resistivity } (\Omega cm) &= \sigma\text{-resistance } (\Omega) \cdot \text{correction factor} \cdot \text{thickness [cm]} \\ &= 0,004 \Omega \cdot 4,4791 \cdot 350E-07cm \\ &= 5,96E-07 \Omega cm \end{aligned}$$

### A3. Cryofox DC procedure

Written by Nis Dam Madsen in corporation with Mathias Hausladen

Generally the system responds slowly to new commands, therefore, **wait 4 sec. before pushing the next button.**

#### Ventilating:

The system will be left in the "standby vacuum" state. Press the Start/Stop bottom to start ventilation of the chamber.

#### Deposition setup:

- **Check the inficon controller that it is set to film 5 under Menu>General Parameter>Process>Film to run: set to 5 and press enter (down).**
- **Recipe:** Go to the recipe tab from the home page.
- **Process structure:** Open the default recipe e.g. ( NDM DC) Set/check, the desired sources for the number of layers desired .This will typically be the DC sputter or one of the E-beam pockets. Save the recipe as a new name if changes are made on this page, this is done by pressing **"Append to recipe"**.
- **Plasma recipe:** Go to the plasma recipe tab and check the values. They should be:
  - o Base pressure: 8.00E-2 mbar
  - o Ar flow: 50 sccm
  - o Plasma pre gas time: 0 min
  - o Plasma clean: 0 min
  - o Lock-load pressure: **7E-2 mbar (important that this value is correct!)**
  - o **Press "Append to Recipe" if changed!**
- **DC sputter:** Change/check the DC sputter recipe:
  - o Base pressure: 5E-5 mbar
  - o Ar flow: 20 sccm
  - o N2 flow: 5 sccm
  - o O2 flow: 2 sccm
  - o Puls on: 4 sec
  - o Puls off: 16 sec
  - o Oxygen pulsing: On
  - o Thickness: 400 nm
  - o Rate: 1.7 Å/s (This value should set higher than the system is capable of at the set maximum power to insure that the system is running at a constant power.)
  - o Tooling factor: 25 %
  - o **Press "Append to Recipe" if changed!**
  - o **GO TO Process structure and PRESS USE RECIPE until CHECK MARK appears!**
  - o **Substrates:** Mount the desired substrates in the substrate holder.
  - o **Check the density and z-ratio under Menu>Film parameter>Source> change values if necessary. Ti: density: 4.500 and Z-ratio: 0.628**

**Deposition start:** Start by checking the substrate rotation setting (press for 4 sec, if no check mark is in the rotation box). Switch the system over to **"coating process"** and press the **"start/stop"** button

to start evacuating the chamber. Press in the load-lock drawer until the pump starts working. Go to the **process trends** page to follow the pressure in chambers. When the load-lock pressure is reached the system will open the load-lock shutter. When this has happened, **tilt the substrate holder to 22.5° towards the DC target**. Here after the system will continue to evacuate the system until the base pressure defined under the “plasma recipe tab” is reached. At this point it will be possible to start the deposition by pressing “**start layer**”.

**Manuel control:** When the sputtering process has initiated **SOAK time 2**. Go to manuel control under the home tab. SOAK time has a total duration of 6 min.

- **Change all manual settings to the same as in the status column!**
- Go to the analog output tab and enter the same flow for N2 and Ar as in the DC recipe settings. E.g.
  - o **Ar flow: 20 sccm**
  - o **N2 flow: 5 sccm**
  - o **O2 flow: 0 sccm**
  - o **Open Ar main chamber valve**
  - o **Open N2 valve**
  - o **Check that the rest are closed.**
- When **4 min.** remains of SOAK time 2 **enable manual control** under the manual control tab.
- While the system is running with nitrogen – **check the deposition rate in the small control box** under the main control box (typically 0.8 Å/s). Check also that the system is running “film nummer 5” which is the DC sputter mode.
- On the inficon control box, **Menu>Film parameter>Deposite>Deposition**. **Change the deposition rate setting to a value 0.4 Å/s above the current deposition rate and press enter (down)**. Otherwise the system will not open the shutter to start the deposition.
- After the 4 min. in SOAK time 2 **return the system to automated control**.
- Now the deposition should proceed automatically here after.

**After deposition:** **tilt the substrate holder to 0°**, otherwise the chamber won't ventilate. Take out the samples and go to the **standby vacuum tab** and press **start/stop** to evacuate the chamber for the next user.

## Cyrofox E-beam deposition procedure:

Use the standard recipe, if another material is to be used just change **tooling factor** and **cup no.**

#### A4. Cryobox error analysis and optimization

Written by Mathias Hausladen in corporation with Nis Dam Madsen

07:00-11:00: Nis and Kasper opened cryobox, exchanged microbalance crystal, dismantled the target shutter and cleaned the chamber. All interior plates and the wafer shutter were cleaned about 2 weeks ago.

11:00-14:00: Nis and Mathias made the hysteresis curves for the power series (deposited around 1200nm of TiN). After 15:00 o'clock Cryobox was opened again due to plasma problems.

Figure 101 shows the baffle valve and the retracted wafer shutter in the load lock chamber. The wafer shutter was jiggled a bit before retraction. It can be seen that a lot of flakes are accumulating. The large flakes on the left have been there before the jiggling of the wafer shutter.

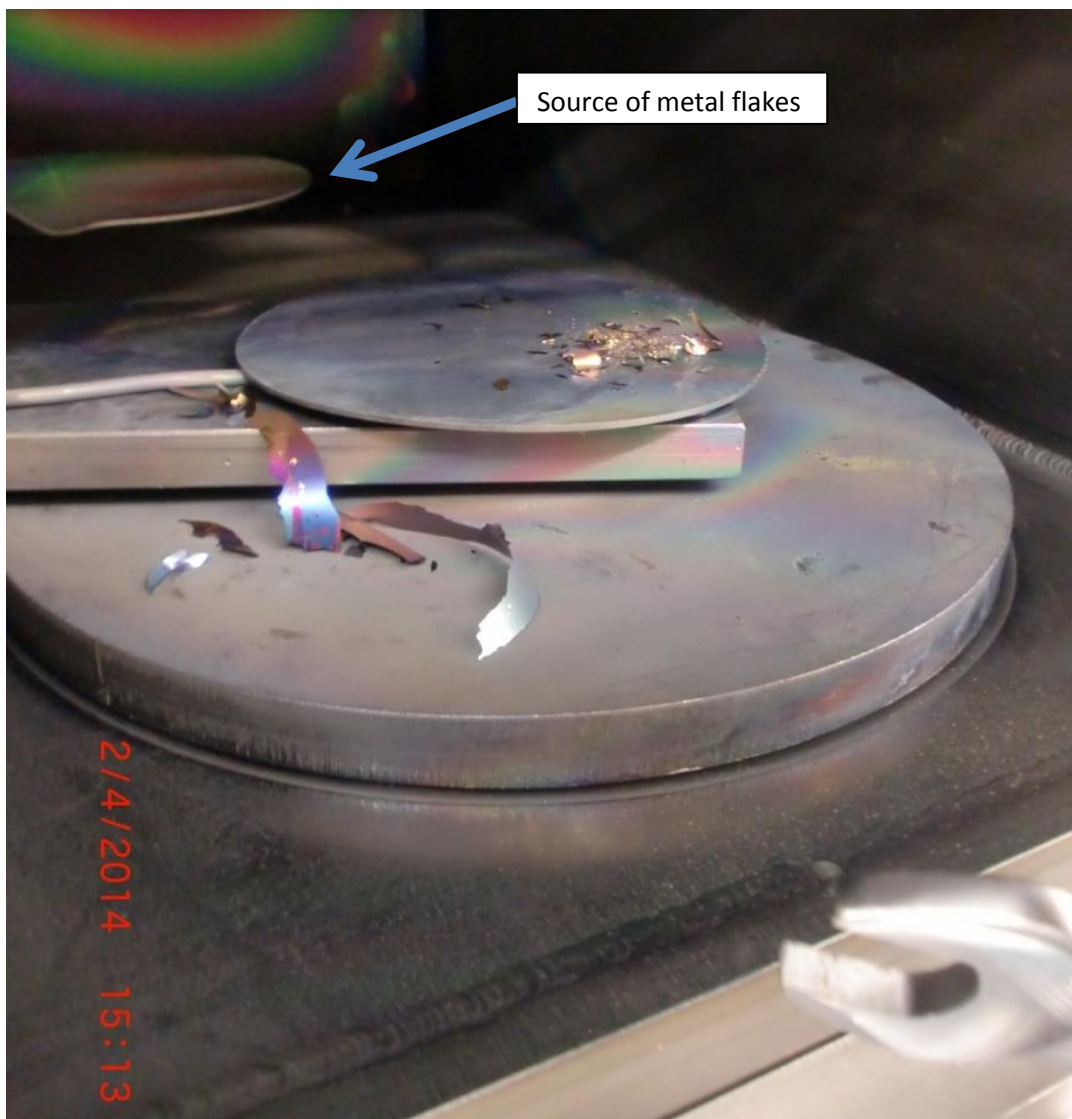


Figure 101 – retracted wafer shutter

Figure 102 shows the wafer shutter bottom side. It can be seen that large areas of metal flakes are loosely hanging from the wafer shutter.

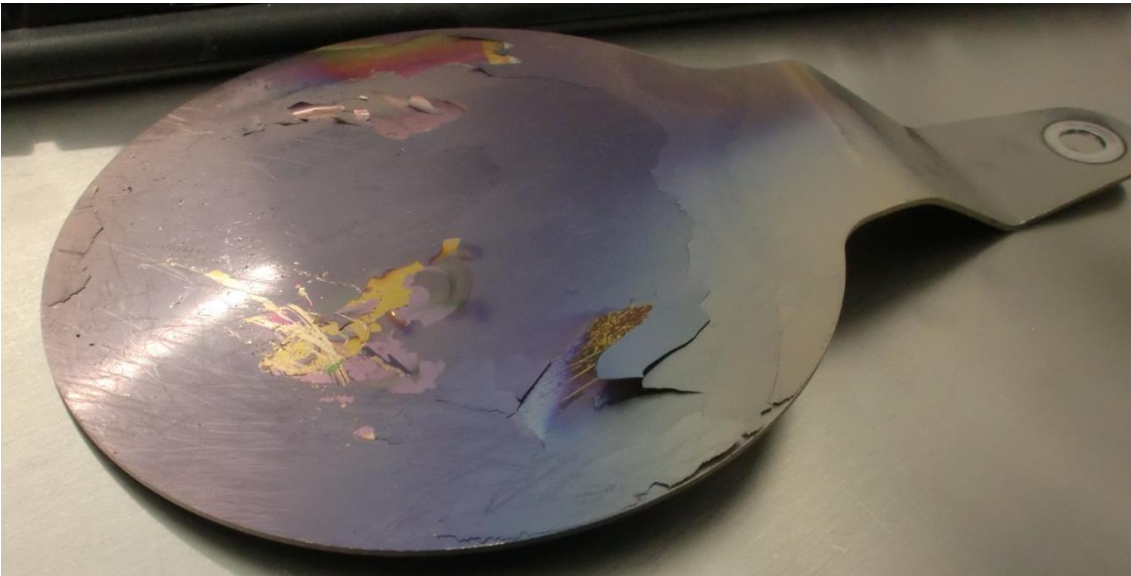


Figure 102 – wafer shutter

Figure 103 shows the target with the sputter head. The DC sputter head shutter was removed in order to test if the contamination will be reduced. Flakes are still accumulating on the target surface and in this case one metal flake got between target and sputter head, causing a short circuit.



Figure 103 – target with DC sputter head and removed target shutter

Figure 104 shows the target and DC sputter head from another position. Note the flake between the target and sputter head causing the plasma to shut down during the deposition.

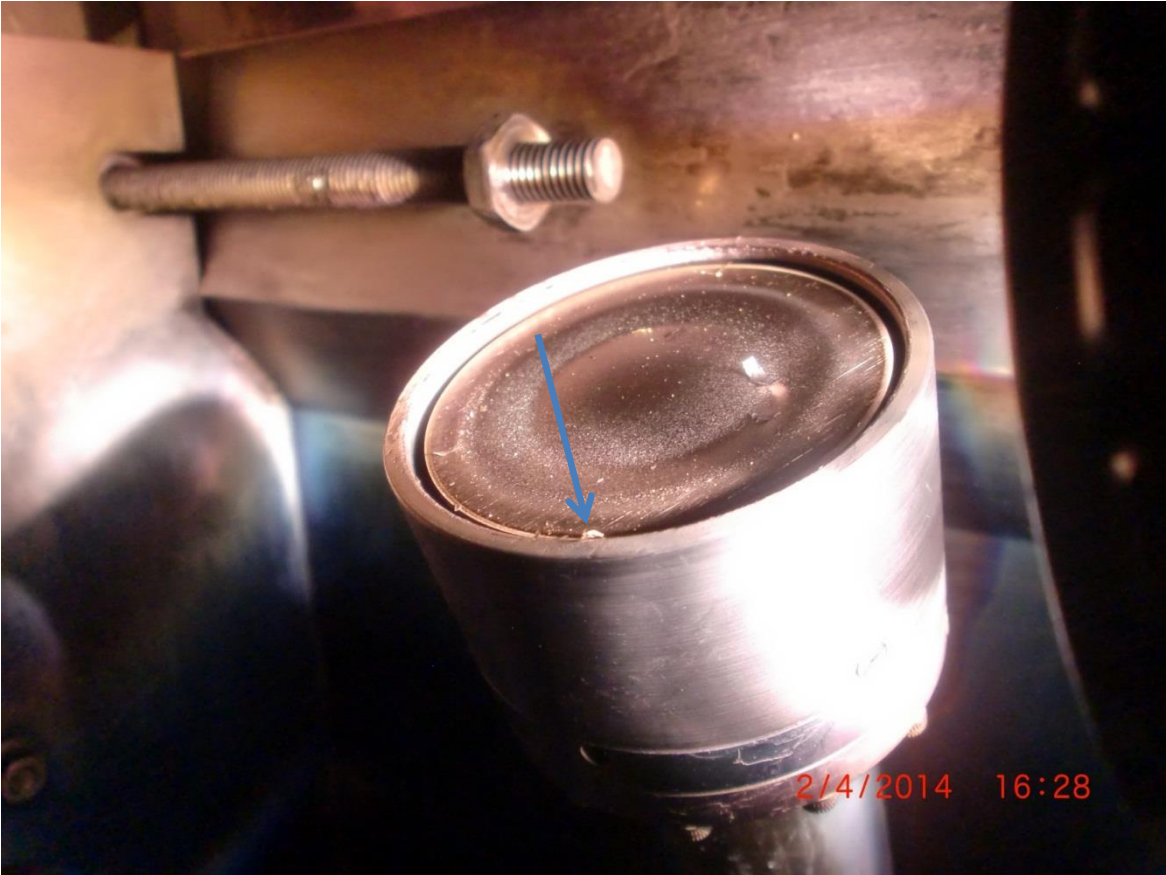


Figure 104 – target with DC sputter head

Figure 105 shows the sputter head with target, the DC sputter head shutter mounting screw and the metal plate above the target head. Note that on the metal plate flakes are accumulating which fall down onto the target. In that case it would be better to let the DC sputter head shutter mounted, so sputtered material will accumulate on the DC-sputter head shutter.



Figure 105 – top metal plate in the proximity of the target sputter head

Figure 106 shows the top metal plate in focus. Note the area where flakes are accumulating, which then fall down in the direction of the sputter head. This plate needs to be removed for proper deposition.

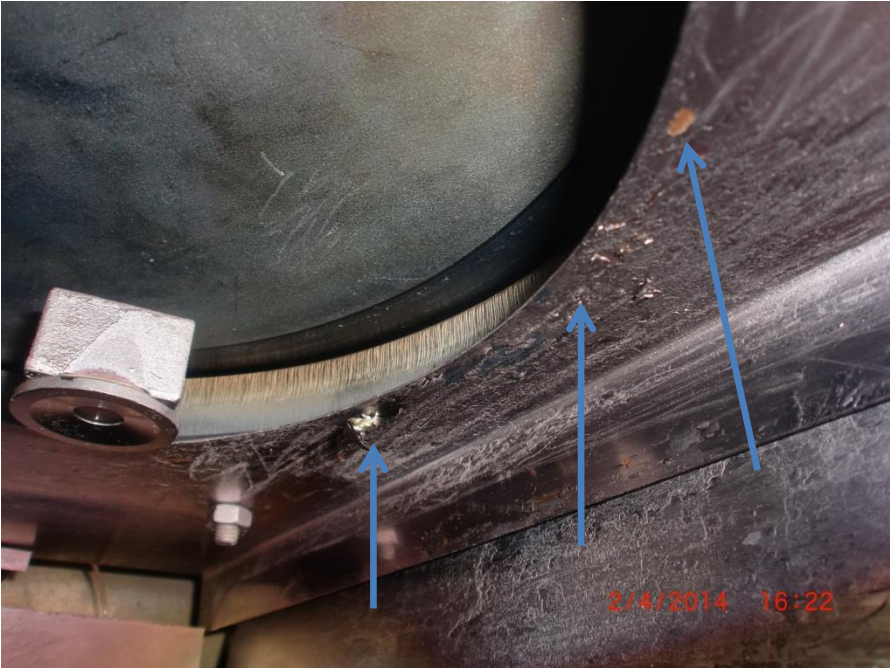


Figure 106 – metal plate in the proximity of the target sputter head

Figure 107 shows the inside of the main chamber with the DC-magnetron sputtering head on the right side together with the target shutter. The target shutter is another source of metal flakes which are falling down onto the target causing plasma problems during the reactive sputtering process.

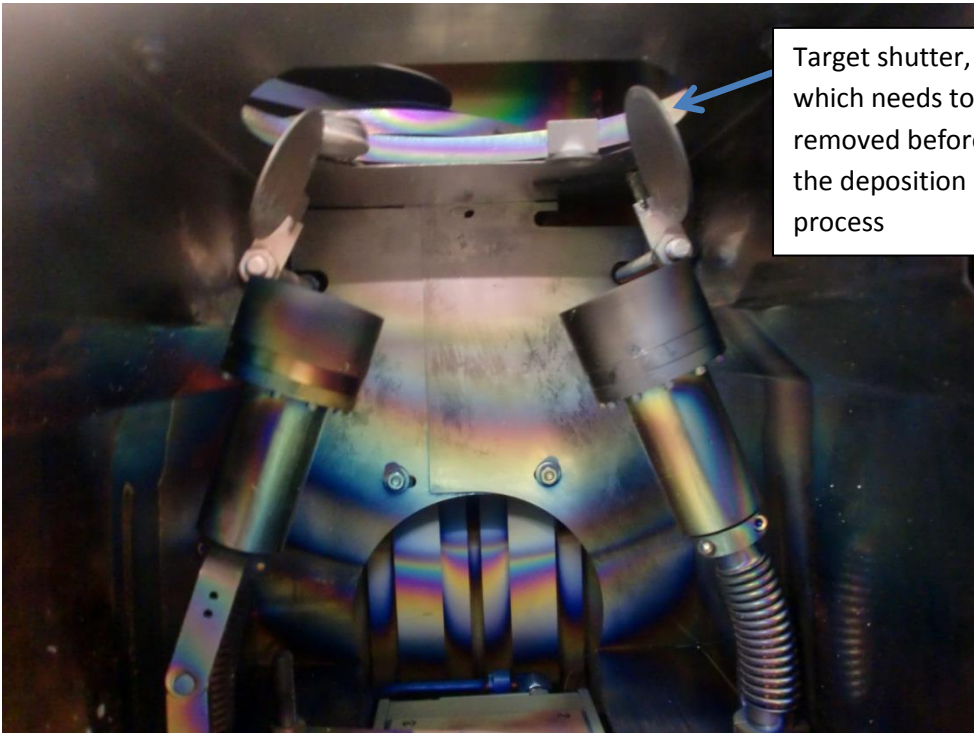


Figure 107– metal plate in the proximity of the target sputter head

Figure 108 shows the target shutter in top-view.



Figure 108 – target shutter top-view

#### **Working solution for increasing the production success rate to almost 100%**

- ➔ The wafer shutter needs to be cleaned with sandpaper from time to time
- ➔ Before each deposition series the following actions should be performed:
  - the quartz microbalance crystal needs to be exchanged (deposition thickness error readings are caused by a mixture of several thin films such as aluminum and titanium nitride, which have been deposited on to the microbalance crystal, resulting in a low adhesion causing flaking of the thin film, which results in a malfunction and error reading for the measured thickness)
  - the top chamber plate from figure 106 should be removed and substituted with aluminum foil before each deposition to avoid metal flakes falling down on the target
  - the target shutter should be removed to avoid metal flakes falling down on the target
  - the target and sputter head should be cleaned
  - the load lock and main chamber should be cleaned with a vacuum cleaner

### A5. Cryofox sample placement

Performed and written by Mathias Hausladen in corporation with Nis Dam Madsen

Goal: an evaluation of the thin film thickness vs. position has been conducted. This is important for the sample placement and repeatability of the experiments.

A titanium nitride thin film (DC-038) of 400nm has been deposited on a Si(100) P1 wafer and the cross-section thickness of the TiN thin film has been measured with an scanning electron microscope at a step size of 0.5 cm. The results can be seen in figure 109.

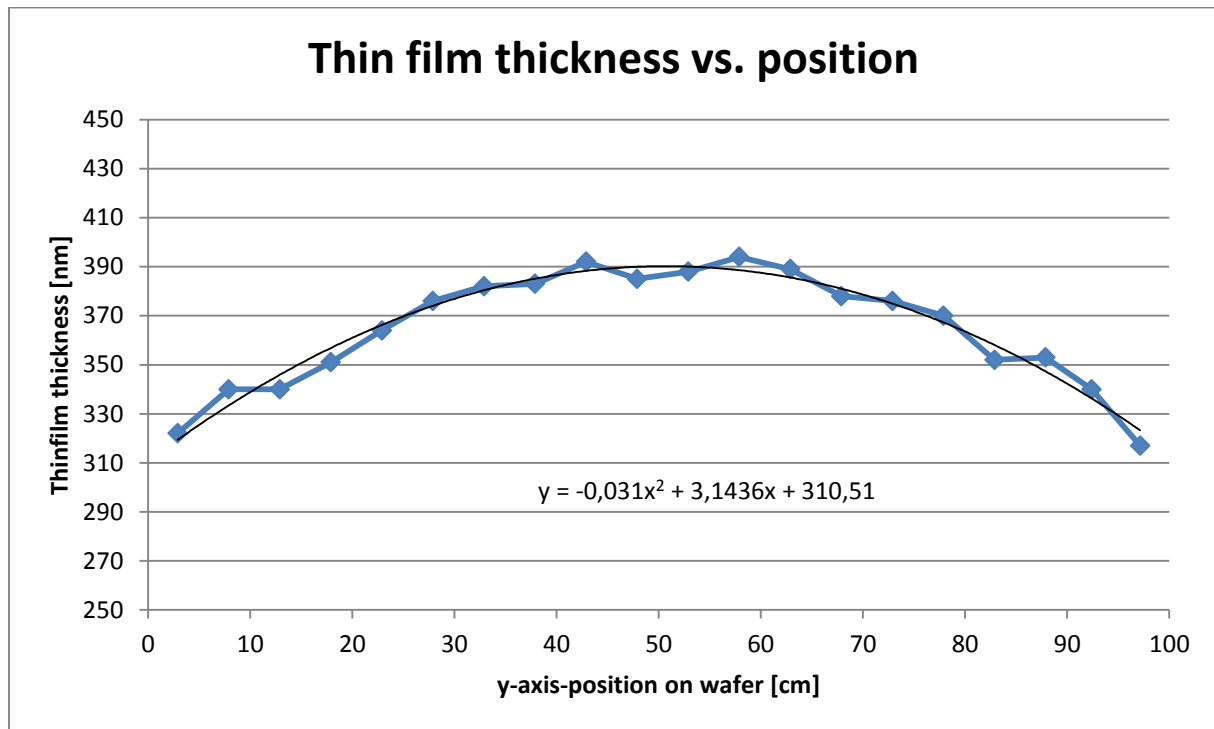


Figure 109 - Thin film thickness vs. position

**Conclusion:** The position of the sample within the holder is affecting the thin film thickness and thus the sheet resistance. There is a difference of 77nm from the maximum to the minimum measured thin film thickness, which corresponds to about 20% error with the center position as reference.

In order to create reproducible results the samples should be placed in the same positions.

## A6. Deposition log book

| Date     | Run    | Plasma clean settings |        |       | Reactive RF-sputtering settings |    |    |    |     |           |             |            |                            |                 | Comment |   |
|----------|--------|-----------------------|--------|-------|---------------------------------|----|----|----|-----|-----------|-------------|------------|----------------------------|-----------------|---------|---|
|          |        | Ar                    | Pregas | Clean | Ar                              | N2 | O2 | On | Off | Power [W] | DC-bias [V] | Rate [Å/s] | Thickness [nm] / tool/life | Pressure [mbar] |         | Temp [°C]   |
| 20-02-13 | RF-001 | 0                     | 0      | 0     | 20                              | 10 | 0  |    |     | 360       |             | 0,7        | 300/30                     | 4,0E-3          | 20      |   |
| 20-02-13 | RF-002 | 0                     | 0      | 0     | 20                              | 20 | 0  |    |     | 360       |             | 0,7        | 300/30                     | 5,7E-3          | 20      |   |
| 20-02-13 | RF-003 | 0                     | 0      | 0     | 40                              | 20 | 0  |    |     | 360       |             | 0,7        | 300/30                     | 7,8E-3          | 20      |   |
| 27-02-13 | RF-004 | 0                     | 0      | 0     | 20                              | 0  | 0  |    |     | 360/18    | 380         | 1,7        | 300/31                     | 2,5E-3          | 20      |   |
| 27-02-13 | RF-005 | 0                     | 0      | 0     | 20                              | 0  | 0  |    |     | 360/18    | 380         | 1,6        | 300/31                     | 2,5E-3          | 20      |   |
| 27-02-13 | RF-006 | 0                     | 0      | 0     | 20                              | 5  | 0  |    |     | 360/16    | 372         | 1,0        | 300/31                     | 3,15E-3         | 20      |   |
| 28-02-13 | RF-007 | 0                     | 0      | 0     | 20                              | 10 | 0  |    |     | 360/15    | 373         | 0,8        | 300/31                     | 4,05E-3         | 20      |   |
| 28-02-13 | RF-008 | 100                   | 0,5    | 1,0   | 20                              | 15 | 0  |    |     | 360/15    | 363         | 0,7        | 300/31                     | 4,95E-3         | 20      | Very unstable rate, bad MB                                |
| 28-02-13 | RF-009 | 0                     | 0      | 0     | 20                              | 20 | 0  |    |     | 360/10    | 373         | 0,6        | 300/31                     | 5,80E-3         | 20      |   |
| 06-03-13 | RF-010 | 0                     | 0      | 0     | 20                              | 0  | 0  |    |     | 360/13    | 345         | 1,6        | 50/32                      | 2,40E-3         | 20      |   |
| 06-03-13 | RF-011 | 0                     | 0      | 0     | 20                              | 5  | 0  |    |     | 360/11    | 359         | 1,1        | 50/32                      | 3,00E-3         | 20      |   |
| 06-03-13 | RF-012 | 0                     | 0      | 0     | 20                              | 10 | 0  |    |     | 360/11    | 360         | 0,8        | 50/32                      | 3,85E-3         | 20      |   |
| 07-03-13 | RF-013 | 50                    | 0,5    | 2     | 20                              | 15 | 0  |    |     | 360/4     | 377         | 0,8        | 50/32                      | 4,70E-3         | 20      |   |
| 07-03-13 | RF-014 | 50                    | 1      | 5     | 20                              | 2  | 0  |    |     | 360/12    | 384         | 1,4        | 50/32                      | 2,55E-3         | 20      |   |
| 07-03-13 | RF-015 | 0                     | 0      | 0     | 20                              | 20 | 0  |    |     | 360/13    | 384         | 0,7        | 50/32                      | 5,47E-3         | 20      |   |
| 07-03-13 | RF-016 | 0                     | 0      | 0     | 20                              | 10 | 2  | 3  | 15  | 360/14    | 382         | 0,8        | 50/32                      | 3,83E-3         | 20      |   |
| 13-03-13 | DC-001 | 0                     | 0      | 0     | 20                              | 0  | 0  |    |     | 200       |             | 1,7        | 50/32                      | 2,50E-3         | 20      |   |
| 13-03-13 | DC-002 | 0                     | 0      | 0     | 20                              | 0  | 0  |    |     | 358       | 365         | 1,7        | 50/20                      | 2,05E-3         | 20      |   |
| 13-03-13 | DC-003 | 0                     | 0      | 0     | 20                              | 5  | 0  |    |     | 358       | 411         | 1,5        | 50/20                      | 2,85E-3         | 20      |   |
| 14-03-13 | RF-017 | 0                     | 0      | 0     | 20                              | 10 | 2  |    |     | 360/7     | 365         | 0,8        | 50/32                      | 4,22E-3         | 20      |   |
| 14-03-13 | RF-018 | 0                     | 0      | 0     | 20                              | 10 | 2  | 6  | 12  | 360/10    | 350         | 0,8        | 50/32                      | 4,00E-3         | 20      |   |
| 14-03-13 | RF-019 | 0                     | 0      | 0     | 20                              | 10 | 2  | 9  | 9   | 360/7     | 355         | 0,8        | 50/32                      | 4,09E-3         | 20      |   |
| 14-03-13 | RF-020 | 0                     | 0      | 0     | 20                              | 10 | 2  | 12 | 6   | 360/14    | 353         | 0,8        | 50/32                      | 3,96E-3         | 20      |   |
| 14-03-13 | RF-021 | 0                     | 0      | 0     | 20                              | 10 | 2  | 15 | 3   | 360/15    | 350         | 0,7        | 50/32                      | 4,04E-3         | 20      |   |
| 14-03-13 | RF-022 | 0                     | 0      | 0     | 20                              | 0  | 2  |    |     | 360/0     | 302         | 0,9        | 50/32                      | 2,67E-3         | 20      |   |
| 22-03-13 | DC-004 | 0                     | 0      | 0     | 20                              | 10 | 0  |    |     | 300       | 389         | 0,9        | 200/20                     | 3,90E-3         | 20      |   |
| 25-03-13 | DC-005 | 0                     | 0      | 0     | 20                              | 10 | 2  | 1  | 17  | 300       | 380         | 0,8        | 100/20                     | 3,85E-3         | 20      |   |
| 25-03-13 | DC-006 | 0                     | 0      | 0     | 20                              | 10 | 2  | 1  | 17  | 300       | 382         | 0,8        | 150/20                     | 3,85E-3         | 20      |   |
| 03-04-13 | DC-007 | 50                    | 0,5    | 5     | 20                              | 5  | 0  |    |     | 300       | NA          | 1,2        | 170/20                     | NA              | 20      | Meas. thickness 178                                       |
| 11-04-13 | DC-008 | 50                    | 0,5    | 5     | 20                              | 5  | 0  |    |     | 300       | NA          | NA         | 400/20                     | NA              | 20      | Plasma stopped at 84nm (insulating TiN surface of target) |
| 11-04-13 | DC-009 | 50                    | 0,5    | 5     | 50                              | 5  | 0  |    |     | 199       | 570         | 1,0        | 400/20                     | 6,30E-3         | 20      | Meas. thickness 521nm, hot target                         |
| 12-04-13 | DC-010 | 50                    | 0,5    | 5     | 50                              | 10 | 0  |    |     | 199       | 540         | 0,8        | 400/20                     | 7,25E-3         | 20      | Meas. thick 522nm -> T=26, hot target                     |

|          |             |    |     |   |    |    |   |    |    |     |     |     |                      |         |                 |   |
|----------|-------------|----|-----|---|----|----|---|----|----|-----|-----|-----|----------------------|---------|-----------------|---|
| 15-04-13 | DC-011      | 0  | 0   | 0 | 50 | 5  | 0 |    |    | 199 | 438 | 0,7 | 400/26               | 6,35E-3 | 20              | Meas. thickness 469 nm  |
| 15-04-13 | DC-012      | 0  | 0   | 0 | 40 | 20 | 0 |    |    | 199 | 439 | 0,4 | 400/26               | 7,60E-3 | 20              | Unstable rate, deposition manual stopped at 150nm. thickness 211nm.   |
| 17-04-13 | DC-013      | 0  | 0   | 0 | 40 | 10 | 0 |    |    | 298 | 445 | 0,8 | 400/26/70            | 6,14E-3 | 20              |   |
| 17-04-13 | DC-014      | 0  | 0   | 0 | 40 | 15 | 0 |    |    | 298 | 438 | 0,7 | 400/28/73            |         | 20              |   |
| 17-04-13 | DC-015      | 0  | 0   | 0 | 40 | 0  | 0 |    |    | 298 |     | 1,8 | 400/24/78            |         | 20              |   |
| 18-04-13 | DC-016      | 50 | 0,5 | 5 | 40 | 10 | 0 |    |    | 298 | 426 | 0,7 | 400/27/1             | 5,90E-3 | 20              | AFM: 417 nm   |
| 18-04-13 | DC-017      | 50 | 0,5 | 5 | 40 | 10 | 2 | 2  | 16 | 298 | 424 | 0,8 | 400/27/8             | 5,93E-3 | 20              | AFM: 380 nm   |
| 18-04-13 | DC-018      | 50 | 0,5 | 5 | 40 | 10 | 2 | 4  | 14 | 298 | 417 | 0,7 | 400/27/14            | 5,93E-3 | 20              | AFM: 373 nm   |
| 18-04-13 | DC-019      | 50 | 0,5 | 5 | 40 | 10 | 2 | 6  | 12 | 298 | 416 | 0,7 | 400/27/20            | 5,93E-3 | 20              | AFM: 374 nm   |
| 22-04-13 | DC-020      | 50 | 0,5 | 5 | 40 | 10 | 2 | 8  | 10 | 298 | 414 | 0,7 | 400/27/43            | 6,00E-3 | 20              | AFM: 366 nm   |
| 24-04-13 | DC-021      | 50 | 0,5 | 5 | 40 | 10 | 2 | 10 | 8  | 298 | 405 | 0,7 | 400/27/61            | 6,00E-3 | 20              | AFM: 364 nm   |
| 25-04-13 | DC-022      | 50 | 0,5 | 5 | 40 | 10 | 2 | 12 | 6  | 298 | 406 | 0,7 | 400/27/66            | 6,00E-3 | 20              | AFM: 353 nm   |
| 25-04-13 | DC-023      | 50 | 0,5 | 5 | 40 | 10 | 2 | 14 | 4  | 298 | 408 | 0,7 | 400/27/71            | 6,21E-3 | 20              | AFM: 338 nm   |
| 25-04-13 | DC-024      | 50 | 0,5 | 5 | 40 | 10 | 2 | 16 | 2  | 298 | 432 | 0,7 | 400/27/76            | 6,27E-3 | 20              | AFM: 348 nm   |
| 06-05-13 | DC-025      | 50 | 0,5 | 5 | 40 | 10 | 2 | 18 | 0  | 298 | 431 | 0,6 | 400/23/14            | 6,21E-3 | 20              | AFM: 395 nm   |
| 23-05-13 | DC-026      | 0  | 0   | 0 | 40 | 10 | 0 |    |    | 298 | 386 | 0,7 | 400/27/16            | 5,95E-3 | 20              | 1 min. Ar pre-sputter time<br>5 min. N2 pre-sputter time<br>AFM: 392nm  |
| 27-05-13 | DC-027      | 50 | 0,5 | 2 | 40 | 10 | 0 |    |    | 298 | 384 | 0,7 | 400/27/30            | 6,00E-3 | 100             | 1 min. Ar pre-sputter time<br>5 min. N2 pre-sputter time<br>AFM: 343nm  |
| 30-05-13 | DC-028      | 50 | 0,5 | 2 | 40 | 10 | 0 |    |    | 298 | 381 | 0,7 | 400/27/37            | 6,00E-3 | -20/-18<br>5min | 1 min. Ar pre-sputter time<br>5 min. N2 pre-sputter time<br>AFM: nm<br>Changed to -18 after 80nm due to fault   |
| 22-11-13 | DC-029      | 50 | 0,5 | 5 | 20 | 5  | 2 | 2  | 16 | 300 | 391 | 0,7 | 400/25/4             | 3,08E-3 | RT              | NDM Stress wafer 1-4 included.  |
| 04-12-13 | DC-030      | 50 | 0,5 | 5 | 20 | 5  | 0 | -  | -  | 298 | 522 | 1,2 | 400/25/61            | 2,92E-3 | 20              | Shadow mask #1 on N11 substrates. Plasma was unstable with many arcs observed, furthermore the plasma was lost several times. After 15 min, the plasma seems stable, still with many arcs. After 35 min only few arcs is observed. <b>New target.</b>   |
| 05-12-13 | DC-031_fail | 0  | 0   | 0 | 20 | 5  | 0 | -  | -  | -   | -   | 0,5 | Stopped after 100nm. | 3.16E-3 | 20              | Shadow mask #1.1 on N11 substrates. The system was running in an undefined mode where both the RF target (InO3-SnO2 DC bias 293V) and the DC target (123W) is running at the same time. See also day-log. The process stopped at 100nm thickness and was running at a deposition rate of 0.5 Å/s. |

|          |        |    |     |   |    |    |   |    |   |              |                    |          |           |  |               |   |
|----------|--------|----|-----|---|----|----|---|----|---|--------------|--------------------|----------|-----------|--|---------------|---|
| 05-12-13 | DC-032 | 0  | 0   | 0 | 20 | 5  | 0 | -  | - | 298          | 505                | 1,2      | 400/25/74 | 2,95E-3                                | 20<br>(21.11) | XRD test samples, the target was only pre-sputtered in N2 for 2 min. Only very few arcs observed. There is a spike in the pressure after 4min. which indicate that the plasma has been lost at that point.              |
| 05-12-13 | DC-033 | 0  | 0   | 0 | 20 | 5  | 0 | -  | - | 298          | 505                | 1,1      | 400/25/78 | 2.99E-3                                | 20<br>(21,13) | Shadow mask #1.1 on N11 substrates. During soak time 2 much glowing debris was observed on target surface (see picture). The glows were gone after 10 min of dep. Time. Similar glow was observed after a heavy arc.    |
| 12-12-13 | DC-034 | 0  | 0   | 0 | 40 | 10 | 0 | -  | - | 298          | 464                | 0,8      | 400/27/7  | 5,86E-3                                | 20            | The deposition ran smoothly.  |
| 12-12-13 | DC-035 | 0  | 0   | 0 | 40 | 10 | 2 | 12 | 6 | 298          | 461/490<br>(oxide) | 0,8      | 400/27/7  | 6,14E-3                                | 21            | The process was stopped to correct recipe before deposition. The microbalance was unstable during manual soak time 2 but stabilized after the deposition was started. The deposition went smooth.                       |
| 30-01-14 | DC-036 | 50 | 0,5 | 2 | 20 | 4  | 0 | -  | - | 298          | 453                | 1,3      | 400/27/26 | 2,76E-3                                | 21            | The plasma clean process could not be seen through the observation window.  |
| 05-02-14 | DC-037 | 50 | 0,5 | 2 | 10 | 4  | 0 | -  | - | 298          | 497                | 1,0      | 400/27/1  | 1.54E-3                                | 21            | During SOAK time the plasma did not ignite, turning the Ar-flow up to 20 sccm ignited the plasma. The plasma was lost at 224nm and restarted by increasing the Ar flow manually. The plasma was lost several more times |
| 12-02-14 | RF-023 | 0  | 0   | 0 | 20 | 10 | 0 | -  | - | 360/26       | 831                | 0,6      | 300/31/   | 3,91E-3                                | 21            | The target has twice the thickness of the targets used in the RF001-RF-010 series. Resulting in a higher DC bias.   |
| 17-02-13 | RF-024 | 0  | 0   | 0 | 20 | 5  | 0 | -  | - | 360/28       | 834                | 0,8      | 300/31    | 3,05E-3<br>(main)<br>4,72E-3<br>(load) | 21            | Note: chose film 6 in Cryofox "deposition controller" (general parameters → film to run) Density: 4.50 g/cm; Z-ratio: 0.628<br>Deposition rate very stable. AFM: 227.5nm  |
| 17-02-14 | RF-025 | 0  | 0   | 0 | 20 | 15 | 0 | -  | - | 360/37       | 750                | unstable | 300/31    | 4,84E-3<br>(main)<br>6,05E-3<br>(load) | 21            | Very unstable rate. Bad MB reading (#####) after 35 min. Power fluctuating between 340-360W. Stopped after 70 minutes<br>MB crystal. AFM: 182nm   |
| 17-02-14 | RF-026 | 0  | 0   | 0 | 20 | 20 | 0 | -  | - | 98W/10<br>2W | 0                  | -        | 300/31    | 2,40E-3<br>(main)<br>4,22E-3<br>(load) | 21            | Error: Refracted power out of range. (Reset with F4). Deposition rate unstable. Power at 98W and refracted power at 102W. Cancelled deposition in case of avoiding damage. Restarted deposition but same error occurs.  |

|          |        |   |   |   |    |    |   |   |     |              |       |                  |        |         |    |  |
|----------|--------|---|---|---|----|----|---|---|-----|--------------|-------|------------------|--------|---------|----|--|
| 19-02-14 | RF-027 | 0 | 0 | 0 | 20 | 15 | 0 | - | -   | 360W/3<br>3W | 763V  | 0,55             | 300/31 | 4,73E-3 | 21 | Used "Cryofox N2 hack" procedure. Rate very stable. Short circuit at 223.7nm thickness (small glowing piece on sputter head) → process stopped   |
| 24-02-14 | RF-028 | 0 | 0 | 0 | 20 | 5  | 2 | 5 | 250 | 360W/4<br>1W | 789V  | 0,7              | 400/31 | 3,16E-3 | 21 | Target track depth: 2 mm. Magnetron cleaned.<br>Cl: 448 Ct: 997  |
| 24-02-14 | RF-029 | 0 | 0 | 0 | 20 | 5  | 0 | 0 | 0   | 360W/4<br>1W | 785V  | 0,7              | 400/31 | 2,95E-3 | 21 | Cl: 448 Ct: 997  |
| 03-03-14 | DC-038 | 0 | 0 | 0 | 20 | 5  | 0 | 0 | 0   | 298W         | 421V  | 1,5              | 400/27 | 2,92E-3 | 21 | No problems occurred, wafer for thickness distribution test.   |
| 06-03-14 | DC-039 | 0 | 0 | 0 | 10 | 5  | 0 | 0 | 0   | 298 W        | 464 V | 0,8<br>initially | 400/27 | 1,79E-3 | 21 | Film 1 in pressure series. Deposition stopped due to bad micro balance after 93:36 min. Chamber opened, target vacuum cleaned and mb replaced.   |
| 06-03-14 | DC-040 | 0 | 0 | 0 | 15 | 5  | 0 | 0 | 0   | 298 W        | 429 V | 0,8<br>initially | 400/27 | 2,40E-3 | 21 | Smooth deposition<br>The last 20 minutes a lot of small sparks on the target were observed   |
| 06-03-14 | DC-041 | 0 | 0 | 0 | 20 | 5  | 0 | 0 | 0   | 298 W        | 417 V | 0,9<br>initially | 400/27 | 2,95E-3 | 21 | Many sparks during deposition were observed<br>Plasma stopped at 298nm. Tried to restart manually with increased argon flow and switching of MP1 power supply but could not restart plasma. Chamber open, target and shutter cleaned and target measured to 2.2 mm. Target is a little dirty should be sputtered in pure Ar for 10-15 minutes. |
| 07-03-14 | DC-042 | 0 | 0 | 0 | 20 | 0  | 0 | 0 | 0   | 251W         | 385 V | 1,6<br>initially | 200/27 | 2,35E-3 | 21 | Deposited 200nm Ti on Bk7 25x25mm and P1 10x10 wafer pieces for cleaning the Ti target   |
| 07-03-14 | DC-043 | 0 | 0 | 0 | 30 | 5  | 0 | 0 | 0   | 298 W        | 408 V | 1,2<br>initially | 400/27 | 4,00E-3 | 21 | Smooth deposition<br>No problems   |

|          |        |   |   |   |    |   |   |   |   |       |       |                  |        |         |    |   |
|----------|--------|---|---|---|----|---|---|---|---|-------|-------|------------------|--------|---------|----|---|
| 07-03-14 | DC-044 | 0 | 0 | 0 | 40 | 5 | 0 | 0 | 0 | 298 W | 395 V | 1,3<br>Initially | 400/27 | 5,06E-3 | 21 | Smooth deposition<br>No problems  |
| 14-03-14 | DC-045 | 0 | 0 | 0 | 15 | 5 | 0 | 0 | 0 | 299 W | 416 V | 0,8<br>Initially | 400/27 | 2,38E-3 | 21 | Microbalance crystal broke at around 135 nm. Set deposite up to 200 Å/s. Constant power at 298W (running on time) Deposition ended at around 70 minutes (no plasma). Plasma could not be restarted. Kasper said that the thickness was reached and Cryofox stopped automatically  |
| 19-03-14 | DC-046 | 0 | 0 | 0 | 10 | 5 | 0 | 0 | 0 | 298 W | 446 V | 0,8              | 400/27 | 1,86E-3 | 21 | Density measurement. 1-1,1-2 and 1-3 weighted. The first one and half minuttess was done in pure Ti due to problem starting the plasma. Deposition time: 95 min. Many arcs observed near the end of the deposition.   |
| 19-03-14 | DC-047 | 0 | 0 | 0 | 40 | 5 | 0 | 0 | 0 | 298 W | 396 V | 1,4              | 400/27 | 5,01E-3 | 21 | Density measurement.<br>Chamber cleaned<br>target racetrack depth: 2,1mm<br>200nm pre-sputtered<br>Deposition time: 57,44 min   |
| 20-03-14 | DC-048 | 0 | 0 | 0 | 9  | 7 | 0 | 0 | 0 | 298   | 465 V | 0,6              | 400/27 | 2,15E-3 | 21 | Deposition failed due to plasma problems<br>Chamber opened, new MB, entire chamber cleaned (plates + target)  |
| 20-03-14 | DC-049 | 0 | 0 | 0 | 9  | 7 | 0 | 0 | 0 | 298   | 462 V | 0,6              | 400/27 | 2,26E-3 | 21 | Data taken at 43 minutes into deposition. Pressure increased from 2,15E-3 mbar to 2,26E-3 mbar during the first 40 minutes Many arcs during deposition (metal flakes on target in middle of plasma). Deposition time: about 130 min<br>Otherwise smooth deposition<br>Wafer shutter cleaned (a lot of metal flakes removed) |

|          |        |   |   |   |    |   |   |   |   |     |       |     |        |          |    |   |
|----------|--------|---|---|---|----|---|---|---|---|-----|-------|-----|--------|----------|----|---|
| 20-03-14 | DC-050 | 0 | 0 | 0 | 12 | 5 | 0 | 0 | 0 | 298 | 468 V | 0,6 | 400/27 | 2,23E-3  | 21 | Data taken at 35 minutes into deposition. Arcs and some metal flakes during deposition observed (not as bad as DC-049). Deposition time: around 105 min<br>Otherwise smooth deposition  |
| 20-03-14 | DC-051 | 0 | 0 | 0 | 16 | 3 | 0 | 0 | 0 | 298 | 437 V | 1,1 | 400/27 | 2,23E-3  | 21 | Cleaned wafer metal ring holder (a lot of material was on the rim)<br>No arcs during SOAK2 (only argon). When Nitrogen valve opened a lot of arcs started to appear throughout the entire deposition, but no metal flakes. Plasma lost at 230 nm, jump started with higher Argon flow and switched back to auto-mode<br>Deposition time: around 75 min<br>Otherwise smooth deposition |
| 25-03-14 | DC-052 | 0 | 0 | 0 | 18 | 1 | 0 | 0 | 0 | -   | -     | -   | -      | -        | -  | Microbalance broke after 10 minutes due to previous aluminum deposition. Deposition was canceled after 20 minutes (plasma went out several times)<br>Target changed   |
| 25-03-14 | DC-053 | 0 | 0 | 0 | 18 | 2 | 0 | 0 | 0 | 298 | 542 V | 2,0 | 400/27 | 2,23E-03 | 21 | Exchanged microbalance<br>Smooth deposition<br>Changed N2=2 sccm to achieve 2,23E-3 mbar chamber pressure<br>Deposition time: about 35 min  |
| 26-03-14 | DC-054 | 0 | 0 | 0 | 20 | 0 | 0 | 0 | 0 | 298 | 519 V | 2,0 | 400/27 | 2,20E-03 | 21 | First attempt failed (no plasma)<br>Kasper cleaned chamber<br>Second attempt went smooth (no arcs, stable plasma)<br>Deposition time: about 35 min  |
| 26-03-14 | DC-055 | 0 | 0 | 0 | 19 | 1 | 0 | 0 | 0 | 298 | 513 V | 2,0 | 400/27 | 2,20E-03 | 21 | Smooth deposition (no arcs, stable plasma)<br>Deposition time: about 33min  |
| 26-03-14 | DC-056 | 0 | 0 | 0 | 16 | 3 | 0 | 0 | 0 | 298 | 495 V | 1,5 | 400/27 | 2,26E-03 | 21 | Deposition failed due to plasma problems in the beginning (flakes on target)  |

|          |        |   |   |   |    |    |   |   |   |       |       |     |        |                      |    |  |
|----------|--------|---|---|---|----|----|---|---|---|-------|-------|-----|--------|----------------------|----|--|
| 02-04-14 | DC-057 | 0 | 0 | 0 | 19 | 1  | 0 | 0 | 0 | 448   | 478 V | 3,0 | 400/27 | 2,20E-03             | 21 | Chamber cleaned, new MB, shutter cleaned, wafer shutter cleaned<br>Power series first sample<br>Smooth deposition<br>Total deposition time: around 25 min  |
| 02-04-14 | DC-058 | 0 | 0 | 0 | 19 | 1  | 0 | 0 | 0 | 448   | 424 V | 0,8 | 400/27 | 2,23E-03             | 21 | Deposition failed – no plasma (flakes on target)   |
| 04-04-14 | DC-059 | 0 | 0 | 0 | 18 | 1  | 0 | 0 | 0 | 149   | 426 V | 1,0 | 400/27 | 2,26E-03             | 21 | Kasper took out the top plate and wafer shutter plus new microbalance. Measurement taken after 25min (state time). Total deposition time: about 65 min. Smooth deposition (no arcs, stable deposition) |
| 04-04-14 | DC-060 | 0 | 0 | 0 | 19 | 1  | 0 | 0 | 0 | 597 W | 486 V | 4,0 | 400/27 | 2,20-2,23E-03        | 21 | Total deposition time: about 16 min<br>Smooth deposition (no arcs, stable deposition) (wrong nitrogen flow used)   |
| 04-04-14 | DC-061 | 0 | 0 | 0 | 19 | 2  | 0 | 0 | 0 | 597 W | 490 V | 4,1 | 400/27 | 2,23-2,26E-03        | 21 | Total deposition time: about 16 min<br>Smooth deposition (no arcs, stable deposition)  |
| 04-04-14 | DC-062 | 0 | 0 | 0 | 6  | 10 | 0 | 0 | 0 | 597 W | 724 V | 1,5 | 400/27 | 2,23E-03 to 2,32E-03 | 21 | Total deposition time: about 45 min<br>Smooth deposition (no arcs, stable deposition)  |
| 07-04-14 | DC-063 | 0 | 0 | 0 | 8  | 9  | 0 | 0 | 0 | 448 W | 548 V | 1,0 | 400/27 | 2,20E-3              | 21 | Total deposition time: about 65 min<br>Smooth deposition (no arcs, stable deposition) (error with photoresist 25x25mm)   |
| 15-04-14 | DC-064 | 0 | 0 | 0 | 17 | 4  | 0 | 0 | 0 | 597 W | 509 V | 3,8 | 400/27 | 2,20E-03             | 21 | First 50 nm at ramped up power while deposition was running<br>Total deposition time: about 19 min<br>Smooth deposition (some arcs, stable deposition)   |
| 15-04-14 | DC-065 | 0 | 0 | 0 | 14 | 6  | 0 | 0 | 0 | 597 W | 539 V | 2,8 | 400/27 | 2,23E-03             | 21 | Total deposition time: about 23 min<br>Material from shutter fell down on target – more arcs observed. Plasma went about 5 times during deposition. Shutter needs to be removed                        |
| 22-04-14 | DC-066 | 0 | 0 | 0 | 17 | 4  | 0 | 0 | 0 | 597 W | 500 V | 3,9 | 400/27 | 2,20E-03             | 21 | Smooth deposition. Total deposition time: about 17 min. No arcs  |

|          |        |   |   |   |    |    |   |   |   |       |       |     |        |          |    |  |
|----------|--------|---|---|---|----|----|---|---|---|-------|-------|-----|--------|----------|----|--|
| 22-04-14 | DC-067 | 0 | 0 | 0 | 13 | 6  | 0 | 0 | 0 | 597 W | 538 V | 2,7 | 400/27 | 2,20E-03 | 21 | Smooth deposition. Total deposition time: about 24 min. No arcs  |
| 22-04-14 | DC-068 | 0 | 0 | 0 | 10 | 8  | 0 | 0 | 0 | 597 W | 560 V | 1,9 | 400/27 | 2,26E-03 | 21 | Smooth deposition. Total deposition time: about 37 min. No arcs<br>Switched from Ar:11 to Ar:10 at t=10 min and from Ar:10 to Ar:9sccm at t=25 min   |
| 23-04-14 | DC-069 | 0 | 0 | 0 | 19 | 1  | 0 | 0 | 0 | 298 W | 416 V | 2,0 | 400/27 | 2,26E-03 | 21 | Stress wafers for metallic production. Transverse and longitudinal gauge factor samples (reproduction of DC-055)   |
| 23-04-14 | DC-070 | 0 | 0 | 0 | 10 | 7  | 0 | 0 | 0 | 298 W | 442 V | 0,7 | 400/27 | 2,26E-03 | 21 | Failed due to plasma problems. A lot of particles on the target. Shutter needs to be removed   |
| 07-05-14 | DC-071 | 0 | 0 | 0 | 19 | 1  | 0 | 0 | 0 | 597 W | 486 V | 3,5 | 400/27 | 2,23E-03 | 21 | Smooth deposition, no arcs, total time: about 16 min   |
| 07-05-14 | DC-072 | 0 | 0 | 0 | 19 | 2  | 0 | 0 | 0 | 597 W | 483 V | 3,7 | 400/27 | 2,26E-3  | 21 | Smooth deposition, no arcs, total time: about 18 min   |
| 15-05-14 | DC-073 | 0 | 0 | 0 | 6  | 10 | 0 | 0 | 0 |       |       |     |        |          |    | Failed due to red glowing target. Stopped at 10nm. The target has been used up.  |
| 15-05-14 | DC-074 | 0 | 0 | 0 | 6  | 10 | 0 | 0 | 0 |       |       |     |        |          |    | Continuation of failed deposition on the 07-05-14 where the target was used up. New target inserted. Deposition failed it was not possible to run at the desired parameters due to a too high voltage on the new target. |

**Units:**

Ar, N2, O2 flow in sccm

Rate: Å/s

Pressure = main chamber pressure

## A7. Wafer substrate information

| Identifier | Diameter   | Thickness | Orientation | Dopant | Resistivity          | Polishing | Film                        |
|------------|------------|-----------|-------------|--------|----------------------|-----------|-----------------------------|
| P1         | 100 mm     | 525±25 µm | <100>       | B      | 1 - 100 Ohm-cm       | SSP       | None                        |
| P2         | 100 mm     | 525 µm    | <100>       | B      | 0,002 - 0,005 Ohm-cm | SSP       | 300 nm SiO2                 |
| P3         | 100 mm     | 525 µm    | <100>       | B      | 1 - 100 Ohm-cm       | SSP       | 300 nm low-stress nitride   |
| P4         | 100 mm     | 500 µm    | <100>       | B      | 0 - 100 Ohm-cm       | DSP       | None                        |
| P5         | 100 mm     | 525 µm    | <100>       | B      | 0 - 30 Ohm-cm        | DSP       | None                        |
| P6         | 100 mm     | 525 µm    | <100>       | B      | 0 - 30 Ohm-cm        | DSP       | 514±12nm low-stress nitride |
| P7         | 100 mm     | 200 µm    | <100>       | B      | 0,1 - 5 Ohm-cm       | DSP       | None                        |
|            |            |           |             |        |                      |           |                             |
|            |            |           |             |        |                      |           |                             |
|            |            |           |             |        |                      |           |                             |
| N1         | 100 mm     | 525 µm    | <100>       | P      | 5 - 10 Ohm-cm        | SSP       | None                        |
| N2         | 100 mm     | 525 µm    | <100>       | Sb     | 0,005 - 0,020 Ohm-cm | SSP       | None                        |
| N3         | 100 mm     | 525 µm    | <100>       | Sb     | 0,005 - 0,020 Ohm-cm | SSP       | 100 nm SiO2                 |
| N4         | 100 mm     | 525 µm    | <100>       | As     | 0,001 - 0,006 Ohm-cm | SSP       | 200 nm SiO2                 |
| N5         | 100 mm     | 400 µm    | <100>       | P      | 6-14 Ohm-cm          | SSP       | None                        |
| N6         | 100 mm     | 525 µm    | <100>       | As     | 0,001 - 0,005 Ohm-cm | SSP       | 100 nm low-stress nitride   |
| N7         | 100 mm     | 400 µm    | <100>       | P      | 6-14 Ohm-cm          | SSP       | 100 nm SiO2                 |
| N8         | 100 mm     | 525 µm    | <100>       | Sb     | 0,005 - 0,020 Ohm-cm | SSP       | 300 nm SiO2                 |
| N9         | 100 mm     | 500 µm    | <100>       | As     | 0,001 - 0,005 Ohm-cm | SSP       | 300 nm SiO2                 |
| N10        | 100 mm     | 381 µm    | <100>       | Sb     | 0,005-0,02 Ohm-cm    | SSP       | None                        |
| N11        | 100 mm     | 525 µm    | <100>       | P      | 5 - 10 Ohm-cm        | SSP       | 492nm±14nm SiO2             |
| N12        | 100 mm     | 525 µm    | <100>       | Sb     | 0,005 - 0,020 Ohm-cm | SSP       | 302nm±5nm SiO2              |
| N13        | 100±0,5 mm | 500±25 µm | <100>       | As     | 0,001 - 0,005 Ohm-cm | SSP       | None                        |

| 1 | Identifier | Diameter | Thickness | Orientation | Notes              | Polishing |
|---|------------|----------|-----------|-------------|--------------------|-----------|
| 2 | G1         | 100 mm   | 500 µm    |             | Pyrex 7740         |           |
| 3 | G2         | 100 mm   | 200 µm    |             | Borofloat          |           |
| 4 | G3         | 100 mm   | 500 µm    |             | BK7 Glass          | DSP       |
| 5 | G4         | 101,6 mm | 1,1 mm    |             | Borosilicate Glass | SSP       |
| 6 | G5         | 100 mm   | 300 µm    |             | BK7 Glass          | DSP       |
| 7 |            |          |           |             |                    |           |

## A8. Four point probe procedure

### *Procedure for making sheet resistivity measurements with 4-point probe*

Written by Nis Dam Madsen in corporation with Mathias Hausladen

#### **Keithley 2450 Setup**

The Keithley sourcemeter needs to be setup for 4-wire resistivity measurement. The good standard settings have been saved in the scripts **Sheetresistance1mA** and **Sheetresistance10mA**, see Fig 111. These can be loaded from Menu->Script column->Run script. Running one of these scripts will setup the instruments with the following values.

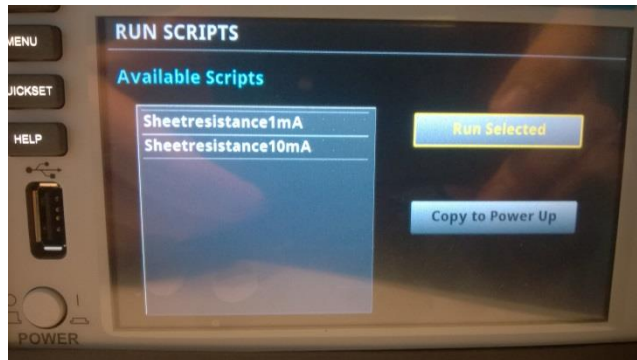


Figure 110: Setup scripts for 4-wire resistivity measurements.

In table 1 the most important settings are shown and standard values are given. These values should be checked on the instrument before the measurements are initiated.

| Setting checklist   | Value       | Explanation   |
|---------------------|-------------|---|
| Source current      | 1/10 mA     | Current driven through the sample                               |
| Source range        | Auto        | Accuracy of the source current measurement                      |
| Filter              | 10 (repeat) | Number of measurements averaged over for each read-out value    |
| NPLC                | 10          | Number of 50 Hz cycles used in each measurement                 |
| Auto zero           | On          | Recalibration of the instrument before each measurement         |
| Offset compensation | On          | Subtracts voltage measurement made at 0 A source current.       |
| Source readback     | On          | Uses the measured source current for calculation of resistance. |

Table 1: Settings for Keithley 2450

In table 2, screenshots of the setting screens are displayed. Go and check these before starting the measurement, the path to the screens are given below each picture. Also check that the 4-point probe is wired correctly to the Keithley.

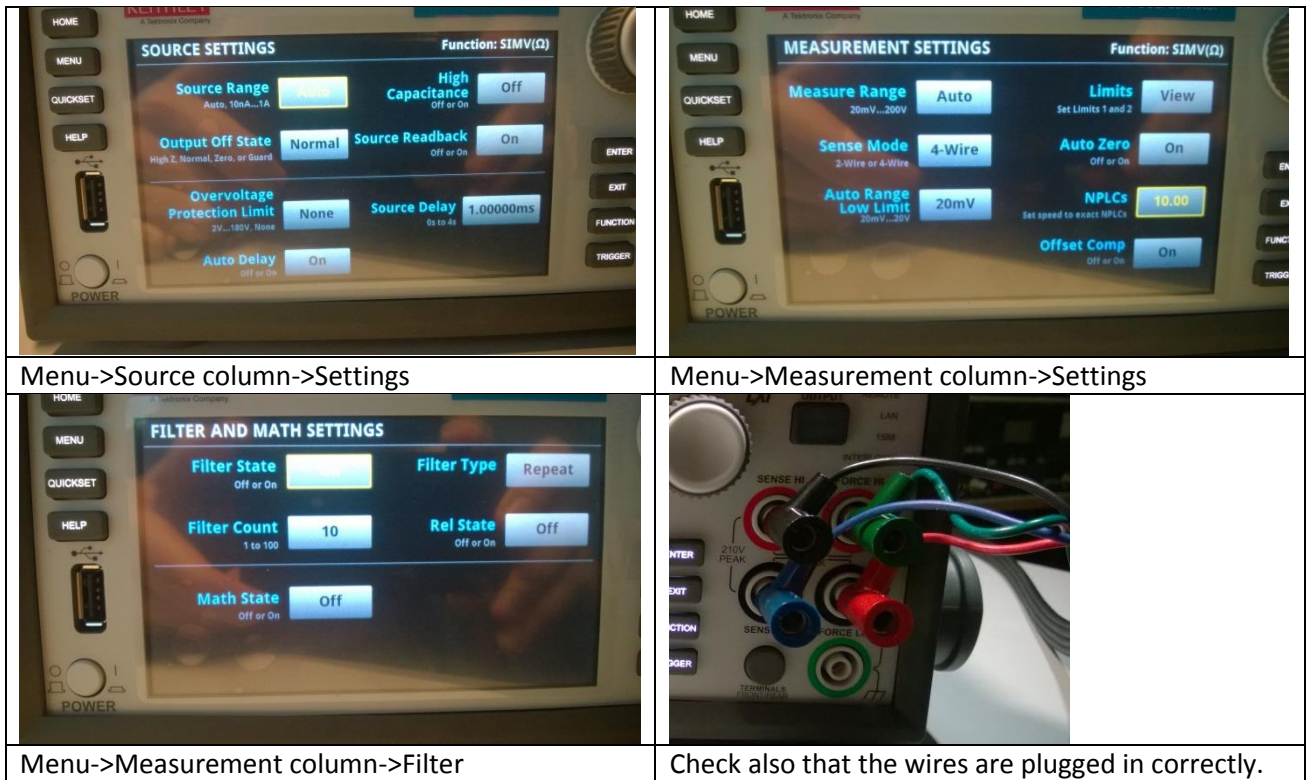


Table 2: The screens to check before starting a measurement.

On the measurement screen, check that the measurement mode is set to continuous measurement by pressing the place “UNVAL” in Fig. 112. Otherwise the instrument will not make measurements.



Figure 111: Check that the measurement mode is set to continuous.

### Four point probe sample placement procedure

Start by lifting up the probe by turning the height adjustment knob shown in Fig. 113 until the probe is 1 cm above the chuck. Now engage the lever so that the probe is in the lowest position. Then place the sample under the probe tips and slowly approach the sample with the tips. **Use reflections and plenty of light to see where the tips are.** When all the tips have contact to the sample - lift up the probe with lever. **Never adjust the height using the lever!**

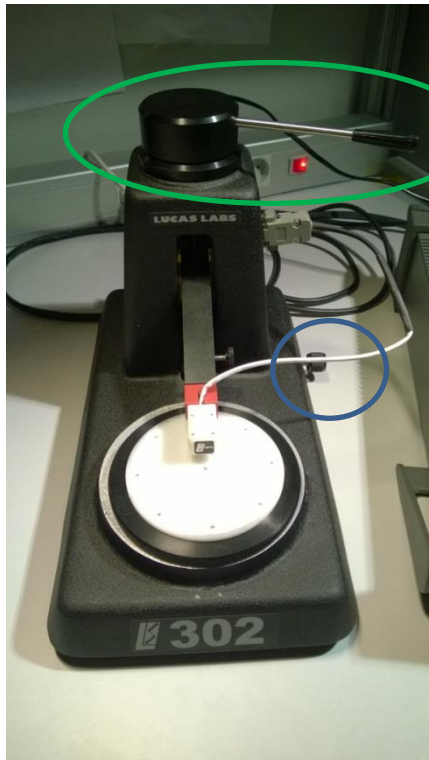


Figure 112: Probe station for 4-point resistivity measurements. The height adjustment knob is marked with a blue circle and the probe engagement lever is marked with a green circle.

Now follow the instructions in table 3 to make the measurements. It is good practice to make at least 4 measurements and it is important to take out the sample between each measurement to obtain the correct statistics for comparing different samples. The number of averages used in the filter and NPLC settings means that each read-out value will take ten seconds or so to produce, this means that it will take a little time before a value is displayed on the Keithley. If the time is long then check that the Keithley is set to continuous measurement

|  |  |  |  |
|--|--|--|--|
|  |  |  |  |
| Align the sample from the front.   |  | ... and from the side.   |  |
|  |  |  |  |
| Engage sample with probe, turn on Keithley and wait for reading. Turn off Keithley before disengaging and disengage. |  | Remember to lift up!<br>Remove sample and rotate sample to repeat measurement. |  |

Table 3: Repeated measurement procedure to obtain statically reliable error bars on the measured samples.

## A9. Four point probe measurement repeatability experiment

Goal: check the relative error related to the placing repeatability of the probe in the middle of the sample area

Description: Probe was placed in the middle of the sample and lowered, measurement were taken, probe was lifted, sample was removed and procedure was performed again

Test sample: RF-023-1

|                   |            |                                     |             |
|-------------------|------------|-------------------------------------|-------------|
| Correction factor | 4,186622   | Resistance standard deviation       | 0,442       |
| Dimensions        | 24 x 24 mm | Sheet resistance standard deviation | 1,851968435 |
| Thickness [nm]    | 263        | Resistivity standard deviation      | 4,87068E-05 |

| Measurement | Resistance ( $\Omega$ ) | Sheet resistance ( $\Omega$ ) | $\rho$ ( $\Omega\text{cm}$ ) |
|-------------|-------------------------|-------------------------------|------------------------------|
| 1           | 31,541                  | 132,05                        | 3,473E-03                    |
| 2           | 31,133                  | 130,34                        | 3,428E-03                    |
| 3           | 31,403                  | 131,47                        | 3,458E-03                    |
| 4           | 31,537                  | 132,03                        | 3,472E-03                    |
| 5           | 31,568                  | 132,16                        | 3,476E-03                    |
| 6           | 31,588                  | 132,25                        | 3,478E-03                    |
| 7           | 31,455                  | 131,69                        | 3,463E-03                    |
| 8           | 32,491                  | 136,03                        | 3,578E-03                    |
| 9           | 32,372                  | 135,53                        | 3,564E-03                    |
| 10          | 32,067                  | 134,25                        | 3,531E-03                    |

mean resistance      31,716  
 relative difference    1,39%      (*standard deviation/mean*)

**Conclusion:** the relative error for the placing of the probe in the middle of the sample over a course of 10 tries is around 1,4% for the 25x25mm sample  
 This error should be considered when evaluating the resistivity vs. time graphs

Test sample: RF-023-3

|                   |              |                                     |             |
|-------------------|--------------|-------------------------------------|-------------|
| Correction factor | 3,551994     | Resistance standard deviation       | 0,725       |
| Dimensions        | 24 x 12.5 mm | Sheet resistance standard deviation | 2,576245683 |
| Thickness [nm]    | 263          | Resistivity standard deviation      | 6,77553E-05 |

| Measurement | Resistance ( $\Omega$ ) | Sheet resistance ( $\Omega$ ) | $\rho$ ( $\Omega\text{cm}$ ) |
|-------------|-------------------------|-------------------------------|------------------------------|
| 1           | 44,218                  | 157,06                        | 4,131E-03                    |
| 2           | 44,525                  | 158,15                        | 4,159E-03                    |
| 3           | 45,881                  | 162,97                        | 4,286E-03                    |
| 4           | 44,719                  | 158,84                        | 4,178E-03                    |
| 5           | 46,035                  | 163,52                        | 4,300E-03                    |
| 6           | 45,903                  | 163,05                        | 4,288E-03                    |
| 7           | 44,775                  | 159,04                        | 4,183E-03                    |
| 8           | 44,500                  | 158,06                        | 4,157E-03                    |
| 9           | 45,596                  | 161,96                        | 4,259E-03                    |
| 10          | 44,280                  | 157,28                        | 4,137E-03                    |

mean resistance      45,043  
relative difference    1,61%      (*standard deviation/mean*)

**Conclusion:** the relative error for the placing of the probe in the middle of the sample over a course of 10 tries is around 1,6 % for the 25x12.5mm sample  
This error should be considered when evaluating the resistivity vs. time graphs

## A10. AFM lift-off structure

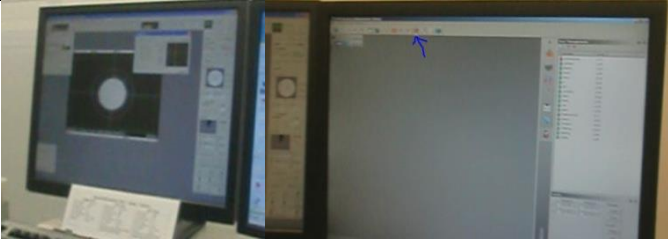
Figure 113 shows the negative photolithographic and lift-off procedure for creating the thin film thickness pattern. In case of a positive process step 6 and 7 can be jumped over.

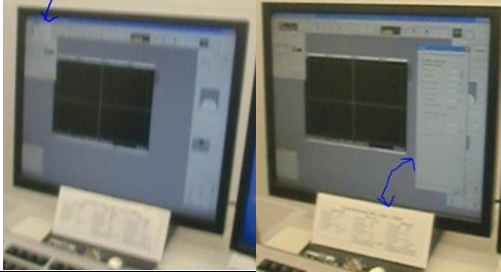
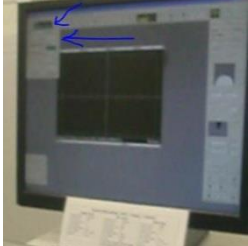
| #  | Process                                 | Description  |
|----|---|--|
| 1  | Starting wafer                          | Si (100), 4", single-sided polished, thickness = 525 $\mu\text{m}$   |
| 2  | Deposit adhesion promoter (HMDS)        | See HMDS oven manual   |
| 3  | Spin on photo resist                    | EBS11 spin coater, resist: AZ 5214E, resist thickness = 1.5 $\mu\text{m}$<br>1. Automatic resist dispense (3s)<br>2. Spin at 500 rpm for 5 s (acc. 5000 rps <sup>2</sup> )<br>3. Spin at 4000 rpm for 30 s (acc. 10000 rps <sup>2</sup> )  |
| 4  | Prebake                                 | Hot plate, 90°C for 60s  |
| 5  | UV exposure                             | KS Mask aligner, exposure time = 2.4 s   |
| 6  | Inversion bake                          | Hot plate 130 °C for 100s  |
| 7  | Flood exposure                          | KS Mask aligner, exposure time = 25 s, not mask!   |
| 8  | Develop                                 | Developer: AZ 351B (mix with DI water, ratio 1:4), 60 s, agitation!  |
| 9  | Rinse and dry                           | Rinse in water (fine rinse bath) for 2 min, spin dry.  |
| 10 | Dicing saw                              | Cutting wafer in 10x10 mm square pieces with dicing saw Disco DAD-2H5)   |
| 10 | Deposit TiO <sub>x</sub> N <sub>y</sub> | <i>Example recipe</i><br>Cryofox, Plasma clean settings: Ar: 50 sccm, Pregas: 0,5 sccm, time: 5min<br>Reactive DC-sputtering settings: Ar: 40 sccm, N2: 10 sccm, O2:2 sccm<br>Pulse on: 4 sec, pulse off: 14s<br>Rate: 0,7 Å/s, Temperature: 20 °C<br>Pressure: 5,93E-3 mbar<br>Thickness: 400nm, tooling factor: 27 |
| 11 | Lift-off                                | Ultrasonic bath, acetone.<br>Wash off with acetone, isopropanol, DI-water. Blow dry with nitrogen  |
| 12 | AFM                                     | Measure thickness of TiO <sub>x</sub> N <sub>y</sub> thin film   |

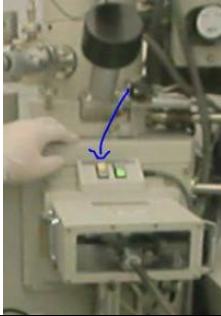
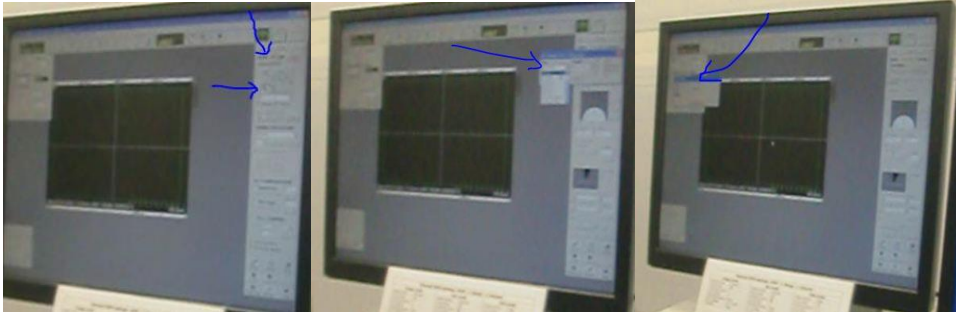
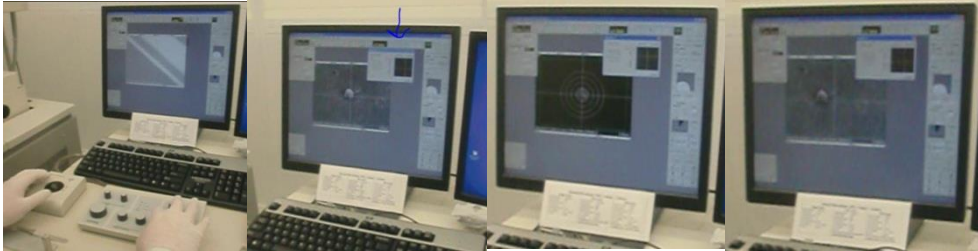
Figure 113- silicon wafer sample production

## A11. EDX procedure

### Characterization procedure for EDX system on SEM in NanoSYD Cleanroom

|   |  |  |
|---|--|--|
| 1 | Press standby off so the cooling is turned on. Normally it take 30 minutes to stabilize.   |    |
| 2 | Check if there is an electron beam.<br>In case there is no beam on left screen log in "Lfy Quantum program" (right computer screen)<br>Choose Administrator – no password<br>Press "intern" and "beam on" – shut down „Lfy“<br>On left screen click - see if beam turns on and then press "beam off" |    |
| 3 | Change to computer for EDX system  |   |
| 4 | Change cables on the backside (For this the electron beam has to be turned off!)<br><br>Plug in cables of EDX computer<br><br>Change SEM interface plug to EDX computer  |  |

|   |   |  |   |
|---|---|--|---|
|   |   |    |   |
| 5 | <p>Press "air chamber"<br/>Put sample on holder<br/>Check standard height<br/>Load the sample and close chamber<br/>Press "evac" (pumping down)</p> |    |   |
| 6 | <p>Install SEM settings<br/>Press "setup" and "column"<br/>Use data from Kasper's table</p>   |   |   |
| 7 | <p>Pick acceleration voltage and current</p>  |  | <p>Look at what material you want to measure. The acceleration voltage depends on the K-L energies levels of the material you want to measure. Pick an acceleration voltage which is at least 3x higher than you highest energy level. In this project we want to measure on Ti and Nitrogen and Oxygen. Titanium has</p> |

|    |  |   |
|----|--|---|
|    |  | K-alpha of about 5ev so we take 15ev as acceleration voltage.                       |
| 8  | <p>Insert sample to chamber<br/>         Press "open"<br/>         Insert arm -&gt; turn handle right (unlock) -&gt; pull arm back until it clicks -&gt; press "close"</p>   |   |
| 9  | <p>Adjust sample size in SEM software<br/>         Go to SEM/Stage/Utilities<br/>         Press "stage" -&gt; and "set"<br/>         It's good to do this to get the right graphical representation of the sample<br/>         + it's good if you want to tilt the sample</p> <p>Set standard height to 15 (no deviation)<br/>         It will start high voltage<br/>         Set to home position when asked. (sample will move to the middle)</p> |   |
| 10 | <p>Calibrating the focus (hard part)<br/>         Move to the edge of the sample<br/>         Switch to high magnification<br/>         Find something particle<br/>         Press "Align"<br/>         Beam alignment should be in the middle<br/>         Press "Aperture alignment"<br/>         Adjust beam so it is stable</p>  |  |

|    |   |  |  |
|----|---|--|--|
|    |   |  |  |
| 11 | <p>Press "Stage"</p> <p>Change home position to 15 mm</p> <p>Do this after you focused on something</p><br><p>Change magnification to the area you want to research</p> |  |  |
| 12 | <p>Start EDX software! (right computer screen) and perform scan</p>   |  |  |

## A12. EDX measurement standard

Login: edx      password: edx

Wait 30 minutes after switching on the EDX cooling

### **Adjust parameters in setup → column**

Probe current: high

Focus: HR

Condenser lens 1: 1-2

Focus depth: 1

Working distance: 15mm

ACC. Voltage: 10kV (at lower voltage EDX is more surface sensitive)

Current: 20uA

Insert detector (press symbol on top right)!!!

### **During measurement:**

Magnification: x50k (1 micrometer)

Always measure in the middle of the sample

### **Acquire spectra:**

Use the automatic option. Change to precise!

### **Analysis:**

Use the **interactive PB-ZAF** automatic standard-less option.

Do a manual analysis (better according to Bruker)

- Press quantify
- Change to logarithmic scale (y-axis)
- Press continue
- Click with right mouse button and drag along spectrum
- Change logarithmic scale
- Press continue, check off “bremsstrahlung”, check off background free, change to error1 sigma (table)
- Add spectrum to report

### **Ending program**

- Check mark “retractor” and “cooling”

### A13. EDX relative concentration and error calculations

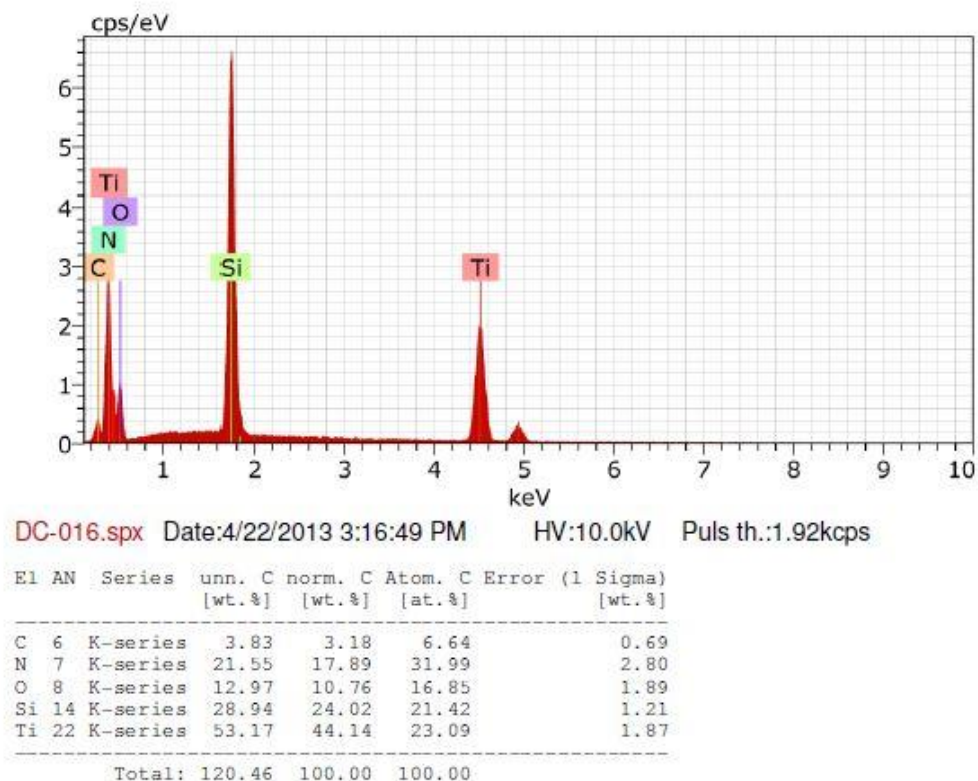


Figure 114 – EDX measurements for sample DC-016

Figure 115 lists the EDX measurement data obtained from Sample DC-016 to DC-025 with the calculated Nitrogen (x) and oxygen (y) concentrations of the  $TiO_xN_y$  thin films.

| Samples | Pulse time [s] | Silicon [at. %] | Carbon [at. %] | Titanium [at. %] | Nitrogen [at. %] | Oxygen [at. %] | Nitrogen [x] | Oxygen [y] |
|---------|----------------|-----------------|----------------|------------------|------------------|----------------|--------------|------------|
| DC-016  | 0              | 21,42           | 6,64           | 23,09            | 31,99            | 16,85          | 1,39         | 0,73       |
| DC-017  | 2              | 23,25           | 7,75           | 21,36            | 27,49            | 20,16          | 1,29         | 0,94       |
| DC-018  | 4              | 23,09           | 5,39           | 22,78            | 25,53            | 23,22          | 1,12         | 1,02       |
| DC-019  | 6              | 24,49           | 4,52           | 22,92            | 21,55            | 26,51          | 0,94         | 1,16       |
| DC-020  | 8              | 25,69           | 5,11           | 23,57            | 17,23            | 28,38          | 0,73         | 1,20       |
| DC-021  | 10             | 24,83           | 6,05           | 23,42            | 13,34            | 32,35          | 0,57         | 1,38       |
| DC-022  | 12             | 25,25           | 4,93           | 23,15            | 11,87            | 34,80          | 0,51         | 1,50       |
| DC-023  | 14             | 25,55           | 4,98           | 23,61            | 4,83             | 41,03          | 0,20         | 1,74       |
| DC-024  | 16             | 26,06           | 4,65           | 23,42            | 2,32             | 43,54          | 0,10         | 1,86       |
| DC-025  | 18             | 22,61           | 2,67           | 24,83            | 1,54             | 47,73          | 0,06         | 1,92       |

Figure 115 – EDX measurement data - sample DC-016 to DC-025

## Calculations for oxygen (x) and nitrogen (y) concentrations for TiOxNy

Example: sample DC-017

$$\text{nitrogen } [x] = \frac{\text{nitrogen } [\%]}{\text{titanium } [\%]} = \frac{27,49 \%}{21,36 \%} = 1,29$$

$$\text{oxygen } [x] = \frac{\text{oxygen } [\%]}{\text{titanium } [\%]} = \frac{20,16 \%}{21,36 \%} = 0,94$$

Figure 116 shows the fabrication parameters and the relative values for the EDX measurements results of titanium, nitrogen and oxygen compositions for sample DC-016 to DC-025 without carbon and silicon. The parameter influencing the sample composition is the oxygen on/off time in seconds, which also is represented as the duty cycle in percentage. The argon flow was kept at 40 sccm, nitrogen at 10 sccm and oxygen at 2 sccm.

| Sample | Duty cycle [%] | O2 On [s] | O2 Off [s] | Titanium [at. %] | Nitrogen [at. %] | Oxygen [at. %] |
|--------|----------------|-----------|------------|------------------|------------------|----------------|
| DC-016 | 0,00           | 0         | 18         | 32,10            | 44,47            | 23,43          |
| DC-017 | 11,11          | 2         | 16         | 30,95            | 39,83            | 29,21          |
| DC-018 | 22,22          | 4         | 14         | 31,85            | 35,69            | 32,46          |
| DC-019 | 33,33          | 6         | 12         | 32,29            | 30,36            | 37,35          |
| DC-020 | 44,44          | 8         | 10         | 34,07            | 24,91            | 41,02          |
| DC-021 | 55,56          | 10        | 8          | 33,89            | 19,30            | 46,81          |
| DC-022 | 66,67          | 12        | 6          | 33,16            | 17,00            | 49,84          |
| DC-023 | 77,78          | 14        | 4          | 33,99            | 6,95             | 59,06          |
| DC-024 | 88,89          | 16        | 2          | 33,80            | 3,35             | 62,85          |
| DC-025 | 100,00         | 18        | 0          | 33,51            | 2,08             | 64,41          |

Figure 116 – Reactive DC sputtering settings for sample DC-016 to DC-025

### Duty cycle calculation for figure 116

Example: sample DC-017

$$\text{duty cycle} = \frac{\text{pulse time } [s]}{\text{pulse period } [s]} * 100\% = \frac{2 \text{ s}}{18 \text{ s}} * 100\% = 11,11\%$$

**Data conversion calculations (relative values)**

**Titanium [%]**

$$Titanium_{adjusted}[\%] = \frac{Titanium [\%]}{(Titanium [\%] + Nitrogen [\%] + Oxygen [\%])} * 100\%$$

**Nitrogen [%]**

$$Nitrogen_{adjusted}[\%] = \frac{Nitrogen [\%]}{(Titanium [\%] + Nitrogen [\%] + Oxygen [\%])} * 100\%$$

**Oxygen [%]**

$$Oxygen_{adjusted}[\%] = \frac{Oxygen [\%]}{(Titanium [\%] + Nitrogen [\%] + Oxygen [\%])} * 100\%$$

Example: sample DC-017

$$Titanium_{adjusted}[\%] = \frac{21,36\%}{(21,36\% + 27,49\% + 20,16\%)} * 100\% = 30,95\%$$

**Error conversion from [wt. %] to [at. %]:**

Re-calculated the error bar for [wt. %] to a relative value, which then is used to calculate the value for [at. %]. The following shows an example with titanium (Ti) from figure 117 for sample DC-019:

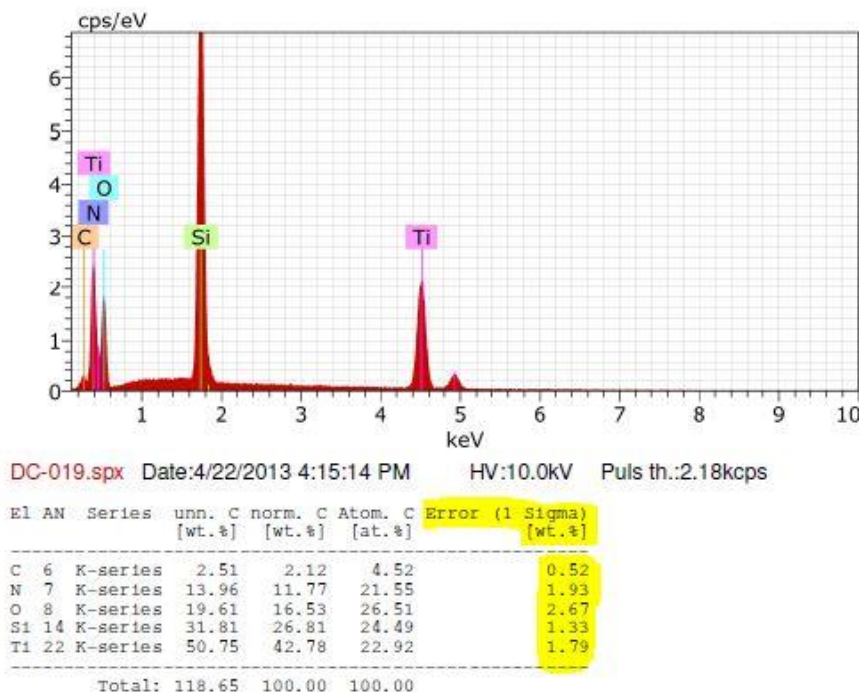


Figure 117 – EDX measurement for sample DC-019

Relative error bar =  $1,79 / 42,78 = 0,0418 = 4,18 \%$   
 This means that the error for the Ti concentration is 4,18%  
 Error bar for [at.%) =  $22,92 * 0,0418 = 0,958$   
 Which means that the Ti-concentration error for [at.%) =  $22,92 +/- 0,958$

Because the data for silicon and carbon have been removed from the measurements the errors also have to be adjusted.

The error for sample 19 [at.%) has been adjusted by calculating the ratio between the titanium [at.%) and Ti error bar [at.%) :  $22,92/0,958 = 23,924$

With this ratio the adjusted ratio for the relative values for Ti have been calculated:

Relative titanium value: 32,29 [at.%)

$32,29/23,875 = 1,35$

This gives the error which fits to the relative value for Ti [at.%)

Figure 118 lists all the calculation results for duty cycle, adjusted titanium, nitrogen, oxygen [at.%) and the adjusted error bars [at.%)

| Sample | Duty cycle [%] | Titanium [at. %] | Ti error bar [at.%) | Nitrogen [at. %] | N <sub>2</sub> error bar [at.%) | Oxygen [at. %] | O <sub>2</sub> error bar [at.%) |
|--------|----------------|------------------|---------------------|------------------|---------------------------------|----------------|---------------------------------|
| DC-016 | 0,00           | 32,10            | 1,36                | 44,47            | 6,96                            | 23,43          | 4,11                            |
| DC-017 | 11,11          | 30,95            | 1,29                | 39,83            | 6,22                            | 29,21          | 4,85                            |
| DC-018 | 22,22          | 31,85            | 1,35                | 35,69            | 5,76                            | 32,46          | 5,38                            |
| DC-019 | 33,33          | 32,29            | 1,35                | 30,36            | 4,98                            | 37,35          | 6,03                            |
| DC-020 | 44,44          | 34,07            | 1,41                | 24,91            | 4,22                            | 41,02          | 6,50                            |
| DC-021 | 55,56          | 33,89            | 1,39                | 19,30            | 3,35                            | 46,81          | 7,16                            |
| DC-022 | 66,67          | 33,16            | 1,37                | 17,00            | 3,13                            | 49,84          | 7,75                            |
| DC-023 | 77,78          | 33,99            | 1,37                | 6,95             | 1,49                            | 59,06          | 8,64                            |
| DC-024 | 88,89          | 33,80            | 1,34                | 3,35             | 0,87                            | 62,85          | 9,00                            |
| DC-025 | 100,00         | 33,51            | 1,33                | 2,08             | 0,62                            | 64,41          | 9,17                            |

Figure 118 - Converted data with error bars

#### A14. SEM top-view and Cross-section images

The top-view images were done at 100k magnification at 500nm resolutions using an acceleration voltage of 5kV. The cross-section view images were done at 250k magnification at 200nm field of view, using an acceleration voltage of 5-10kV and a beam current of 10 microampere. The working distance is 8 mm.

For the cross-section measurements the samples needed to be cut in half in order to achieve information about the thin film structure. For this the sample was placed on a tissue and a cut was applied to the sample at the edge with a diamond pencil. By applying a force to the diamond pencil while cutting the sample will flake in the middle, resulting in to two pieces. (See figure 119)

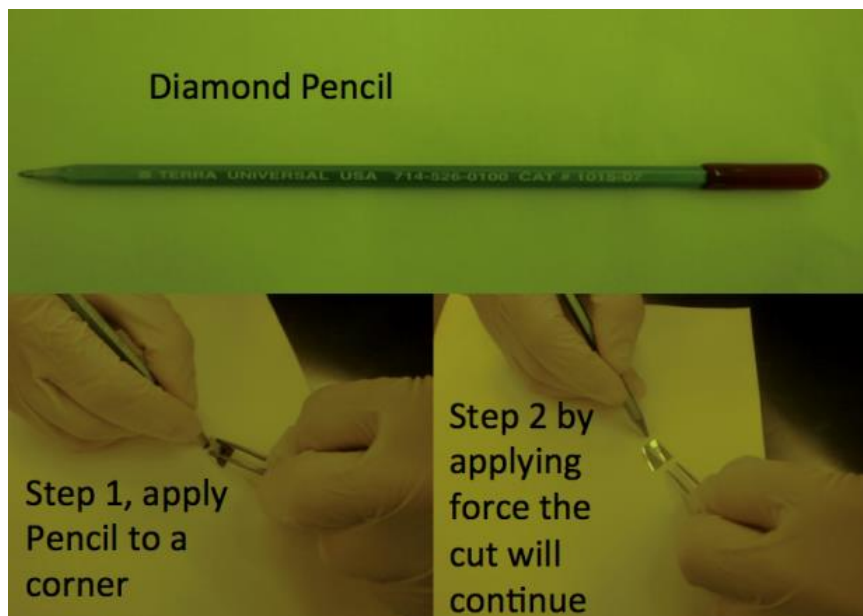


Figure 119 - Sample cutting with diamond pencil

In order to increase the SEM image resolution of the cross-section the samples were sputter coated with a few nanometer (1-3nm) Au/Pd (60:40) mixture with a "Cressington 208HR" sputter coater in order to avoid charging effects by the SEM electron beam. The tooling factor has been adjusted to 6.6 nm after initial experiments.

## A15. Stress wafer measurements and calculations

The wafer radius for the stress measurements were performed with a contact profilometer (Veeco Dektak 150) using a diamond stylus which is laterally moved in contact mode across the sample. The substrates were 25x3 mm P7 silicon wafers with a thickness of 200 micro meters.

On the backside of the stress wafer an identification number is written with a diamond cutter. The wafer should be placed with the number facing the black marking on the Dektak platform. The diamond stylus should be placed about 2-3 mm from the wafer edge on top of the wafer (see figure 120).

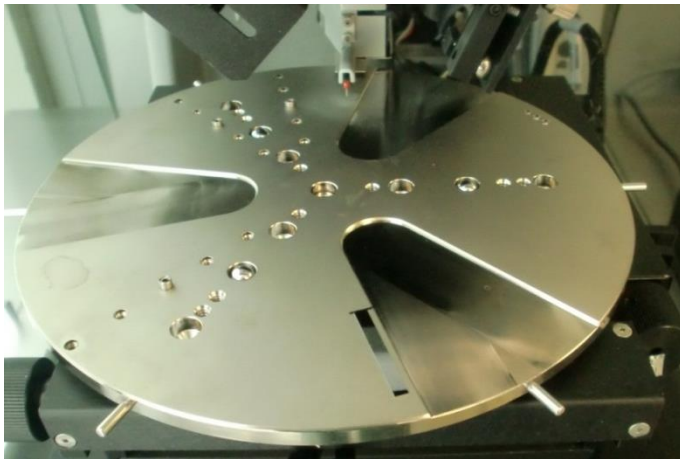


Figure 120 – Dektak with placed stress wafer

The scan parameters are shown in figure 121.

Scan length: 15 micro meters

Scan duration: 30 sec

Analytical functions: radius

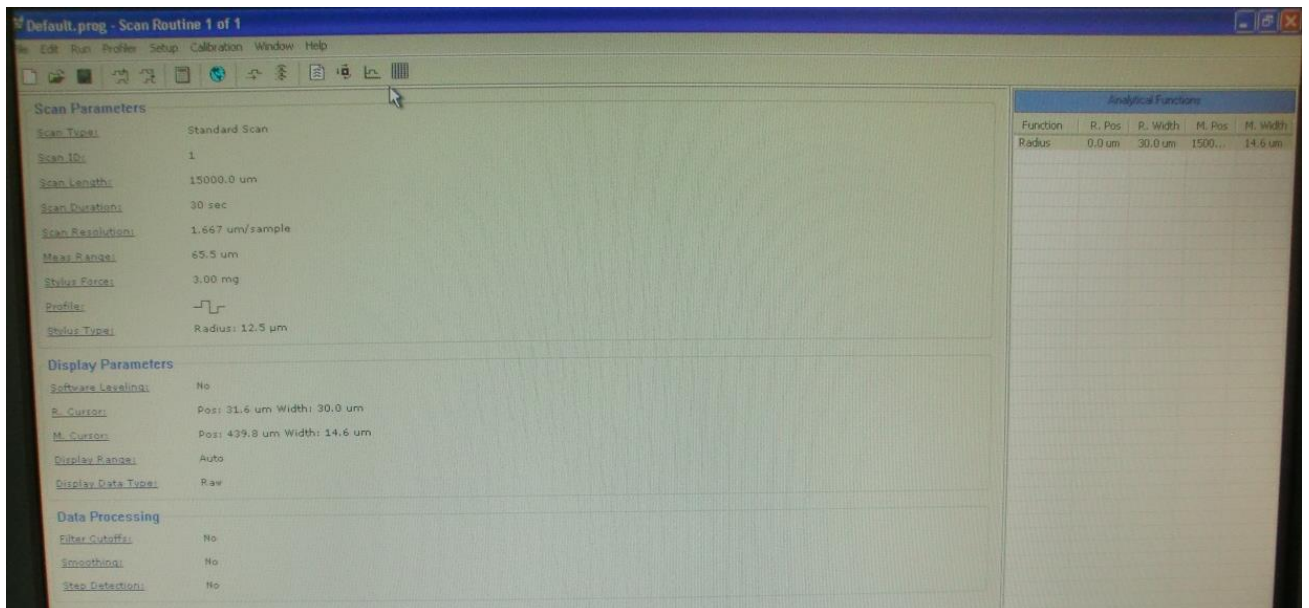


Figure 121 – Dektak scanning parameters

Figure 122 and figure 123 show examples of the dektak measurement data, plotting the thin film curvature in height [ångström] vs. distance [micrometer]. If the thin film was facing upwards and the data result in an upwards pointing parable the residual stress is tensile. In case where the parable was pointing downwards the sample had to be turned so the thin film was facing downwards in order to measure the curvature. In that case the stress is defined to be compressive.

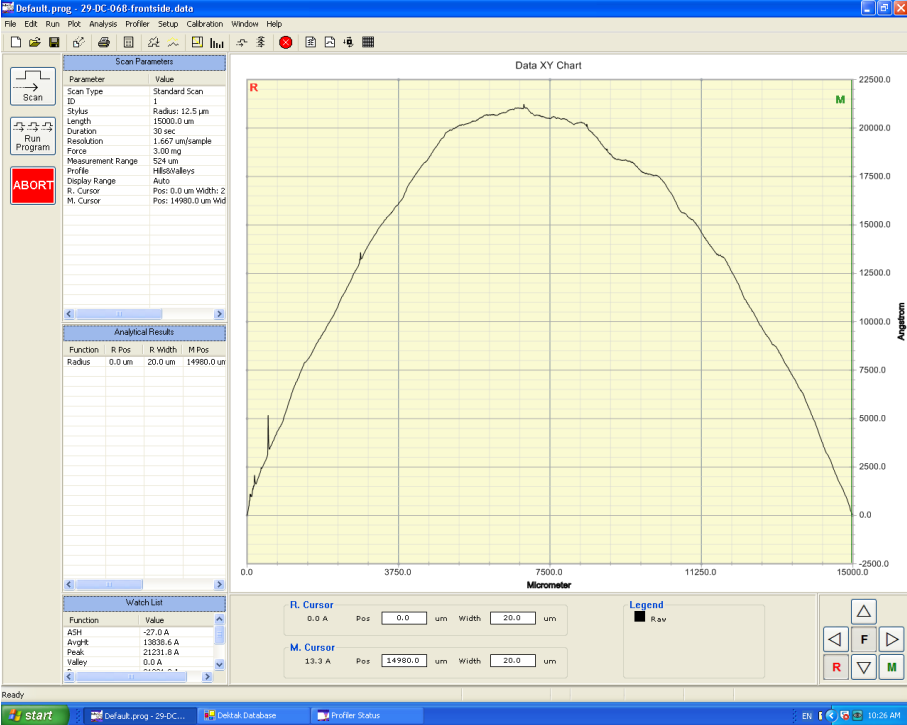


Figure 122 – DC-68 measured with thin film facing upwards (tensile stress)

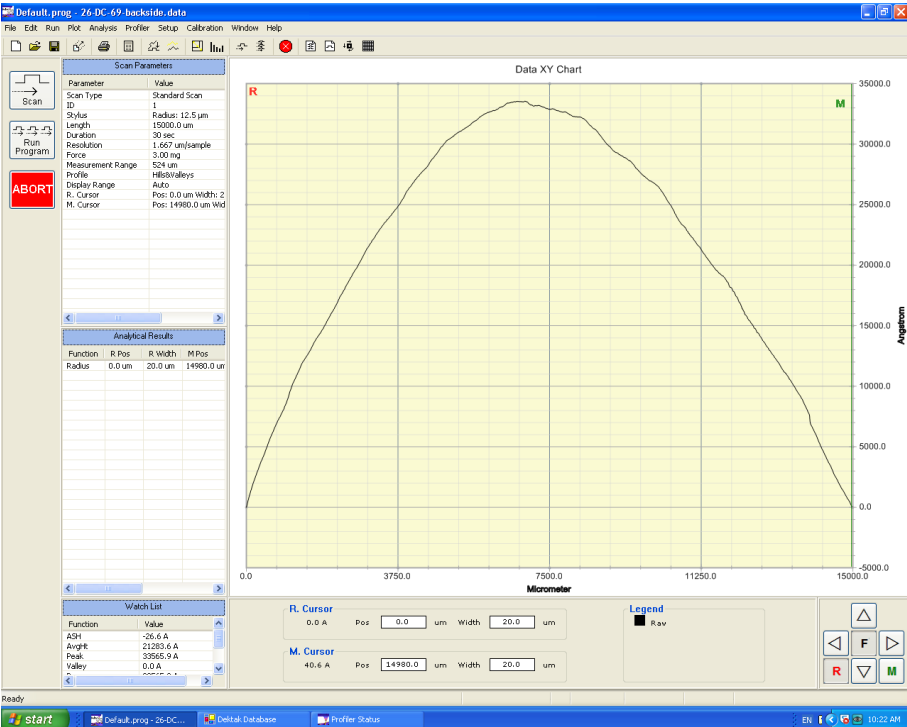


Figure 123 – DC-69 - measured with thin film facing downwards (compressive stress)

## Stress calculation

SampleDC-069 wafer number 33

Extracted values:

$$M_{(100)}^{Si} = 180 \text{ GPa}$$

$$h = 200 \text{ micrometer} = 200\text{E-}06 \text{ m}$$

$$t_f = 321 \text{ nm} = 321\text{E-}09 \text{ m}$$

$$R_{post} = 9,25 \text{ m}$$

$$R_{pre} = 404 \text{ m}$$

$$\sigma_{Si(100)} = \frac{180 \text{ GPa} \cdot h^2}{6 \cdot t_f} \cdot \left( \frac{1}{R_{post}} - \frac{1}{R_{pre}} \right) \quad (\text{eq.1})$$

$$= \frac{180 \text{ GPa} \cdot (200\text{E} - 06 \text{ m})^2}{6 \cdot 321\text{E} - 09\text{m}} \cdot \left( \frac{1}{9,25\text{m}} - \frac{1}{404\text{m}} \right)$$

$$= 0,394889 \text{ GPa}$$

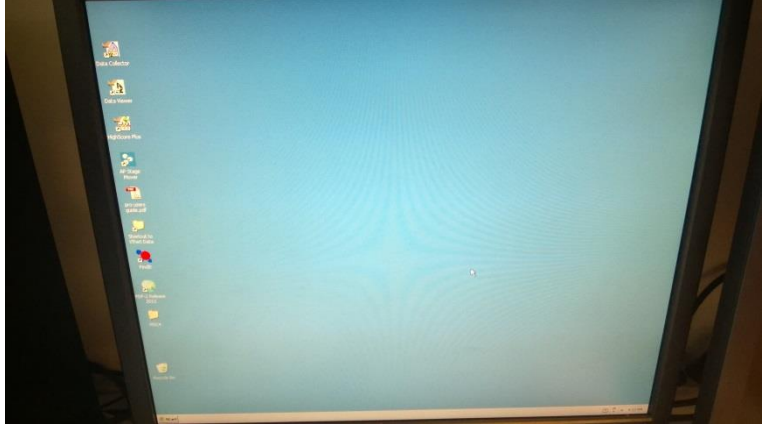
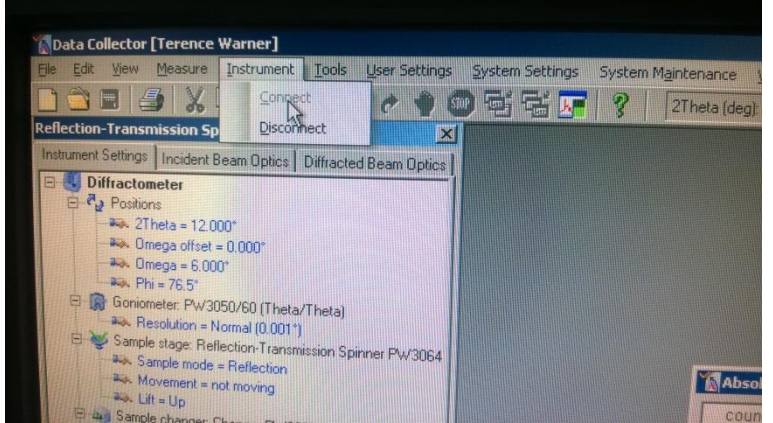
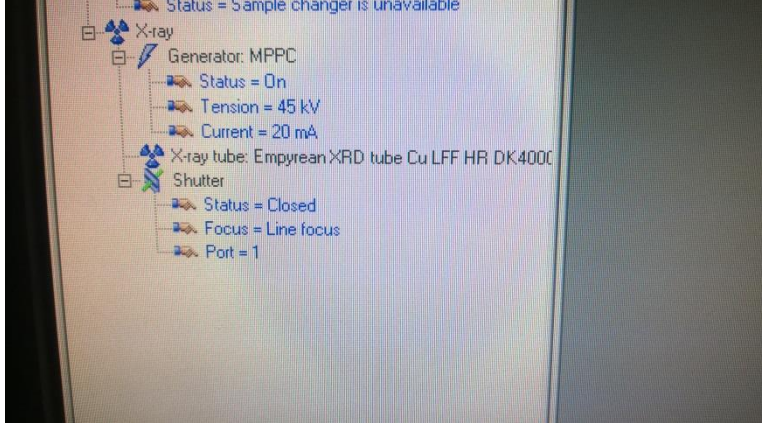
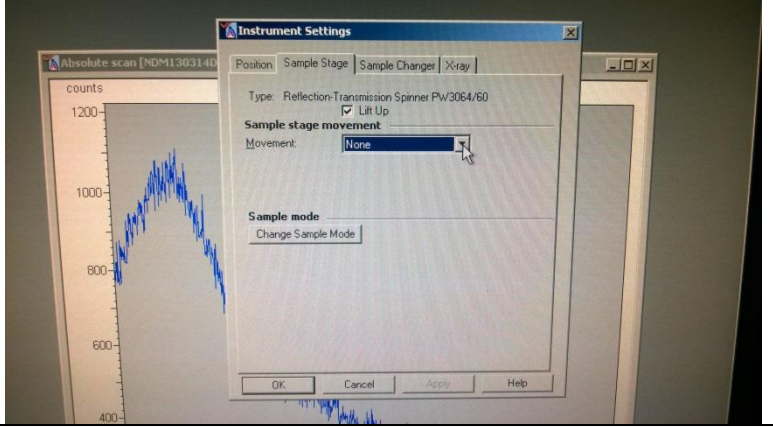
Convention used for the stress analysis:

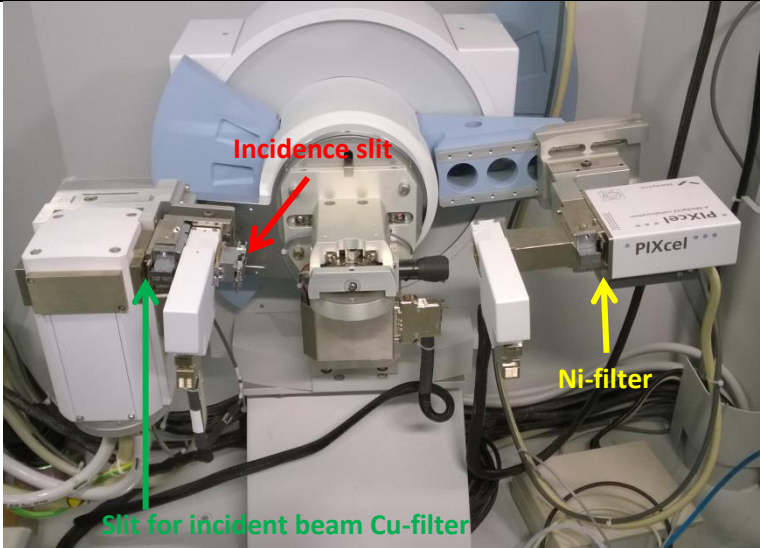
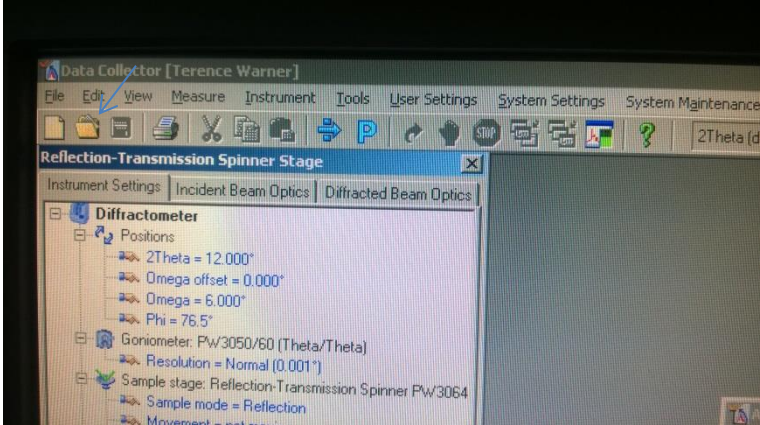
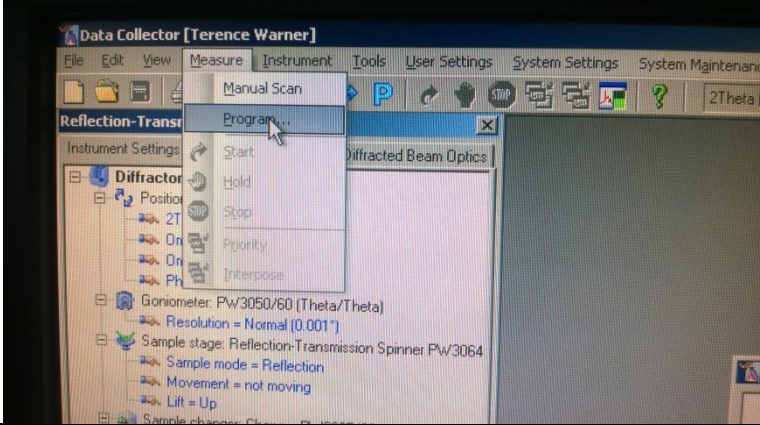
Compressive = negative stress value

Tensile = positive stress value

## A16. XRD quick start guide

### Quick Start guide for X-ray Diffractometer at FKF in Odense by Nis Dam Madsen

|  |  |
|--|--|
| <p>Open Data Collector.<br/>User: tew<br/>Password: england</p>                |    |
| <p>Connect to instrument.</p>  |   |
| <p>Set generator to 45 kV and 40 mA by clicking on the generator settings.</p> |  |
| <p>Lift down sample by clicking on "Lift=up".</p>                              |  |

|   |  |
|---|--|
| <p>Open enclosure</p> <p>Change slits to the desired sizes. Current slit settings for grazing incidence: Incident anti-scatter slit: 0.25° (default 2°) and check that the Ni-filter is inserted on the detector side. The remaining slits are set by the automation program.</p> |    |
| <p>Prepare sample-holder and sample. The distance pieces should be on the same side as the sample. The sample should be centered in the holder as precise as possible.</p>  |  |
| <p>Insert sample in stage.</p>  |  |
| <p>Lift up sample.</p>  |  |
| <p>Open program (e.g. NDM...) and change the values if needed. Close the program <b>and SAVE changes</b>.</p>   |   |
| <p>Go to Measure and choose Program. Click the browse icon and choose the location and name for the file. The typical naming is todaysdate as (ddmmyy-A-samplename) where A is changed for each run.</p>  |  |
| <p>Fill out the Excel XRD measurement log book with the parameters for the run.</p>   |  |

## A17. Tube furnace annealing procedure

1. Put a cooling pad into the water beaker which cools the oil (thickens the oil and decreases air backflow into oven)
2. Mount the samples which have to be annealed on the carrier wafer (be sure to position them in the middle of the oven → stable temperature profile)
3. Open oven and load carrier wafer
4. Outgas oven for minimum 10 minutes at 0,1-0,3 scfh (strong bubble flow should be visible in the oil)
5. Put wet paper towel at the glass near the bearing
6. Increase temperature up to 500°C (press „state“ → „run“ and increase temperature with the „up-arrow“ button. The furnace display switches from “OP2” to “OP1”)
7. Put the flow to around 0.1 scfh (bubbles should be well separated and it should be a steady flow)
8. From the time where the oven reached 500°C count 60 minutes
9. After 60 minutes decrease temperature to 0°C with the “bottom down key”. The furnace display switches from “OP1” to “OP2”.
10. Take samples out when the temperature reached 100 °C (reduces oxygen on post-annealing)

## b. Post-annealing experiments

The experiments were conducted together with Nis Dam Madsen

### Annealing of layered and non-layered TiN films

**Purpose:** To study the effect of introducing periodic pulse of O<sub>2</sub> gas into the deposition of titanium nitride thin films. Furthermore, the effect of annealing on the grain sizes, morphology and resistivity will be studied at two different temperatures and compared to the as-deposited samples.

#### Experimental procedure

The deposition will be carried out using RF sputtering with the Cryofox 600 Explorer deposition system. The deposition parameters are given in figure 124. The thickness of 400 nm is chosen in order to be able to carry out a more accurate EDX analysis. The pulsing period is chosen to so that the titanium nitride layer thickness will be 20 nm per layer. It is assumed that 5 second of oxygen flow at 2 sccm should be enough to produce a few monolayers of oxide on top of the titanium nitride layers to interrupt the columnar growth.

| Deposition Parameters:            | Film A (RF-029) | Film B (RF-028) |
|-----------------------------------|-----------------|-----------------|
| Target                            | 2-inch Ti       | 2-inch Ti       |
| RF Power                          | 360 W           | 360 W           |
| N <sub>2</sub> flow               | 5 sccm          | 5 sccm          |
| O <sub>2</sub> flow (pulse)       | 0               | 2 sccm          |
| Ar flow                           | 20 sccm         | 20 sccm         |
| Base Pressure                     | 5,00E-5 mbar    | 5,00E-5 mbar    |
| Substrate temperature             | 20 °C           | 20 °C           |
| Thickness                         | 400 nm          | 400 nm          |
| Tooling factor                    | 31              | 31              |
| Expected rate                     | 0,8 Å/s         | 0,8 Å/s         |
| T <sub>on</sub> /T <sub>off</sub> | 0 / 99.9s       | 5 s / 250 s     |
| Layer thickness                   | 400 nm          | 20 nm           |
| No. of layers                     | 1               | 20              |

Figure 124 - Deposition parameters for the layered annealing series.

Figure 125 lists the substrates which have been included in each deposition.

| Substrate:                                 | Name | Number: | Dimensions: | Purpose:   |
|--|------|---------|-------------|--|
| Si (100) with 500nm SiO <sub>2</sub> (N11) | N11  | 6       | 15x15 mm    | 4-point probe measurement and TEM samples                    |
| Si (100) with photo resist                 | P1B  | 3       | 10x10 mm    | Lift-off AFM thickness measurement and SEM cross-section/EDX |
| BK7 glass (G3)                             | BK7  | 1       | 25x25 mm    | 4-point probe (electrical characteristics)                   |
| Si (100)                                   | P1A  | 3       | 15x15 mm    | XRD analysis   |
| Si (100)                                   | P1C  | 3       | 10x10 mm    | TEM template effect test samples                             |

Figure 125 - Substrates to be included in the layered annealing experiment

The samples have been placed with carbon tape on a carrier silicon wafer figure 126

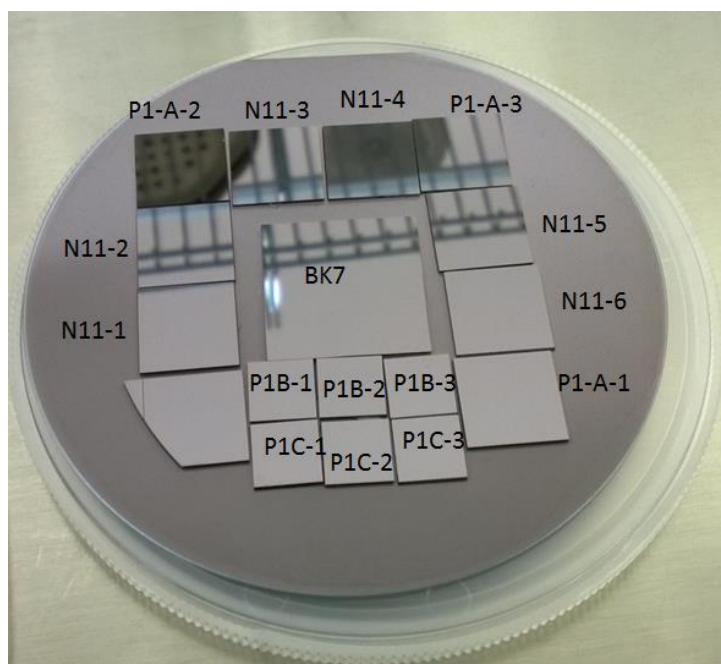


Figure 126 – sample placement with carbon tape on carrier wafer

The annealing parameters are listed in figure 127

| Annealing Parameters:         | Annealing 1                                    | Annealing 2                                   |
|-------------------------------|--|---|
| T <sub>max</sub>              | 500 °C   | 900 °C  |
| Outgassing                    | Min. 15 minutes @ 1 scfh, Ar 4.0 (99.99%) flow | Min. 15 minutes @ 1 scfh Ar 4.0 (99.99%) flow |
| Hold time at T <sub>max</sub> | 1 h  | 1 h   |
| Heating time                  | 6-7 min  | 12-13 min                                     |
| Cooling time                  | 1,5h (samples are exposed to air at 100 °C)    | 2h (samples are exposed to air at 100 °C)     |
| Ar flow rate                  | 0.5 L/min                                      | 0.5 L/min                                     |
| Pressure                      | Flow through vacuum oil cooled to 0 °C         | Flow through vacuum oil cooled to 0 °C        |

Figure 127 - Annealing parameters for Film A and Film B.

The Ar is bubbled through vacuum oil cooled with ice to insure an oil partial pressure below 10<sup>-8</sup> mbar. The oil should prevent back diffusion of oxygen into the furnace. However, the atmosphere is not expected to be Oxygen free since the Argon gas purity isn't perfect as well as the tubing to the furnace.

| Samples       | Annealing 1                         | Annealing 2                         |
|---------------|-------------------------------------|-------------------------------------|
| <b>Film A</b> | N11-2, N11-5, P1-A-2, P1-B-2, P1C-2 | N11-3, N11-6, P1-A-3, P1-B-3, P1C-3 |
| <b>Film B</b> | N11-2, N11-5, P1-A-2, P1-B-2, P1C-2 | N11-3, N11-6, P1-A-3, P1-B-3, P1C-3 |

Table 4: Completed annealings marked with green.

The samples are placed in the furnace at RT. The tube is outgassed with Ar for 15 minutes before the heating is started to insure clean atmosphere (or at least constant atmosphere) during annealing. The time was calculated from the tube volume and the flow rate. After the annealing is done the samples were taken out below 100 °C to reduce oxygen reaction post-annealing (see also document

for annealing procedure). The sheet resistance is measured right before and right after the annealing procedure. The procedure for resistivity measurements is described elsewhere.

### Annealing oven setup



Figure 128 – tube furnace setup connected to argon bottle via red tube

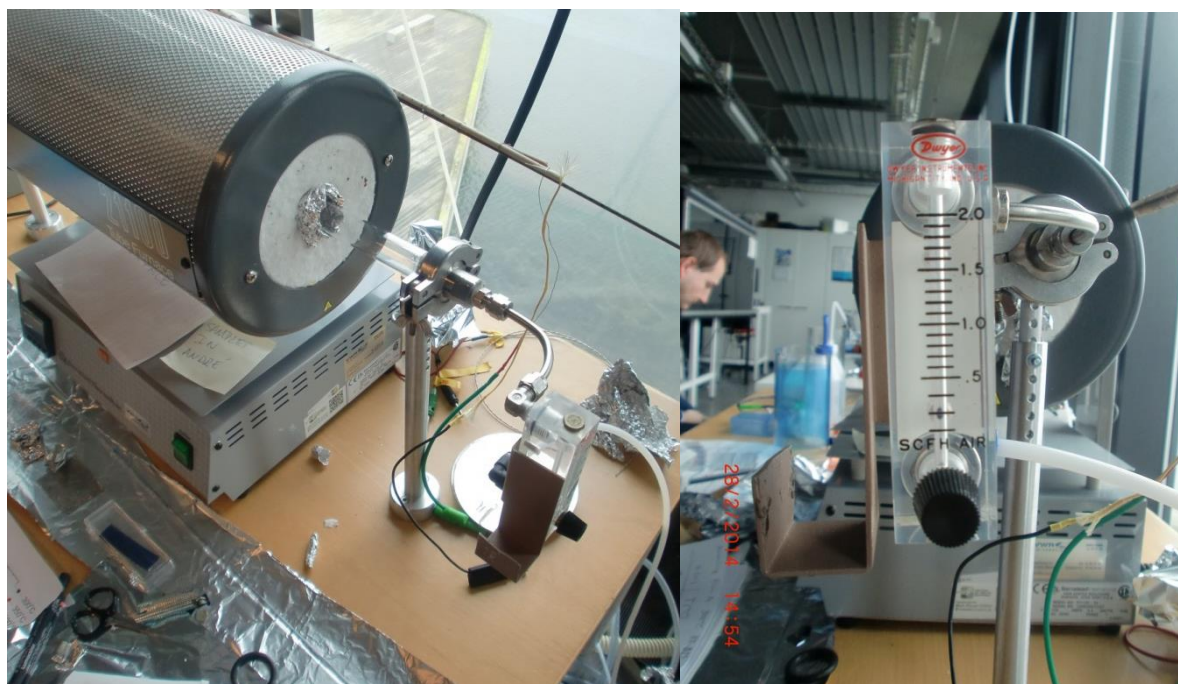


Figure 129 – flow meter connected to argon gas bottle (left) and close up of flow meter (right)

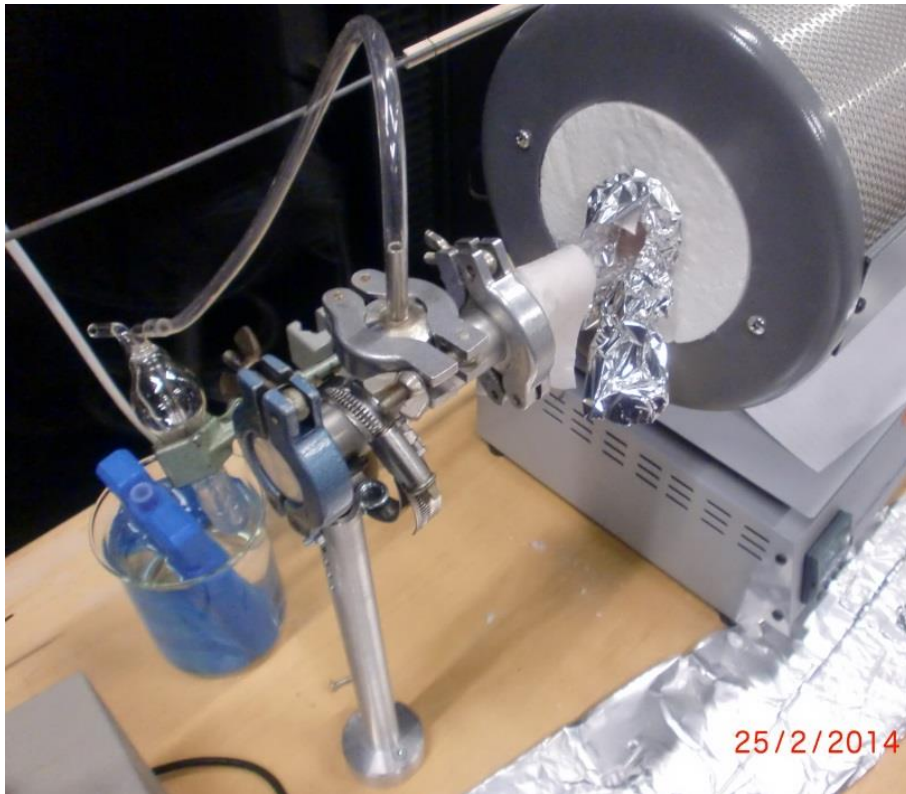


Figure 130 – Exhaust tube - The Ar is bubbled through vacuum oil cooled with ice to insure an oil partial pressure below  $10^{-8}$  mbar. The oil should prevent back diffusion of oxygen into the furnace.

## Results

**Observations:** At 900 °C the thin film color changes to white

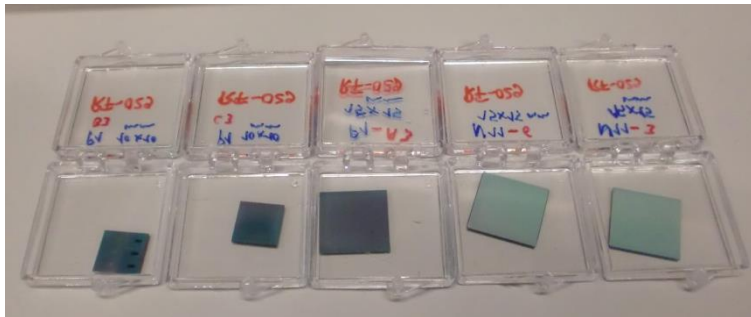


Figure 131 - Film A RF-029 after annealing at 900 °C

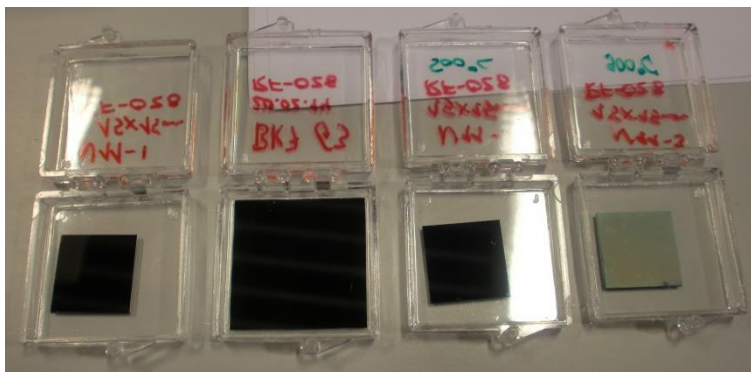


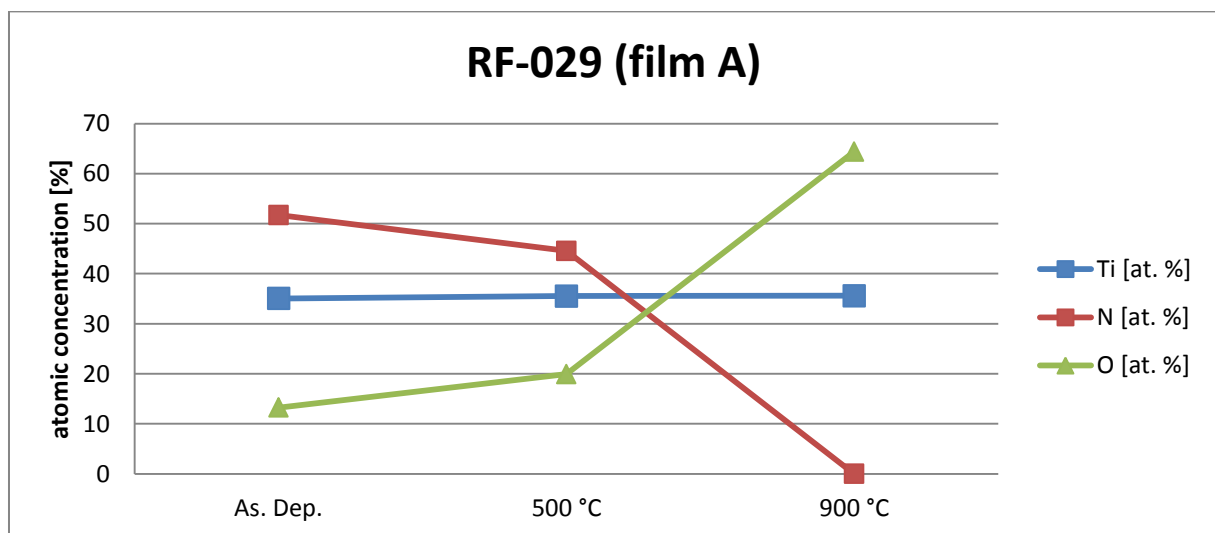
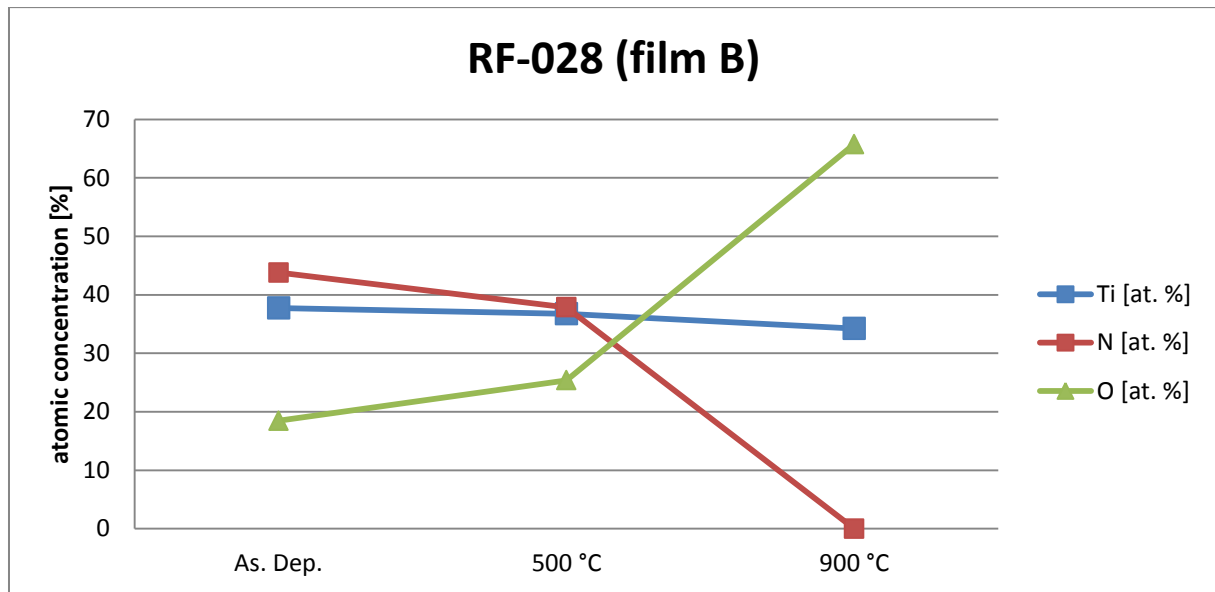
Figure 132 – Film B RF-029 after annealing at 900 °C

**EDX**

The EDX measurements have been performed according to the “EDX measurement procedure”

| Film   | Annealing | EDX composition |             |           |            |           |            |
|--------|-----------|-----------------|-------------|-----------|------------|-----------|------------|
|        |           | Ti [at. %]      | σTi [at. %] | N [at. %] | σN [at. %] | O [at. %] | σO [at. %] |
| Film B | -         | 37,74897        | 1,525279    | 43,79493  | 5,790306   | 18,4561   | 2,734237   |
| Film B | 500       | 36,7587         | 1,512532    | 37,86059  | 5,171434   | 25,38071  | 3,694004   |
| Film B | 900       | 34,25459        | 1,335436    | -         | -          | 65,74541  | 8,247285   |
| Film A | -         | 35,04084        | 1,461645    | 51,73862  | 7,570432   | 13,22054  | 2,524621   |
| Film A | 500       | 35,52663        | 1,505141    | 44,54438  | 6,599167   | 19,92899  | 3,493918   |
| Film A | 900       | 35,59676        | 1,39517     | -         | -          | 64,40324  | 8,90514    |

Table 5: Results from EDX measurements.



**Observations:** it can be seen that with increasing temperature the nitrogen content is decreasing and the oxygen content is increasing for both thin films. The measured titanium content is stable for film A and decreasing slightly for film B. At 900 °C no nitrogen content is measured, which indicates that the measured thin film composition is that of titanium dioxide (TiO<sub>2</sub>).

#### 4-point probe measurements:

The film A (non-layered) was measured to have a resistivity of 1.58 mΩ·cm, while film B (layered) had a resistivity of 4.35 mΩ·cm. Both in the as-deposited state right after deposition.

#### Accelerated life test

Accelerated life test: samples of “layered TiN” (RF-028) and “one layer TiN” (RF-029) were placed in an oven at 100°C, at ambient environment in order to accelerate the resistivity change over time. The samples were measured with the four point probe according to the “four point probe measurement standard”. An initial measurement was taken before the test, and then the samples were placed in an oven (elektrolux). After 1 hour the samples were measured again. The samples were then placed for 3 hours more in the oven at 100°C and measured at the end of the experiment.

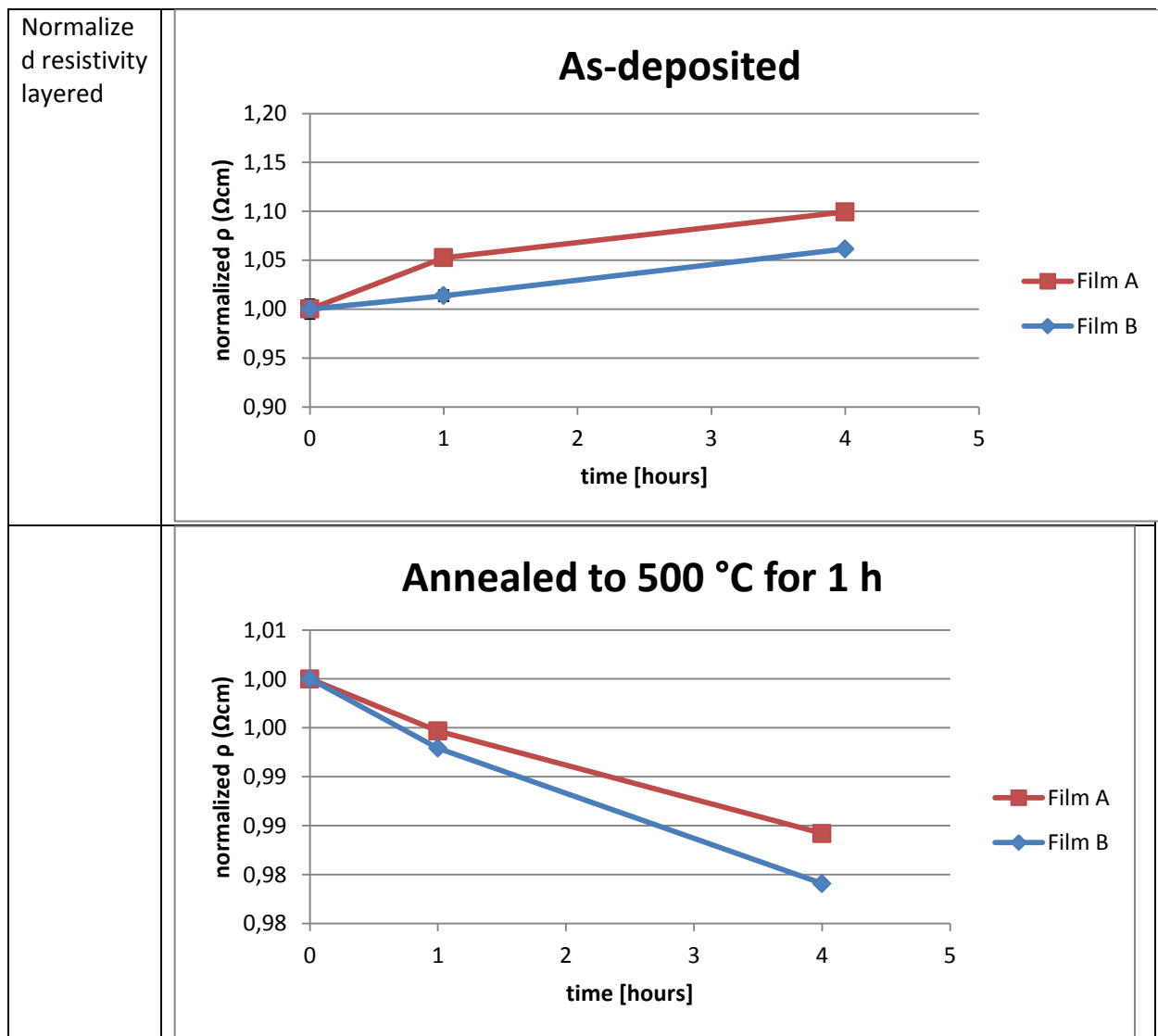
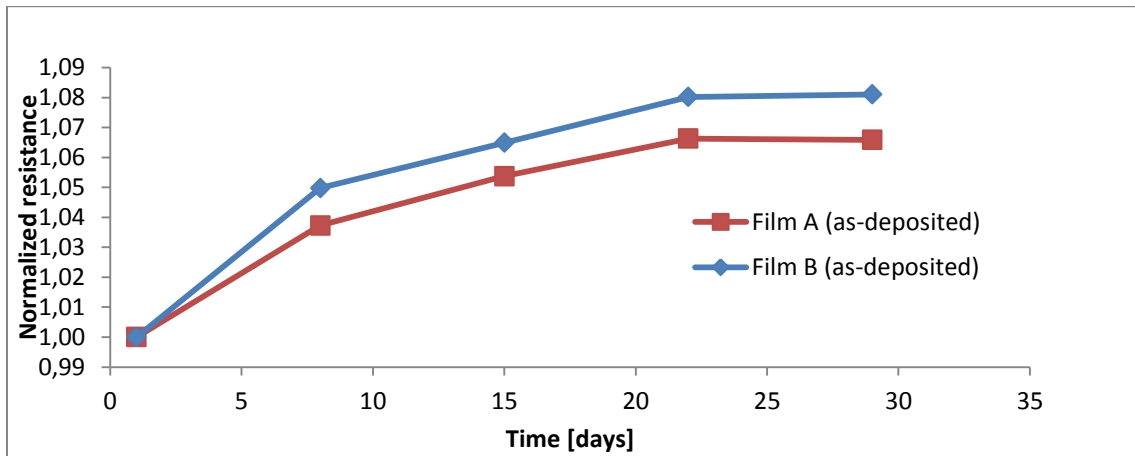


Table 6: The change in resistivity versus hours exposed to 100 °C.

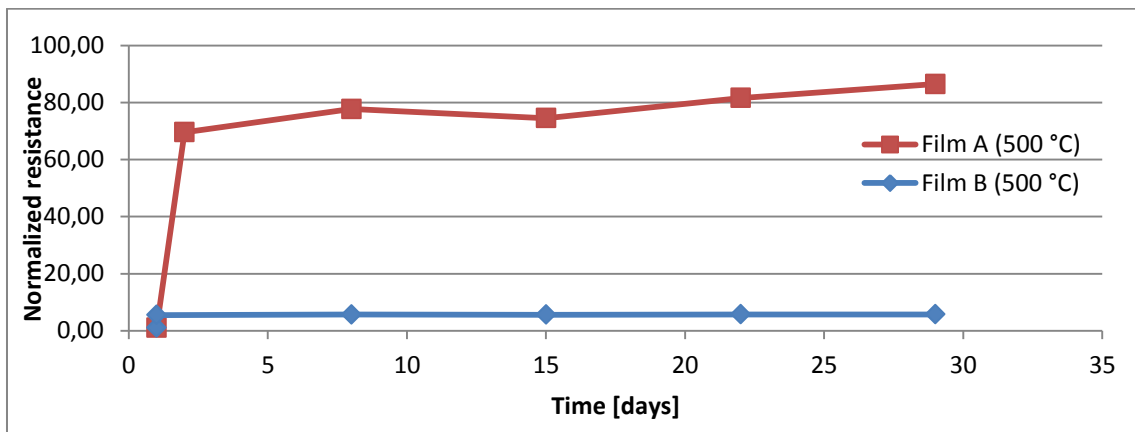
**Observations:** it can be observed that the resistivity of the none-annealed samples is increasing over time when placed in the oven at 100°C. “RF-028-N11-4” shows an increase of about 10% and “RF-029-N11-4” about 6% after 4 hours. The samples which had been annealed at 500 °C before show a decrease in resistivity.

### Stability at room temperature:

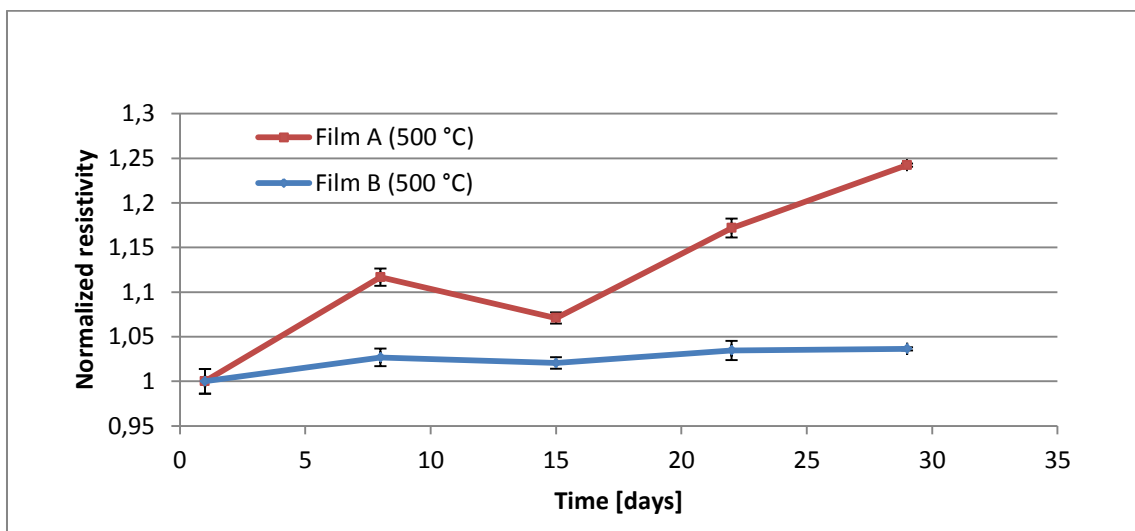
The evolution of the film resistivity for the **as-deposited samples**. Film B is the layered film and film A is the non-layered film.



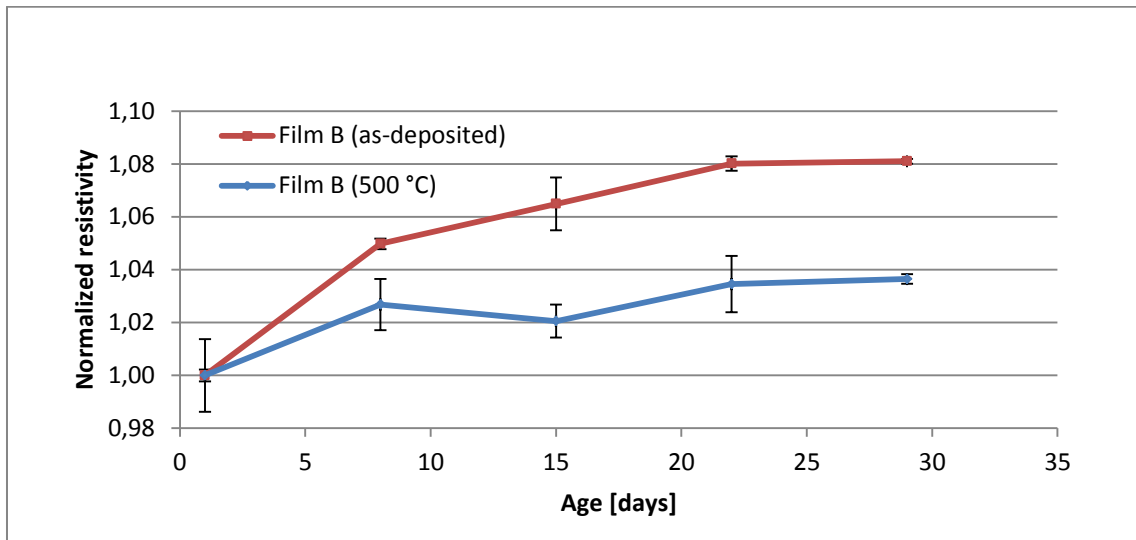
The evolution of the film resistivity for the samples **annealed to 500 °C**. The large increase observed for film A compared to film B after annealing is most likely due to the **leakage** of the annealing tube during annealing of film A.



Same as above but with the resistivity normalized by the post-annealing resistivity



The evolution of the resistivity of film B (layered) versus time after deposition. The resistivity of **the annealed sample appears to be more stable than the as-deposited sample**. The annealed film has been normalized by the post-annealing resistivity. The resistivity of the annealed sample increased by a factor of 5.5 as a result of the annealing.



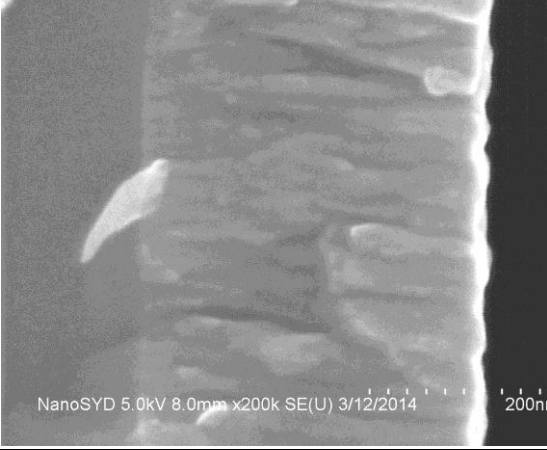
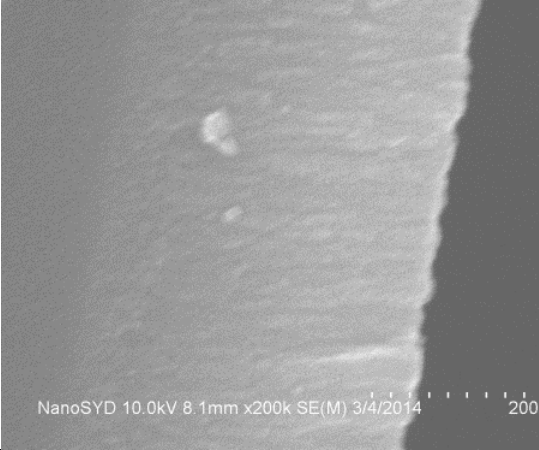
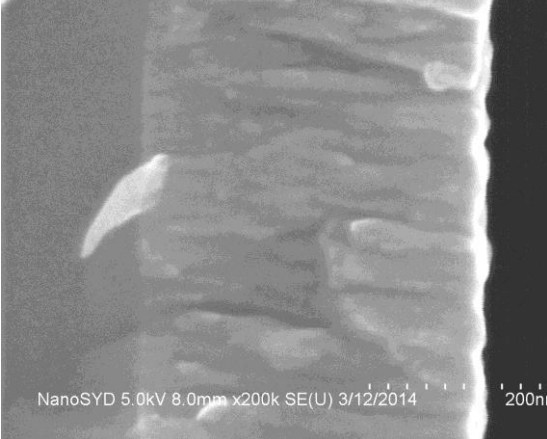
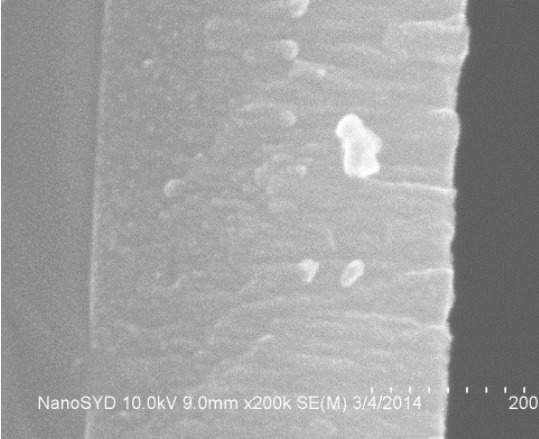
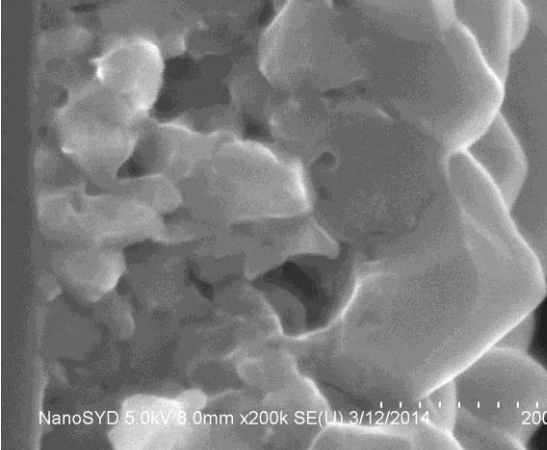
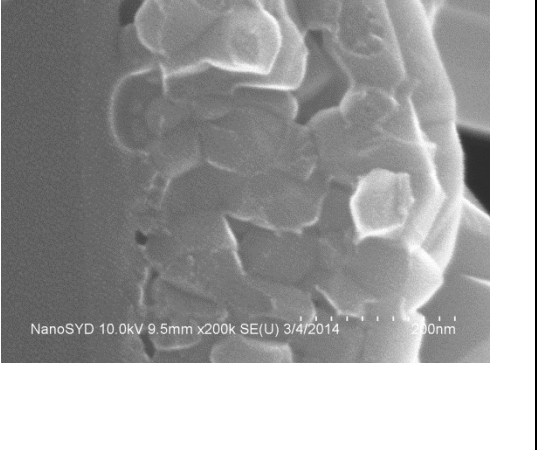
Two important observations are made from these data:

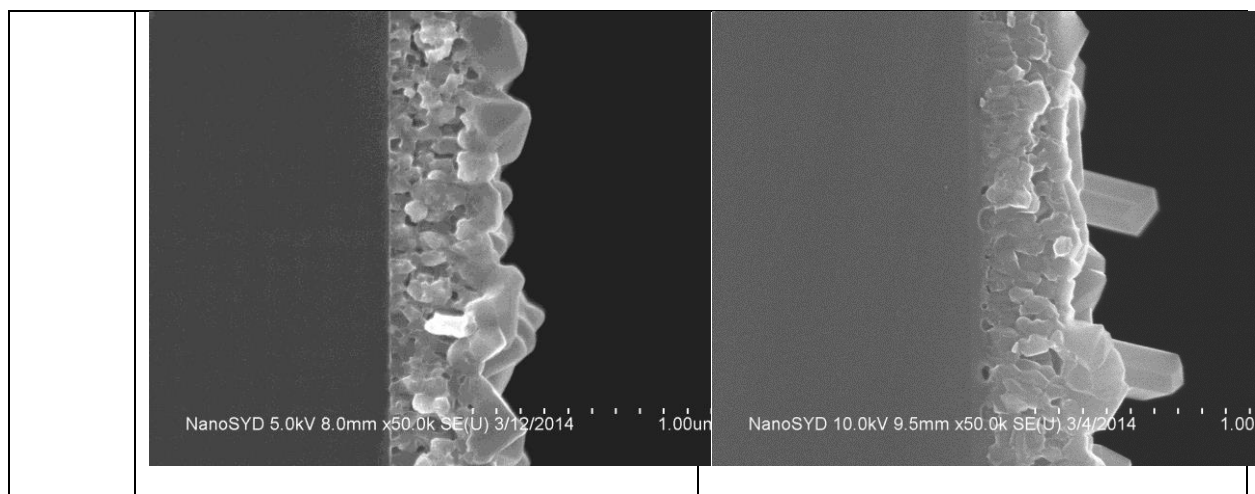
- The resistivity of the as-deposited non-layered sample is slightly more stable than the layered sample during aging at room temperature.
- The layered film annealed to 500 °C is more stable than the non-annealed sample during aging at room temperature.

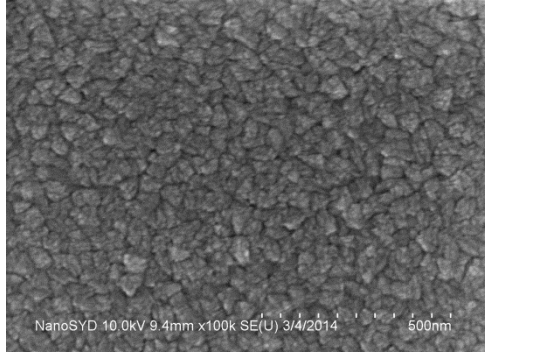
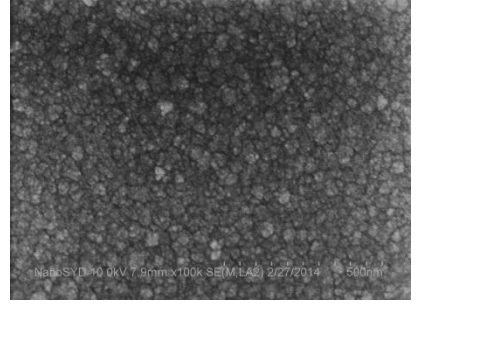
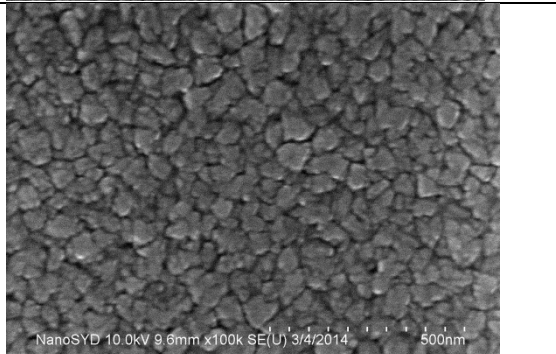
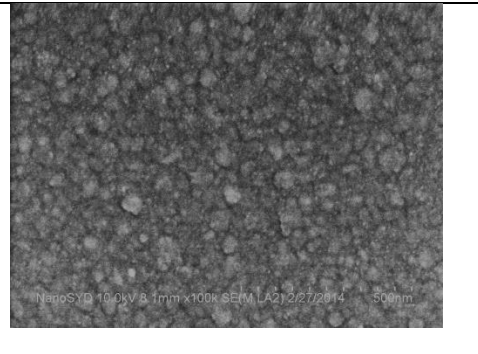
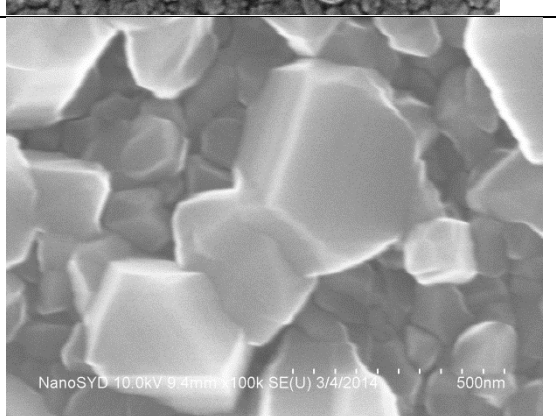
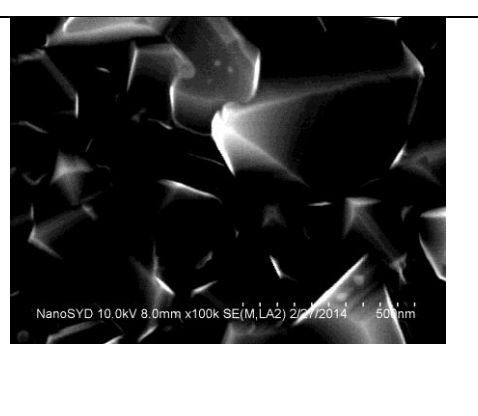
It is not possible to make conclusions regarding the performance of the layered vs. non-layered annealed samples because of the fracture that occurred in the quartz tube during the annealing experiment. However, by comparing the time evolution of the resistivity of the samples annealed to 500 °C and the samples used in the accelerated life test, there is an indication that the resistivity of the non-layered films are more susceptible to heat (oxidation?) than the layered films.

**SEM:**

The introduction of oxygen pulses introduced a large difference in the observed film morphology. The columnar structure is much finer in the layered case.

| Cross-section SEM           | Film A – non layered (No coating)  | Film B – layered. (1.0 nm Au-Pd coating deposited on cross-section)   |
|-----------------------------|--|---|
| As dep.                     |  <p>NanoSYD 5.0kV 8.0mm x200k SE(U) 3/12/2014 200nm</p>   |  <p>NanoSYD 10.0kV 8.1mm x200k SE(M) 3/4/2014 200nm</p>   |
| Annealed to 500 °C for 1 h. |  <p>NanoSYD 5.0kV 8.0mm x200k SE(U) 3/12/2014 200nm</p>  |  <p>NanoSYD 10.0kV 9.0mm x200k SE(M) 3/4/2014 200nm</p>  |
| Annealed to 900 °C for 1 h. |  <p>NanoSYD 5.0kV 8.0mm x200k SE(U) 3/12/2014 200nm</p> |  <p>NanoSYD 10.0kV 9.5mm x200k SE(U) 3/4/2014 200nm</p> |



|         | Film A  | Film B   |
|---------|---|--|
| As dep. |   |   |
| 500 °C  |  |  |
| 900 °C  |  |  |

**Observations:** For the SEM cross-section images it can be seen that at 900 °C annealing, crystals are forming (TiO<sub>2</sub>). For the SEM top images an increase in surface roughness is observed.

Goal: test the impact of 900C annealing for 30 minutes on a BK7 (G3) glass wafer

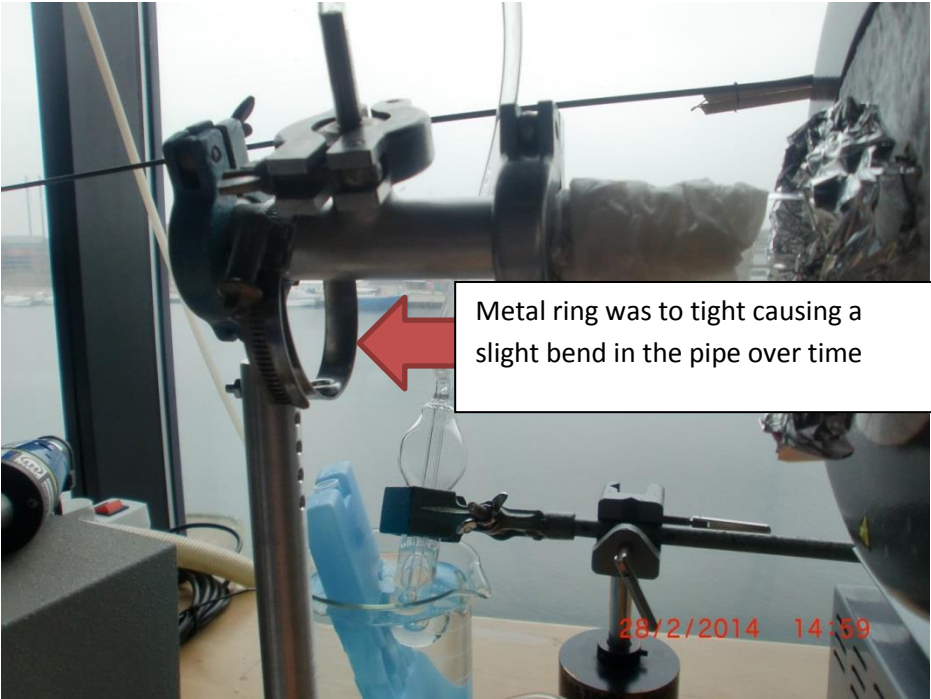
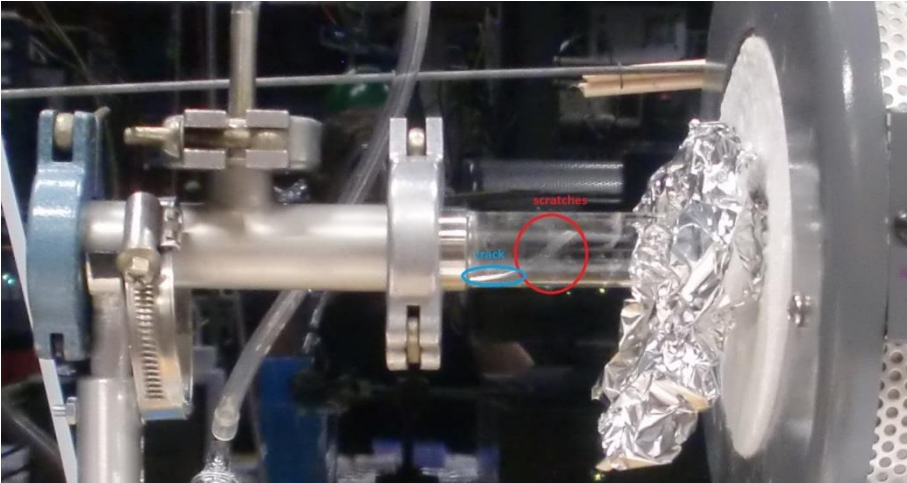
Result: the wafer shattered / melted. Furthermore we proved that the equipment can tolerate a temperature of 900C, which means that we can

easily operate in the regions of 500-600C.



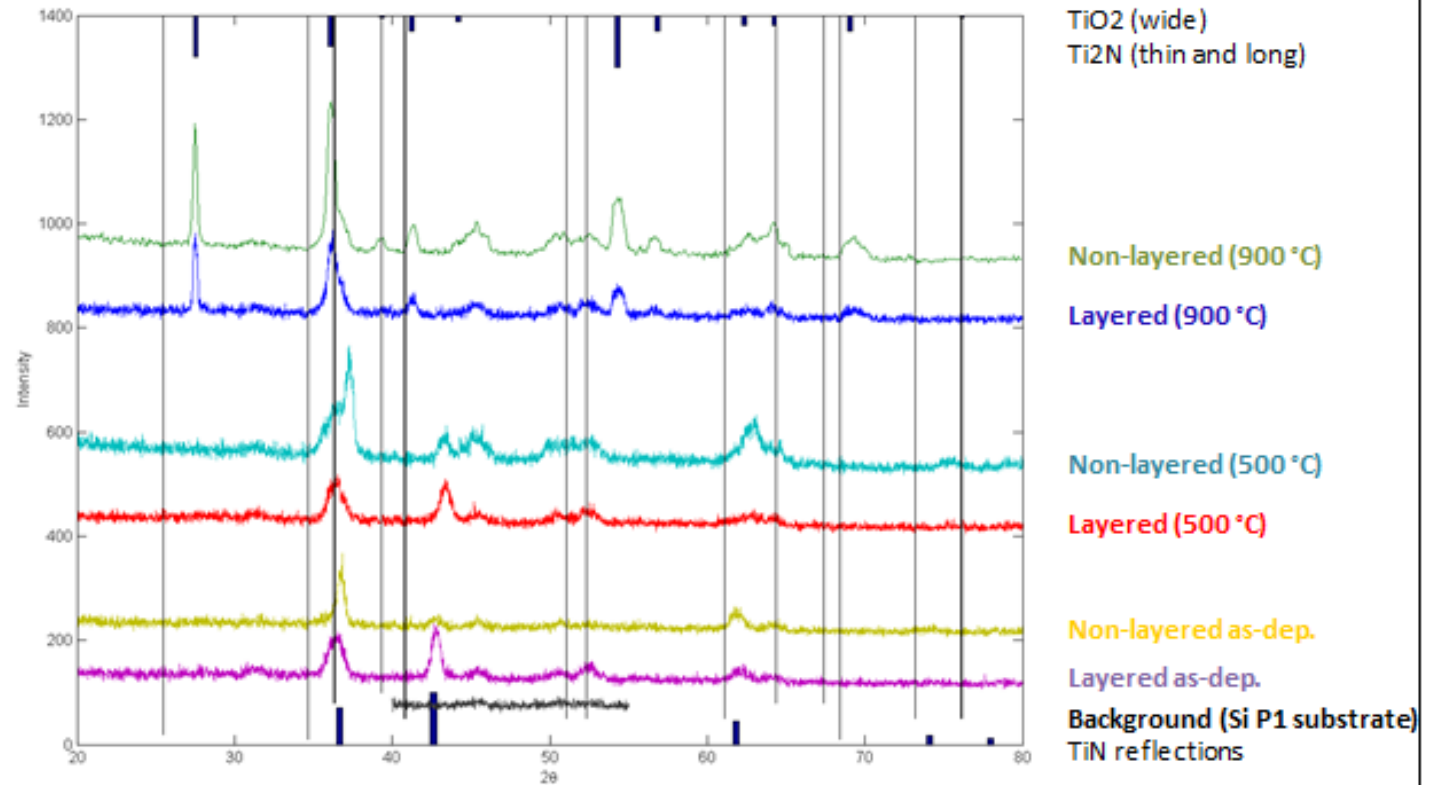
**Failure analysis**

A crack in the quartz tube pipe resulted in corrupted measurements at 900



## XRD

Gracing incidence  
XRD spectra. ( $\omega=7^\circ$ ).  
XRD performed on Si  
P1-A substrates.



### c. Pressure series appendix

#### C1. Substrates and placement – pressure series

A variation of substrates had to be used for the different characterization techniques (see figure 133)

| Substrate                  | Name   | Number | Dimensions | Purpose   |
|----------------------------|--------|--------|------------|---|
| Si (100)                   | P1-A1  | 1      | 10x10 mm   | EDX composition and SEM top-view                |
| Si (100)                   | P1-A2  | 1      | 10x10 mm   | EDX accelerated life time test                  |
| Si (100)                   | P1-A3  | 1      | 10x10 mm   | SEM cross-section                               |
| Si (100)                   | P1-A4  | 1      | 10x10 mm   | reserve   |
| Si (100) with photo resist | P1-B1  | 1      | 10x10 mm   | Lift-off AFM thickness measurement              |
| Si (100) with photo resist | P1-B2  | 1      | 10x10 mm   | Accelerated life test                           |
| BK7 glass (G3)             | BK7-A1 | 1      | 25x25 mm   | 4-point probe measurement room temperature      |
| BK7 glass (G3)             | BK7-A2 | 1      | 25x25 mm   | 4-point probe measurement accelerated life test |
| BK7 glass (G3)             | BK7-B1 | 1      | 15x15 mm   | XRD analysis                                    |
| BK7 glass (G3)             | BK7-B2 | 1      | 15x15 mm   | XRD analysis accelerated life test              |

Figure 133 - Substrates needed for the analysis of the films

The substrates were fixed using carbon tape on a carrier wafer to have the substrates tightly placed to minimize effects of thickness variations and variations in the energy content of the sputter flux (see figure 134 )

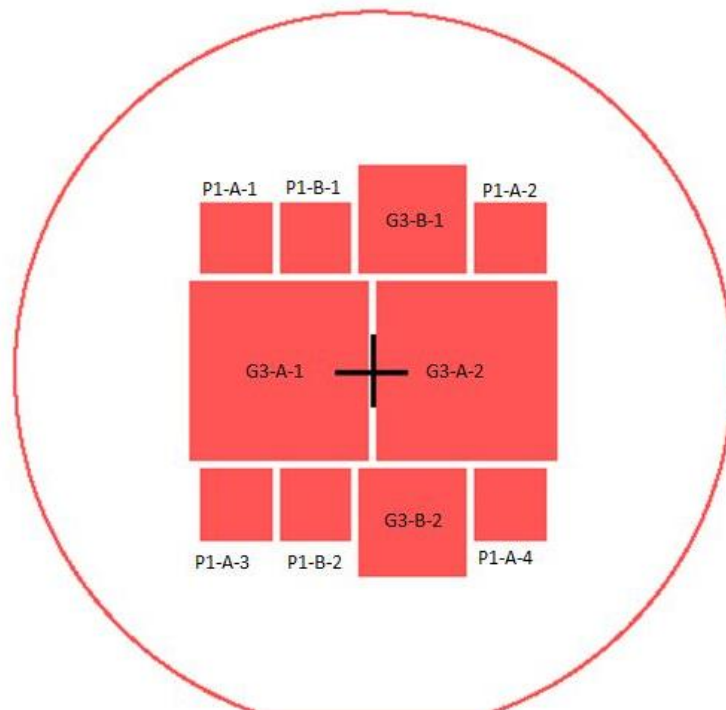


Figure 134 - Substrate placement on 4 inch wafer

## C2. Accelerated lifetime testing experiment

**Goal:** acceleration of the resistivity increase by placing target samples in an oven at 100°C for 60 minutes per run

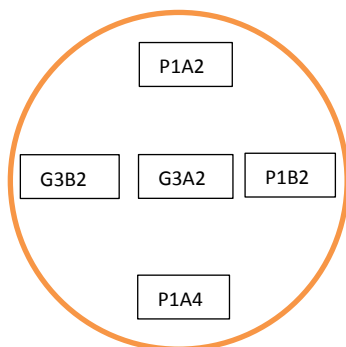
**Setup:** Samples were placed on porcelain plates. A thermocouple attached to a Fluke179 multi-meter measured the temperature in the middle of the oven (brown wire). Oven set temperature was put to 85°C, which resulted in a reading of 100°C on both the multi-meter and the scale on the oven.



| Oven calibration experiment |                             |                           |
|-----------------------------|-----------------------------|---------------------------|
| Fluke 179 multi-meter [°C]  | Oven scale temperature [°C] | Oven set temperature [°C] |
| 92,4                        | 90                          | 80                        |
| 104,1                       | 102,5                       | 85                        |
| 111,6                       | 105                         | 90                        |
| 123,1                       | 115                         | 100                       |
| 134,3                       | 122                         | 120                       |

**Note:** waited over 5 minutes for stabilization of temperature. Adjust oven set temperature to around 82.5 – 85 °C to achieve a temperature of around 100 °C in the oven.

**Sample placement on plates:**



| Experimental documentation   |       |                     |
|------------------------------|-------|---------------------|
| Run                          | Time  | Temperature (Fluke) |
| 1 <sup>st</sup> run started  | 11:40 | 102,4               |
|                              | 12:13 | 106,5               |
|                              | 12:38 | 108,1               |
|                              | 12:40 | 107,2               |
| Sheet resistance measurement |       |                     |
| 2 <sup>nd</sup> run started  | 13:30 | 100                 |

|                              |       |       |
|------------------------------|-------|-------|
|                              | 14:30 | 109,9 |
| Sheet resistance measurement |       |       |
| 3 <sup>rd</sup> run started  | 15:20 | 100   |
|                              | 16:00 | 101,5 |
|                              | 16:20 | 104,4 |
| Sheet resistance measurement |       |       |
| 4 <sup>th</sup> run started  | 17:10 | 100   |
|                              | 18:10 | 107   |

### C3. Pre and post EDX for accelerated life test samples

Figure 135 shows the difference between the atomic concentration in percentage between the pre and post accelerated life time measurements. The observed difference is much lower than the corresponding measurement error. Based on this observations it seems that the accelerated life time tests at 100 °C have no measurable effect on the thin film stoichiometry.

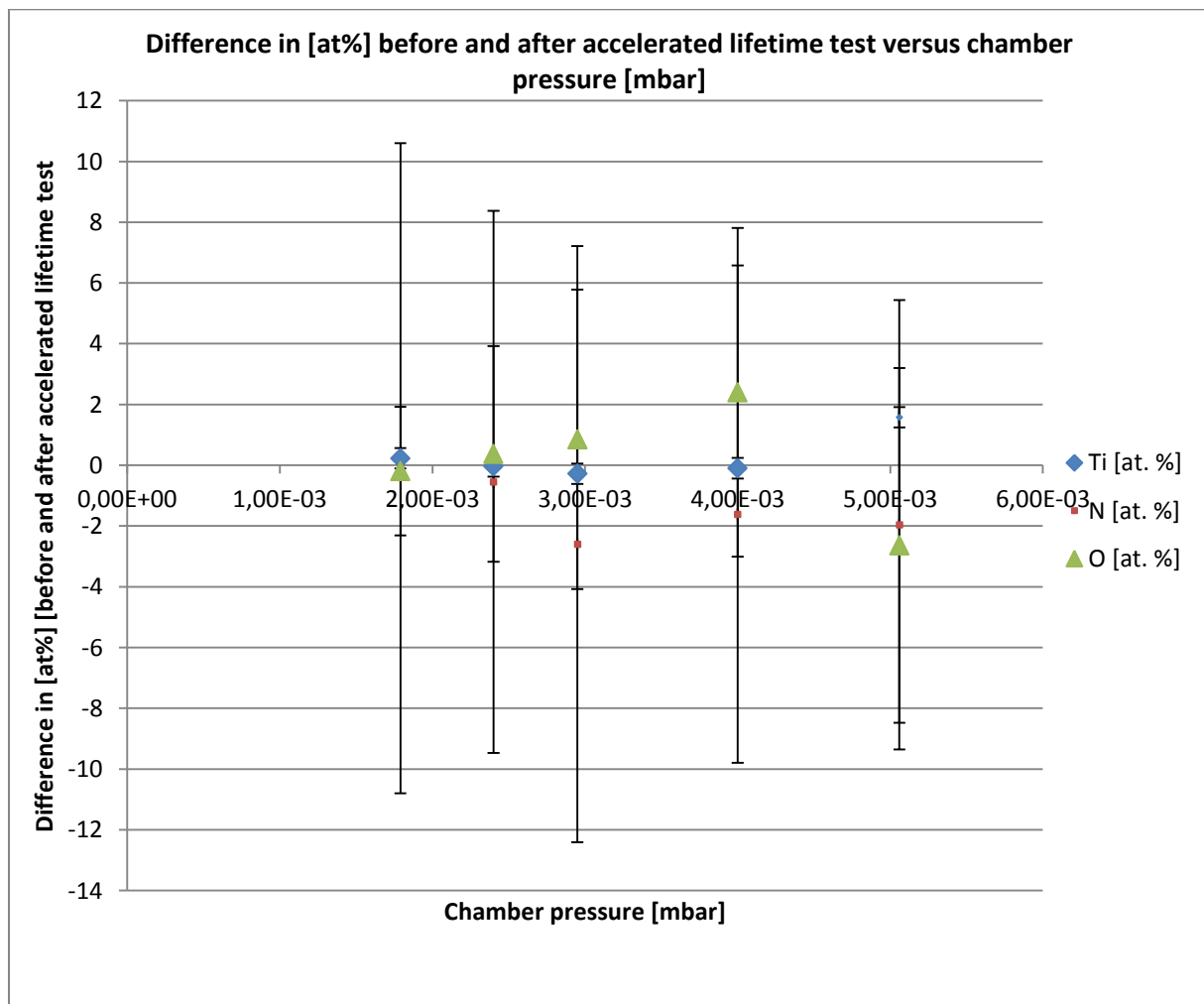


Figure 135 - Difference in [at%] before and after accelerated lifetime test versus chamber pressure [mbar]

#### C4. AFM and SEM thickness measurements

Figure 136 shows the thin film thickness [nm] vs. chamber pressure during deposition [mbar]. Sample DC-039 stopped due to a broken microbalance crystal after 93:36 min and sample DC-041 had plasma problems at 298 nm due to metal flakes on the target. The DC-040, DC-043 and DC-044 were deposited without interruptions to a nominal thickness of 400 nm as measured by the micro balance crystal. Despite of the deposition problems it seems that the thin film thickness is increasing with increasing chamber pressure. Note that a micro balance measures the mass added to the crystal. The larger thickness measured for DC-044 and DC-043 compared to DC-040, therefore, could indicate that the low pressure films are denser.

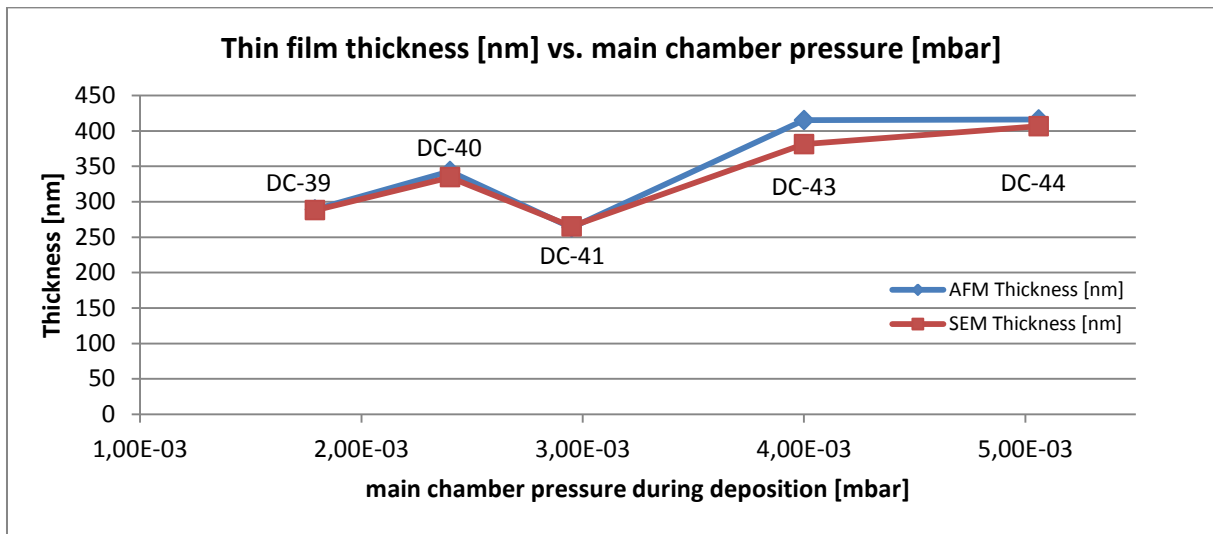
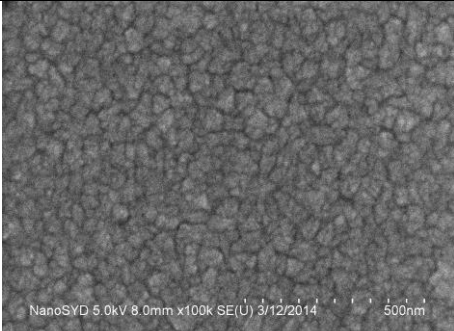
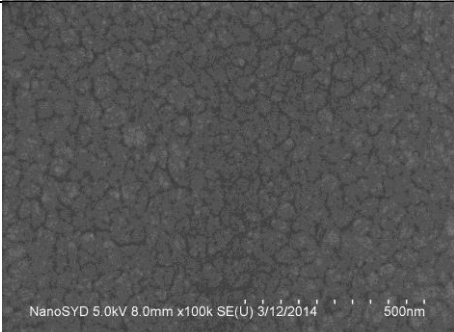
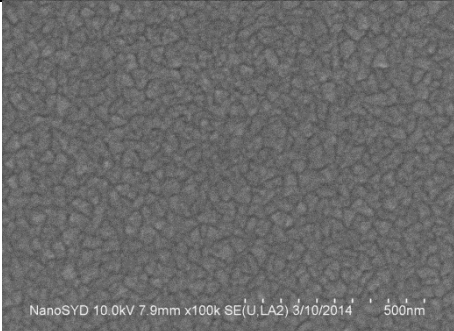
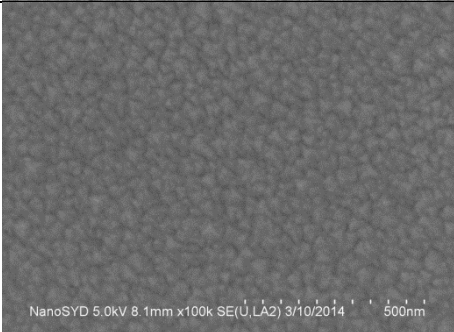
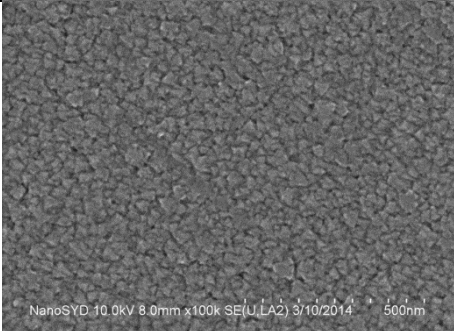
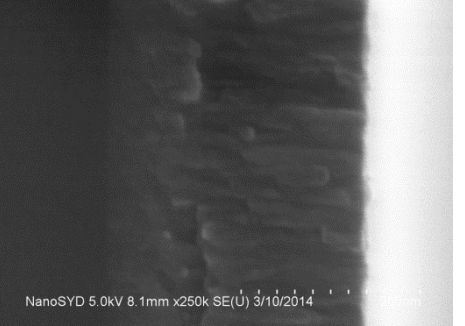
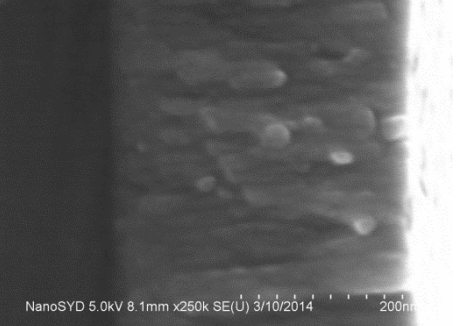
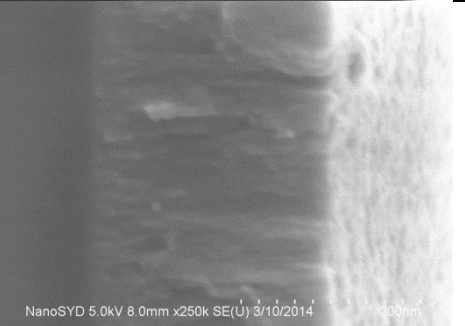
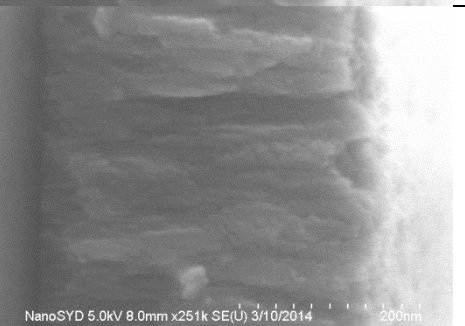
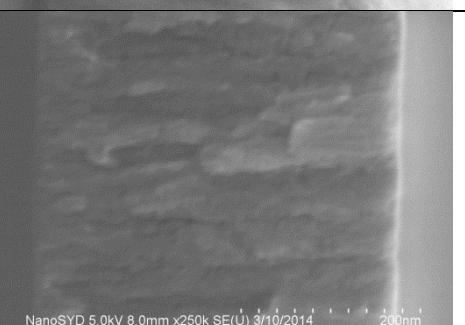


Figure 136 - SEM and AFM thickness of depositions made at various pressures

The difference between the AFM and SEM cross-section measurements are neglectable, which means that both methods will in most cases measure a similar thin film thickness.

C5. SEM top-view and cross-section view images

| Sample   | Top-view image (pre-accelerated)   |
|--|--|
| DC-039-P1A-3<br>Argon flow: 10 sccm<br>SEM thickness: 288 nm   |    |
| DC-040-P1A-3<br>Argon flow: 15 sccm<br>SEM thickness: 334.5 nm |    |
| DC-041-P1A-3<br>Argon flow: 20 sccm<br>SEM thickness: 265 nm   |   |
| DC-043-P1A-3<br>Argon flow: 30 sccm<br>SEM thickness: 381.2 nm |  |
| DC-044-P1A-3<br>Argon flow: 40 sccm<br>SEM thickness: 406.5 nm |  |

| Samples  | Cross-section image (pre-accelerated)  |
|--|--|
| DC-039-P1A-3<br>Argon flow: 10 sccm<br>SEM thickness: 288 nm   |    |
| DC-040-P1A-3<br>Argon flow: 15 sccm<br>SEM thickness: 334.5 nm |    |
| DC-041-P1A-3<br>Argon flow: 20 sccm<br>SEM thickness: 265 nm   |   |
| DC-043-P1A-3<br>Argon flow: 30 sccm<br>SEM thickness: 381.2 nm |  |
| DC-044-P1A-3<br>Argon flow: 40 sccm<br>SEM thickness: 406.5 nm |  |

## C6. Density measurement experiment

By Nis Dam Madsen and Kasper Thilsing-Hansen

To investigate the change in density with pressure two additional depositions will be carried out. The parameters are set to check the highest and lowest pressure. In each deposition 3xBK7 25x25mm substrates, 2xP1-A 10x10 and 2xP1-B 10x10 substrate is included. The BK7 substrates have been weighted before the deposition to an accuracy of 0.05 mg. The substrates are placed in a shadow mask. To test the accuracy of the method three BK7 substrates are included in each deposition. The P1-A-A and P1-B-A are placed closer to the center and the P1-A-B and P1-B-B are placed in the outer positions in the mask.

| Sample name | Argon flow | Nitrogen flow | Power | Substrates          | Placement  | Comment   |
|-------------|------------|---------------|-------|---------------------|--|---|
| DC-046      | 10 sccm    | 5 sccm        | 300 W | 3xBK7,2xP1-A,2xP1-B | The A samples are closer to the center. 1-2 is in the center and 1-1 and 1-3 are in the outer positions. | The first one and half minutes was done in pure Ti due to problem starting the plasma. Deposition time: 95 min. Many arcs observed near the end of the deposition. The center sample was misplaced during deposition. |
| DC-047      | 40 sccm    | 5 sccm        | 300 W | 3xBK7,2xP1-A,2xP1-B | The A samples are closer to the center. 1-5 is in the center and 1-4 and 1-6 are in the outer positions. | Chamber and target cleaned before deposition. Smooth deposition<br>Deposition time: 57,44 min   |



The density has been measured using a Mettler Toledo XS205 Dual range microbalance situated at FKF in Odense. The reading precision of the balance is 0.01 mg and it was observed to give very reproducible readings under repeated weighting.

| Substrate |          |                 |             |            | Film   |          |                         |                |                                |                   |             |                              |
|-----------|----------|-----------------|-------------|------------|--------|----------|-------------------------|----------------|--------------------------------|-------------------|-------------|------------------------------|
| Name      | Material | Dimensions [mm] | Weight [mg] | Date       | Name   | Material | Area [cm <sup>2</sup> ] | Thickness [nm] | Weight (substrate + film) [mg] | Date [dd-mm-yyyy] | Weight [mg] | Density [g/cm <sup>3</sup> ] |
| 1-1       | BK-7     | 25x25           | 779.58      | 13-03-2014 | DC-046 | TiN      | 5.76                    | 300.71         | 780.25                         | 27-03-2014        | 0.67        | 3.868160169                  |
| 1-2       | BK-7     | 25x25           | 779.15      | 13-03-2014 | DC-046 | TiN      | 5.52                    | 300.71         | 779.85                         | 27-03-2014        | 0.7         | 4.217072735                  |
| 1-3       | BK-7     | 25x25           | 780.14      | 13-03-2014 | DC-046 | TiN      | 5.76                    | 300.71         | 780.85                         | 27-03-2014        | 0.71        | 4.099095105                  |
| 1-4       | BK-7     | 25x25           | 779.6       | 13-03-2014 | DC-047 | TiN      | 5.76                    | 453.175        | 780.32                         | 27-03-2014        | 0.72        | 2.758316324                  |
| 1-5       | BK-7     | 25x25           | 780.63      | 13-03-2014 | DC-047 | TiN      | 5.76                    | 453.175        | 781.4                          | 27-03-2014        | 0.77        | 2.949866068                  |
| 1-6       | BK-7     | 25x25           | 780.27      | 13-03-2014 | DC-047 | TiN      | 5.76                    | 453.175        | 780.94                         | 27-03-2014        | 0.67        | 2.566766579                  |

As states above, the samples 1-1, 1-3 and 1-4, 1-6 were placed in the outer positions in the shadow mask. The samples for the thickness measurement were placed in the same radial distance. Therefore, the densities of the samples are most accurately determined for the outer samples. The **average density for the low pressure sample is 4.0 g/cm<sup>3</sup>, while the average density for the high pressure sample is 2.7 g/cm<sup>3</sup>**. This is a clear demonstration that the low pressure films are denser than the high pressure films. As a reference the tabulated value for the density of TiN is 5.22 g/cm<sup>3</sup>, while pure Ti has a density of 4.51 g/cm<sup>3</sup>.

## d. Nitrogen flow series at 300 W appendix

### D1. Substrates and placement

It was decided not to include extra analysis samples for post accelerated-life test other than the 4-point probe samples (see figure 137)

| Substrate:                 | Name   | Number: | Dimensions: | Purpose:                            |
|----------------------------|--------|---------|-------------|-------------------------------------|
| Si (100)                   | P1-A1  | 1       | 10x10 mm    | EDX composition                     |
| Si (100)                   | P1-A2  | 1       | 10x10 mm    | SEM cross-section                   |
| Si (100) with photo resist | P1-B1  | 1       | 10x10 mm    | AFM thickness                       |
| BK7 glass (G3)             | BK7-A1 | 1       | 25x25 mm    | 4-point probe reference             |
| BK7 glass (G3)             | BK7-A2 | 1       | 25x25 mm    | 4-point probe accelerated life test |
| BK7 glass (G3)             | BK7-B1 | 1       | 15x15 mm    | XRD analysis                        |

Figure 137 - substrates needed for the analysis of the films

The substrates will be fixed using carbon tape on a wafer to have the substrates tightly placed to minimize effects of thickness variations and variations in the energy content of the sputter flux (see figure 138)

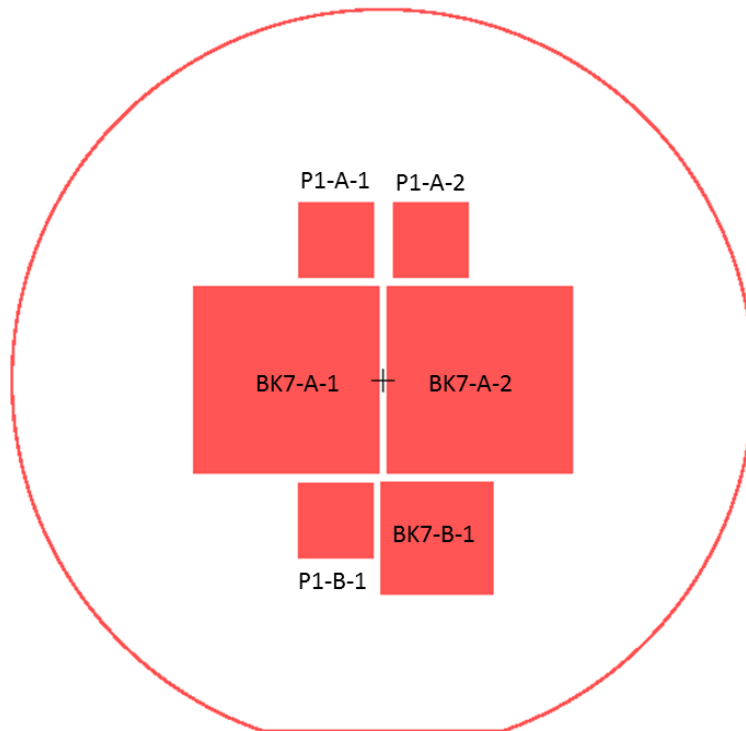


Figure 138 - substrate placement on wafer

## D2. Sample thickness

Figure 139 shows the thickness [nm] versus the N<sub>2</sub>-total flow ratio. The tooling factor was kept constant for all depositions.

| Sample | AFM Thickness [nm] | SEM Thickness [nm] | N2/total flow ratio |
|--------|--------------------|--------------------|---------------------|
| DC-049 | 338,57             | 350                | 0,44                |
| DC-050 | 313,23             | 335                | 0,29                |
| DC-051 | 320,45             | 373                | 0,16                |
| DC-053 | 323,97             | 340                | 0,1                 |
| DC-054 | 283,24             | 315                | 0                   |
| DC-055 | 289,95             | 294                | 0,05                |

Figure 139 – AFM and SEM thickness measurement data

From figure 140 it can be observed that the thin film thickness is slightly increasing with an increasing N<sub>2</sub>-total flow ratio.

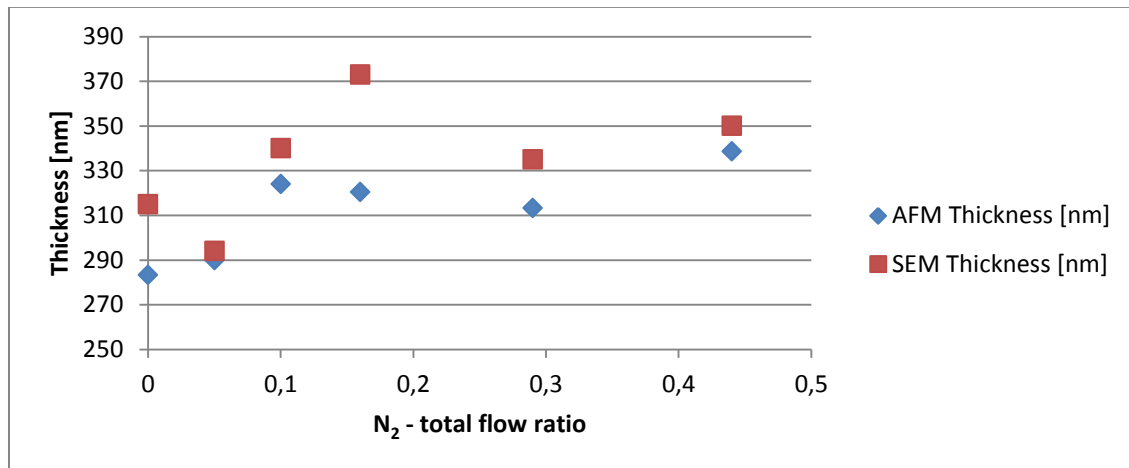


Figure 140 – thin film thickness vs. N<sub>2</sub>-total flow ratio

### D3. Sample deposition data observations

| DC-049 (Argon: 9 sccm, N2: 7 sccm) |                              | Production date: 20.03.2014 | Total flow   | 16         | N2/total flow ratio   | 0,44 |
|------------------------------------|------------------------------|-----------------------------|--------------|------------|---|------|
| State time [min]                   | Main chamber pressure [mbar] | Power [W]                   | DC-volt [V]  | Rate [Å/s] | Comment   |      |
| 10                                 | 2,18E-03                     | 298                         | 457          | 0,6        | Observations: during the deposition many arcs have been observed on the target. |      |
| 20                                 | 2,20E-03                     | 298                         | 457          | 0,6        |   |      |
| 32                                 | 2,23E-03                     | 298                         | 458          | 0,6        |   |      |
| 43                                 | 2,26E-03                     | 298                         | 462          | 0,6        |   |      |
| 60                                 | 2,26E-03                     | 298                         | 470          | 0,6        |   |      |
| 70                                 | 2,26E-03                     | 298                         | 476          | 0,5        |   |      |
| 80                                 | 2,26E-03                     | 298                         | 481          | 0,6        |   |      |
| 90                                 | 2,26E-03                     | 298                         | 486          | 0,5        |   |      |
| 100                                | 2,26E-03                     | 298                         | 490          | 0,5        |   |      |
| 110                                | 2,26E-03                     | 298                         | 493          | 0,5        |   |      |
|                                    |                              |                             | Average rate | 0,56       |   |      |

| DC-050 (Argon: 12 sccm, N2: 5 sccm) |                              | Production date: 20.03.2014 | Total flow   | 17         | N2/total flow ratio              | 0,29 |
|-------------------------------------|------------------------------|-----------------------------|--------------|------------|----------------------------------|------|
| State time [min]                    | Main chamber pressure [mbar] | Power [W]                   | DC-volt [V]  | Rate [Å/s] | Comment                          |      |
| 10                                  | 2,06E-03                     | 298                         | 459          | 0,8        | manually set argon to 13 sccm    |      |
| 15                                  | 2,23E-03                     | 298                         | 453          | 0,7        |                                  |      |
| 20                                  | 2,31E-03                     | 298                         | 449          | 0,7        | back to automode (argon 12 sccm) |      |
| 35                                  | 2,23E-03                     | 298                         | 468          | 0,6        |                                  |      |
| 40                                  | 2,20E-03                     | 298                         | 467          | 0,6        |                                  |      |
| 45                                  | 2,20E-03                     | 298                         | 471          | 0,6        | 190nm thickness                  |      |
| 50                                  | 2,23E-03                     | 298                         | 471          | 0,6        |                                  |      |
| 60                                  | 2,20E-03                     | 298                         | 482          | 0,6        |                                  |      |
| 70                                  | 2,23E-03                     | 298                         | 485          | 0,6        |                                  |      |
| 80                                  | 2,20E-03                     | 298                         | 487          | 0,6        |                                  |      |
| 90                                  | 2,23E-03                     | 298                         | 488          | 0,6        |                                  |      |
|                                     |                              |                             | Average rate | 0,64       |                                  |      |

| DC-051 (Argon: 16 sccm, N2: 3 sccm) |                              | Production date: 20.03.2014 | Total flow   | 19         | N2/total flow ratio  | 0,16 |
|-------------------------------------|------------------------------|-----------------------------|--------------|------------|--|------|
| State time [min]                    | Main chamber pressure [mbar] | Power [W]                   | DC-volt [V]  | Rate [Å/s] | Comment  |      |
| 5                                   | 2,23E-03                     | 298                         | 434          | 1,2        |  |      |
| 15                                  | 2,23E-03                     | 298                         | 442          | 1,1        |  |      |
| 20                                  | 2,23E-03                     | 298                         | 450          | 1          |  |      |
| 25                                  | 2,26E-03                     | 298                         | 457          | 1          | thickness 162nm  |      |
| 30                                  | 2,28E-03                     | 298                         | 465          | 1          | thickness 193nm, switched to manual (argon 15 sccm, N2: 3 sccm)  |      |
| 40                                  | 2,20E-03                     | 298                         | 469          | 1          | Plasma lost at 236nm, jump started within 15 seconds, switched back to auto (argon: 16 sccm, N2: 3 sccm) |      |
| 50                                  | 2,31E-03                     | 298                         | 475          | 0,9        |  |      |
| 55                                  | 2,23E-03                     | 298                         | 485          | 0,9        | switched to manual (argon 15 sccm, N2: 3 sccm)   |      |
| 60                                  | 2,23E-03                     | 298                         | 489          | 0,8        |  |      |
| 70                                  | 2,23E-03                     | 298                         | 495          | 0,8        |  |      |
|                                     |                              |                             | Average rate | 0,97       |  |      |

| DC-053 (Argon: 18 sccm, N2: 2 sccm) |                              | Production date: 25.03.2014 | Total flow   | 20         | N2/total flow ratio   | 0,1 |
|-------------------------------------|------------------------------|-----------------------------|--------------|------------|---|-----|
| State time [min]                    | Main chamber pressure [mbar] | Power [W]                   | DC-volt [V]  | Rate [Å/s] | Comment   |     |
| 5                                   | 2,23E-03                     | 298                         | 543          | 1,8        | Increased N2 manually: 2 sccm during first 5 minutes to adjust pressure instead of argon flow. (Error: should have adjusted argon flow, but the positive thing is that this is the only sample with a golden colour (characteristic for TiN)) |     |
| 10                                  | 2,23E-03                     | 298                         | 543          | 1,8        |   |     |
| 20                                  | 2,23E-03                     | 298                         | 542          | 1,9        |   |     |
| 30                                  | 2,26E-03                     | 298                         | 538          | 2          |   |     |
| 35                                  | 2,26E-03                     | 298                         | 539          | 2          |   |     |
|                                     |                              |                             | Average rate | 1,9        |   |     |

| DC-054 (Argon: 19 sccm, N2: 0 sccm) |                              | Production date: 25.03.2014 | Total flow   | 19         | N2/total flow ratio   | 0 |
|-------------------------------------|------------------------------|-----------------------------|--------------|------------|---|---|
| State time [min]                    | Main chamber pressure [mbar] | Power [W]                   | DC-volt [V]  | Rate [Å/s] | Comment   |   |
| 5                                   | 1,95E-03                     | 298                         | 524          | 1,9        | changed manually to argon: 19 sccm, N2: 0 sccm (argon: 20 sccm results in p=2,32E-03 mbar)  |   |
| 7                                   | 2,18E-03                     | 298                         | 520          | 2          |   |   |
| 8                                   | 2,20E-03                     | 298                         | 520          | 2          |   |   |
| 15                                  | 2,20E-03                     | 298                         | 519          | 2          |   |   |
| 20                                  | 2,20E-03                     | 298                         | 517          | 2          |   |   |
| 30                                  | 2,23E-03                     | 298                         | 514          | 2          | thickness: 350nm. pressure fluctated with 0,08E-03 mbar                                     |   |
| 32                                  | 2,23E-03                     | 298                         | 513          | 2          | switched back to auto (argon: 18 sccm, N2: 0 sccm). Total deposition time: about 35 minutes |   |
|                                     |                              |                             | Average rate | 1,99       |   |   |

| DC-055 (Argon: 18 sccm, N2: 1 sccm) |                              | Production date: 25.03.2014 | Total flow   | 19         | N2/total flow ratio                             | 0,05 |
|-------------------------------------|------------------------------|-----------------------------|--------------|------------|---|------|
| State time [min]                    | Main chamber pressure [mbar] | Power [W]                   | DC-volt [V]  | Rate [Å/s] | Comment   |      |
| 5                                   | 2,18E-03                     | 298                         | 514          | 2          | switched to manual (argon: 19 sccm, N2: 1 sccm) |      |
| 10                                  | 2,18E-03                     | 298                         | 513          | 2,1        |   |      |
| 15                                  | 2,20E-03                     | 298                         | 511          | 2          |   |      |
| 20                                  | 2,18E-03                     | 298                         | 508          | 2          |   |      |
| 25                                  | 2,20E-03                     | 298                         | 504          | 2          | thickness 261nm                                 |      |
| 30                                  | 2,20E-03                     | 298                         | 503          | 2          | Total deposition time: about 32,5 min           |      |
|                                     |                              |                             | Average rate | 2,02       |   |      |

#### D4. Pressure evolution during deposition

From figure 141 it can be seen that the main chamber pressure [mbar] needed to be adjusted for DC-050 and DC-054 in the beginning of the deposition. Otherwise the small pressure fluctuations can be neglected. Sample DC-049 with the highest N<sub>2</sub>-total flow ratio seems to have the most stable main chamber pressure.

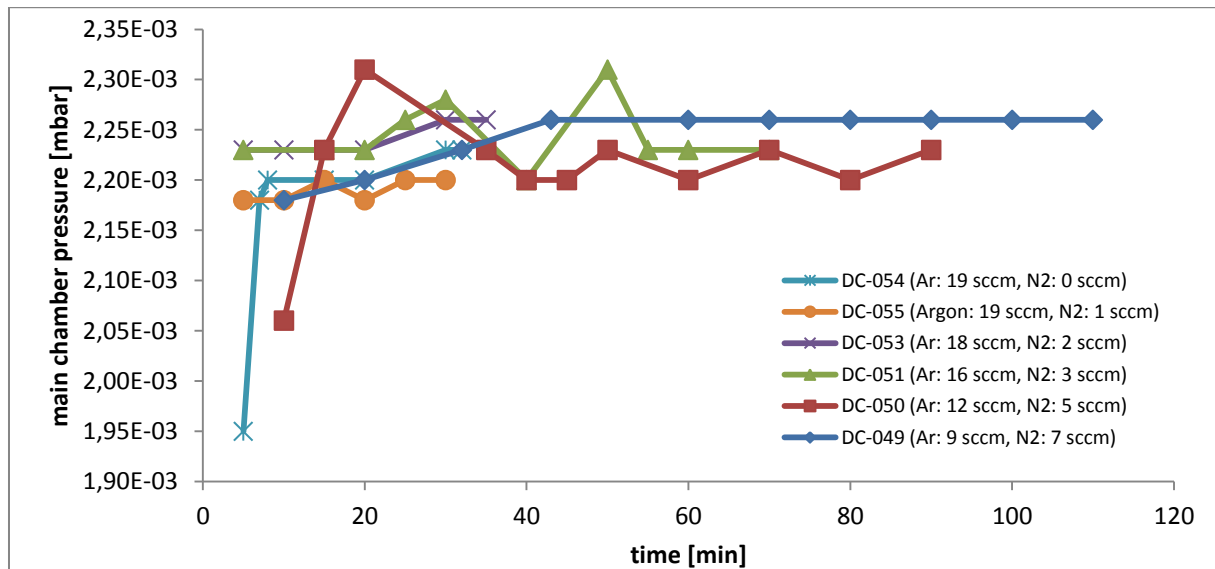


Figure 141 - main chamber pressure [mbar] vs. time [min]

#### D5. Target arcing investigations

Figure 142 shows an evaluation of the number of arcs on the target surface observed during the deposition with the goal to determine if it's necessary to reproduce the nitrogen series. No arcing was observed for the new target, which was half the thickness and mounted with a copper back plate to the sputter head in order to keep the same target height. The old target showed many arcs.

Comparing the electrical stability of the samples produced with the new and old target it can be stated, that there is no significant observable correlation between resistivity drift and observed arcing on target surface during deposition, which is why it is believed that it's not necessary to reproduce the series, which saves more than 1 week in production time.

| Sample | Ar flow [sccm] | N <sub>2</sub> flow [sccm] | Ar/N <sub>2</sub> ratio | Number of arcs as observed through looking glass. (3 most arcs) | Stability ranking | Target | Target state  |
|--------|----------------|----------------------------|-------------------------|---|-------------------|--------|---------------|
| DC-054 | 19             | 0                          | 20                      | 0   | 4                 | new    | Metallic mode |
| DC-055 | 19             | 1                          | 19                      | 0   | 2                 | new    | Metallic mode |
| DC-053 | 18             | 2                          | 9                       | 0   | 6                 | new    | Intermediate  |
| DC-051 | 16             | 3                          | 5,3                     | 3   | 5                 | old    | Intermediate  |
| DC-050 | 12             | 5                          | 2,4                     | 2   | 1                 | old    | Poisoned mode |
| DC-049 | 9              | 7                          | 1,3                     | 2.5   | 3                 | old    | Poisoned mode |

Figure 142 - Influence of arcs and target age on resistivity stability of films

To avoid arcing in the future productions the old titanium target has been analyzed. Figure 143 and figure 144 show the qualitative EDX mapping of the old titanium target used for the production of sample DC-049, 50, 51. The position is on the racetrack of the target, which is about 2.1 mm deep. Orange shows the detection of titanium, yellow shows nitrogen and violette shows carbon. It can be seen that nitrogen is incorporated into the target.

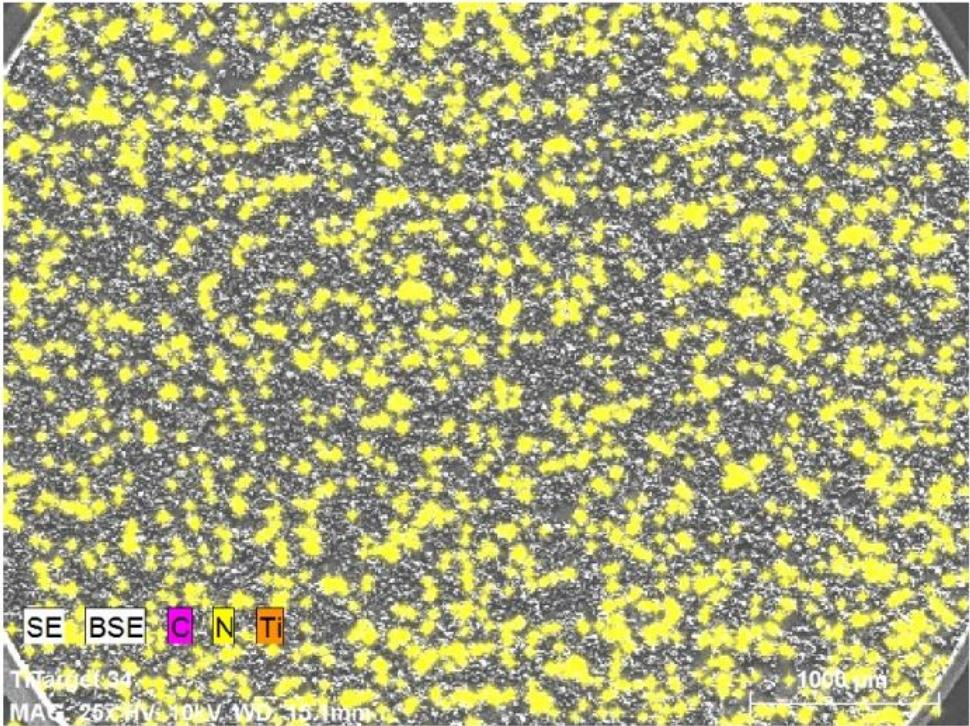
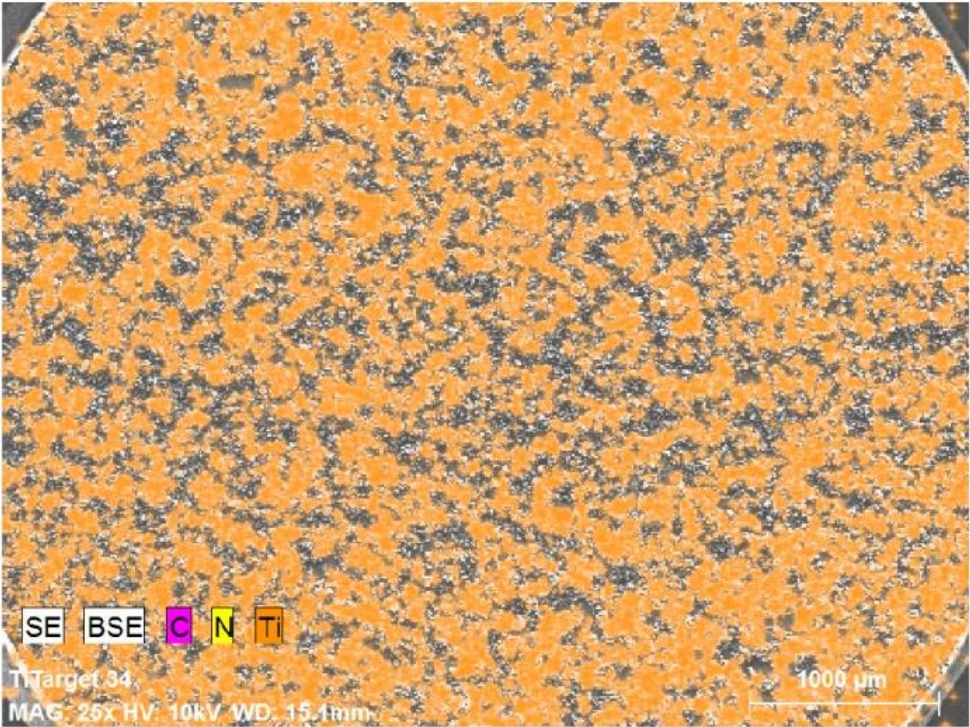


Figure 143 – Qualitative EDX mapping of old titanium target part 1

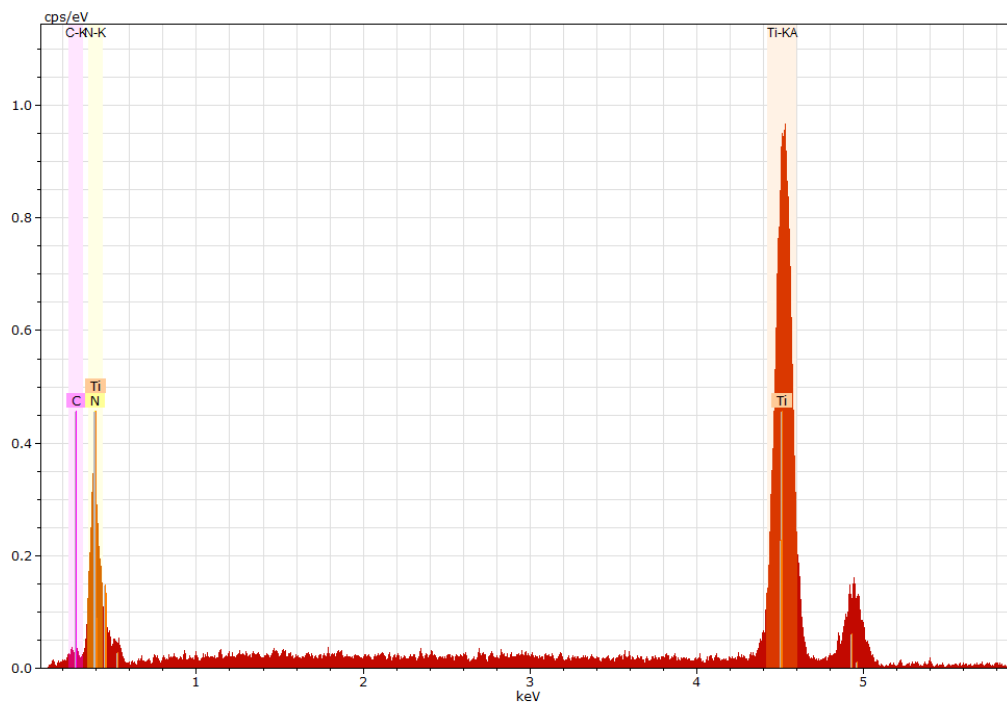
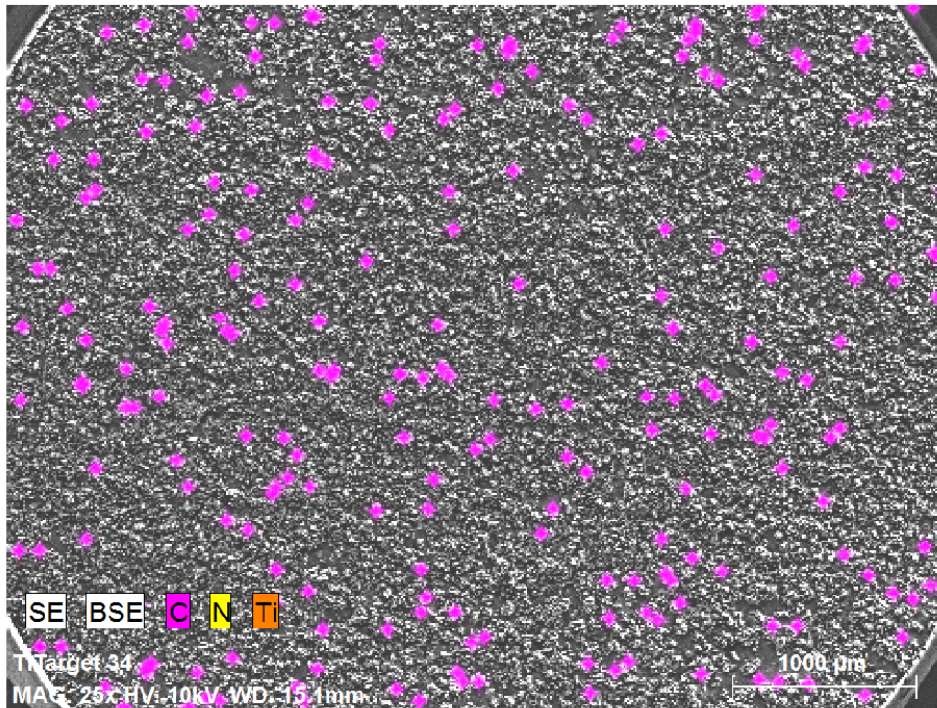


Figure 144 – Qualitative EDX mapping of old titanium target part 2

SEM images of the middle in the racetrack showed a very rough surface. It can be seen that small islands have been formed on top of the smoother titanium target surface (see figure 145).



Figure 145 – SEM image of racetrack (upper image) and image of titanium target (lower image)

A qualitative EDX mapping of a 5x5um area detected nitrogen and oxygen in the “islands” which could indicate that the islands are  $TiO_xN_y$  target contaminations causing the heavy arcing on the titanium target surface during the PVD process (see figure 146).

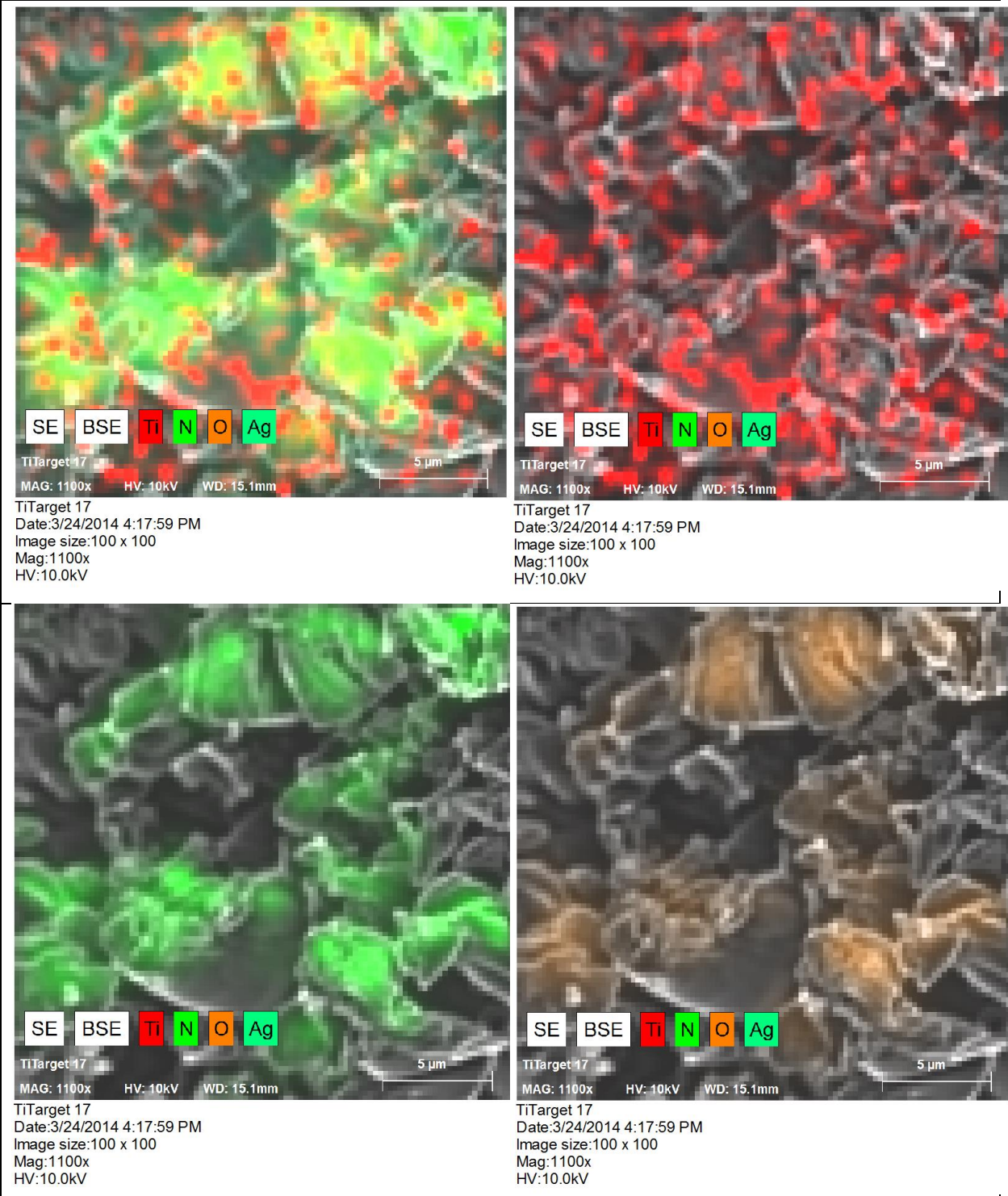
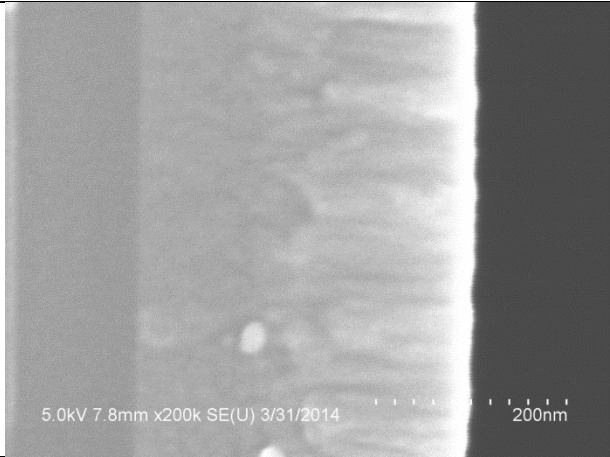
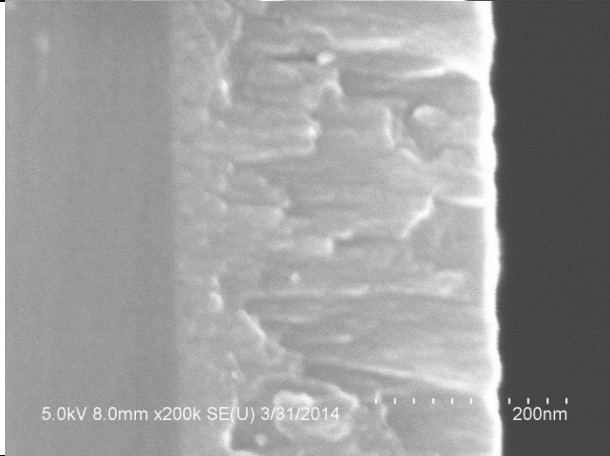
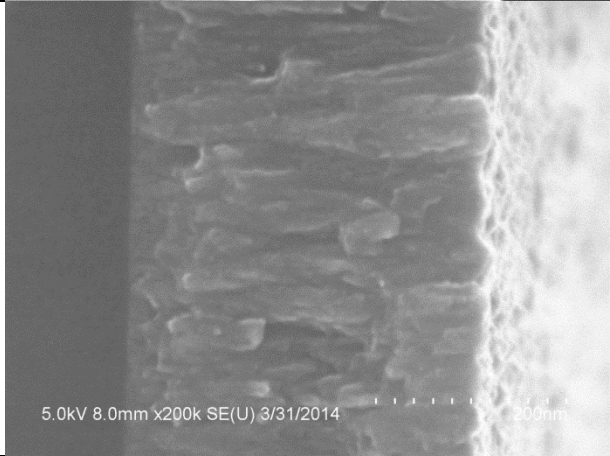


Figure 146 - qualitative EDX mapping of a 5x5um on target racetrack

The consequences for the future could be to polish the target in case the racetrack is getting to deep and also to increase the pre-cleaning time of the target in pure argon at the beginning of the deposition process (SOAK2) from 6 to 15 minutes in order to get rid of target contaminations.

## D6. SEM cross-section images

The thickness and cross-sectional morphology of the sample was investigated. The images were taken with a magnification of x200k. Figure 147 show the cross-view SEM images of the produced samples. The target was changed midway in this deposition series, so there might be some influence to the thickness from this change.

| SEM images  |  |
|---|--|
| DC-049-P1A-2<br>Nitrogen flow: 9 sccm<br>Argon flow: 7 sccm<br>SEM thickness: 350 nm  |    |
| DC-050-P1A-2<br>Nitrogen flow: 5 sccm<br>Argon flow: 12 sccm<br>SEM thickness: 335 nm |   |
| DC-051-P1A-2<br>Nitrogen flow: 3 sccm<br>Argon flow: 16 sccm<br>SEM thickness: 373 nm |  |

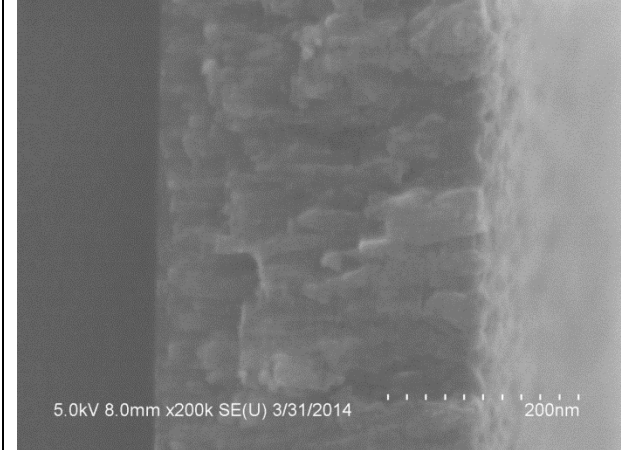
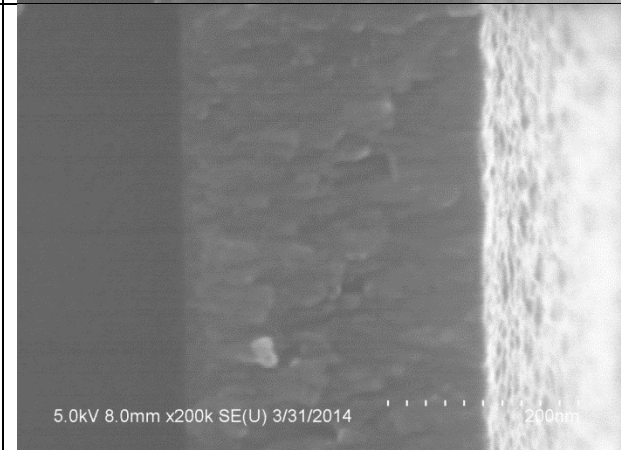
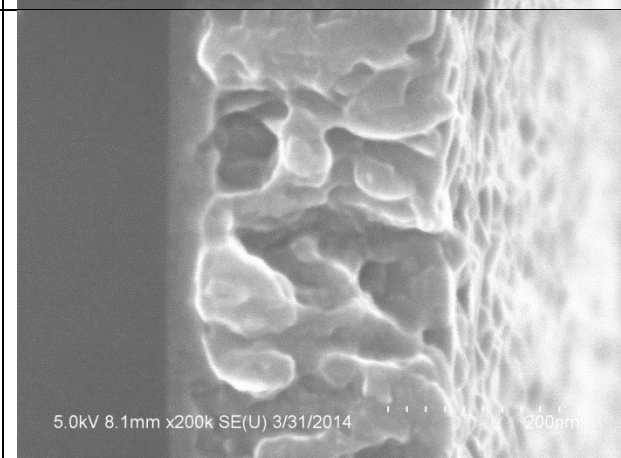
|  |   |
|--|---|
| <p>DC-053-P1A-2<br/>         Nitrogen flow: 2 sccm<br/>         Argon flow: 18 sccm<br/>         SEM thickness: 340 nm</p> |  <p>5.0kV 8.0mm x200k SE(U) 3/31/2014 200nm</p>   |
| <p>DC-055-P1A-2<br/>         Nitrogen flow: 1 sccm<br/>         Argon flow: 19 sccm<br/>         SEM thickness: 315 nm</p> |  <p>5.0kV 8.0mm x200k SE(U) 3/31/2014 200nm</p>  |
| <p>DC-054-P1A-2<br/>         Nitrogen flow: 0 sccm<br/>         Argon flow: 19 sccm<br/>         SEM thickness: 294 nm</p> |  <p>5.0kV 8.1mm x200k SE(U) 3/31/2014 200nm</p> |

Figure 147 – cross-section view image for “nitrogen series 300W”

## e. Power series appendix

### E1. Substrates and placement – power series

We have decided not to include extra analysis samples for post accelerated-life test other than the 4-point probe samples.

| Substrate:                 | Name   | Number: | Dimensions: | Purpose:  |
|----------------------------|--------|---------|-------------|---|
| Si (100)                   | P1-A1  | 1       | 10x10 mm    | EDX composition   |
| Si (100)                   | P1-A2  | 1       | 10x10 mm    | SEM cross-section (to be canceled. Not conclusive enough) |
| Si (100) with photo resist | P1-B1  | 1       | 10x10 mm    | Lift-off<br>AFM thickness measurement                     |
| BK7 glass (G3)             | BK7-A1 | 1       | 25x25 mm    | 4-point probe measurement reference                       |
| BK7 glass (G3)             | BK7-A2 | 1       | 25x25 mm    | 4-point probe measurement accelerated life test           |
| BK7 glass (G3)             | BK7-B1 | 1       | 15x15 mm    | XRD analysis  |
| Si P7                      | P7-A1  | 1       | 3x25 mm     | Dektak - Stress measurements                              |
| Si P7                      | P7-A2  | 1       | 3x25 mm     | Dektak - Stress measurements                              |

Figure 148 - substrates needed for the analysis of the films

The substrates will be fixed using carbon tape on a wafer to have the substrates tightly placed to minimize effects of thickness variations and variations in the energy content of the sputter flux.

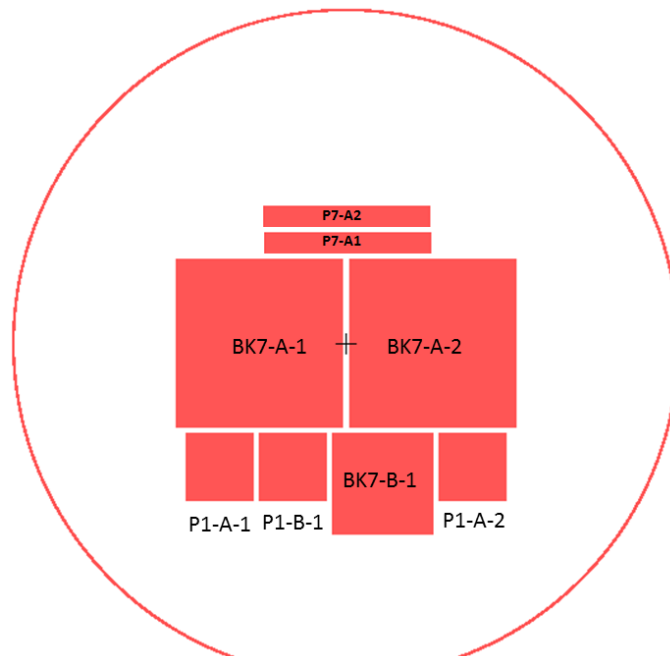


Figure 149 - sample placement on wafer

## E2. Sample deposition data observations

|   |                              |                             |             |              |   |                                  |        |
|---|------------------------------|-----------------------------|-------------|--------------|---|----------------------------------|--------|
| DC-049 (Ar: 9 sccm, N <sub>2</sub> : 7 sccm, 300W)  |                              | Production date: 20.03.2014 |             | Total flow   | 16  | N <sub>2</sub> /total flow ratio | 0,44   |
| State time [min]                                    | Main chamber pressure [mbar] | Power [W]                   | DC-volt [V] | Rate [Å/s]   | Comment   |                                  |        |
| 10  | 2,18E-03                     | 298                         | 457         | 0,6          | Observations: during the deposition many arcs have been observed on the target.   |                                  |        |
| 20  | 2,20E-03                     | 298                         | 457         | 0,6          |   |                                  |        |
| 32  | 2,23E-03                     | 298                         | 458         | 0,6          |   |                                  |        |
| 43  | 2,26E-03                     | 298                         | 462         | 0,6          |   |                                  |        |
| 60  | 2,26E-03                     | 298                         | 470         | 0,6          |   |                                  |        |
| 70  | 2,26E-03                     | 298                         | 476         | 0,5          |   |                                  |        |
| 80  | 2,26E-03                     | 298                         | 481         | 0,6          |   |                                  |        |
| 90  | 2,26E-03                     | 298                         | 486         | 0,5          |   |                                  |        |
| 100   | 2,26E-03                     | 298                         | 490         | 0,5          |   |                                  |        |
| 110   | 2,26E-03                     | 298                         | 493         | 0,5          |   |                                  |        |
| Average pressure                                    |                              | 2,26E-03                    |             | Average rate |   |                                  |        |
| DC-055 (Ar: 18 sccm, N <sub>2</sub> : 1 sccm, 300W) |                              | Production date: 25.03.2014 |             | Total flow   | 19  | N <sub>2</sub> /total flow ratio | 0,0526 |
| State time [min]                                    | Main chamber pressure [mbar] | Power [W]                   | DC-volt [V] | Rate [Å/s]   | Comment   |                                  |        |
| 5   | 2,18E-03                     | 298                         | 514         | 2            | switched to manual (argon: 19 sccm, N <sub>2</sub> : 1 sccm)  |                                  |        |
| 10  | 2,18E-03                     | 298                         | 513         | 2,1          |   |                                  |        |
| 15  | 2,20E-03                     | 298                         | 511         | 2            |   |                                  |        |
| 20  | 2,18E-03                     | 298                         | 508         | 2            |   |                                  |        |
| 25  | 2,20E-03                     | 298                         | 504         | 2            | thickness 261nm   |                                  |        |
| 30  | 2,20E-03                     | 298                         | 503         | 2            | Total deposition time: about 32,5 min   |                                  |        |
| Average pressure                                    |                              | 2,19E-03                    |             | Average rate | 2,02  |                                  |        |
| DC-057 (Ar: 19 sccm, N <sub>2</sub> : 1 sccm, 450W) |                              | Production date: 02.04.2014 |             | Total flow   | 20  | N <sub>2</sub> /total flow ratio | 0,0500 |
| State time [min]                                    | Main chamber pressure [mbar] | Power [W]                   | DC-volt [V] | Rate [Å/s]   | Comment   |                                  |        |
| 5   | 2,18E-03                     | 448                         | 479         | 3            | manually Ar:20 results in 2,31E-03 mbar   |                                  |        |
| 7,5   | 2,20E-03                     | 448                         | 479         | 3            |   |                                  |        |
| 10  | 2,20E-03                     | 448                         | 482         | 3            |   |                                  |        |
| 12,5  | 2,20E-03                     | 448                         | 478         | 3            |   |                                  |        |
| 15  | 2,23E-03                     | 448                         | 477         | 3            |   |                                  |        |
| 17,5  | 2,23E-03                     | 448                         | 477         | 3            |   |                                  |        |
| 20  | 2,23E-03                     | 448                         | 476         | 3            |   |                                  |        |
| 22,5  | 2,23E-03                     | 448                         | 477         | 3            |   |                                  |        |
| Average pressure                                    |                              | 2,21E-03                    |             | Average rate | 3   |                                  |        |
| DC-059 (Ar: 18 sccm, N <sub>2</sub> : 1 sccm, 150W) |                              | Production date: 04.03.2014 |             | Total flow   | 19  | N <sub>2</sub> /total flow ratio | 0,0526 |
| State time [min]                                    | Main chamber pressure [mbar] | Power [W]                   | DC-volt [V] | Rate [Å/s]   | Comment   |                                  |        |
| 5   | 2,20E-03                     | 149                         | 427         | 0,9          | changed manually from Ar: 19 to Ar: 18 sccm   |                                  |        |
| 10  | 2,20E-03                     | 149                         | 427         | 0,9          |   |                                  |        |
| 15  | 2,20E-03                     | 149                         | 427         | 0,9          |   |                                  |        |
| 20  | 2,23E-03                     | 149                         | 426         | 1            |   |                                  |        |
| 25  | 2,23E-03                     | 149                         | 426         | 1            |   |                                  |        |
| 30  | 2,26E-03                     | 149                         | 425         | 1            |   |                                  |        |
| 35  | 2,26E-03                     | 149                         | 425         | 1            |   |                                  |        |
| 40  | 2,26E-03                     | 149                         | 424         | 1            |   |                                  |        |
| 45  | 2,26E-03                     | 149                         | 424         | 1            |   |                                  |        |
| 50  | 2,26E-03                     | 149                         | 423         | 1            |   |                                  |        |
| 55  | 2,26E-03                     | 149                         | 422         | 1            |   |                                  |        |
| 60  | 2,26E-03                     | 149                         | 422         | 1,1          |   |                                  |        |
| 65  | 2,26E-03                     | 149                         | 420         | 1,1          |   |                                  |        |
| Average pressure                                    |                              | 2,24E-03                    |             | Average rate | 0,99  |                                  |        |
| DC-061 (Ar: 19 sccm, N <sub>2</sub> : 2 sccm, 600W) |                              | Production date: 04.04.2014 |             | Total flow   | 21  | N <sub>2</sub> /total flow ratio | 0,0952 |
| State time [min]                                    | Main chamber pressure [mbar] | Power [W]                   | DC-volt [V] | Rate [Å/s]   | Comment   |                                  |        |
| 1   | 2,23E-03                     | 597                         | 493         | 4,1          |   |                                  |        |
| 2   | 2,23E-03                     | 597                         | 493         | 4,1          |   |                                  |        |
| 6   | 2,26E-03                     | 597                         | 492         | 4,1          |   |                                  |        |
| 10  | 2,26E-03                     | 597                         | 491         | 4,1          |   |                                  |        |
| 15  | 2,26E-03                     | 597                         | 490         | 4,1          |   |                                  |        |
| Average pressure                                    |                              | 2,25E-03                    |             | Average rate | 4,10  |                                  |        |
| DC-062 (Ar: 6 sccm, N <sub>2</sub> : 10 sccm, 600W) |                              | Production date: 04.04.2014 |             | Total flow   | 16  | N <sub>2</sub> /total flow ratio | 0,6250 |
| State time [min]                                    | Main chamber pressure [mbar] | Power [W]                   | DC-volt [V] | Rate [Å/s]   | Comment   |                                  |        |
| 1   | 2,20E-03                     | 597                         | 726         | 1,5          | manually adjusted Ar: 6sccm, N <sub>2</sub> :10sccm (poisoned mode)   |                                  |        |
| 5   | 2,23E-03                     | 597                         | 717         | 1,5          |   |                                  |        |
| 10  | 2,26E-03                     | 597                         | 714         | 1,5          |   |                                  |        |
| 15  | 2,28E-03                     | 597                         | 712         | 1,5          |   |                                  |        |
| 20  | 2,28E-03                     | 566                         | 800         | 1,5          | about 180nm   |                                  |        |
| 25  | 2,32E-03                     | 597                         | 712         | 1,5          | manually adjusted Ar: 5sccm N <sub>2</sub> : 10 sccm (pressure was at p=2,31E-03 mbar), but plasma got shortly lost. Switched back to Ar:6 sccm N <sub>2</sub> : 10sccm |                                  |        |
| 30  | 2,32E-03                     | 597                         | 712         | 1,5          |   |                                  |        |
| 35  | 2,32E-03                     | 597                         | 712         | 1,5          |   |                                  |        |
| 40  | 2,32E-03                     | 597                         | 711         | 1,5          |   |                                  |        |
| 45  | 2,32E-03                     | 597                         | 711         | 1,5          |   |                                  |        |
| Average pressure                                    |                              | 2,29E-03                    |             | Average rate | 1,50  |                                  |        |
| DC-063 (Ar: 8 sccm, N <sub>2</sub> : 9 sccm, 450W)  |                              | Production date: 07.04.2014 |             | Total flow   | 17  | N <sub>2</sub> /total flow ratio | 0,5294 |
| State time [min]                                    | Main chamber pressure [mbar] | Power [W]                   | DC-volt [V] | Rate [Å/s]   | Comment   |                                  |        |
| 0   | 2,20E-03                     | 448                         | 548         | 1            |   |                                  |        |
| 10  | 2,23E-03                     | 448                         | 547         | 1            | 63 nm   |                                  |        |
| 20  | 2,26E-03                     | 448                         | 547         | 1            | 130 nm  |                                  |        |
| 30  | 2,28E-03                     | 448                         | 547         | 1            | 190 nm  |                                  |        |
| 40  | 2,28E-03                     | 448                         | 546         | 1            | 250 nm  |                                  |        |
| 50  | 2,28E-03                     | 448                         | 546         | 1            | 310 nm  |                                  |        |
| 60  | 2,31E-03                     | 448                         | 546         | 1            | 370 nm  |                                  |        |
| 65  | 2,31E-03                     | 448                         | 546         | 1            | 400 nm  |                                  |        |
| Average pressure                                    |                              | 2,27E-03                    |             | Average rate | 1,00  |                                  |        |

## f. Nitrogen flow series 600W appendix

### F1. XRD – nitrogen series 600W

XRD measurements were performed by Kasper Thilasing-Hansen with the goal of analyzing the phase content of the thin films. Figure 150 shows the XRD results. There is no clear indication in how far the texture is influencing the resistivity stability for the 600 W nitrogen series.

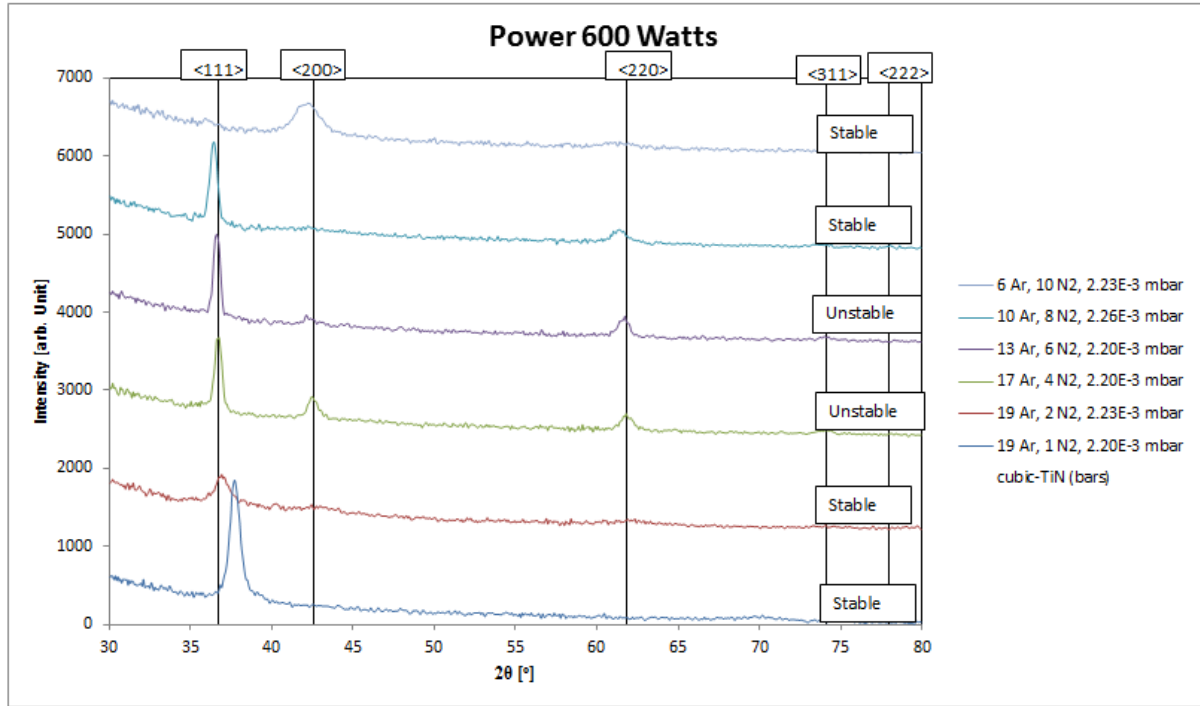


Figure 150 - XRD spectra - Grazing incident X-ray diffraction patterns ( $\omega=7^\circ$ ). The reflection angles from cubic TiN are shown as bars. The large “bumps” in the spectra stem from the amorphous BK-7 glass substrates.

## g. Gauge factor experiments

### G1. Ansys and Comsol beam deflection models

By Nis Dam Madsen and Mathias Hausladen

Figure 151 and figure 152 show ANSYS and COMSOL finite element models for the beam deflection.

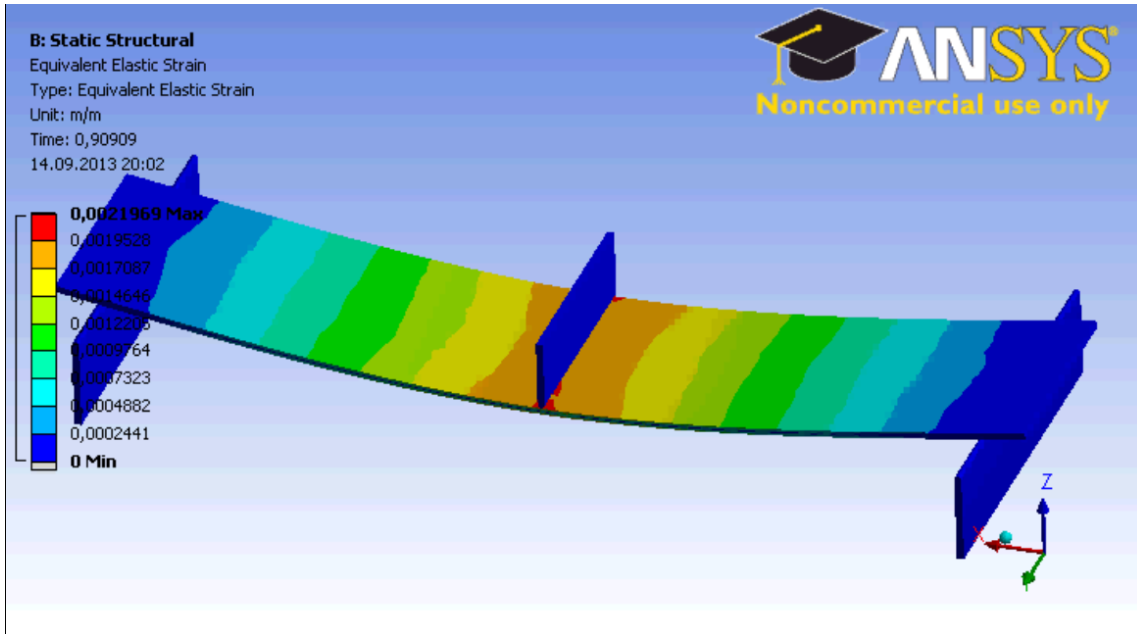


Figure 151 – ANSYS model showing strain for various loads

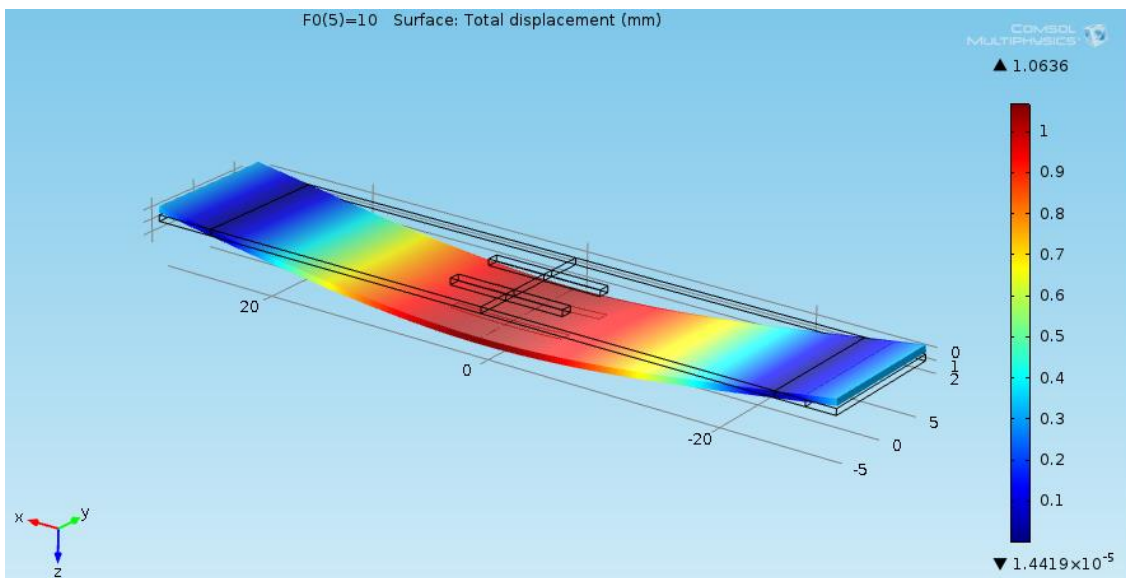


Figure 152 – COMSOL model showing the total displacement at 10



## G2. Initial gauge factor measurement

This chapter is intended to only give a brief impression of the work which preceded the newest gauge factor holder design and setup.

Figure 154 shows the initial testing setup with manual loading by Nis Dam Madsen and Mathias Hausladen:

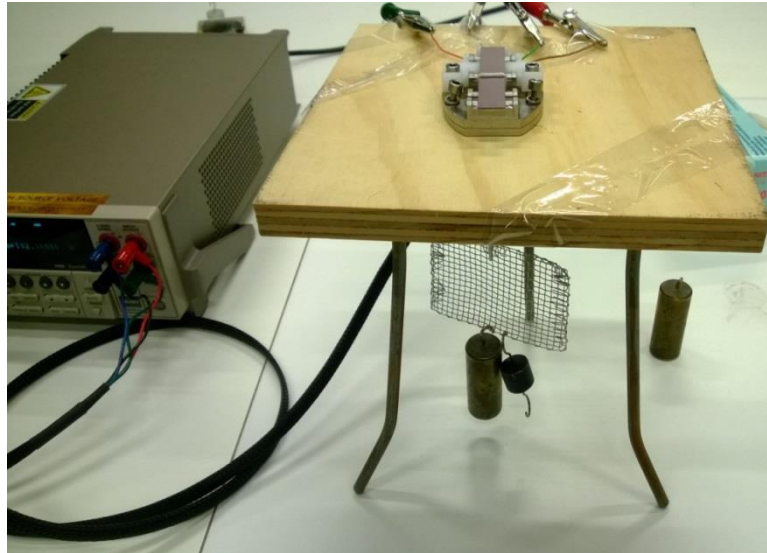


Figure 154 – initial testing setup

Figure 155 shows a close-up of the holder with the extension, which is able to measure electrical resistance using 4-spring loaded pins, which are touching the gold contacts of the substrates

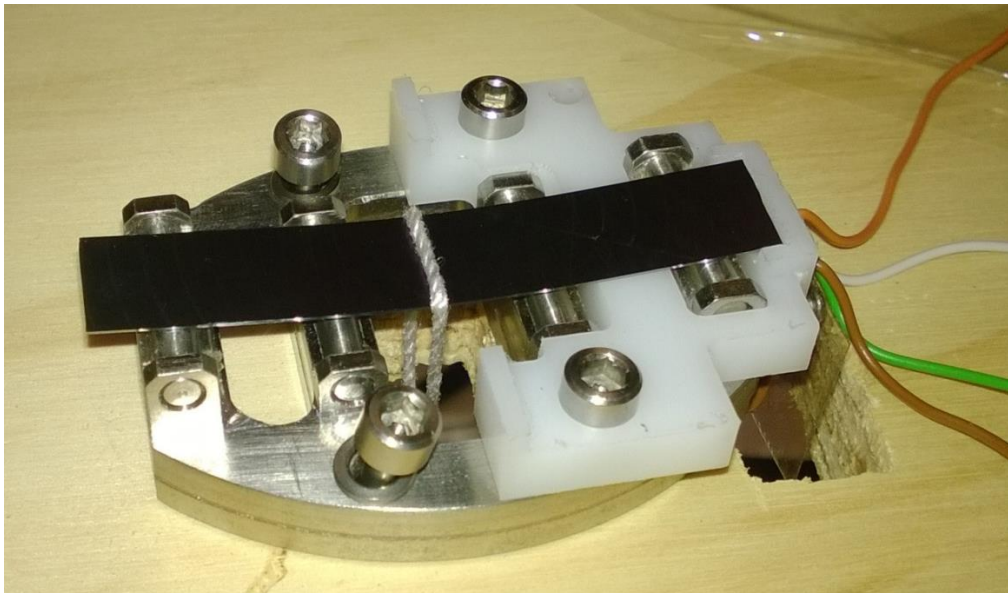


Figure 155 – close-up of the initial gauge factor setup

Figure 156 shows the initial longitudinal, Wheatstone bridge and transverse resistors designs (top contact) sample DC-30 used for the initial gauge factor experiments. Note that the wheat stone bridge sample could not be measured because due to shadow effects of the deposition mask the resistors were not balanced (which is crucial for a wheat stone bridge)

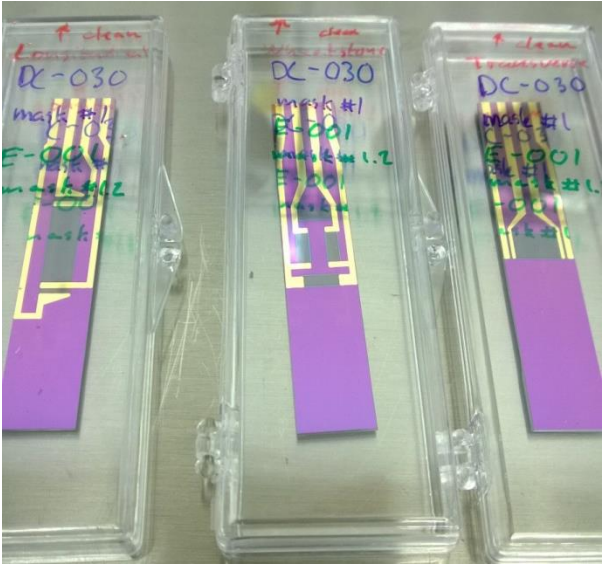


Figure 156 - initial longitudinal, Wheatstone bridge and transverse resistors designs (DC-30)

Figure 157 shows the gauge factor of test sample DC-30 (transverse) with a gauge factor of 3,6.

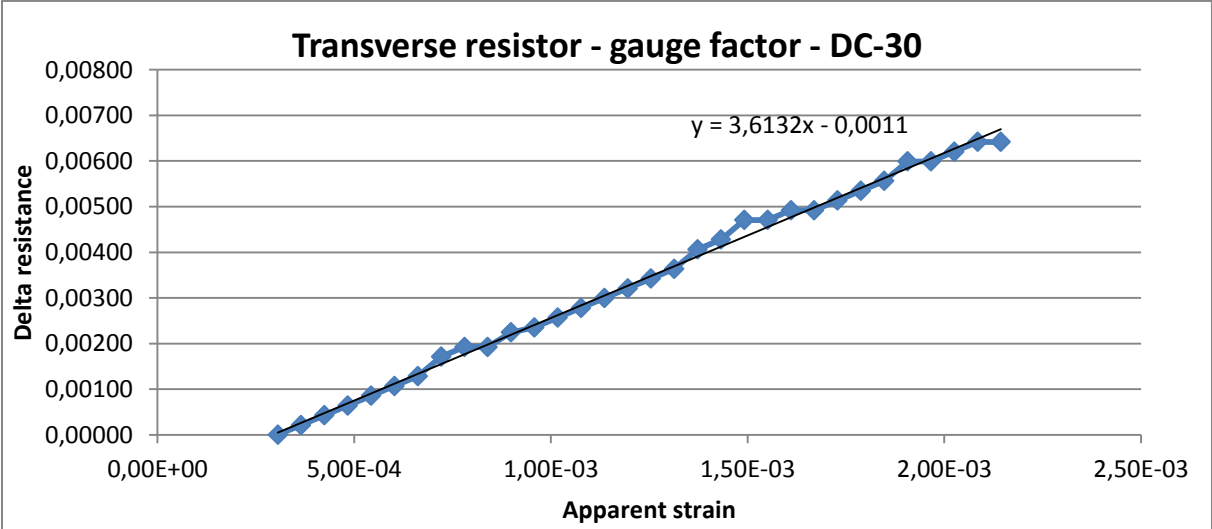


Figure 157 – gauge factor – transverse resistor – DC-30

Figure 158 shows the gauge factor of test sample DC-30 (longitudinal) with a gauge factor of 5,4.

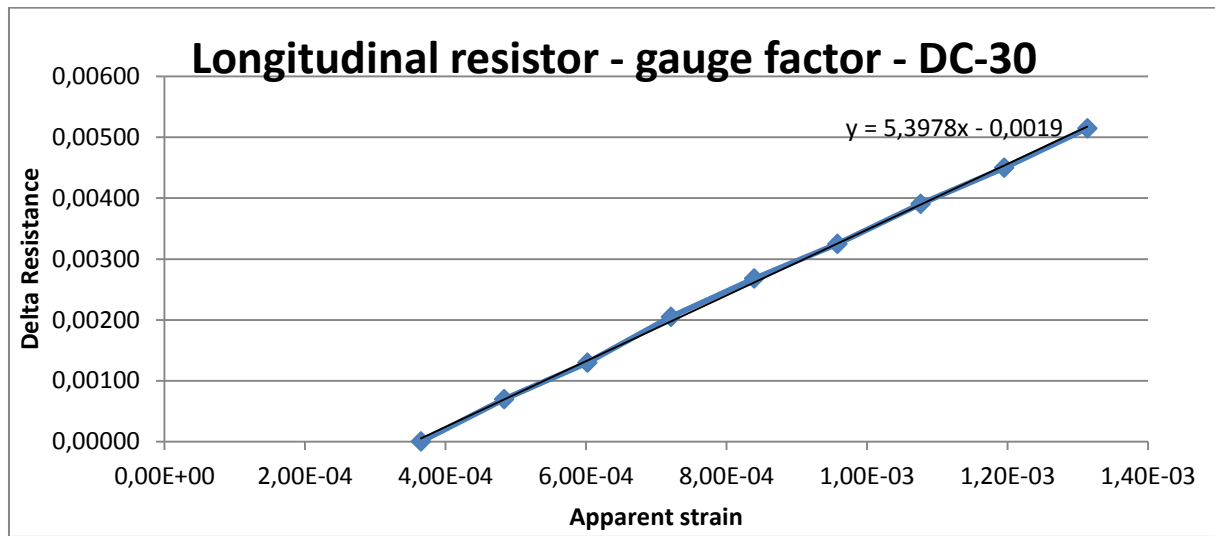


Figure 158 – gauge factor - longitudinal resistor – DC-30

The strain is denoted apparent strain because the wafer is resting on the springs until ~7N was applied. Furthermore, issues with anisotropy and thickness will also influence the strain.

The strain was calculated based on Bernoulli’s beam theory using the following data for the longitudinal sample:

|  |   |             |
|--|---|-------------|
| <b>Parameters:</b>                             | Keithley using filter: 10 measurements averaged (average count) |             |
| <b>z0 [m]</b>                                  | (This increased the accuracy. 1st digit after comma was stable  |             |
| 0,0002625                                      | 2nd digit was fluctuating within a small range                  |             |
| <b>Youngs modulus (E) [Pa]</b>                 | Resistor length (mm):   | 15          |
| 1,69E+11                                       | Resistor width (mm):  | 5           |
| <b>beam width (b) [m]</b>                      | Film thickness (nm):  | 400         |
| 0,012  | Film resistivity:   | 9,55933E-05 |
| <b>beam height (h) [m]</b>                     |   |             |
| 0,000525                                       |   |             |
| <b>length (l) [m]</b>                          |   |             |
| 0,05   |   |             |
| <b>Area moment inertia (I) [m<sup>4</sup>]</b> |   |             |
| 1,4470E-13                                     |   |             |

$$I_x = \frac{1}{12}bh^3$$

And for the transverse sample:

**Parameters:**

**z0 [m]**  
0,0002625

**Youngs modulus (E) [Pa]**  
1,69E+11

**beam width (b) [m]**  
0,012

**beam height (h) [m]**  
0,000525

**length (l) [m]**  
0,05

**Area moment inertia (I) [m<sup>4</sup>]**  
1,4470E-13

$$I_x = \frac{1}{12} b h^3$$

**transverse resistor width (l<sub>0</sub>)**  
**[mm]**  
0,005

Resistor length (mm): 7,8  
Resistor width (mm): 5  
Film thickness (nm): 400  
Film resistivity: 1,20E-04

Also a prototype measurement with the DMA was setup:

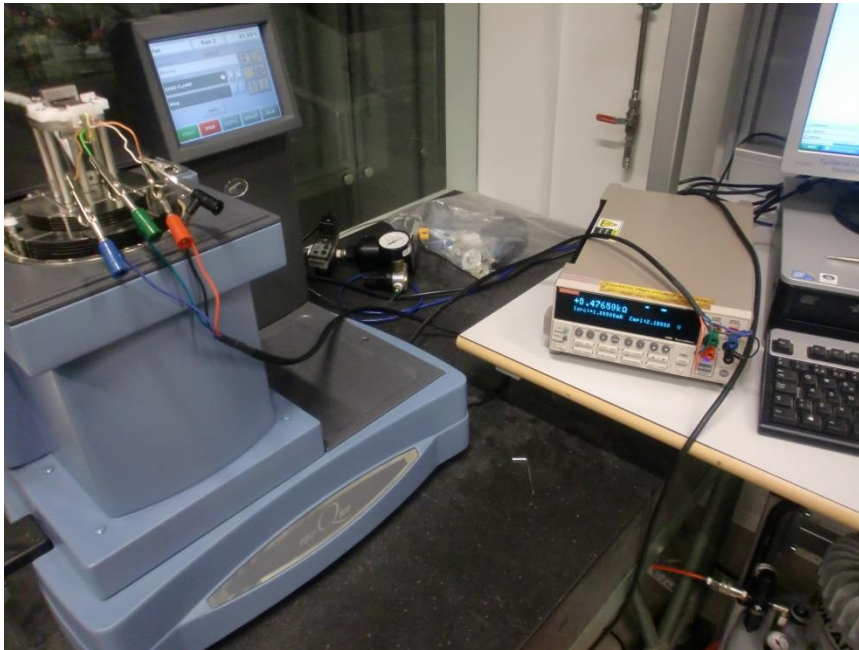


Figure 159 – initial holder extension connected to the DMA setup

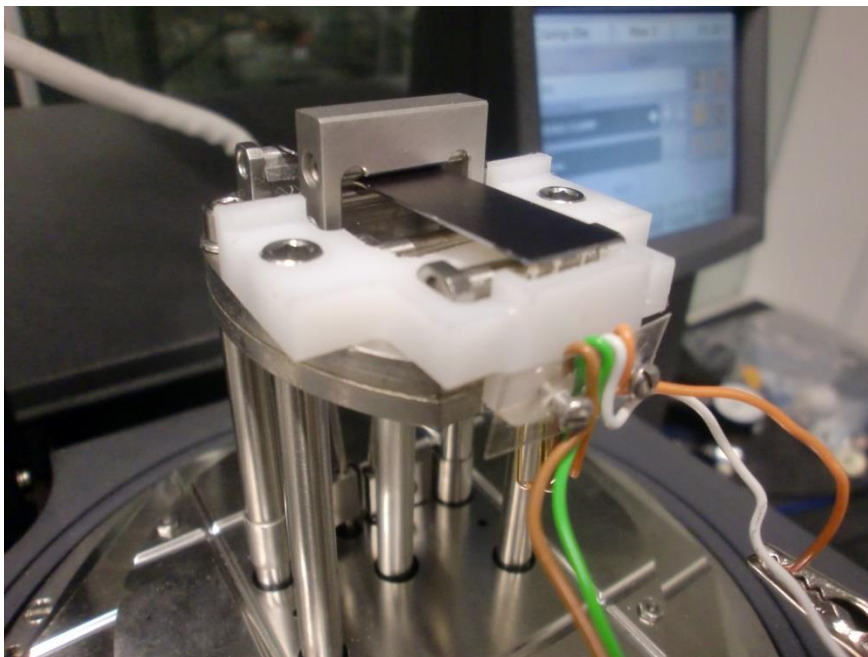


Figure 160 – zoom-in of initial holder extension with four spring loaded probes connected to the DMA setup

#### Main problems:

- ➔ The strain is not centered. The sample is resting on the four spring loaded probes. For an accurate gauge factor measurement the load should be centered.
- ➔ The setup is not good for high temperature measurements.
- ➔ Electrical contact problems due to the non-uniform contact pressure of the spring loaded probes

### G3. DMA software measurement steps

| #  | Running Segment Description         |
|----|-------------------------------------|
| 1  | Initial temperature 40.00 °C        |
| 2  | Ramp force 15.000 N/min to 7.500 N  |
| 3  | Ramp force -15.000 N/min to 2.000 N |
| 4  | External event Off                  |
| 5  | External event On                   |
| 6  | Ramp force 15.000 N/min to 7.500 N  |
| 7  | Ramp force -15.000 N/min to 1.900 N |
| 8  | Ramp force 15.000 N/min to 7.500 N  |
| 9  | Ramp force -15.000 N/min to 1.900 N |
| 10 | Ramp force 10.000 N/min to 2.000 N  |
| 11 | Isothermal for 0.50 min             |
| 12 | External event Off                  |
| 13 | External event On                   |
| 14 | Isothermal for 0.40 min             |
| 15 | Ramp force 5.000 N/min to 3.000 N   |
| 16 | Isothermal for 0.10 min             |
| 17 | External event Off                  |
| 18 | External event On                   |
| 19 | Isothermal for 0.40 min             |
| 20 | Ramp force 5.000 N/min to 4.000 N   |
| 21 | Isothermal for 0.10 min             |
| 22 | External event Off                  |
| 23 | External event On                   |
| 24 | Isothermal for 0.40 min             |
| 25 | Ramp force 5.000 N/min to 5.000 N   |
| 26 | Isothermal for 0.10 min             |
| 27 | External event Off                  |
| 28 | External event On                   |
| 29 | Isothermal for 0.40 min             |
| 30 | Ramp force 5.000 N/min to 6.000 N   |
| 31 | Isothermal for 0.10 min             |
| 32 | External event Off                  |
| 33 | External event On                   |
| 34 | Isothermal for 0.40 min             |
| 35 | Ramp force 5.000 N/min to 7.000 N   |
| 36 | Isothermal for 0.10 min             |
| 37 | External event Off                  |
| 38 | External event On                   |
| 39 | Isothermal for 0.40 min             |
| 40 | Ramp force -5.000 N/min to 6.000 N  |
| 41 | Isothermal for 0.10 min             |
| 42 | External event Off                  |
| 43 | External event On                   |
| 44 | Isothermal for 0.40 min             |
| 45 | Ramp force -5.000 N/min to 5.000 N  |
| 46 | Isothermal for 0.10 min             |
| 47 | External event Off                  |
| 48 | External event On                   |
| 49 | Isothermal for 0.40 min             |
| 50 | Ramp force -5.000 N/min to 4.000 N  |
| 51 | Isothermal for 0.10 min             |
| 52 | External event Off                  |
| 53 | External event On                   |
| 54 | Isothermal for 0.40 min             |
| 55 | Ramp force -5.000 N/min to 3.000 N  |
| 56 | Isothermal for 0.10 min             |
| 57 | External event Off                  |
| 58 | External event On                   |
| 59 | Isothermal for 0.40 min             |
| 60 | Ramp force -5.000 N/min to 2.000 N  |
| 61 | Isothermal for 0.10 min             |
| 62 | External event Off                  |
| 63 | External event On                   |
| 64 | Isothermal for 0.40 min             |
| 65 | Increment by 10.00 °C               |
| 66 | Repeat segment 11 until 70.00 °C    |
| 67 | Ramp force -15.000 N/min to 0.000 N |

Figure 161 -

#### G4. Load displacement performance experiment

By Nis Dam Madsen

Load-displacement curves from the 3-point bend tests in the Q800 DMA has been produced for the 4x0 and 2x2 configuration and without contact wires in the holder. A 12x64x0.5 mm Si (100) [110] beam was used in all the load-displacement experiments. The curves are shown in Fig. 5. The bends observed in all curves near the origin is due the clamp not being tightened to avoid the gap between sample and clamp. In 3-point bending the displacement is expected to be linear proportional to the load. This is also seen to be case at higher loads. There is a non-linear component to the reponse in the load case without wires, which may be due the material properties of the prototype and/or insufficient compliance calibration. For the two other load case, a load of 5-6 N is needed before a linear response is observed. The slope of the load-displacement curve, at higher loads, is the same in the three cases. The 2x2 wire configuration is more compliant than the 4x0 configuration.

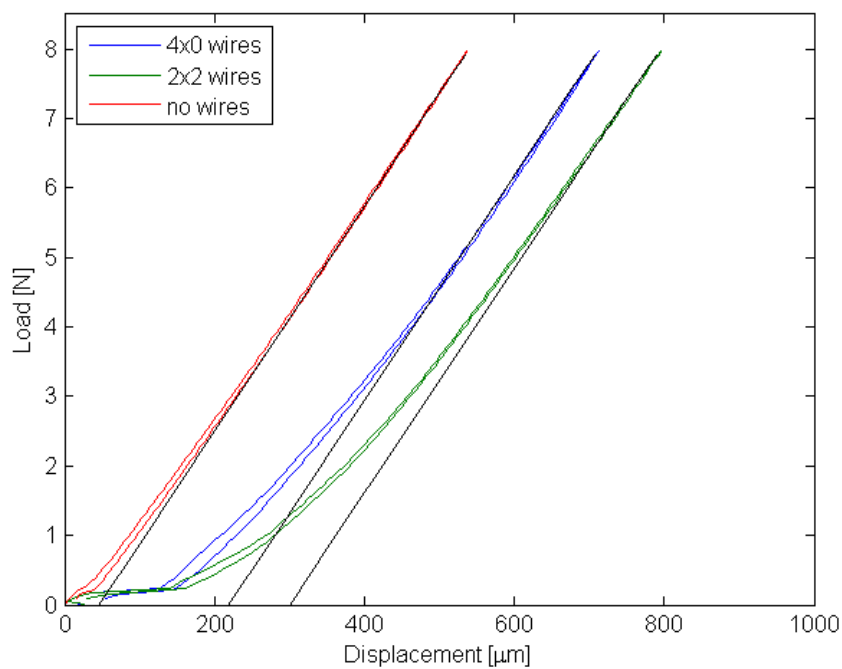


Figure 162 – load displacement curves for 4x0 (all four wires on one end of holder), 2x2 (two wires on one end and two wires on other end of holder) and without piano wire configuration. The black lines have the same slope which comes from a fit to the upper part of the “no wires” curve by Nis Dam Madsen

G5. Strain sensitive resistor substrate design

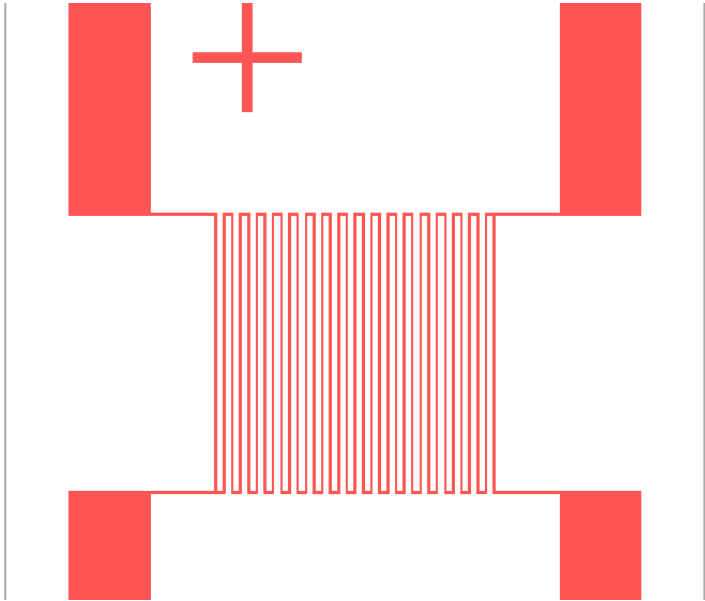


Figure 163 - Longitudinal meander structure (L-edit design) (5150x5150um) – lines 50um thick and spacing of 100um

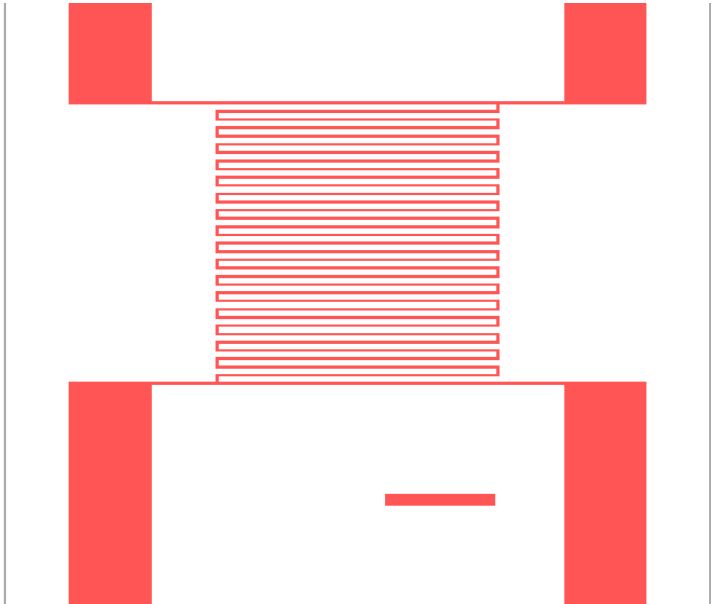


Figure 164 – Transverse meander structure (L-edit design) (5150x5150um) – lines 50um thick and spacing of 100um

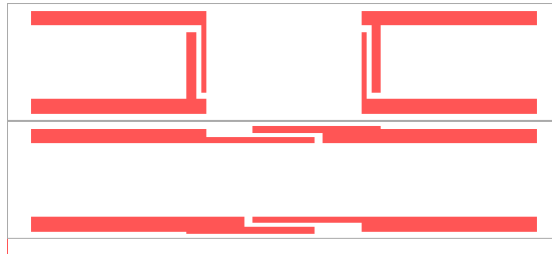


Figure 165 – bottom electrode design – longitudinal (left) and transverse (right)

**Dimensions:**

Longitudinal bottom contact resistor: 20mm x 5mm

Transverse bottom contact resistor: 12mm x 5x mm

High resolution thin film mask from “Microlitho”

### High Resolution Film

---

|   |  |
|---|--|
| <ul style="list-style-type: none"> <li>▪ Features down to 5µm.</li> <li>▪ Stable fine grain emulsion .007 film.</li> <li>▪ Superior line definition.</li> </ul> | <ul style="list-style-type: none"> <li>▪ Consistent density.</li> <li>▪ Flexible - easy to cut.</li> <li>▪ A4 to 28" x 32" sizes.</li> </ul> |
|---|--|

Figure 166 – high resolution film mask properties, source: <http://www.microlitho.co.uk> (28.05.2014)

Figure 167 shows an example of the high resolution thin film lithography mask which was used for the titanium/gold bottom contacts



Figure 167- Example of high resolution thin film lithography mask: bottom contacts pattern

Shadow mask for the cryofox deposition system

Longitudinal resistor dimensions are 20mm x 5mm with a target thickness of 400nm

Transverse resistor dimensions are 12mm x 5mm with a target thickness of 400nm



Figure 168 - Shadow mask for the cryofox deposition system

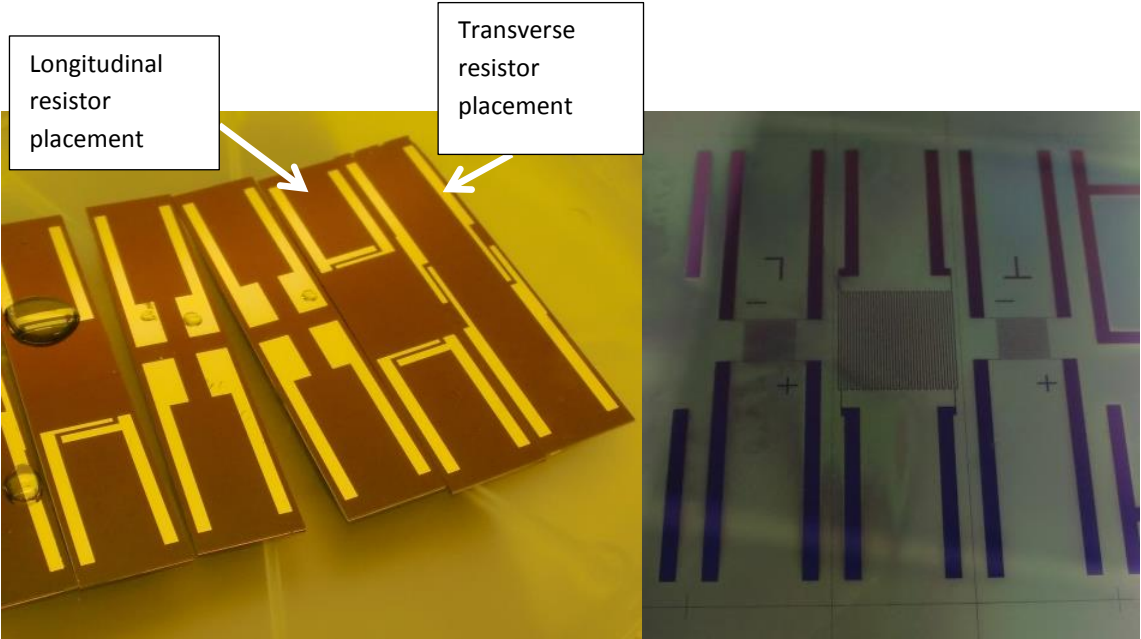


Figure 169 – Ti/Au bottom contact Ti:5nm, Au:100nm for Wheatstone bridge, longitudinal and transverse resistor placement (left), meander structures (right)

## G6. Gauge factor measurement test

By Nis Dam Madsen and Mathias Hausladen

A test of the setup's ability to measure gauge factors has also been carried out. The sample (DC-045) was made for the old setup, therefore, the resistor have not been centered with respect to the maximum strain in the sample. Generally, very stable resistivity measurements were made with the Keithley 2450. A five digit precision on the resistivity measurement was obtained with a little drift on the last digit. This translates into a force sensitivity of approximately 50 mN in this case. As seen in Fig. 7, the holder produce very accurate gauge factor data despite the many small corrections that have to be made to the design.

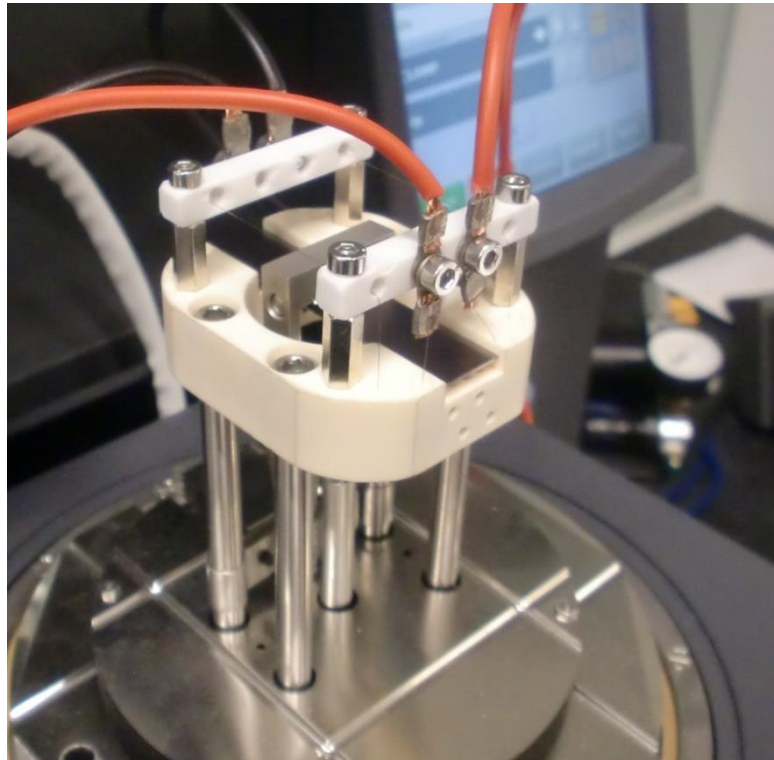
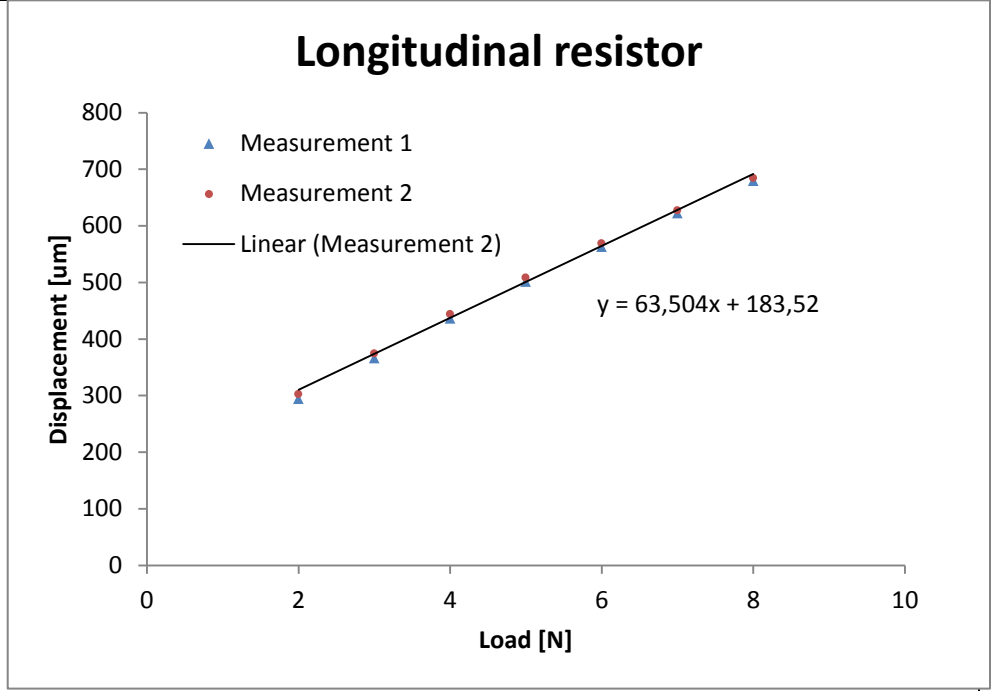
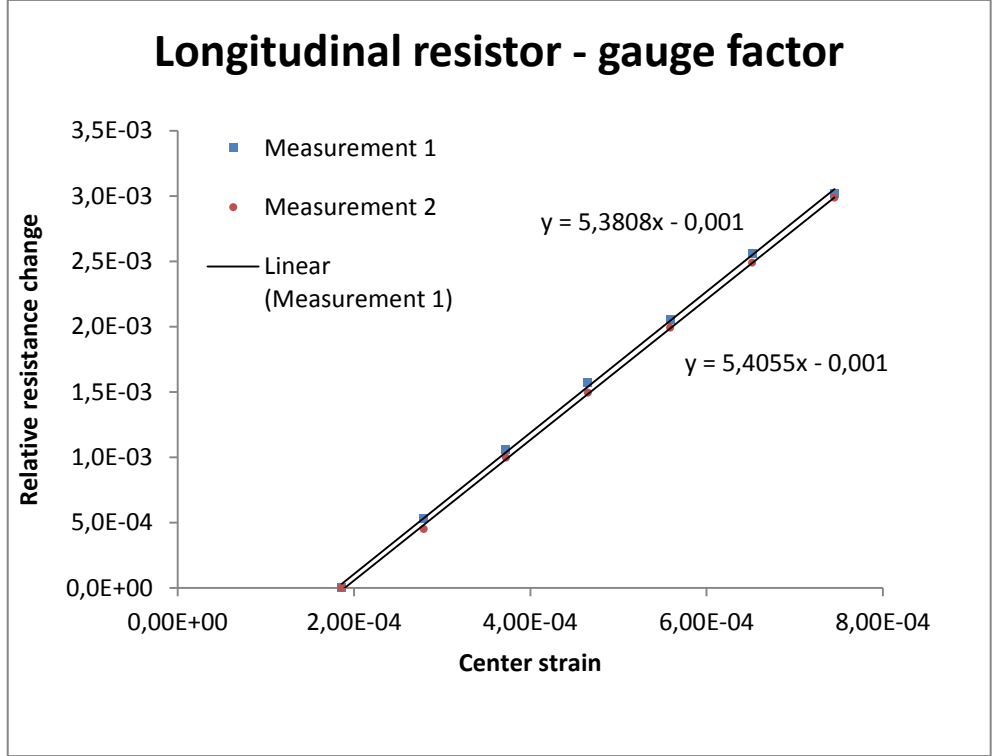


Figure 170 – prototype DMA setup for measuring a gauge factor

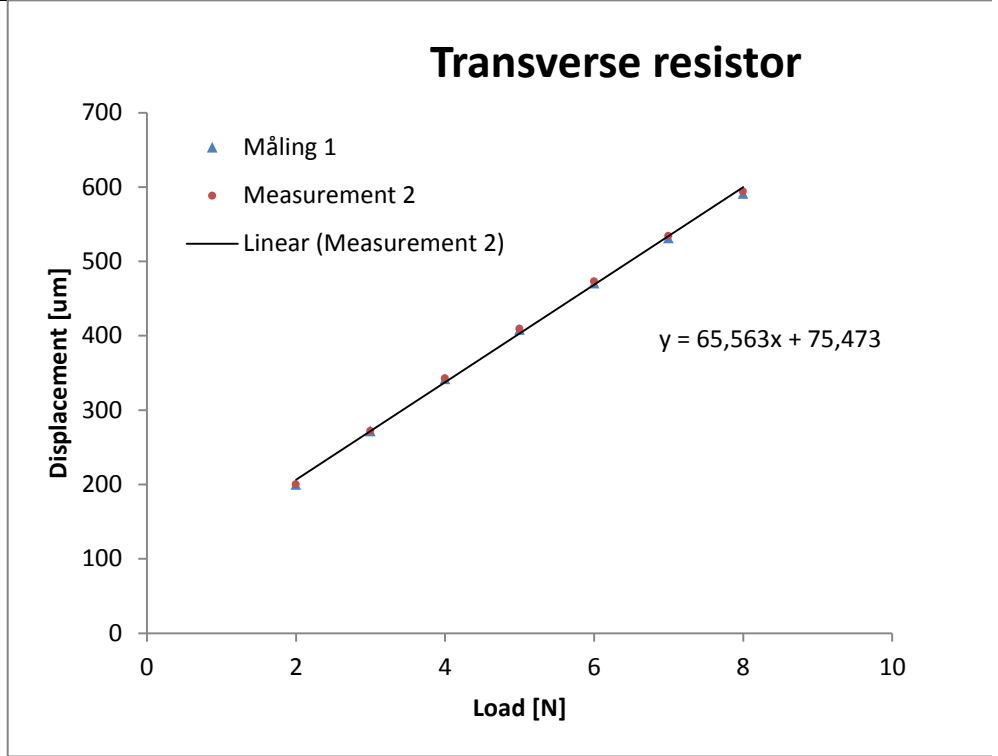
The load-displacement measurements of the longitudinal sample.



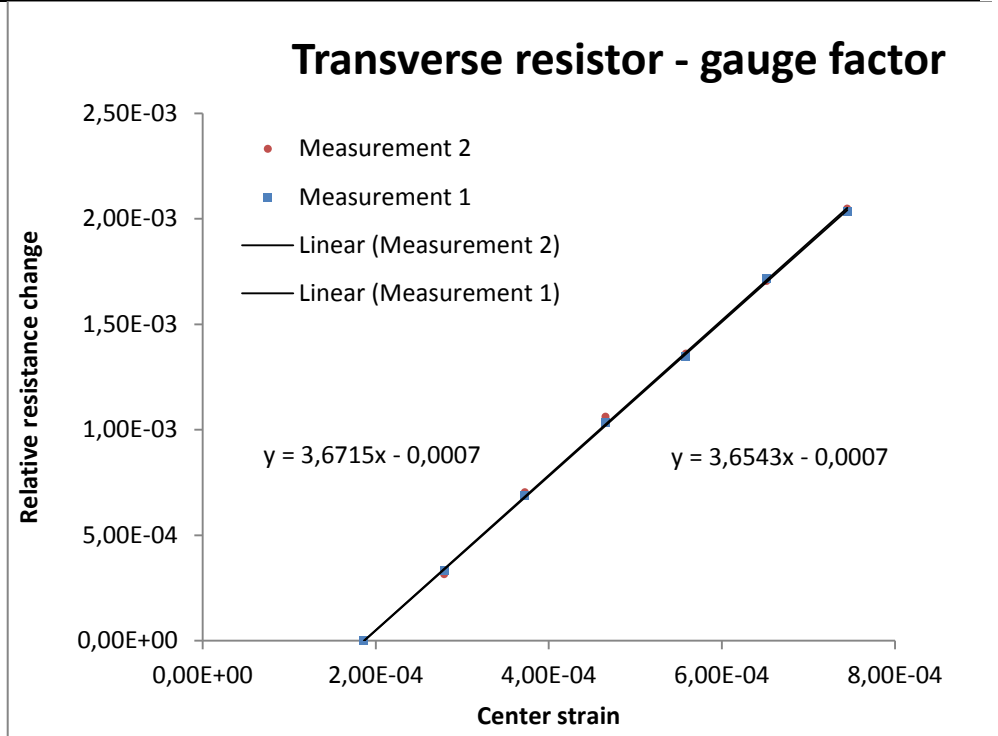
Two consecutive gauge factor measurements obtained on the longitudinal sample.



The load-displacement measurements of the transverse sample.



Two consecutive gauge factor measurements obtained on the transverse sample.



|   |                 |                           |                   |          |  |
|---|-----------------|---------------------------|-------------------|----------|--|
| DC-045 longitudinal DMA                           |                 |                           |                   |          |  |
| Measurement performed using: DMA and Keithley.    |                 |                           |                   |          |  |
| date: 18.03.2014                                  |                 |                           |                   |          |  |
| Current:  | 1 mA            | Note: auto mode           |                   |          |  |
| Compl.:   | 21 V            |                           |                   |          |  |
| Filter:   | none            |                           |                   |          |  |
|   |                 |                           |                   |          | Parameters:                                      |
|   |                 |                           |                   |          | z0 [m]   |
| Measurement 1 - prototypetest DC_45_transverse004 |                 |                           |                   |          | 0,0002625  |
| P (load) [N]                                      | Resistance [Ω]  | relativ resistance change | Displacement [um] | Strain   | Youngs modulus (E) [Pa]                          |
| 2,000   | 622,78          | 0,00000                   | 294,36            | 1,86E-04 | 1,69E+11   |
| 3,000   | 623,11          | 0,00053                   | 366,24            | 2,79E-04 |  |
| 4,000   | 623,44          | 0,00106                   | 436,21            | 3,73E-04 |  |
| 5,000   | 623,76          | 0,00157                   | 501,35            | 4,66E-04 | beam width (b) [m]                               |
| 6,000   | 624,06          | 0,00206                   | 562,92            | 5,59E-04 | 0,0121   |
| 7,000   | 624,37          | 0,00255                   | 622,39            | 6,52E-04 |  |
| 8,000   | 624,66          | 0,00302                   | 679,64            | 7,45E-04 | beam height (h) [m]                              |
|   |                 |                           |                   |          | 0,000525   |
| Measurement 2 - prototypetest DC_45_transverse005 |                 |                           |                   |          |  |
| P (load) [N]                                      | Resistance [kΩ] | relativ resistance change | Displacement [um] | Strain   | length (l) [m]                                   |
| 2,000   | 622,9           | 0,00000                   | 301,91            | 1,86E-04 | 0,04   |
| 3,000   | 623,18          | 0,00045                   | 374,07            | 2,79E-04 |  |
| 4,000   | 623,52          | 0,00100                   | 443,35            | 3,73E-04 | Area moment inertia (I) [m <sup>4</sup> ]        |
| 5,000   | 623,83          | 0,00149                   | 507,95            | 4,66E-04 | 1,4591E-13                                       |
| 6,000   | 624,14          | 0,00199                   | 568,89            | 5,59E-04 |  |
| 7,000   | 624,45          | 0,00249                   | 626,98            | 6,52E-04 |  |
| 8,000   | 624,76          | 0,00299                   | 684,16            | 7,45E-04 |  |
|   |                 |                           |                   |          | $I_x = \frac{1}{12}bh^3$                         |
|   |                 |                           |                   |          | transverse resistor width (l <sub>0</sub> ) [mm] |
|   |                 |                           |                   |          | 0,005  |

Figure 171 – raw data for the load-displacement and gauge factor plots (DC-45 longitudinal)

|   |                 |                           |                   |          |  |
|---|-----------------|---------------------------|-------------------|----------|--|
| DC-045 Transverse DMA                             |                 |                           |                   |          |  |
| Measurement performed using: DMA and Keithley.    |                 |                           |                   |          |  |
| date: 18.03.2014                                  |                 |                           |                   |          |  |
| Current:  | 1 mA            | Note: auto mode           |                   |          |  |
| Compl.:   | 21 V            |                           |                   |          |  |
| Filter:   | none            |                           |                   |          |  |
|   |                 |                           |                   |          | Parameters:                                      |
|   |                 |                           |                   |          | z0 [m]   |
|   |                 |                           |                   |          | 0,0002625  |
| Measurement 1 - prototypetest DC_45_transverse003 |                 |                           |                   |          |  |
| P (load) [N]                                      | Resistance [Ω]  | relativ resistance change | Displacement [um] | Strain   | Youngs modulus (E) [Pa]                          |
| 2,000   | 669,41          | 0,00000                   | 200               | 1,86E-04 | 1,69E+11   |
| 3,000   | 669,63          | 0,00033                   | 271,64            | 2,79E-04 |  |
| 4,000   | 669,87          | 0,00069                   | 341,7             | 3,73E-04 | beam width (b) [m]                               |
| 5,000   | 670,1           | 0,00103                   | 408,07            | 4,66E-04 | 0,0121   |
| 6,000   | 670,31          | 0,00134                   | 470,61            | 5,59E-04 |  |
| 7,000   | 670,56          | 0,00172                   | 531,28            | 6,52E-04 | beam height (h) [m]                              |
| 8,000   | 670,77          | 0,00203                   | 591,32            | 7,45E-04 | 0,000525   |
| Measurement 2 - prototypetest DC_45_transverse002 |                 |                           |                   |          |  |
| P (load) [N]                                      | Resistance [kΩ] | relativ resistance change | Displacement [um] | Strain   | length (l) [m]                                   |
| 2,000   | 669,33          | 0,00000                   | 199,98            | 1,86E-04 | 0,04   |
| 3,000   | 669,54          | 0,00031                   | 271,51            | 2,79E-04 | Area moment inertia (I) [m <sup>4</sup> ]        |
| 4,000   | 669,8           | 0,00070                   | 342,21            | 3,73E-04 | 1,4591E-13                                       |
| 5,000   | 670,04          | 0,00106                   | 409,22            | 4,66E-04 |  |
| 6,000   | 670,24          | 0,00136                   | 472,8             | 5,59E-04 |  |
| 7,000   | 670,47          | 0,00170                   | 533,74            | 6,52E-04 |  |
| 8,000   | 670,7           | 0,00205                   | 593,55            | 7,45E-04 |  |
|   |                 |                           |                   |          | $I_x = \frac{1}{12}bh^3$                         |
|   |                 |                           |                   |          | transverse resistor width (l <sub>0</sub> ) [mm] |
|   |                 |                           |                   |          | 0,005  |

Figure 172 – raw data for the load-displacement and gauge factor plots (DC-45 transverse)

## G7. Substrate and substrate placement

A variation of substrates had to be used for the different characterization techniques

| Sample | Substrate                                  | Number | Purpose                          |
|--------|--|--------|----------------------------------|
| GF-T-B | N9 - Transverse                            | 1      | Gauge factor/TCR                 |
| GF-L-B | N9 - Longitudinal                          | 1      | Gauge factor/TCR                 |
| GF-W-B | N9 - Wheatstone                            | 1      | Gauge factor/TCR                 |
| GF-T-M | N9 - Transverse                            | 1      | Gauge factor/TCR                 |
| GF-L-M | N9 - Longitudinal (LT-011)                 | 1      | Gauge factor/TCR                 |
| BK7-A  | G3 (BK-7)                                  | 1      | XRD                              |
| P1-A   | P1 (10x10 mm)                              | 1      | EDX                              |
| P1-B   | P1 lift off (10x10 mm)                     | 1      | AFM thickness /SEM cross-section |
| P7-A   | P7 (200 micron) (3x25 mm) (Lowest number)  | 1      | Stress measurement               |
| P7-B   | P7 (200 micron) (3x25 mm) (Highest number) | 1      | Stress measurement               |

Figure 173 - Substrates needed for the analysis of the films

**GF-X-B:** Gold bottom contact samples, (5 nm Ti / 100 nm Au)

**GF-X-M:** Lift-off meander structure samples

Figure 174 shows the placement of the substrates during the deposition. The shadow mask was used to place the GF-X-B samples in and the remaining samples were mounted with carbon tape on the outside of the mask.

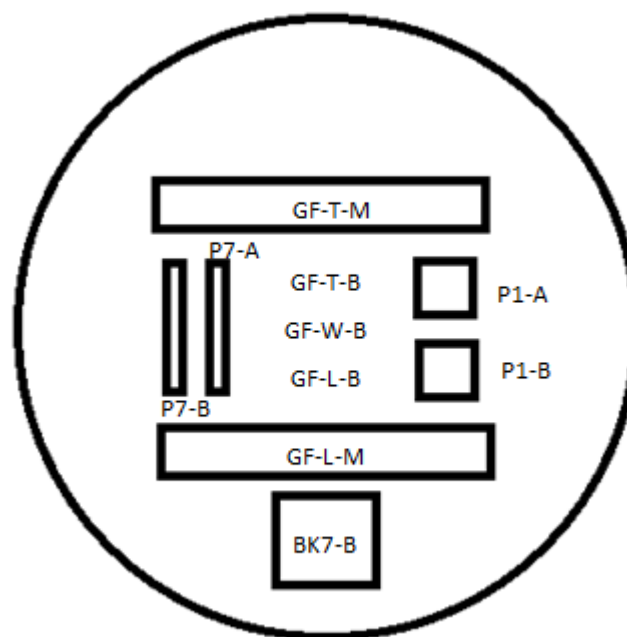


Figure 174 – Substrate placement on 4 inch wafer

Figure 175 shows the lithography parameters for producing the meander structure for DC-68 and DC-72

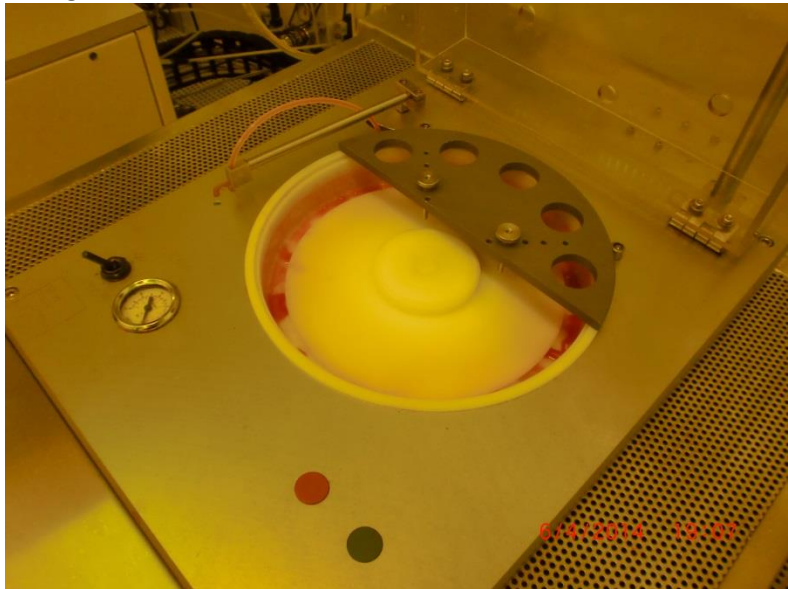
| Date       | Run    | Wafer type | Spin coating   | Pre-bake               | Mask                 | Exposure 1   | Inversion bake                | Exposure 2   | Development   | DC-Deposition |
|------------|--------|------------|--|------------------------|----------------------|--|-------------------------------|--|---|---------------|
| 14.04.2014 | LT-007 | N9         | Step 1: 3 s dispense, speed 0, ramp 5000; Step 2: 5 s, speed 500 rpm, ramp 5000 rpm/s; Step 4: 30 s, speed 4000 rpm, ramp 10000 rpm/s. | Hotplate: 90 C @ 1 min | Meander structure #1 | 2.5 s. Alignment gab: 5 micron. Exposure gap: 5 micron | Hotplate: 130 C @ 1 min, 40 s | 25 s Alignment gab: 5 micron. Exposure gap: 5 micron | Developer time: 1 min. Rough rinse: 1 min. Fine rinse: 1 min. Blow dry.                   | DC-068        |
| 06.05.2014 | LT-009 | N9         | Step 1: 3 s dispense, speed 0, ramp 5000; Step 2: 5 s, speed 500 rpm, ramp 5000 rpm/s; Step 4: 30 s, speed 4000 rpm, ramp 10000 rpm/s. | Hotplate: 90 C @ 1 min | Meander structure #1 | 2.5 s. Alignment gab: 5 micron. Exposure gap: 5 micron | Hotplate: 130 C @ 1 min, 40 s | 30 s Alignment gab: 5 micron. Exposure gap: 5 micron | Developer time: 1 min 20 sek. In beaker. Rough rinse: 1 min. Fine rinse: 1 min. Blow dry. | DC-072        |

Figure 175 – lithography parameters

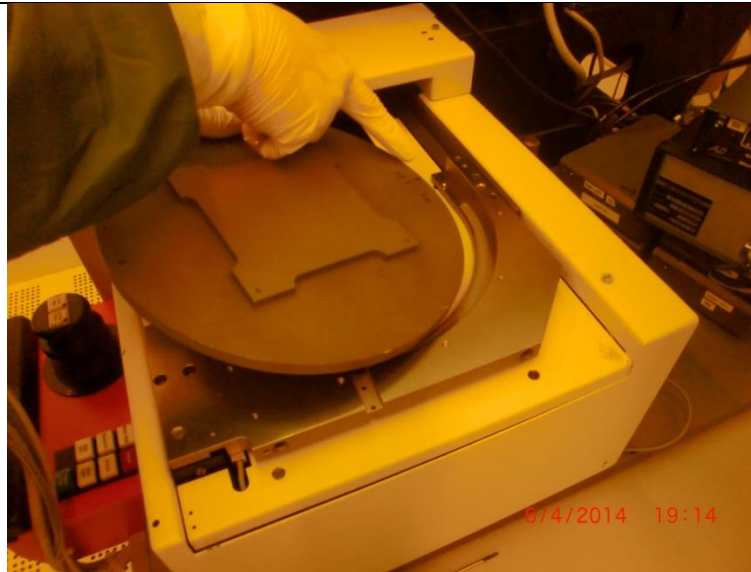
## G8. Step by step production instructions

Written by Nis Dam Madsen in corporation with Mathias Hausladen

| Stepwise recipe for making structured samples using a lift-off process |                            |  |  |
|--|----------------------------|--|--|
| Step number  | Action                     | Parameters   | Comment  |
| 1  | Chose wafer from inventory | Depends on the purpose.  | Remember to write in wafer log   |
| 2  | HDMS                       |  |  |
| 2.1  | Apply HDMS                 | Set the HDMS oven to 120 °C  | The oven takes approx. 30 min to heat up.  |
| 2.2  |                            | Follow the standard instructions as described on the note near the oven.   | The HDMS procedure takes approx. 40 min to complete.   |
| 4.1  | Lithography                | Turn on the mask aligner.<br> | First push the large green botton on the left. Then turn on the lamp, on the switch in the upper right corner. Turn on the computer on the large switch in the middle. When the instrument is reading ready in the display push the start button underneath the lamp switch. This button may be difficult to push on. The lamb has to read 275 and the light from it can be seen on the back wall. |
| 3  | Spin coating               |  |  |
| 3.1  |                            | Turn on the spin coater. And place the screening disk and then the wafer   | This can be done before the  |

|         |  |  |   |
|---------|--|--|---|
|         |  | chuck in the spin coater. Check the photo resist bottle.   | HDMS process finishes   |
| 3.2/5.1 |  | Turn on the two hotplates. The left hotplate must be set to 130 °C and the right hotplate to 90 °C.  | The temperature settings, the plates takes a long time to cool down if the temperature is set too high. |
| 3.3     |  | Place test wafer on the dedicated wafer chuck and use the alignment devise to align the wafer.<br>                |   |
| 3.4     |  | <b>Turn on vacuum</b> , remove alignment devise and close lid  |   |
| 3.5     |  | Chose program number and check the parameters:<br><b>Step 1:</b><br>Spin Time: 3 s<br>Rotation: 0 rpm<br>Ramping: 5000 rpm/s<br>Dispense on<br><b>Step 2:</b><br>Spin Time: 5 s<br>Rotation: 500 rpm |   |

|          |                    |   |  |
|----------|--------------------|---|--|
|          |                    | Ramping: 5000 rpm/s<br><b>Step 3:</b><br>Spin Time: 30 s<br>Rotation: 4000 rpm<br>Ramping: 10000 rpm/s<br><b>Step 4:</b><br>Spin Time: 0<br>Rotation: 0<br>Ramping: 10000 rpm/s                   |  |
| 3.6      |                    | Close lid and press the green bottom to start the spin coating procedure.   |  |
| 3.7      | Pre-bake           | Take out wafer from spin coater and place on the left hotplate (90 °C ) for 1 min. Remember to have the ventilation pipe over the wafer while it is drying, the fumes are not healthy.            | To remove solvent from the photoresist. It is important to be precise with the time                                    |
| 3.8      | Repeat             | Repeat steps 3.3 to 3.7 for the wafers with HDMS applied.   |  |
| 3.9      | Clean              | <b>Clean the spin coater with acetone. Avoid inhaling the fumes if possible. Turn of the 90 °C hotplate when done with spin coating.</b>  |  |
| <b>4</b> | <b>Lithography</b> |   | Turn on mask aligner if not already done in step 4.1 above. Note that the mask aligner takes a few minutes to warm up. |
| 4.2      |                    | Log on to the computer. Username: p, password: p  |  |
| 4.3      |                    | Insert mask in the mask aligner. Push the mask button in the upper left corner in the display. And chose load mask. Take the mask chuck in the rack on the wall and place it in the mask aligner. |  |

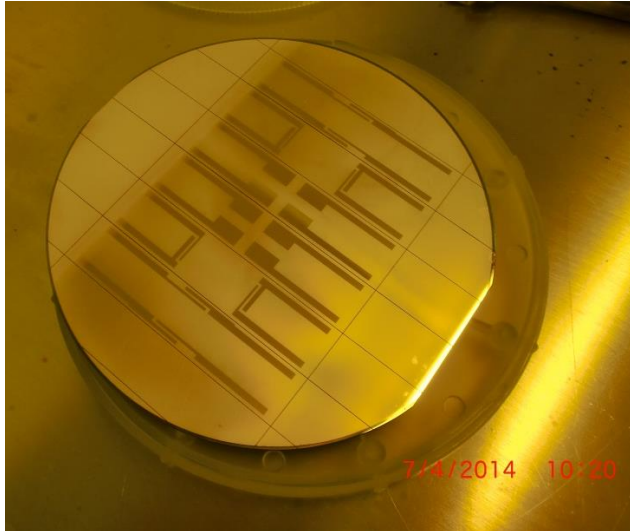


Note that the pins in the mask aligner has to fit the holes in the chuck. Handle the chuck with care. Follow the on screen instructions on the mask aligner.

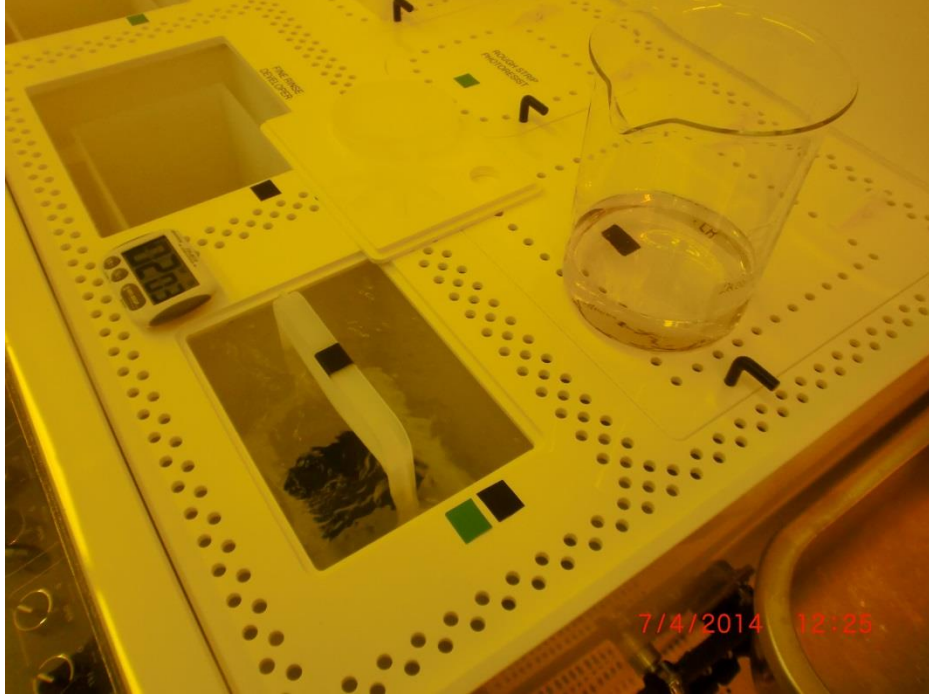
|     |  |  |  |
|-----|--|--|--|
| 4.4 |  | Place the appropriate mask on the mask chuck and align the corners carefully.  |  |
| 4.5 |  | Push the start button to insert the mask.  |  |
| 4.6 |  | Take out the mask chuck and place it in the rack again.  |  |
| 4.7 |  | Insert the wafer chuck into the mask aligner.  |  |
| 4.8 |  | Place wafer on the wafer chuck and align it with the stubs on the chuck. If a foil mask is going to be used place this on top of the wafer and check that the correct side is facing up. | The readable side should be facing up in the case of the MicroLitho masks. |

|      |  |   |   |
|------|--|---|---|
|      |  |                                   |   |
| 4.9  |  | Follow the on screen instructions to load the wafer.  |   |
| 4.10 |  | Set the exposure time (2.5 s) and check remaining parameters.<br>Alignment gab: 50 micron<br>Exposure gab: 5 micron | Push the field where the exposure time is listed to open this menu. |

|          |                       |   |  |
|----------|-----------------------|---|--|
|          |                       |   |  |
| 4.11     |                       | Expose: Push start, press the alignment complete button on the joystick and press expose. Take out wafer when done.                           |  |
| 4.12     |                       | Repeat step 4.8 to 4.11 for the remaining wafers.   |  |
| <b>5</b> | <b>Inversion bake</b> |   | Turn on left hotplate if not already done at step 3.2.                                     |
| 5.2      |                       | Place the exposed wafer on the right hotplate at 130 °C for 100 s (1 min 40 s). It is important this time and temperature is kept accurately! | Set the stop watch to 1 min 45 s and be ready to place the wafer when it reach 1 min 40 s. |
| 5.3      |                       | Turn off hotplate when done.  |  |
| <b>6</b> | <b>Float Exposure</b> |   |  |
| 6.1      |                       | Change the mask to the blank mask if it is not already in the mask aligner by repeating steps 4.3 to 4.7.                                     |  |
| 6.2      |                       | Expose the wafer for 25 s by repeating step 4.8 to 4.11. <b>Remember to change</b>  |  |

|          |                      |  |  |
|----------|----------------------|--|--|
|          |                      | <b>the exposure time to 25 s!!!</b>  |  |
| 6.3      |                      | Repeat for the remaining samples.  |  |
| 6.4      |                      | Take out the mask. First remove wafer chuck and put in the mask chuck. Unload the mask from the load menu.   |  |
| 6.5      |                      | Turn off mask aligner when done. Opposite procedure as turning it on. (first the computer and then the lamp)   |  |
| <b>7</b> | <b>Dicing</b>        |  |  |
| 7.1      |                      | Take the sample out of the clean room and dice the wafer.<br>   | A separate instruction is available for this step.         |
| <b>8</b> | <b>Development</b>   | <b>It is important to put on the safety equipment for the development procedure. This includes the apron, the sturdy chemicals gloves, an extra pair of gloves and the face screen.</b>  | Ask someone to help if you are not comfortable doing this. |
| 8.1      | Development solution | The wafers are developed in a 1:4 mixture of AZ 351 B Developer and deionized water. Take 400 ml of <b>deionized water</b> from the tap in fume hood and put into a large beaker. Take 100 ml of <b>AZ 351 B Developer</b> and mix into the water in the beaker. | The beaker must be large enough to hold a whole wafer.     |

|     |  |   |  |
|-----|--|---|--|
|     |  |   |  |
| 8.2 |  | Take the development solution to the development wetbench and place it on top of the developer lid. Turn on the rough rinse vessel. |  |

|     |  |   |   |
|-----|--|---|---|
|     |  |   |   |
| 8.3 |  | Place the wafer in the developer for 2 min while the liquid in the beaker is gently swirled.  | This is important to keep this time fairly accurate. It can however be difficult to get the wafer up from the beaker. It may be a good idea to practice this with water and a test wafer before starting. |
| 8.4 |  | Take up the wafer and place it in the rough rinse vessel for at least 1 min. Turn on the fine rinse vessel.   | The contact for the fine rinse require a little push action to work.  |
| 8.5 |  | Put the sample in the fine rinse for 1 min.   | Time not critical.  |
| 8.6 |  | Take up sample and blow dry in nitrogen from fume hood. <b>Be careful not to drip water on the floor since this will put of the spillage alarm!</b> |   |
| 8.7 |  | Repeat steps 8.3 to 8.6 for remaining wafers.   |   |

|           |                              |   |  |
|-----------|------------------------------|---|--|
| 8.8       |                              | Turn off the rinse vessels when done. Dispose the developer according to the <b>waste regulations</b> listed on the side of the fume hood. Clean beakers and tools.   |  |
| <b>9</b>  | <b>Deposit film</b>          |   |  |
| 9.1       |                              | Check the structure in the microscope and blow it with nitrogen before starting the deposition. Turn off microscope.  |  |
| 9.2       |                              | Deposit the film, a separate instruction is available for this.   |  |
| <b>10</b> | <b>Lift-off</b>              |   |  |
| 10.1      |                              | Depending on the deposition and if the wafer was cut the procedure may vary. However, the general procedure is to place the samples in acetone and expose them the ultra-sonication. The time is usual between 2 min to 10 min. Be careful not to use too high ultra-sonication power. If the film still persists it can be attempted to gently wipe the sample with a tissue while the sample and tissue are submerged into acetone. |  |
| 10.2      |                              | When the excess film has been stripped. Flush the sample with new acetone and then with isopropanol followed by deionized water. Blow dry with nitrogen the finish the sample cleaning.   |  |
| 10.3      |                              | Check the structure in the microscope and clean up beakers, tools etc.  |  |
| 10.4      |                              | <b>The sample is done 😊</b>   |  |
| 11        | <b>Clean up and check up</b> | Check that everything is cleaned and put back on the shelves. Check that there is no mask in the mask aligner and that it is turned off. Check that the spin coater is clean and turned off. Check the development wet bench is tidy and off. Make sure the fume looks good and no beakers are left. Turn off microscope if not already done.   |  |

